Numerical approximation and analysis of mathematical models arising in cells movement

Monika Twarogowska

UNIVERSITÀ DEGLI STUDI DELL'AQUILA

Dipartimento di Matematica Pura e Applicata

Dottorato in Matematica - XXIV Ciclo

Tesi di Dottorato in Matematica
Settore Scientifico Disciplinare: MAT/05

Numerical approximation and analysis of mathematical models arising in cells movement

Relatori

Prof. Roberto Natalini

Candidato

Monika Twarogowska

Dr. Magali Ribot

Coordinatore del corso di Dottorato

Prof. Anna De Masi

ANNO ACCADEMICO 2010/2011

I hereby declare that this Thesis is my own work and effort. Where other sources of information have been used, they have been acknowledged.

Acknowledgments

Looking back over these three years of the PhD studies I see moments which were full of joy as well as those tough, when everything seemed to be against me and despondency appeared. I am very grateful for all of them. They certainly shaped me as a person I am today. One of this joyful moments is now, when I can thank all those without whom this thesis would not be possible.

I owe my deepest gratitude to the supervisor of my thesis Roberto Natalini, who took care of my PhD research at a difficult moment time, after the earthquake in L'Aquila. I am thankful for his time, ideas and support that were irreplaceable, for introducing me to the field of numerical analysis and for showing interesting and challenging topics. In addition, I would like to thank for his patience, guidance and dedication in the preparation of this thesis. Through all these years, the joy and enthusiasm he has for Mathematics has been motivational for me.
I would also like to express my sincere thanks to Magali Ribot, who became my co-advisor. Her presence and contribution to my research enriched my experience and understanding of numerical methods and implementation of algorithms. Moreover, her openness, kindness and support made the time I spent in France unforgettable.

I am heartily thankful to Bruno Rubino for his help, care and encouragement since my first day in L'Aquila. I am really grateful for the support I have received from him during these years and for the ceaseless sensation that in any difficulty I can turn to him. It is so comforting while being far from my family.

I wish to thank Federica Di Michele, my room mate for two years and companion at University, for a great friendship and being always available to help, give advice or just listen. I am grateful for her understanding and encouragement, for fruitful discussions, for making time in L'Aquila more interesting, coffees more tasty and running more enjoyable.
I devote special thanks to my best friends in Poland. Especially to Joanna Kamińska and Weronika Pelc-Garska for irreplaceable encouragement and company in the moments of homesickness.

I would also like to thank Prof. P. Marcati and Marco Di Francesco for introducing me to the field of mathematical modelling and for all the support during my PhD studies.
I thank the people in the Laboratoire J. A. Dieudonné at Université de Nice-Sophia Antipolis for hospitality and for giving me the possibility to broaden my knowledge in the field of numerical analysis. In addition, I would like to thank Christophe Berthon for an invitation to Laboratoire de Mathématiques Jean Leray at Université de Nantes and for very interesting and fruitful discussions.
I express also my gratitude to Prof. P. Marcati , Prof. L.C. Berselli and Prof. D. Benedetto for accepting to be members of my thesis committee.

Monika Twarogowska

To my Mother
and my Sister

Contents

Introduction

The aim of this thesis is to investigate some mathematical models arising in cells movement, from both analytical and numerical point of view.

Migration of cells in the fibrous environment is an essential feature of normal and pathological, biological phenomena such as embryonic morphogenesis, wound healing, angiogenesis or tumour invasion. In the simplest case we can consider a tissue as a tridimensional structure consisting of fibres (Extracellular matrix ECM) and cells attached to them. Many experimental studies (see for instance [42]) give a good insight into how the cells move. It is known that they interact with the tissue matrix as well as with other cells using different biological and physical mechanisms. The forces driving the cells motion are generated by controlled remodelling of the actin network within the cell as a response to mechanical and chemical signals. The movement itself is strongly influenced by the spatial and temporal configuration of the fibres. Moreover, it depends on the contact-guidance phenomenon and attached-detached processes. Also their behaviour can be altered by the presence of some stimulus giving rise to the so called taxis movements. Basically it means to change the direction, in which the cell moves, for example, according to the gradient of some quantities such as adhesion forces (haptotaxis), electric field (galvanotaxis), chemical substances (chemotaxis), oxygen concentration (aerotaxis). In this thesis we focus our attention to the chemotaxis that is a directed movement of mobile species towards the lower/higher concentration of a chemical substance in the surrounding environment.

Since the first description of chemotaxis in bacteria by T.W.Engelmann (1881) and W.F.Pfeffer (1884), our knowledge about this phenomenon has been continuously expanding. Changes in the behaviour due to the presence of some stimulus have been observed in many kinds of organisms and are decisive in biological processes. For example, some bacteria can move towards higher concentration of food such as glucose molecules. Moreover, they can aggregate while starving. Amoebae like organism, Dictystelium Discoiduum, secretes the cyclic Adenosine Monophosphate (cAMP), which attracts other amoebae, leading to the formation of a multicellular organisms (see [117]). White, blood cells, neutrophil granulocytes, migrate to the cites of inflammation following chemokines released by macrophages after the encountering an antigen. During tumour invasion the cancerous cells secrete various growth factors, which attract and stimulate endothelial cells, in order to form a blood network around the tumour (see [40]).

The movement of cells under the effect of a stimulus has been a widely studied topic in the last decades by biologists as well as by mathematicians and many models have been proposed [89], [90]. Of course they differ in complexity, that is for example how many constituents are taken into account or which phenomena are to be considered, but the mathematical framework of any model depends on the scale at which we describe the problem. In particular, at the macroscopic level we consider cells as continuum medium and describe their behaviour via the population density. This approach leads to models built in the form of systems of partial differential equations of reaction-advection-diffusion type. The most classical model describing the chemotaxis in this framework is due to Patlak [96] and subsequently to Keller and Segel

[70]. One of the models we consider in this thesis is of this type. It describes the density $\rho(x,t)$ of cells and the concentration of chemoattractant $\phi(x,t)$ and it writes as

$$\begin{cases} \rho_t = \Delta(P(\rho)) - \chi \nabla \cdot (\rho \nabla \phi), \\[2ex] \phi_t = D\Delta\phi + a\rho - b\phi. \end{cases} \tag{1}$$

The fibrous character of the tissue is modeled by the nonlinear function

$$P(\rho) = \varepsilon \rho^\gamma, \quad \varepsilon > 0, \gamma > 1. \tag{2}$$

The positive parameters D, a, b are respectively diffusion coefficient, production and degradation rates of chemoattractant, while χ measures the strength of the response of cells to its presence. This model has been widely studied in the recent years. It is known that in the case of linear diffusion the solutions exist globally in time in one dimension and there is the possibility of some pointwise blow-up in higher ones if the initial mass is big enough. To overcome this problem, modifications were introduced to prevent from overcrowding and guarantee the global existence of solutions. For example, it was proposed to use a density dependent diffusion, such as (2), having a volume filling effect (see [95], [23]) or a nonlinear chemosensitive function $\chi = \chi(\rho, \phi)$ instead of the constant parameter [99].

In this framework, in Chapter 2 we propose a reaction-diffusion system with a chemotaxis term and nutrient-based growth of tumour. The formulation of the model considers also an influence of tumour and pharmacological factors on the nutrient concentration. It is based on the one presented in [101]. Denoting by ϕ the tumour density and by c the nutrient concentration it writes as

$$\begin{cases} \phi_t = \nabla \cdot (\phi \nabla F(\phi)) - \nabla \cdot (\omega \phi \nabla c) + \alpha(\phi, c) \\[2ex] c_t = D\triangle c + \beta(\phi, c) \end{cases} \tag{3}$$

with

$$\alpha(\phi, c) = \gamma_1 \widehat{p}\left(\frac{c}{c^*} - 1\right)\phi\widehat{H}(\phi^* - \phi) - \gamma_2 \widehat{p}\left(1 - \frac{c}{c^*}\right)\phi - \delta\phi \tag{4}$$

$$\beta(\phi, c) = -dc\phi + G\phi - Rc, \tag{5}$$

where $\hat{H}(x), \hat{p}(x)$ are regularized approximations of the Heaviside and the 'positive part' function $(x)_+$ respectively. In this thesis we study the convergence of solutions to constant steady states in one dimensional case for small perturbations from the equilibria. The nonlinear stability results are obtained by means of the classical symmetrization method and energy estimates.

Macroscopic, parabolic type of models describe very well the aggregation phenomena but fail when the network structures have to be reproduced. This can be observed when studying the experiments with human vascular, endothelial cells. Randomly seeded on the plain gel substratum, these cells migrate and aggregate to finally form a complex network seen as the beginning of vascularization, that is de novo formation of blood capillaries. The Patlak-Keller-Segel model cannot explain this process as well as cannot describe the 'run and tumble' movement of, for example, Eusterichia Coli. This is because it is mainly directed to the long

time scales evolutions [37]. This is why in recent years there is a tendency to use hyperbolic systems, which correspond to models at the lower, mesoscopic scale. They are able to capture the particular features of the modeled quantity and as a consequence can better describe short time behaviour of physical problems.

In this thesis we consider a hyperbolic model of chemotaxis introduced by Gamba et.al in [44] to describe the vasculogenesis process. It is a simple system, which takes into account only two constituents. It describes the evolution of the density ρ of endothelial cells and a concentration of chemoattractant ϕ and has the form

$$
\begin{cases}
\rho_t + \nabla \cdot (\rho u) = 0 \\[2mm]
(\rho u)_t + \nabla(\rho u \otimes u + P(\rho)) = -\rho u + \chi \rho \nabla \phi \\[2mm]
\phi_t = D \Delta \phi + a\rho - b\phi
\end{cases}
\tag{6}
$$

The pressure law for $P(\rho)$ is given by the constitutive law for isentropic gases (2). It models the short range interaction between cells and the fact that they have their own volume and cannot be penetrable by others. The friction term $-\rho u$ describes the adhesion of cells to the structure, while $\chi \rho \nabla \phi$ is the directional response to the chemical gradient.

From the mathematical point of view the Keller-Segel type model (1) is a parabolic system with cross diffusion, nonlinear terms, while the system (6) is a degenerate, hyperbolic-parabolic problem. They are connected also for long time asymptotics. More precisely, in [61],[62], for $1 \leq \gamma \leq 3$, the convergence of the solutions to the isentropic gas dynamics with friction to the porous medium equation was studied, while for the chemotaxis models the long time behaviour was analyzed in [41]. Despite this connection between the two models, our knowledge of them differs very much. Behaviour of parabolic, degenerate equations is now quite well understood, while in the case of hyperbolic, degenerate systems, even without chemotaxis, there are still many open problems. For example, as finite time blow-up was proved for the Keller-Segel model, no similar results are available in the case of the hyperbolic one. Another aspects concerns the behaviour of solutions in the presence of vacuum, where the density vanishes. It is especially interesting from the point of view of the application, as it is very reasonable to consider for example in the modelling of tumour growth or biofilm, places without cells and to study the evolution of the interface between the region with strictly positive density and the vacuum. However, the presence of states with vanishing density complicates the situation from the mathematical point of view. In the case of the isentropic gas dynamics system, at the interface the eigenvalues coincide and become zero. The system becomes degenerate, cannot be any more symmetrizable with real coefficients and standard theories cannot be applied.

Our approach to better understanding the behaviour of the isentropic gas dynamics system with damping and the hyperbolic model of chemotaxis (6) is to study the problem numerically. More precisely, in the case of a pure diffusion problem we focus our attention on the waiting time phenomena and the behaviour near the interface under the physical boundary condition in one dimension. The analysis of the chemotaxis model concerns the study of solutions on the bounded domain with no-flux boundary conditions. In particular, we are interested in non constant steady states, which appear to contain vacuum even for the strictly positive initial data, and compare the behaviour with the parabolic model (1).

Numerical approximation

In order to study numerically any kind of problem we need a stable and consistent numerical scheme. Besides, a good scheme has to reproduce all of the important features of the original model, which arise from the physical background of the problem. First of all the scheme has to preserve the non negativity of solutions as we deal with densities and concentrations. Then, if we consider bounded domains with no-flux boundary conditions, the numerical approximation has to conserve the total mass. Conservation laws with reaction terms are characterized by a special balance between the fluxes and the sources, which can lead to non constant stationary solutions. Their preservation is essential and in the case of geometric sources, containing for example space derivatives, it is impossible by using standard schemes treating the flux and the source at different time steps. Moreover, the presence of the vacuum states brings another difficulty as many schemes produce oscillations at the interface between the regions, where the density is strictly positive and where it vanishes. In order to study the behaviour of the free boundary, the approximate solution not only has to be free from oscillations, but also it has to deal with steep fronts and also has to be characterized by small artificial viscosity. Constructing a numerical scheme for parabolic and hyperbolic model of chemotaxis satisfying all these properties is not an easy task.

In fact, for the pure diffusion problem, there is a vast amount of stable, very accurate schemes. In particular, for the porous medium equation we apply a fully implicit discretization in time with centered, conservative approximation of the diffusion term, while for the isentropic gas dynamics system with friction we use a finite volume scheme based on the approximate Riemann solver. As the damping has a stiff nature we treat it implicitly solving an ODE at the additional step.

In the case of the chemotaxis models the situation is more complicated. For the parabolic system the presence of the advection term can lead to the loss of the total mass and steep, traveling fronts, where oscillations may occur. In this thesis we compare two approaches, the IMEX scheme with implicit-explicit splitting and a scheme based on the relaxation technique introduced in [6]. On the model of angiogenesis (see [25]) we show that IMEX approach works very well, with the accurate approximation of the interface if the solution is smooth enough, however, in the presence of steep fronts it produces spurious oscillations. On the other hand, the second method is fully explicit and requires a solution of the system of linear, transport equations. This is why it is characterized by a higher numerical viscosity that smooths the oscillations, but at the same time gives large error at the free boundary. To fix this problem we considered high resolution schemes based on the flux-limiters approach and chose the limiter functions suitable to diminish artificial diffusion. Unfortunately both of these methods need a special treatment of boundary conditions in order to conserve the total mass.

Hyperbolic model of chemotaxis could be also approximated by the above scheme, however, a more suitable approach is to use the finite volume method, which can handle shocks, contact discontinuities and by definition preserves the total mass. Moreover, to construct a scheme in one dimension for conservation laws we are endowed with a powerful tool, which is the Riemann problem. Using its approximate solutions for the homogeneous part and well-balancing reconstruction of the variables at interfaces of each cell to treat the sources, we can

construct a consistent scheme that preserves the steady states with constant velocity. Additionally to the well-balanced property, the scheme preserves the non negativity of densities. Moreover, as for the approximate Riemann solver, we use Suliciu relaxation solver adapted to treat the vacuum states presented in [17]. We prove all these properties for a semi-discrete scheme and give a weak stability condition for the fully discrete approximation.

Numerical analysis

The numerical analysis we present in this thesis is divided into two parts. We start by considering the evolution into vacuum of the isentropic gas described by the compressible Euler equation with damping. In particular we focus our attention on two problems, which have been extensively studied in the case of degenerate parabolic equations such as the porous medium equation. It is well known that the degeneracy implies a finite speed of propagation. Equivalently it means that when the initial density has compact support, it will remain compact for all times [94]. Moreover, it induces an interface ξ between the region where the density is bigger than zero and the one where it vanishes. After being set in motion, the interface is a strictly positive function of time [72]. However, under special conditions on the initial data, it may remain motionless for a finite, positive time t^*, called the waiting time, then it starts to move and never stops.

In the case of the porous medium equation, sufficient and necessary conditions that guarantee the occurrence of this phenomenon are available [120], together with the bounds on the waiting time [9], [10], [97]. Moreover it was proved in [12], [60] that the interface is a C^∞ function after the waiting time. On the other hand, the Euler system with damping for the isentropic gas is singular at the vacuum and currently available theories cannot deal with. As a consequence, there are no results concerning the waiting time phenomenon for the hyperbolic model. This is the reason why in this thesis, in order to give a better insight into the process, we study numerically the behaviour of solutions in one dimension for different initial data such that $\rho_0(x) = g(x)$ if $x < \xi$ and $\rho_0(x) = 0$ elsewhere, for any function g strictly positive up to the interface ξ.

For the porous medium equation the length of the waiting time can depend locally on the initial density, that is on its profile near the interface, or globally. In [10] a special function was introduced

$$t^*(x) := \frac{\gamma}{2(\gamma + 2)} \frac{(x - \xi)^2}{\rho_0^\gamma}.$$

The limit $x \to \xi$ for any initial data indicates with which situation we are dealing. In particular, when $\lim_{x \to \xi} t^*(x) = 0$ the interface starts to move immediately, while if $\lim_{x \to \xi} t^*(x)$ is finite and non vanishing the waiting time is bounded and depends locally on the initial date. Finally, in the case $\lim_{x \to \xi} t^*(x) = \infty$ the length of the waiting time has to be determined from the global distribution of the mass. We perform a simulation for the isentropic gas dynamics with the adiabatic coefficient of the pressure function $\gamma = 2$ for different initial data giving respectively finite, bounded limit and infinity. The results of the porous medium equation are in agreement with the theory, while for the hyperbolic model suggest that its behaviour is much more sensitive to the initial data then the parabolic equation. Moreover, we observe that changing the mass center with respect to the interface leads to different waiting times

and different initial velocities of the interface. A particular attention is needed to the fact that while for the porous medium equation these features changes correspondingly to the location of the mass center, for the hyperbolic model they seem to be irregular. More precisely, more the initial density is concentrated with respect to the free boundary, and more abrupt is the behaviour of the interface. Besides, we also give some numerical estimates on the waiting times for different adiabatic exponents $\gamma = 2, ..., 9$ and different initial data. However, we point out that the obtained values may contain a big error due to the numerical approximation. But, even if they are not optimal, they illustrate the differences between the porous medium equation and the hyperbolic system.

The second phenomenon that we study is the canonical, singular behaviour of the free boundary characteristic for the porous medium equation. In [78] it was conjectured that near the boundary ξ the enthalpy of the isentropic gas dynamics with damping at any point x is proportional to the distance from the interface. As a consequence, at ξ the pressure i_x has a bounded, non zero effect on the interface. It can be stated in the following condition

$$0 < \left| \frac{\partial c^2}{\partial x} \right| < \infty, \tag{7}$$

where $c = \sqrt{P'(\rho)}$ is the sound speed, called the physical boundary condition. It imposes a special regularity on the solution near the free boundary, which causes that the system cannot be symmetrizable with regular coefficients and standard theories cannot be used. In fact, only recently due to [65] and [28], some local existence results were obtained, however, there are still many open questions left. Here we analyze how the regularity of the density changes near the interface. To obtain this goal we use the parameter α, which characterizes the smoothness of ρ, defined at each time t for points near the interface $\xi(t)$ by

$$\rho(x, t) \sim |x - \xi(t)|^\alpha.$$

The value $\alpha = \frac{1}{\gamma - 1}$ corresponds to the physical boundary condition. Smaller or larger values give respectively more irregular or smoother solution.

It is expected that asymptotically, for every initial data of the same type as in the previous problem, this is the regularity of the solution near the boundary and our simulations confirm that. However, how it is reached remains an open question. In order to give a better insight in this process, we study the time evolution of the parameter α starting from the initial profiles with different regularity near the free boundary. In the case of the porous medium equation the parameter α approaches $\frac{1}{\gamma - 1}$ monotonically, while for the isentropic gas dynamics system with friction we observe oscillations before. Moreover, the smoother the solution is initially, the larger are the oscillations. It suggests that they are connected with the oscillating redistributions of the mass. More precisely, when it starts to move it gains velocity and approaches the interface. It accumulates there, but it is also partially "reflected" due to the fact that its velocity is higher then the one of the interface. Then it moves back towards the left boundary of the domain and the oscillation starts again until reaching the distribution corresponding to the physical boundary condition. This explanation is motivated by the fact that accumulation of mass near the interface can lead to steep gradients that is low values of the parameter α, which are observed. We underline that it is only an empirical analysis and deeper mathematical studies are needed, however, it shows that the behaviour of the hyperbolic model and the

properties of the solutions are not trivial.

The next step in our study is the numerical and analytical investigation of the behaviour of one dimensional hyperbolic model of chemotaxis (6) defined on a bounded domain with the homogeneous Neumann boundary conditions. In particular, we are interested in the formation of non constant stationary solutions. They are given by the following system of equilibrium equations

$$
\begin{aligned}
u &= 0 \\
P(\rho)_x &= \chi\rho\phi_x \\
-D\phi_{xx} &= a\rho - b\phi
\end{aligned}
\tag{8}
$$

and coincide with steady states of the parabolic model (1). Moreover, for $\gamma > 1$, they are composed of regions, where the density is strictly positive, and regions, where it vanishes. There equilibria have a form of a series of "bumps", which can be associated with the location of vascular network chords observed in the experiments.

The first aim is to describe the existence and structure of these equilibria. In Section 7.2.1 we give a detailed analysis for $\gamma = 2$ in the case of only one region with strictly positive density. Otherwise, we present formulas assuming that the mass distribution among the bumps is known. However, in this case the existence of such solutions is not proved. Moreover, how the system choses the particular configuration of bumps at the steady state is also an open problem. Our next goal, presented in Section 7.2.2 is to study numerically these type of stationary solutions using finite volume scheme that we have constructed, with well-balanced property.

At first we analyze stability of non constant steady states of the form of one lateral bump. We show numerically their stability under small perturbations and give a better insight into the mechanisms of the convergence process.

Then we study the influence of the system parameters on the number and form of bumps. More precisely, we consider the dependence on the length of the domain L, chemosensitivity constant χ, adiabatic exponent γ and initial mass. Simulations in case $\gamma = 2$ indicate that the non constant equilibria are formed if there is enough free space or the response to the chemoattractant is strong enough. Increasing any of them leads to the formation of new bumps. The numerical results suggest that there exists a maximal number of regions, where $\rho > 0$, for each value of L. However, again, no rigorous proof is available.

Adiabatic exponent γ models how fast the repeling force between cells increases when their density grows. In fact, the value $\gamma = 2$ is used in the similar model, the Saint-Venant system, for shallow water equations, which describe various geophysical flows. Cells are much bigger than the molecules of water, occupy a finite volume and are impenetrable, which implies higher internal pressure at compression. Numerical analysis shows that increasing γ the bumps become wider and their maximal density decreases. Moreover, growing supports of the bumps may merge diminishing the number of regions with $\rho > 0$ for higher γ. A constant state is observed at values large enough, which is expected as the chemotaxis effect is dominated by the internal forces leading to the homogenization of the structure.

The study of the dependence of solutions on the initial mass is motivated by the experimental results on the vasculogenesis process. It was observed in [107] that for different threshold initial densities transitions from a disconnected structure to the vascular-like network and to

the so called "Swiss cheeses" configuration occur. Comparison between $\gamma = 2$ and $\gamma = 3$ of how the equilibria change for different total masses show that in the first case the model fails to reproduce the experimental results. Only the hight of the bumps increases, while their support remains constant. On the other hand, $\gamma = 3$ implies stronger repealing forces at high densities and the unnatural overcrowding is prevented. Moreover, in Section 7.2.2 we also show that in this case there is a threshold mass, above which steady states are constant.

From the mathematical point of view the analysis of the equilibria is simpler for $\gamma = 2$ due to the linear relation between ρ and ϕ. For $\gamma = 1$ the relation becomes exponential, while $\gamma > 2$ implies $\rho \sim \phi^{\frac{1}{\gamma-1}}$ at steady state. This nonlinearity creates non trivial numerical problem to balance correctly the source term and the flux in the numerical approximation. For instance our scheme fails at $\gamma > 5$. Moreover, in the case $\gamma = 1$ the understanding of some results is still poor. For example, for some choice of system parameters, we observe solutions converging to states of the form of a series of Dirac masses. So far their appearance and meaning are not understood.

The last part of our research is devoted to the comparison of long time behaviour of the parabolic and hyperbolic model of chemotaxis. It is known that the former cannot reproduce complex network structures. In Section 7.4 we observe that solutions composed of several bumps are not stable.There is a constant exchange of mass between them. As a result, over large times they move toward each other and finally merge. New metastable state is reached and the mechanism repeats until only one bumps at the boundary remains. This mechanism was described by many authors for the Keller-Segel type model with linear pressure and logistic sensitivity function. We analyze and compare behaviour of the two models. Our simulations show the solutions to the parabolic model are metastable in the case $\gamma = 2$, while for the hyperbolic system persistent equilibria containing more than one bump are observed.

Plan of the thesis

The thesis is organized as follows:

In Chapter 1 we give an introduction to the mathematical modelling of biological phenomena. At the beginning we present some backgrounds on cells movement in a tissue and tumour growth. Then we describe the parabolic and hyperbolic models of chemotaxis. First we give details on the Patlak-Keller-Segel model. Therefore we present two methods to derivate the hyperbolic model of chemotaxis. The moment closure and the phenomenological approach are considered.

In Chapter 2 we study a model of reaction-diffusion system with nonlinear diffusion, chemotaxis and nutrient-based growth of tumour, which is based on the one presented in [101] and describes the time evolution of the density of tumour cells and the concentration of a nutrient being a chemoattractant. First we present its description explaining the biological origin of all the terms. Then we study the convergence of solutions to constant, stationary states in one dimensional case for small perturbations of the equilibria. The classical symmetrization methods combined with the Sobolev type energy estimates are used to prove nonlinear stability. The results have been first presented in [35].

Chapter 3 is devoted to an introduction to the numerical methods for systems of partial differential equations. First we consider finite difference approach and describe basic, conservative schemes. Then we introduce the high resolution method with flux-limiters functions and the advanced explicit schemes based on the relaxation technique, which will be used to approximate the parabolic model of chemotaxis. In the second part of the chapter we focus on the finite volume methods for conservation laws. A special attention is give to Godunov type schemes and approximate Riemann solvers for the isentropic gas dynamics system. Then we introduce the concept of well-balancing as a method to treat the source with preservation of stationary solutions. In the end, a description of the approximation of boundary conditions is given.

In Chapter 4 we focus on the numerical approximation of the parabolic models with nonlinear diffusion of the porous medium type and chemotaxis. We present and compare two types of schemes. First we introduce the implicit-explicit splitting method. Then we give details of the explicit scheme based on the relaxation approximation. The comparison is performed on the model of angiogenesis introduced in [25].

Chapter 5 is devoted to the numerical study of the one dimensional Euler equations for isentropic gas dynamics with damping. We present the existing theory on the evolution of gas into the vacuum in the case of the porous medium equation and the hyperbolic model. In particular, we give details on the waiting time phenomenon and the behaviour of solutions under the physical boundary condition. Then we approximate the isentropic gas dynamics system using finite volume scheme with Suliciu Relaxation solver adopted to treat the vacuum and discuss possible approximations of the location of the interface. In the second part we analyze numerically the aspects of the evolution. We compare the behaviour of the parabolic equation with the hyperbolic system, give some estimates of the waiting times and discuss the regularity of the solutions near the free boundary.

In Chapter 6 we present numerical schemes for the hyperbolic model of chemotaxis. First we explain why a standard, explicit methods fails. Then we construct a consistent, finite volume, well-balanced scheme, which besides preserving the non negativity of density, preserves also stationary solutions with constant velocity and is able to treat the vacuum states. We prove the above properties for a semi-discrete scheme and give a weak stability condition in a fully discrete case.

In the final chapter we focus on the analytical and numerical analysis of the hyperbolic model of chemotaxis (6) in one space dimension defined on a bounded domain with no-flux boundary conditions. At the beginning we study non constant stationary solutions containing vacuum and intervals with strictly positive density for the particular case of $P(\rho) = \varepsilon\rho^2$. We give a detailed description of the equilibria with one bump and present a general approach under the assumption that the mass distribution between the bumps is known. Then we study numerically these types of states. First we analyze some numerical schemes approximating the model. After choosing the most accurate method we study the stability of steady states and their dependence on the system parameters such as length of the domain and chemosensitivity

constant. Moreover, we consider different values of the adiabatic exponent γ and analyze their influence on equilibria. In particular, the effect of the increase of total mass is compared in two cases, $\gamma = 2$ and $\gamma = 3$. Then, we discuss the results in the case $\gamma = 1$, which is still a fully open problem. The last section of the chapter is devoted to the comparison of the long time behaviour of the parabolic (1) and hyperbolic (6) models. In particular, their capability of reproducing the experimental results is analyzed.

MATHEMATICAL MODELLING OF CELLS MOVEMENT

Migration of cells in the fibrous environment is an essential feature of normal and pathological, biological phenomena such as embryonic morphogenesis, wound healing, angiogenesis or tumour invasion. In the simplest case we can consider a tissue as a tridimensional structure consisting of fibres, which form a so called extracellular matrix (ECM), and cells attached to them. Many experimental studies (see,[42]) give a good insight into how cells move. It is known that they interact with the tissue matrix as well as with other cells using different biological and physical mechanisms. Forces driven the cell motion are generated by a controlled remodelling of the actin network within the cell in a response to mechanical and chemical signals. The movement itself is strongly influenced by the spatial and temporal configuration of the fibres. Moreover, it depends on the contact-guidance phenomenon and attached-detached processes. Also behaviour of cells can be altered by the presence of some stimulus given rise to the so called taxis movements. Basically it means to change the direction, in which a cell moves, according to the, for example gradient, of some quantity such as adhesion force (hapto-taxis), electric field (galvanotaxis), chemical substance (chemotaxis) or oxygen concentration (aerotaxis).

In this thesis we focus on the chemotaxis phenomena that is a directed movement of mobile species towards the lower/higher concentration of a chemical substance dissolved in the surrounding environment. Change of behaviour due to the presence of some stimulus has been observed in many kinds of organisms and is decisive in biological processes. It is an essential method of communication between cells and leads to complex phenomena such as aggregation or pattern formation.

Since the first description of chemotaxis in bacteria by T.W.Engelmann (1881) and W.F.Pfeffer (1884), our knowledge about this phenomenon has been continuously expanding. For example, some bacteria can move towards higher concentration of food such as glucose molecules. Moreover, they can aggregate under starvation conditions. Amoeba like organism, Dictystelium Discoiduum, secretes the substance called cyclic Adenosine Monophosphate (cAMP) which attracts other amoeba leading to the formation of a multicellular organism (see [117]). White blood cells, neutrophil granulocytes, migrate to the cites of inflammation following chemokines released by macrophages after encountering an antigen. During tumour invasion the cancerous cells secrete various growth factors, which attract and stimulate en-

dothelial cells, in order to form a blood network around the tumour (see [40]).

The movement of cells under the effect of a stimulus has been a widely studied topic in the last decades by biologists as well as by mathematicians and many models have been proposed [89], [90]. Of course, they differ in complexity, that is for example how many constituents are taken into account or which phenomena are to be considered, but the mathematical framework of any model depends on the scale at which we describe the problem. Moreover, it is essential to choose a correct level of description in order to capture all the features of the underlying physical and biological phenomena. In the macroscopic approach cells are considered as a continuum medium and the description of their behaviour is done using populations densities. In this case models have the form of reaction-advection -diffusion systems and particularly well explain the aggregation phenomena. However, they fail when complex network structures have to be reproduced or the so called 'run and tumble' movement is to be explained. The reason for this is that parabolic models are mainly directed to the long time scales evolutions. This is why in recent years there is a tendency to use hyperbolic systems, which correspond to the description at lower mesoscopic scale. They are able to capture particular features of the modeled quantity and as a consequence can describe short time behaviour of physical problems.

In this chapter we are going to present some backgrounds on biological phenomena, such as vasculogenesis and tumour growth, and mathematical modelling of them. First we describe an approach based on the mixture theory. Then we introduce two systems of partial differential equations modelling chemotaxis. At the beginning parabolic models based on the classical Patlak-Keller Segel system are presented. Then we focus on the hyperbolic system modelling the vasculogenesis process.

1.1 Biological background

Cells movement in a tissue is a complex process that occurs at many different scales from subcellular phenomena to macroscopic behaviour. It starts from reactions in the nucleus, which activate signal pathways or generate mutations. Then, at the cells boundary, the response to external signals and absorption of nutrients takes place. At the cellular level the interactions between individuals are observed leading to proliferation, compression or death for instance. When the number of cells increases, phenomena typical for continuum medium occur. Diffusion, convection or phase transitions are the most visible macroscopic effects of dynamics at subcellular and cellular level.

In order to model processes at any of these scales the knowledge of the underlying chemical, mechanical and biological mechanisms has to be known. This is the reason why before presenting particular mathematical modes of chemotaxis, first we give some details on the process that they describe.

Vasculogenesis

Vasculogenesis is a precess of a formation of blood vessels by producing endothelial cells from mesoderm, when there are no pre-existing ones. First, endothelial precursor cells in a response to local signals, such as growth factors, migrate and differentiate into endothelial cells. Then, the latter ones diffuse and release chemical factors , Vascular Endothelial Growth

Factor (VEGF) for instance, to interact with each other. These chemical substances serve as chemoattractans which direct the movement of cells towards their higher concentrations. As a result, an assemble of cells is able to reorganize and form complex networks of blood vessels. This process was studied in vitro in two dimensional setting in the experiments of Serini et al. [107]. On a Petri dish, coated with an amount of Matrigel, human endothelial cells were seeded randomly. Initially a horizontal movement of cell on the substratum was observed and after a sufficient amount of time complex structures appeared (see also [118] and [2] for a review on the models of vasculogenesis).

In the literature two main approaches explaining mechanisms of the formation of networks are the most diffused. The first one is called mesenchymal motion and was introduced by Murray, Oster and coworkers in [83], [91]. It is based on the assumption that cells, moving on the substratum, create tensional fields sensed by other cells which, as a result, move along the tensional lines. In this way a local indirect information about the cells concentration is spread. Mathematical and numerical analysis based on this assumption shows the formation of network structures. However, before the mesenchymal motion influences cells velocity fields, a faster, driven by the presence of chemical factors amoeboid-type migration occurs.

An important result concerns experiments performed for different initial number of cells. They show that there exist threshold, initial masses which induce two transitions between different configurations. More precisely, in the works performed by Serini et al. [107] a vascular-like network develops if cell density ranges from 100 to 400 cell/mm^2. These values correspond to two transitions. The first one, which occurs at the critical density of 100 cell/mm^2, is a percolative transition. Below this value cells group into disconnected structures. After the second threshold value, 400 cell/mm^2, the network chords become thicker. Increasing the density further leads to the formation of so called "Swiss cheese" structure, which is a continuous carpet of cells with holes.

In the subsequent part of this chapter we describe a mathematical model of partial differential equations introduced by Gamba et al. in [44] to describe the above process. Chapters 6 and 7 are devoted respectively to the numerical approximation of this model and analytical and numerical study of its stationary solutions.

Hallmarks of cancer

The evolution of a cancer in a living organism is a multistep process. Numerous researches are devoted to reveal the mechanisms, which lead to the appearance and invasion of the tumor. Despite this fact, there are still many elements of the tumor behavior that must be understood.

The cancerous cell doesn't posses normal, biological limiting regulators. Living organism is for it nothing more then a source of nutrients. Normal cells are subjected to a strict control. Special regulating substances can force a cell to divide in the processes called mitosis only when it is necessary. They don't multiply in improper moments. In many tissues of an adult organism clonal expansion is constantly blocked. The multiplication mechanisms are activated only when it is necessary to replace the neighboring cells, which died or were destroyed. Tumor cells are such cells that managed to avoid this kind of control and can multiply continuously.

It is known that cancer is a disease caused by the changes in gene expressions, called oncogene [86]. Using the techniques of artificial DNA recombination scientists identified some

genes, which malfunctions are connected with the transformation of a normal cell into a cancerous one.

The growth and division of cells can be initiated by one or more substances known as growth factors. This substances connect to specific receptors on the surface of a cell and start a cascade of processes inside it. Usually it means activating specific enzymes, which are capable of activating transcription factors initiating growth and mitosis. Different genes code different growth factors or their receptors. If they are expressed incorrectly a cell can interpret the signals wrongly and can respond by growth and multiplication [122]. Cells, which lost regulating mechanisms as a consequence of defective genes, multiply in an uncontrolled way. Moreover if such a cell divides, all the cells that were born during the mitosis are also changed.

The most important defects characterizing cancerous cells are fast rate of the cell division, avoiding apoptosis, which is a programmed cell death, and improper relations with surrounding cells. In contrast to healthy cells, which respect mutual borders and form tissues in an organized way, cancerous cells grow chaotically and overtake health tissue. Probably they are not capable of reception signals from surrounding cells or cannot react correctly to them. Research results indicates that many cancers reach only few millimeters and their evolution is stopped even for many years. Then in one moment they start to produce special chemical substance, which stimulate the development of new blood vessels growing through the tumor [122]. With the instant when the tumor is supplied with blood reach in nutrients, it starts to grow dynamically and very soon become a thread to life. The metastasis phase occurs when cells migrate from the original place using the blood and lymphatic system.

In Chapter 2 we present a model of non linear partial differential equations of reaction diffusion type, with cross diffusion terms, describing the evolution of a density of tumor cells, which depends on the concentration of a nutrient. The interaction is mutual: the cells use the nutrient in their metabolism and also stimulate the organism to increase its concentration. We also consider a pharmacological factor regulating nutrient concentration. Then we study the convergence of solutions to constant steady states in one dimensional case for small perturbations from the equilibria.

1.2 Macroscopic modelling: mixture theory

The mathematical description of the phenomena differs from the biological one. The reason is the impossibility to describe the processes happening at different scales by the same mathematical framework. The most general view is to divide the processes into micro and macroscopic phenomena. The microscopic description is when we model behavior of a single cell. To present its physical state we describe the processes inside and on its membrane. We refer to it as a subcellular level of description and we model the evolution using ordinary differential equations. At the cellular level, when the number of cells increases and the interactions between them takes place, the system of ordinary differential equations is replaced by the kinetic cellular theory, which provides a statistical description of the evolution of large populations of cells characterized by one or more activation states [15]. On the other hand, at the macroscopic level cells are considered as a continuum medium. Individual cells are indistinguishable. Population of cells are characterized by their density and described by systems of partial differential equations. Every higher scale has to consist the lover ones. Describing the macroscopic processes such as diffusion or advection, the processes inside a cell and at its boundary have to be

considered as the main generators of the observed behavior. Even what happens at the smallest of the scales is important and has an effect at higher ones.

Each scale of description has some advantages and disadvantages. The main part of this work is devoted to the macroscopic modeling, in which partial differential equations are used to describe time evolution of densities and concentrations. This is the reason why we are going to describe it in more details on the example of tumour growth.

Evolution of a tumour consists of many different kinds of elements such as various cells, extracellular matrix, nutrients or chemical factors. We can consider it as a mixture of this constituents, which can be divided into two groups according to their properties (see [3], [5], [49] for more details). The first one consists of cells and ECM, which occupy a finite volume of space and are impenetrable. To the second group belong all nutrients and chemical substances diffused in the surroundings. They are much smaller and their relative dimensions can be neglected.

Let us assume, for simplicity, that the system is composed only of different populations of cells and chemical substances. In the mixture theory a variable describing the evolution of the i-th cells population is a volume ratio ϕ_i, between the volume occupied by the population and the total volume of the domain. The so called saturation constrain implies that sum of all ϕ_i has to be limited. On the other hand, chemical substances are described by a concentration function. Each of these variables depend on time and space. In order to build a mathematical model in this setting we have to write mass and momentum balance equations for cells and reaction-diffusion equations describing evolution of chemical substances. As the behaviour of the later is relatively simple with respect to the former, let us focus on the description of cells movement.

In order to write the mass balance equation for the i-th population of cells we define its mass in a control volume V with boundary ∂V and normal vector $\vec{n}$ as

$$M_i = \int_V \rho \phi_i dV,$$

where ρ is a density assumed to be equal for all types of cells. Then, denoting by u_i the velocity of the i-th population and by Γ_i the production/degradation rate, the time evolution of the mass is given by

$$\frac{d}{dt} M_i = - \underbrace{\int_{\partial V} \rho \phi_i \vec{u}_i \cdot \vec{n} d\Sigma}_{\text{motion through the boundary} \partial V} + \underbrace{\int_V \rho \Gamma_i dV}_{\text{growth/death}}.$$

Using the divergence theorem we obtain the mass balance equation of the form

$$(\rho \phi_i)_t + \nabla \cdot (\rho \phi_i \vec{u}_i) = \rho \Gamma_i. \tag{1.2.1}$$

In a closed mixture there is only exchange of mass between constituents so $\sum_i \Gamma_i = 0$.

To complete the construction of the model we have to close it by defining the velocity field $\vec{u_i}$, which includes the description of how cells move. This can be done either by a phenomenological description or by writing a momentum balance equations. The second approach generalizes the first one and we are going to focus on it.

The starting point is to distinguish processes that lead to the change of the momentum.

More precisely, we have

$$\frac{d}{dt}\int_V \rho\phi_i\vec{u}_i dV \;=\; -\underbrace{\int_{\partial V}\rho\phi_i\vec{u}_i(\vec{u}_i\cdot\vec{n})d\Sigma}_{\substack{\text{motion of cells through}\\\text{the boundary}}} \;+\; \underbrace{\int_{\partial V}\widetilde{T}_c\cdot\vec{n}d\Sigma}_{\substack{\text{contact forces}\\\text{with other cells}}}$$

$$+\underbrace{\int_V \widetilde{m}_c dV}_{\substack{\text{contact forces}\\\text{due to the interaction}\\\text{with other constituents}}} \;+\; \underbrace{\int_V \rho\Gamma_i\vec{u}_i dV}_{\substack{\text{momentum supply due to}\\\text{the mass exchange}}}$$

$$+\underbrace{\int_V \rho\phi_i\vec{b}_i dV}_{\substack{\text{body forces}\\\text{(ex. chemotaxis)}}}\quad,$$

where $\widetilde{T}_c$ is a partial stress tensor, $\widetilde{m}_c$ denotes interaction forces and $\vec{b}_i$ describes body forces, for example can contain gradient of a concentration of some chemical in the case of chemotaxis. Using the divergence theorem and the mass balance equation the above relation becomes

$$\rho\phi_i\left(\partial_t\vec{u}_i + \vec{u}_i\cdot\nabla\vec{u}_i\right) = \nabla\cdot\widetilde{T}_c + \rho\phi_i\vec{b}_i + \widetilde{m}_c \qquad (1.2.2)$$

which is the momentum balance equation. At this point the cell-cell interactions have to be precised. This can be obtained by writing constitutive laws for partial stress tensor and interaction forces. The latter is very often assumed to be proportional to the difference in the velocity between the constituents, while the former in the simplest case for elastic fluids is $\widetilde{T}_c = -\Sigma_i\mathbb{I}$, where Σ is positive in compression.

However, in order to make the model more realistic other constituents, such as the extracellular matrix and liquid or blood vessels, should be taken into account leading to so called multicomponent systems. Then in the constitutive laws for the stress tensor the contributions of all elements of the system have to be considered. Moreover, liquid-solid interactions and adhesion process between cells and extracellular matrix have to be determined as well. Finally the reactions terms describing production and degradation of constituents have to be modelled. For further information we sent to, for example, [101],[16], [15], [13], [102].

This general approach leads to the mathematical models of hyperbolic type. However, neglecting inertial and persistence terms, an assumption which corresponds to immediate adjustment of cells to the limit velocity leads to classical parabolic models of chemotaxis. In the following sections we give details of both types of these systems.

1.3   Parabolic models of chemotaxis

Chemotaxis is a directed movement of mobile species towards the lower or higher concentration of a chemical substance in the surrounding environment. It can be described at the macroscopic level by considering the populations of single individuals as a continuum medium.

Based on this approach, Patlak in 1953 [96] and subsequently in 1970 Keller and Segel [70], [?] presented a system of partial differential equations of parabolic type to model the behaviour of a single-cell amoebae organism, slime mold. When food resources are exhausted it secretes a chemical substance called cAMP being a chemoattractant. It attracts other cells, which move towards regions of its higher concentration. As a consequence, the aggregating phenomenon corresponding to the formation of a multicellular organism, is observed.

The simplest version of the Keller-Segel type model describes the evolution of the density $\rho(x,t)$, $t \geq 0$, $x \in \mathbf{R}^d$ of one type of cells and the concentration $\phi(x,t)$ of the chemical attracting substance. A general form of the system reads

$$\begin{cases} \rho_t = \nabla \cdot (\nabla P(\rho)) - \nabla \cdot (\rho \chi(\rho, \phi) \nabla \phi) \\ \phi_t = D \triangle \phi + a\rho - b\phi, \end{cases} \tag{1.3.1}$$

The motion of cells is described by a continuity equation in which the flux is biased by diffusion and chemotactic transport up to a gradient of a nutrient. Denoting the velocity of cells as $\overrightarrow{u}$, the flux equals $\rho \overrightarrow{u} = -\nabla(P(\rho)) + \chi(\rho)\nabla \phi$. Here P denotes a nonlinear diffusion function due to the presence of a density dependent random mobility for the cells, while $\chi(\rho, \phi)$ is a chemosensitivity function and describes the response of cells to the presence of chemoattractant. Considering different forms of these functions we can obtain many variations of the above model.

Typical examples for the function $P(\rho)$ defining the diffusive flux are given by

- Fick's law (classical linear diffusion): $P(\rho) = \varepsilon \rho$, $\varepsilon > 0$

- Darcy's law (porous medium type diffusion): $P(\rho) = \varepsilon \rho^\gamma$, $\varepsilon > 0, \gamma > 1$

The porous medium type diffusion reflects the density dependent random motility, which models volume filling effects due to the finite volume and finite compressibility of cells [22], [73], [95]. In the case of the chemosensitivity function the simplest form corresponds to the sensitivity of cells independent on the concentration of the chemical, i.e. $\chi(\rho, \phi) = \chi_0$ is constant, where $\chi_0 > 0$ for positive chemotaxis. However, various modification were introduced to model quorum sensing, volume filling or signal limiting responses. For example

- Signal dependent sensitivity function:

  - "receptor" : $\chi(\rho, \phi) = \dfrac{\chi_1}{(\chi_2 + \phi)^2}$, $\chi_1, \chi_2 > 0$
  - "logistic": $\chi(\rho, \phi) = \dfrac{\chi_1 + \chi_0}{\phi + \chi_0}$, $\chi_0 > 0$

- Density dependent sensitivity function ("volume filling"): $\chi(\rho, \phi) = \chi_0 \left(1 - \dfrac{\rho}{\rho_{\max}}\right)$, $\chi_0 > 0, \rho_{\max} > 0$

One of the characteristic features of the system (1.3.1) is the balance between pressure forces, which are modelled by diffusion, and chemotaxis. More precisely, expanding the equation for ρ in (1.3.1) with constant function $\chi(\rho, \phi) = \chi$ we get

$$\rho_t = \triangle P(\rho) - \chi \rho \triangle \phi - \chi \nabla \rho \cdot \nabla \phi.$$

Contribution of the "Laplacian" terms have different signs. This suggests to think of diffusion as stabilizing force, while chemotaxis can be seen to have a destabilizing effect. Balance between these two processes can result in some steady spatial patterns in ρ and ϕ, or in some unsteady traveling wave solutions. On the other hand, if the chemotactic force is sufficiently strong, there is a possibility of a blow-up of solutions in finite time. The blow-up of solutions may in fact can happen, for example in a simplified version of Keller-Segel type model in two space dimensions, where the parabolic equation for the concentration of chemical is substituted by an elliptic one and the decay of ϕ is dropped. If the initial mass is larger than some threshold values, then the solution concentrates into a Dirac's delta in finite time.

The blow-up phenomena is sometimes considered as the weakens of the classical Keller-Segel system. This motivates the introduction of nonlinear diffusion $P(\rho)$ and chemosensitivity function $\chi(\rho, \phi)$ that we presented earlier, to achieve a more refined balance between diffusion and chemotaxis and guarantee the global existence of solution.

1.4 Hyperbolic models of chemotaxis

Macroscopic, parabolic type of models describe very well the aggregation phenomena but fail when the network structures have to be reproduced. This was observed while studying the experiments on the vasculogenesis process. The Patlak-Keller-Segel model cannot explain this process as well as cannot describe the 'run and tumble' movement of, for example, Eusterichia Coli. This is because it is mainly directed to the long time scales evolutions [37]. As a consequence, in recent years there is a tendency to use hyperbolic systems, which correspond to models at the lower, mesoscopic scale. The main difference between the two approaches is that diffusion systems describe the evolution via the density of the population whereas hyperbolic models are based on the individual movement behaviour. They take into account the fine structure of the problem and are able to capture the particular features of the modeled quantity. Moreover, they account for finite propagation speed. Lower level of description implies also that some relevant model parameters, for example turning rates, can be measured from the individual movement patterns. This results in more realistic description on phenomena occurring at short time scales.

This two classes of systems are linked by long time asymptotics. Moreover, both can be derived following the theory of mixtures or using the kinetic transport equation of the velocity-jump process

$$\partial_t f + v \cdot \nabla_x f = \mathcal{T}(\phi, f)$$

where $\mathcal{T}$ is a turning operator modelling the change of direction of cells. In the later case, hyperbolic models can be obtained under the hydrodynamical scalling $t \to \epsilon t$, $x \to \epsilon x$, while parabolic systems are recovered as a limit of transport kinetic equations with diffusive scalling $t \to \epsilon^2 t$, $x \to \epsilon x$.

We focus now on describing a hyperbolic system proposed by Gamba et.al [44] to describe vasculogenesis process that we explained in the beginning of this chapter. As was mentioned before, it can be derived as a hydrodynamic limit of kinetic transport equations or from the phenomenological observations and continuum mechanics. We give details of the second approach, which basically follows the mixture theory approach, in which only one population of cells and one type of a chemical substance is considered.

The model of vasculogenesis describes the early formation of vascular-like network from randomly seeded, human endothelial cells. It concerns the time evolution of the density of cells $\rho(x, t)$, their velocity $u(x, t)$ and the concentration of the chemoattractant $\phi(x, t)$. In order to reproduce the behaviour observed in the experiments of Serini et. at [107], for example transitions between disconnected structures and complex network or characteristic length of chords, the construction of the model is based on the following assumptions:

- endothelial cells show persistence in their motion

- endothelial cells communicate via the release and absorption of a soluble growth factor (VEGF-A)

- the chemical factors released by cells diffuse and degrade in time

- endothelial cells neither duplicate nor die during the process

- cells are slowed down by friction due to the interaction with the fixed substratum

- closely packed cells mechanically respond to avoid overcrowding

Now, following the approach based on the mixture theory presented in Section 1.2, we have to write the mass and momentum balance equations. Following the analysis presented in general case, under the model assumptions, we have

$$
\begin{cases}
\rho_t + \nabla \cdot (\rho u) = 0, \\
(\rho u)_t + \nabla \cdot (\rho u \otimes u) = \mathcal{F}, \\
\phi_t = D \triangle \phi + a\rho - b\phi.
\end{cases}
$$

The first equation is a mass balance equation. Due to the absence of the source terms, based of the model assumptions, the total mass of ρ is conserved in time. The last equation is e reaction-diffusion equation describing the time evolution of the chemoattractant. It diffuses with constant velocity $D > 0$, is produced by cells at rate $a > 0$ and degrades with a half life $\frac{1}{b}$. The velocity field of cells is described by the second equation, where $\mathcal{F}$ states for all phenomena that can influence the direction of cells movement. In order to finalize the construction, we have to describe them.

The model assumes that cells can change direction or the speed due to the three main mechanisms that is

$$
\mathcal{F} = \mathcal{F}_{\text{chem}} + \mathcal{F}_{\text{diss}} + \mathcal{F}_{\text{vol}}.
$$

More precisely,

1. Body force:
$$
\mathcal{F}_{\text{chem}} = \rho \chi(\rho, \phi) \nabla \phi
$$

It describes a change of the cells velocity due to the presence in the environment of the growth factor ϕ, chemotaxis process. The chemosensitive function $\chi(\rho, \phi)$ models how the cells are responding to the gradient of its concentration. If it is constant, then the strength of the response is the same for all concentrations.

2. Contact force due to the interaction with the environment:

$$\mathcal{F}_{\text{diss}} = -\alpha\rho u$$

Damping modelling the presence of a friction between the cells and the substratum. It implies a dissipation of the momentum and leads to the decrease of the velocity.

3. Contact forces with other cells

$$\mathcal{F}_{\text{chem}} = -\nabla[\rho\pi(\rho)]$$

Internal force, with $\pi(\rho)$ strictly positive, modelling the impenetrability of cells and giving rise to stronger repealing effect at higher cells densities.

Together with the above assumptions the model of vasculogenesis can be written in the form

$$\begin{cases} \rho_t + \nabla \cdot (\rho u) = 0, \\ (\rho u)_t + \nabla \cdot (\rho u \otimes u + P(\rho)) = -\alpha\rho u + \chi\rho\nabla\phi, \\ \phi_t = D\triangle\phi + a\rho - b\phi. \end{cases}$$

where

$$P(\rho) = \int \frac{1}{\rho}\frac{d}{d\rho}(\rho\pi)d\rho.$$

In this thesis we present numerical and analytical study of the above model in one space dimension with $P(\rho) = \varepsilon\rho^\gamma$, $\varepsilon > 0$, $\gamma \geq 1$.

ASYMPTOTIC STABILITY OF CONSTANT STATIONARY STATES FOR A 2×2 REACTION-DIFFUSION SYSTEM ARISING IN CANCER MODELLING

2.1 Introduction

In this chapter we consider a model, based on the one presented in [101], of nonlinear partial differential equations of reaction diffusion type, with cross diffusion terms, describing the evolution of a density of tumor cells, which depends on the concentration of a nutrient. The interaction is mutual: the cells use the nutrient in their metabolism and also stimulate the organism to increase its concentration. We also consider a pharmacological factor regulating nutrient concentration. In this section we denote by ϕ the tumor cells density and by c the nutrient concentration. A general form of the system reads

$$\begin{cases} \dfrac{\partial \phi}{\partial t} = \nabla \cdot (\phi \nabla F(\phi)) - \nabla \cdot (\omega \phi \nabla c) + \alpha(\phi, c) \\ \dfrac{\partial c}{\partial t} = D \triangle c + \beta(\phi, c), \end{cases} \tag{2.1.1}$$

posed on a bounded domain $\Omega \subset \mathbf{R}^3$ with smooth boundary and subject to periodic boundary conditions on a torus.

The motion of the tumor cells is described via the density ϕ, which evolves according to the first equation in (2.1.1). It is a continuity equation in which the flux of cells is biased by diffusion and chemotactical transport up the gradient of a nutrient with constant chemotactic sensitivity $\omega > 0$. The nutrient moves according to linear diffusion with constant coefficient $D > 0$. Both equations are endowed with terms describing production and degradation (reac-

tion) processes. They are represented by the reaction terms $\alpha(\phi, c), \beta(\phi, c)$ having the form

$$\alpha(\phi, c) = \gamma_1 \widehat{p} \left(\frac{c}{c^*} - 1 \right) \phi \widehat{H}(\phi^* - \phi) - \gamma_2 \widehat{p} \left(1 - \frac{c}{c^*} \right) \phi - \delta \phi \qquad (2.1.2)$$

$$\beta(\phi, c) = -dc\phi + G\phi - Rc. \qquad (2.1.3)$$

Production of tumour cells, described by the first term of (2.1.2), depends on the availability of the nutrient and free space between the surrounding cells. There exist threshold values c^* and ϕ^*, which switches cells stage from proliferating to quiescent one. This behaviour is obtained by the use of the functions $\widehat{H}(x), \widehat{p}(x)$, which are regularized approximations of the Heaviside function and the 'positive part' function $(x)_+$ respectively. The second term of equation (2.1.2) represents degradation of cells, when the nutrient concentration drops below c^*. Production and degradation rates, γ_1 and γ_2 respectively, are assumed to be constant and unequal. Moreover, the system is endowed with an additional death term, $-\delta\phi$. It models death of cells regardless feeding conditions. Production of the nutrient, with constant rate $G > 0$, is due to the presence of tumour cells . Its degradation is a result of two processes. The first is connected with the consumption of the nutrient by healthy and cancerous cells. It happens with constant consumption rate $d > 0$. The second models pharmacological factor, which decreases the amount of available nutrient with constant degradation rate $R > 0$.

After a short presentation of the model, we follow with its detailed description. As mentioned before, the flux of cells is biased by diffusion and chemotactic transport up to a gradient of a nutrient. Denoting the velocity of cells as $\overrightarrow{u}$, the flux equals $\phi\overrightarrow{u} = -\phi\nabla(F(\phi)) + \omega\phi\nabla c$. Here F denotes a nonlinear diffusion function due to the presence of a density dependent random mobility for the tumor cells. We define $f'(\phi) = \phi F'(\phi)$ so that $f(\phi) = \int_0^\phi \xi F'(\xi) d\xi$. From now on we assume $F'(\phi) > 0$, which implies $f'(\phi) > 0$. Typical examples for the function $F(\phi)$ are $F(\phi) = \log \phi$ (classical linear diffusion), $F(\phi) = \phi^\gamma$ with $\gamma > 0$ (porous medium type diffusion) which models a divergent value for the random mobility as $\phi \to +\infty$ due to volume filling effects (cf. e. g. [22, 73]), or $F(\phi)$ being an increasing function such that the corresponding $f(\phi)$ has a finite limit as $\phi \to +\infty$, which models saturation for large densities. All the above cases can be included (as we shall work under in a small perturbation framework). The last term in the definition of the flux describes a directional movement of tumor cells towards higher concentration of nutrient. The parameter $\omega > 0$ is the *chemotactic sensitivity* of the tumor cells. The motion of the nutrient has a linear diffusion term with constant diffusivity $D > 0$. The above mentioned rules define the flux in the continuity equation for the cells and the nutrient. The source term is represented by the equations (2.1.2), (2.1.3). The first and the second term on the right hand side of the equation (2.1.2) contain functions $\widehat{H}(x), \widehat{p}(x)$, which are regularized approximations of the Heaviside function and the 'positive part' function $(x)_+$ respectively [13]. The use of these mollifiers is motivated by the finite response time of cells to the changes in the surrounding environment. The analysis of the asymptotic behavior of the system requires α and β to be at least C^1 functions. More precisely we define

$$\widehat{H}(x) = \widehat{H}_\sigma(x) = \begin{cases} 0 & x < 0 \\ h_\sigma(x) & 0 \leq x \leq \sigma \\ 1 & \sigma < x \end{cases}, \qquad (2.1.4)$$

with $h_\sigma(0) = 0$, $h_\sigma(\sigma) = 1$ and $h_\sigma \in C^\infty([0, \sigma])$. The second function is

$$\widehat{p}(z) = \widehat{p}_\epsilon(z) = \begin{cases} 0 & z < 0 \\ \frac{1}{2\epsilon} z^2 & 0 \le z \le \epsilon \\ z - \frac{\epsilon}{2} & \epsilon < z \end{cases} . \qquad (2.1.5)$$

The positive parameters σ, ϵ, as described in [13], define the thickness of the transition between the two phases.

The first term in (2.1.2) describes the increase of the density of tumor cells as a result of multiplication in the mitosis cycle and the growth of cells. These processes depend on the number of cells undergoing duplication and the amount of essential nutrient. In the model we assume the presence of two threshold processes. The function $\widehat{H}_\sigma(\phi^* - \phi)$ describes the reduction of free space available to the cells and possibly, after crossing the threshold value ϕ^*, the stopping of their growth. The rapidity of the switch from the proliferating stage to the quiescent one is controlled by the parameter σ. As a second switch off factor we consider the minimal nutrient concentration c^* necessary for the cells to sustain their biological cycles. Following [102], [101] we assume that the concentration of nutrient below the threshold value results not only in limiting the growth but also in the cell's death, which is modeled by the second terms in (2.1.2). The parameters γ_1 and γ_2 are constant growth and death rates respectively. Based on [54] let us assume $\gamma_1 > \gamma_2$, which reflects independence of tumor on growth factors, its insensitivity to growth inhibitors and dependence on alternative, less demanding in nutrients, metabolisms such as in the Warburg effect [124].

The last term in (2.1.2) models the natural death of cells (apoptosis) which occurs after a definite number of multiplications. Telomeres are responsible for this intrinsic counting mechanism, capping both ends of chromosomes [51]. They are being shortened at every mitosis cycle. After reaching the threshold length, suspension of replication occurs obeying so called 'end-replication problem' stated by James D.Watson in 1970. The enzyme telomerase is responsible for elongation of telomeres. Researches in this field showed that although telomerase is absent in somatic cells its activity is reported in 90% of all cancers. In chromosomes of tumor cells the threshold length of telomeres is passed leading to their further shortening, however, this process is accompanied by telomerase activation. Eventually telomeres are stabilised at a constant length, which gives tumor cells immortality and an ability to proliferate indefinitely. As highlighted in [123] immortality is not sufficient for the healthy cell to become cancerous one, however, it gives a significant advantage. Apart from apoptosis, this death term can be seen as an effect of radiotherapy, which destroys tumour cells and surrounding tissue.

By the presence of two, separate death terms we stress the difference between the processes that they represent. First, $-\gamma_2 \widehat{p}\left(1 - \frac{c}{c^*}\right)\phi$, disappear when the nutrient concentration is higher then the threshold value c^*. In the avascular stage of a cancer growth this condition is satisfied only in the external parts of the tumour. It leads to a formation of a necrotic core of death cells. On the other hand, the term $-\delta\phi$, models apoptosis or radiotherapy and concerns all cells of a tumour regardless their position with respect to the tumour centre. In the view of cancer treatment, this kind of separation gives more possible strategies to consider.

Nutrients such as oxygen, glucose or iron are the essential ingredients used in cell cycles. Molecules are supplied by capillary network and consumed by cells. The minimal concentration of nutrient must be available for the cells to survive. While the tumor grows, uncontrolled processes and unnaturally high demand for nutrients cause occurrence of regions of death cells.

One of the characteristic features of tumor cells is their capacity of increasing the availability of nutrient by stimulating formation of capillary network. Based on [102], [101] consumption and degradation of nutrient is modeled by the first and second term in (2.1.3). The rates d and G are assumed to be constant.

The last term in (2.1.3), with $R > 0$, models a pharmacological therapy the aim of which is to limit the feeding ability motivated by [40], where killing tumor by starvation is suggested. The first target would be destroying blood vessels supplying tissue in nutrients. In [52] a new group of drugs, acting on specific parts of signalling pathways, is described. One of the type of these molecular directed drugs works against angiogenesis by neutralizing VEGF (vascular endothelial growth factor), which stimulates multiplication of endothelial cells forming internal layer of capillaries. Approved in 2004 bewacyzumab is an antibody acting in that way. However, further research showed that antiangiogenic drugs don't help unless augmented with conventional chemotherapy. It was discovered that in the first phase of drug action the blood network around tumour, which is chaotic and of poor quality, is being normalized [64]. Remaining capillaries deliver drugs and nutrients more effectively, causing in some cases even increase in the rate of proliferation in some parts of tumour. In our model, as a simplification, we consider only a constant decrease of nutrient as a result of pharmacological therapy.

The mathematical structure of the system (2.1.1) is that of a nonlinear reaction–diffusion system with cross–diffusion terms. The literature related with the existence theory and the stability vs. instability properties of such systems is pretty large. The books [1, 106] are a good reference for the existence of global solutions of systems of reaction–diffusion type, see also [26, 110, 84], whereas the more recent [39, 32, 33] used Lyapunov functions and entropy methods to achieve asymptotic stability of stationary solutions. The dichotomy between stability and instability is a classical problem which goes back to [116] and it has still many open issues.

Several applied contexts in which reaction–diffusion systems appear feature cross–diffusion terms, meaning that one species can be transported via a velocity field directed up the gradient of another species, such as in chemotaxis models. Starting from the earliy 80's, Mimura and other authors [88, 85, 87] addressed the problem of the asymptotic behavior of Lotka–Volterra type systems with cross diffusion, in terms of formation of inhomogeneous steady states (segregation) vs. stability of constant states (self–diffusion). See also the more recent papers by Ni and other authors [81, 93]. The recent [66] is a very exhaustive review for reaction–cross–diffusion systems.

Our results use as a main tool the classical *symmetrization method*, see for instance [71, 43, 108] in which this technique has been used for hyperbolic systems of conservation laws, and the more recent [34] which applies symmetrization and entropy methods to reaction–diffusion systems arising in the context of semiconductor modeling. Our nonlinear stability result is proven via energy Sobolev estimates and it holds for small perturbation of constant states. The symmetrization method works in any dimension for the linearized systems. However, due to the complexity of the Sobolev type energy estimate, we shall prove the nonlinear result only in one space dimension. The main technical difficulty in our computation lies in the fact that the diffusion matrix and the reaction matrix after linearization can never be symmetrized simultaneously in such a way to produce two negative definite quadratic forms. Therefore, the (symmetrized) diffusion term will compensate the lack of negativity in the quadratic form induced by the linearized reaction matrix.

The chapter is organized as follows. In section 2.2 we provide a precise statement of

the problem and we state our main results (cf. subsection 2.2.2). This subsection contains the precise statement of the structural conditions on the parameters needed to achieve stability of steady states together with a suitable interpretation of the result in Remark 2. In section 2.3 we show how to apply the classical symmetrization method needed to prove the main stability result to the linearized model. Finally, in section 2.4 we prove the main nonlinear stability result.

2.2 Preliminaries and results

2.2.1 Constant stationary states

Let us rewrite system (2.1.1) in a form

$$
\begin{cases}
\dfrac{\partial \phi}{\partial t} = \Delta f(\phi) - \nabla \cdot (\omega \phi \nabla c) \\
\qquad + \gamma_1 \widehat{p}\left(\dfrac{c}{c^*} - 1\right) \phi \widehat{H}(\phi^* - \phi) - \gamma_2 \widehat{p}\left(1 - \dfrac{c}{c^*}\right)\phi - \delta \phi \\
\dfrac{\partial c}{\partial t} = D\triangle c - dc\phi + G\phi - Rc
\end{cases}
\tag{2.2.1}
$$

and seek for constant, positive, stationary states (ϕ_∞, c_∞). The reaction terms involves regularised approximations of Heaviside $\widehat{H}$ and 'positive part' $\widehat{p}$ functions. The smoothing regions, characterized by the structural constants σ, ϵ, are quadratic polynomials. To simplify the analysis we assume the solutions to be outside the smoothing regions. It means that

$$
c \in [0, c^* - \epsilon] \cup \{c^*\} \cup [c^* + \epsilon, \infty] \qquad \text{and} \qquad \phi \in [0, \phi^* - \sigma] \cup [\phi^*, \infty].
\tag{2.2.2}
$$

Under this assumption we state the following simple lemma.

Lemma 1. *If*

$$
\begin{cases}
\dfrac{c^* R\left(1 + \frac{\delta}{\gamma_1} + \frac{\epsilon}{2c^*}\right)}{G - dc^*\left(1 + \frac{\delta}{\gamma_1} + \frac{\epsilon}{2c^*}\right)} \le \phi^* - \sigma \\
\dfrac{1}{2}\epsilon < c^* \dfrac{\delta}{\gamma_1} \\
G > c^* d\left(1 + \dfrac{\delta}{\gamma_1} + \dfrac{\epsilon}{2c^*}\right)
\end{cases}
\tag{2.2.3}
$$

then the system (2.2.1) has a constant, non trivial steady state

$$
(\phi_\infty, c_\infty) = \left(\dfrac{c^* R\left(1 + \frac{\delta}{\gamma_1} + \frac{\epsilon}{2c^*}\right)}{G - dc^*\left(1 + \frac{\delta}{\gamma_1} + \frac{\epsilon}{2c^*}\right)}, c^*\left(1 + \dfrac{\delta}{\gamma_1} + \dfrac{\epsilon}{2c^*}\right)\right).
\tag{2.2.4}
$$

Moreover, if one of conditions (2.2.3) is not satisfied, then the only steady states of system (2.2.1) in the range (2.2.2) is the trivial solution $(0,0)$.

Proof. To see this let us assume that $c_\infty > c^* + \epsilon$. From the condition $\beta(\phi_\infty, c_\infty) = 0$ we obtain $c_\infty = \frac{G\phi_\infty}{R + d\phi_\infty}$ and the previous assumption turns to

$$
\phi_\infty > \dfrac{(c^* + \epsilon)R}{G - d(c^* + \epsilon)}.
\tag{2.2.5}
$$

The condition $\alpha(\phi_\infty, c_\infty) = 0$ takes the form

$$\gamma_1 \left(\frac{G\phi_\infty}{c^*(R + d\phi_\infty)} - 1 - \frac{\epsilon}{2c^*} \right) \phi_\infty \widehat{H}(\phi^* - \phi_\infty) - \delta\phi_\infty = 0.$$

Now let us assume

$$\phi_\infty \leq \phi^* - \sigma. \tag{2.2.6}$$

Then the above condition becomes

$$\gamma_1 \left(\frac{G\phi_\infty}{c^*(R + d\phi_\infty)} - 1 - \frac{\epsilon}{2c^*} \right) \phi_\infty - \delta\phi_\infty = 0$$

and yields the non trivial solution

$$\phi_\infty = \frac{c^* R \left(1 + \frac{\delta}{\gamma_1} + \frac{\epsilon}{2c^*} \right)}{G - dc^* \left(1 + \frac{\delta}{\gamma_1} + \frac{\epsilon}{2c^*} \right)}. \tag{2.2.7}$$

Inserting (2.2.7) into $c_\infty = \frac{G\phi_\infty}{R + d\phi_\infty}$ yields (2.2.4). To simplify the notation, from now on let us denote $\Gamma = 1 + \frac{\delta}{\gamma_1} + \frac{\epsilon}{2c^*}$. Then $\phi_\infty = \frac{c^* R\Gamma}{G - dc^*\Gamma}$. It satisfies (2.2.5) if $\frac{1}{2}\epsilon < c^* \frac{\delta}{\gamma_1}$ and (2.2.6) if

$$\frac{c^* R\Gamma}{G - dc^*\Gamma} \leq \phi^* - \sigma.$$

On the other hand, if $\phi_\infty > \phi^*$ then the only solution is $\phi_\infty = 0$, which is a contradiction.

When $c_\infty < c^* - \epsilon$, the only constant stationary solution is a trivial one $(\phi_\infty, c_\infty) = 0$, because $\alpha(\phi_\infty, c_\infty) = 0$ reduces to

$$-\gamma_2 \left(1 - \frac{c_\infty}{c^*} - \frac{\epsilon}{2c^*} \right) \phi_\infty - \delta\phi_\infty = 0.$$

$\square$

Remark 1. In the limit $\delta \to 0$, which models evolution of tumour resistent to apoptosis, the constant, non-trivial, stationary solution takes the form

$$(\phi_\infty, c_\infty) = \left(\frac{c^* R}{G - dc^*}, c^* \right) \qquad \text{if} \qquad G > dc^*. \tag{2.2.8}$$

Moreover, if there exists $p > 0$ such that

$$\begin{cases} p > \phi^* \\ p > \frac{Rc^*}{G - dc^*} \end{cases}$$

and $G > dc^*$, then the system (2.1.1) with $\delta = 0$ has a family of equilibrium states characterised by a parameter p in the form

$$(\phi_\infty, c_\infty) = \left(p, \frac{Gp}{R + dp} \right).$$

This is motivated by the fact that assuming $c_\infty > c^* + \epsilon$ the condition

$$\gamma_1 \widehat{p} \left(\frac{c_\infty}{c^*} - 1 \right) \phi_\infty \widehat{H}(\phi^* - \phi_\infty) - \gamma_2 \widehat{p} \left(1 - \frac{c_\infty}{c^*} \right) \phi_\infty = 0$$

takes the form

$$\gamma_1 \left(\frac{c_\infty}{c^*} - 1 - \frac{\epsilon}{2c^*} \right) \phi_\infty \widehat{H}(\phi^* - \phi_\infty) = 0$$

and is satisfied for $\phi_\infty > \phi^*$.

2.2.2 Results

In the previous section we described a system of reaction-diffusion type with cross diffusion terms and found its constant, positive, stationary states. Now we state our results concerning with the asymptotic behavior of the solutions near these equilibria. Due to complexity of a three dimensional analysis we restrict our results to one spatial dimension. Let us introduce vector notation

$$U = (\phi, \quad c)^T \in (\mathbb{R} \times [0, \infty))^2.$$

Then the system (2.1.1), reduced to one spatial dimension, can be written as

$$\frac{\partial}{\partial t} U = (\mathbf{D} U_x)_x + \vec{\varphi}(U), \tag{2.2.9}$$

where

$$\mathbf{D} = \begin{pmatrix} f'(\phi) & -\omega\phi \\ 0 & D \end{pmatrix}, \qquad \vec{\varphi}(U) = \begin{pmatrix} \alpha(\phi, c) \\ \beta(\phi, c) \end{pmatrix}.$$

To simplify the analysis we consider periodic boundary conditions on the torus.

Structural conditions

As we already stated above, our results uses symmetrization as a fundamental tool and there's a compensation between the symmetrized diffusion and the symmetrized reaction part. This leads to structural assumptions on the constants involved in the model which are quite involved. For the sake of completeness we state these structural conditions here and make some comments afterwards.

We shall prove our results under the following structural assumptions.
Two conditions ensuring positive definiteness of the symmetriser of the linearised problem:

$$\frac{D - \widehat{f}}{c^*\omega R\Gamma} \left[\left(D - \widehat{f}\right) \frac{\gamma_1}{c^*\omega} - \frac{RG}{G - c^*d\Gamma} \right] > 1, \tag{2.2.10}$$

$$\frac{1}{\omega c^*} \left(D - \widehat{f}\right) \left[\frac{(G - c^*d\Gamma)^2 + \gamma_1 R\Gamma}{R\Gamma} \right] > \frac{Rc^*}{G - c^*d\Gamma}. \tag{2.2.11}$$

One condition ensuring positive definiteness of the symmetrised diffusion matrix:

$$\frac{(D - \widehat{f})}{\omega c^*} \left(\frac{(G - dc^*\Gamma)^2}{R\Gamma} \widehat{f} + D\gamma_1 \right) > R\omega c^*\Gamma + \frac{GDR}{G - c^*d\Gamma}, \tag{2.2.12}$$

and one ensuring a spectral gap of the energy of the symmetrised linear system:

$$-E\frac{(RG + Dg)}{g^2} + \frac{R\Gamma(\omega c^* + \gamma_1)}{2gC_\Omega} + \frac{g}{2C_\Omega}\left(1 - \widehat{f}\frac{D - \widehat{f}}{\omega c^* R\Gamma}\right)$$
$$-\frac{1}{2C_\Omega}\left[\left(\frac{D - \widehat{f}}{\omega c^* R\Gamma}g\widehat{f} + \frac{DE}{g} - \frac{\omega c^* R\Gamma}{g}\right)^2 - 4D\widehat{f}\left(\frac{D - \widehat{f}}{\omega R\Gamma c^*}E - 1\right)\right]^{\frac{1}{2}} \tag{2.2.13}$$
$$+\left[\left(\frac{\gamma_1 R\Gamma}{g} - \frac{RG}{g^2}E + g\right)^2 + 4\gamma_1 R\Gamma\left(\frac{D - \widehat{f}}{\omega c^* R\Gamma}E - 1\right)\right]^{\frac{1}{2}} < 0,$$

where $E := \left(\gamma_1 \frac{D - \widehat{f}}{\omega c^*} - \frac{RG}{G - dc^* \Gamma} \right)$, $g := G - dc_0 \Gamma$, and $\widehat{f} = f' \left(\frac{c^* R \Gamma}{G - dc^* \Gamma} \right)$ to simplify the notation, C_Ω is the Poincaré constant of the domain and $\Gamma := 1 + \frac{\delta}{\gamma_1} + \frac{\epsilon}{2c^*}$.

Theorem 1. *Suppose (2.2.3),(2.2.10),(2.2.11), (2.2.12), (2.2.13) are satisfied. Additionally let*

$$\| U_0 - U_\infty \|_{H^2(\Omega)} \leq \eta$$

for η small enough. Then, the non trivial equilibrium of the system (2.2.9)

$$U_\infty = \left(\frac{c^* R \Gamma}{G - dc^* \Gamma}, \quad c^* \Gamma \right)^T$$

is asymptotically stable and

$$\|U - U_\infty\|_{H^2(\Omega)} \leq C_1 e^{-C_2 t} \|U_0 - U_\infty\|_{H^2(\Omega)},$$

where C_1 and C_2 are positive constants depending on the structure parameters of the system.

Remark 2. A precise interpretation of the above structural conditions from a physiological point of view is pretty hard. However, it is easily check that, assuming $D > \widehat{f}$, conditions (2.2.10), (2.2.11) and (2.2.12) are satisfied if ω is small enough, which is reasonable as chemotaxis typically being a phenomenon which causes instabilities. The assumption $D > \widehat{f}$ can be justified by the macroscopic differences between the two groups: cells and molecules [101],[16]. While the latter move freely in the extracellular liquid, cells are attached to themselves and to extracellular matrix [13], [102]. One can also easily observe that conditions (2.2.10), (2.2.11) and (2.2.12) are satisfied for large enough value of G and small enough value of R. Such combination of values of the parameters has a strong effect on the production of nutrient and consequently on the production of tumor cells. In principle, that could be seen as a destabilizing factor for the system. However, the higher the density of cells and the concentration of nutrient, the stronger the degradation of the latter. This results in the decrease in the tumor growth and as a consequence can imply stability. Choosing G and R on the contrary as above: G small enough, R large enough, the conditions (2.2.10), (2.2.11) and (2.2.12) are not satisfied. In this case the degradation dominates and concentration of nutrient goes to zero causing that the non-trivial equilibrium may be unstable. Condition (2.2.13) is definitely more a technical one: as it will be clear from the proof of theorem 1, it has to be interpreted as a *diffusion–dominated* assumption.

Remark 3. Our result, stated in Theorem 1, holds also in the case of $\delta = 0$ for a constant, non-trivial equilibrium (2.2.8). The proof is the same as for the Theorem 1 so we omit it.

2.3   Stability of a linearised model

A standard approach in showing local stability of non linear systems is to study at first stability of the linearised problem. The null solution and the non trivial equilibrium (2.2.4) are taken into account. The results on the linearized problem are valid in any space dimension.

Let, in the vector notation introduced previously, U_∞ be an equilibrium and $\widetilde{U}$ a small perturbation from it. Supposing the solution can be written as

$$U = U_\infty + \widetilde{U},$$

the linearised system (2.2.9) is

$$\widetilde{U}_t = \mathbf{D} \triangle \widetilde{U} + \mathbf{R}\widetilde{U}. \tag{2.3.1}$$

The matrices $\mathbf{D}, \mathbf{R} \in M_{2x2}(\mathbb{R})$, (diffusion and reaction matrix respectively), are

$$\mathbf{D} = \begin{pmatrix} f'(\phi_\infty) & -\omega\phi_\infty \\ 0 & D \end{pmatrix}, \tag{2.3.2}$$

$$\mathbf{R} = \begin{pmatrix} L_1 & L_2 \\ G - dc_\infty & -(R + d\phi_\infty) \end{pmatrix}, \tag{2.3.3}$$

where $L_1 = \frac{\partial\alpha(\phi,c)}{\partial\phi}\big|_{(\phi_\infty,c_\infty)}$ and $L_2 = \frac{\partial\alpha(\phi,c)}{\partial c}\big|_{(\phi_\infty,c_\infty)}$.

The following theorem, describing the stability of the stationary states of the system (2.3.1), holds under the structural conditions (2.2.10), (2.2.11), (2.2.12), (2.2.13).

Theorem 2. *The trivial solution of the linearized system (2.3.1) is asymptotically stable for any choice of the parameters. Moreover,under the structural conditions (2.2.10), (2.2.11), (2.2.12), (2.2.13), if the condition (2.2.3) is satisfied, the non trivial equilibrium point (2.2.4) is asymptotically stable and we have the estimate*

$$||U - U_\infty||_{L^2(\Omega)} \leq C_1 e^{-C_2 t}||U_0 - U_\infty||_{L^2(\Omega)},$$

where C_1 and C_2 are positive constants depending on the structure parameters of the system.

Proof. The proof of the stability result for the trivial stationary state is obtained by simple estimate of L_2 norm of $\widetilde{U}$ using the energy method. We are going to present a proof only in the case of non trivial equilibrium, since the computation follows the same strategy as for the trivial state.

The linearized diffusion and reaction matrices in this case have the form (2.3.2) and (2.3.3) respectively. The elements L_1 and L_2 of the reaction matrix are

$$
\begin{aligned}
L_1 &= \gamma_1\widehat{p}\left(\frac{c_\infty}{c^*} - 1\right)\left(\phi\widehat{H}(\phi^* - \phi)\right)'_{(\phi_\infty,c_\infty)} - \gamma_2\widehat{p}\left(1 - \frac{c_\infty}{c^*}\right) - \delta = \\
&= \delta\left(\widehat{H}(\phi^* - \phi_\infty) - \phi_\infty\widehat{H}'(\phi^* - \phi)|_{\phi_\infty}\right) - \delta = \delta \cdot 1 - 0 - \delta = 0, \\
L_2 &= \gamma_1\phi_\infty\widehat{H}(\phi^* - \phi_\infty)\left[\widehat{p}\left(\frac{c}{c^*} - 1\right)\right]'_{(\phi_\infty,c_\infty)} - \gamma_2\phi_\infty\left[\widehat{p}\left(1 - \frac{c}{c^*}\right)\right]'_{(\phi_\infty,c_\infty)} = \\
&= \frac{\gamma_1}{c^*}\phi_\infty - 0 = \frac{\gamma_1}{c^*}\phi_\infty > 0.
\end{aligned}
$$

Now we want to show that under the structural conditions on parameters there exists a symmetric, positive definite matrix S such that the matrices SD, SR are symmetric. The matrix S is determined up to a multiplying constant. Let us assume that

$$S = \begin{pmatrix} S_1 & 1 \\ 1 & S_2 \end{pmatrix},$$

with $S_1, S_2 \in \mathbb{R}$. Then

$$S\mathbf{D} = \begin{pmatrix} S_1 f'(\phi_\infty) & -S_1\omega\phi_\infty + D \\ f'(\phi_\infty) & -\omega\phi_\infty + S_2 D \end{pmatrix}$$

and

$$SR = \begin{pmatrix} G - dc_\infty & S_1 L_2 - (R + d\phi_\infty) \\ S_2(G - dc_\infty) & L_2 - S_2(R + d\phi_\infty) \end{pmatrix}.$$

We want these matrices to be symmetric so

$$f'(\phi_\infty) = -S_1 \omega \phi_\infty + D \quad \Rightarrow \quad S_1 = \frac{D - f'(\phi_\infty)}{\omega \phi_\infty},$$

$$S_2(G - dc_\infty) = S_1 L_2 - (R + d\phi_\infty) \quad \Rightarrow$$

$$\Rightarrow S_2 = \frac{1}{G - dc_\infty}\left(\frac{D - f'(\phi_\infty)}{\omega \phi_\infty} L_2 \quad - \quad (R + d\phi_\infty)\right).$$

The matrix S takes the form

$$S = \begin{pmatrix} \frac{D - f'(\phi_\infty)}{\omega \phi_\infty} & 1 \\ 1 & \frac{1}{G - dc_\infty}\left(\frac{D - f'(\phi_\infty)}{\omega}\frac{\gamma_1}{c^*} - (R + d\phi_\infty)\right) \end{pmatrix} = \begin{pmatrix} S_1 & 1 \\ 1 & S_2 \end{pmatrix}.$$

It is positive definite if the parameters of the system satisfy the conditions

$$\begin{cases} S_1 S_2 - 1 > 0 \\ S_1 + S_2 > 0, \end{cases}$$

which are equivalent to structural conditions (2.2.10), (2.2.11). Moreover, we require that the matrix SD is positive definite, which means

$$det(SD) > 0 \quad \text{and} \quad tr(SD) > 0.$$

Because

$$det(SD) = (S_1 S_2 - 1)Df'(\phi_\infty)$$

and $S_1 S_2 - 1 > 0$, the determinant of the symmetrised diffusion matrix is always positive. It's trace is positive if

$$tr(SD) = (S_1 f'(\phi_\infty) - \omega \phi_\infty + S_2 D) > 0,$$

which corresponds to the condition (2.2.12). For the symmetrised reaction matrix we obtain

$$det(SR) = (S_1 S_2 - 1)(-L_2(G - dc_\infty)),$$

which is always negative. It means that the matrix SR has eigenvalues with the opposite sign.

Now we prove the asymptotic convergence of the solution to the stationary state in the L_2 norm under the conditions specified in the theorem. In the proof we use the energy method. We define the energy as a positive, quadratic form

$$E(t) = \frac{1}{2}\int_\Omega \widetilde{U} \cdot S\widetilde{U}\,dx,$$

where $\widetilde{U} = U - U_\infty$.

Because the matrix S is symmetric there exists an orthogonal matrix F such that $F^T S F = \Lambda_s$ and Λ_s is diagonal with the two eigenvalues of S as entries. Using this property we obtain

$$\int_\Omega \widetilde{U}^T S\widetilde{U}\,dx = \int_\Omega \widetilde{U}^T F F^T S F F^T \widetilde{U}\,dx = \int_\Omega \widetilde{W}^T \Lambda_s \widetilde{W}\,dx,$$

where $\widetilde{W} = F^T\widetilde{U}$. Denoting by $\min S$ the smallest eigenvalue of the matrix S we get the estimate

$$\int_\Omega \widetilde{U}^T S\widetilde{U} dx \geq \min(S) \int_\Omega |\widetilde{W}|^2 dx = \min(S) \int_\Omega |\widetilde{U}|^2 dx.$$

In the last step we used the fact that the orthogonal transformation doesn't change the L_2 norm. From the above inequality we have

$$||\widetilde{U}||^2_{L_2(\Omega)} \leq \frac{1}{\min(S)} \int_\Omega \widetilde{U} \cdot S\widetilde{U} dx. \tag{2.3.4}$$

To show the convergence of the solution U to the stationary state U_∞ it is sufficient to show that the quadratic form $E(t)$ goes to zero asymptotically. We therefore estimate time derivative of the energy. Let us remark that in the case of the trivial equilibrium, the matrix $S\mathbf{R}$ is negative semi-definite, which helps the solution to get to equilibrium. Here the situation is different as $S\mathbf{R}$ has eigenvalues with different sign. Let us denote by $\mathrm{pos}(S\mathbf{R})$ the positive eigenvalue of $S\mathbf{R}$.

$$\begin{aligned}
\frac{d}{dt}E(t) &= \frac{1}{2}\frac{d}{dt}\int_\Omega \widetilde{U} \cdot S\widetilde{U} dx = \int_\Omega \widetilde{U}^T S\widetilde{U}_t dx \leq \\
&\leq \left(-\frac{|\min(S\mathbf{D})|}{C(\Omega)} + \mathrm{pos}(S\mathbf{R})\right) \int_\Omega |\widetilde{U}|^2 dx \leq \\
&\leq \frac{1}{\min(S)}\left(-\frac{|\min(S\mathbf{D})|}{C(\Omega)} + \mathrm{pos}(S\mathbf{R})\right) \int_\Omega \widetilde{U} \cdot S\widetilde{U} dx,
\end{aligned}$$

where we used the fact that matrix $S\mathbf{D}$ is positive definite, the Poincaré inequality, and (2.3.4).

To prove the convergence using the symmetrization method we suppose

$$M = -\frac{|\min(S\mathbf{D})|}{C(\Omega)} + \mathrm{pos}(S\mathbf{R}) < 0.$$

which corresponds to the condition (2.2.13). Under this assumption, applying Gronwall's lemma we obtain

$$E(t) \leq E(0)exp\left[-\frac{2}{\min(S)}|M|t\right]. \tag{2.3.5}$$

Using a similar argument as in (2.3.4) we have

$$E(0) = \frac{1}{2}\int_\Omega \widetilde{U}_0 \cdot S\widetilde{U}_0 dx \leq \frac{1}{2}\max(S) \int_\Omega |\widetilde{U}_0|^2 dx. \tag{2.3.6}$$

Further estimate of (2.3.4) by (2.3.5) and (2.3.6) with $\widetilde{U} = U - U_\infty$ gives

$$||U - U_\infty||_{L^2(\Omega)} \leq \sqrt{\frac{\max(S)}{\min(S)}}e^{-\frac{1}{\min(S)}|M|t}||U_0 - U_\infty||_{L^2(\Omega)},$$

where $C_1 = \sqrt{\frac{\max(S)}{\min(S)}}$ and $C_2 = \frac{1}{\min(S)}|M|$ as stated in theorem (2). $\qquad\square$

2.4 Proof of the main theorem

In the previous section we proved linear stability of the non-trivial stationary state (2.2.4) far from the smoothing region in any dimension and for any choice of the initial data in the case our structural conditions are satisfied (the trivial equilibrium is stable regardless the system parameters).

In the non linear case we study the asymptotic behavior of a one dimensional model (2.2.9), for which we stated a theorem of convergence of solutions to the constant, stationary states in H^2 norm. In this section we present its proof.

As for the linear case, we shall rely on the standard symmetrization method. We consider a solution as a perturbation $\widetilde{U}$ from the equilibrium U_∞, that is $U = U_\infty + \widetilde{U}$, and rewrite the system (2.2.9)

$$\widetilde{U}_t = \left(\mathbf{D}(U_\infty + \widetilde{U})\widetilde{U}_x\right)_x + \vec{\varphi}(U_\infty + \widetilde{U}),$$

where

$$\vec{\varphi}(U) = \left(\begin{array}{c} \gamma_1 \widehat{p}\left(\frac{c}{c^*} - 1\right)\phi\widehat{H}(\phi^* - \phi) - \gamma_2\widehat{p}\left(1 - \frac{c}{c^*}\right)\phi - \delta\phi \\ -dc\phi + G\phi - Rc \end{array} \right)$$

and

$$\mathbf{D}(U) = \left(\begin{array}{cc} f'(\phi) & -\omega\phi \\ 0 & D \end{array} \right).$$

Expanding the vector $\vec{\varphi}(U_\infty + \widetilde{U})$ in the Taylor series

$$\vec{\varphi}(U_\infty + \widetilde{U}) = \vec{\varphi}(U_\infty) + J\vec{\varphi}(U_\infty)\widetilde{U} + h.o.t.$$

with $\vec{\varphi}(U_\infty) = 0$ and the Jacobian $J\vec{\varphi}(U_\infty) = \mathbf{R}$ corresponding to the reaction matrix of the linear case, we get

$$\widetilde{U}_t = \mathbf{D}(U_\infty)\widetilde{U}_{xx} + \left(\left[\mathbf{D}(U_\infty + \widetilde{U}) - \mathbf{D}(U_\infty)\right]\widetilde{U}_x\right)_x + \mathbf{R}\widetilde{U} + \vec{H}(\widetilde{U}). \qquad (2.4.1)$$

The function $\vec{H}(\widetilde{U}) = \vec{\varphi}(U_\infty + \widetilde{U}) - \mathbf{R}\widetilde{U}$ is continuous and $\vec{H}(\widetilde{U} = 0) = 0$.

To prove the convergence of the solution to the stationary state in the H_2 norm we estimate L_2 norms of $\widetilde{U}, \widetilde{U}_x, \widetilde{U}_{xx}$ using the energy method. As usual, when dealing with linearised stability, we assume a priori that

$$\| \widetilde{U} \|_{H^2} < \eta \qquad \text{for} \qquad \eta \ll 1.$$

A simple continuation argument implies that $\forall_{t>0} \| \widetilde{U}(t) \|_{H^2} \leqslant \eta$ assuming the initial data is such that $\| \widetilde{U}_0 \|_{H^2} \leqslant \eta$. For the sake of clarity, we state the continuation principle.

Theorem 3. *Suppose* $\| \widetilde{U}(t) \|_{H^2} \to 0$ *as* $t \to +\infty$ *under the a priori assumption* $\forall_{t>0}$ $\| \widetilde{U}(t) \|_{H^2} \leqslant \eta \ll 1$. *Then* $\forall_{t>0} \| \widetilde{U}(t) \|_{H^2} < \eta$ *under the assumption on the initial datum* $\| \widetilde{U}_0 \|_{H^2} \leqslant \eta$.

Following the proof of Theorem 1 we define our first energy functional

$$E_1(t) = \frac{1}{2}\int_\Omega \widetilde{U} \cdot S\widetilde{U}\,dx$$

and estimate its time derivative

$$
\begin{aligned}
\frac{d}{dt}E_1 &= \int_\Omega \widetilde{U} \cdot S\widetilde{U}_t dx = \int_\Omega \widetilde{U} \cdot \mathbf{D}(U_\infty)\widetilde{U}_{xx} dx + \\
&+ \int_\Omega \widetilde{U} \cdot S\left(\left[\mathbf{D}(U_\infty + \widetilde{U}) - \mathbf{D}(U_\infty)\right]\widetilde{U}_x\right)_x + \\
&+ \int_\Omega \widetilde{U} \cdot S\mathbf{R}\widetilde{U} dx + \int_\Omega \widetilde{U} \cdot S\vec{H}(\widetilde{U}) dx = \sum_{i=1}^4 I_i.
\end{aligned}
$$

The I_1 and I_3 integrals are the same as in the linear case so we have

$$
\begin{aligned}
I_1 &\leq -\min(S\mathbf{D}(U_\infty)) \int_\Omega |\widetilde{U}_x|^2 dx, \\
I_3 &\leq \operatorname{pos}(S\mathbf{R}) \int_\Omega |\widetilde{U}|^2 dx.
\end{aligned}
$$

The I_2 and I_4 integrals we rewrite componentwise

$$
\begin{aligned}
I_2 &= \int_\Omega \widetilde{U} \cdot S\left(\left[\mathbf{D}(U_\infty + \widetilde{U}) - \mathbf{D}(U_\infty)\right]\widetilde{U}_x\right)_x = \\
&= -\int_\Omega \widetilde{U}_x \cdot S\left[\mathbf{D}(U_\infty + \widetilde{U}) - \mathbf{D}(U_\infty)\right]\widetilde{U}_x dx = \\
&= -\left(S_1 \int_\Omega \Psi(\widetilde{\phi})\widetilde{\phi}_x^2 dx - S_1\omega \int_\Omega \widetilde{\phi}\widetilde{\phi}_x\widetilde{c}_x + \int_\Omega \Psi(\widetilde{\phi})\widetilde{\phi}_x\widetilde{c}_x dx - \omega \int_\Omega \widetilde{\phi}\widetilde{c}_x^2 dx\right) \leq \\
&\leq |S_1| \int_\Omega |\Psi(\widetilde{\phi})|\widetilde{\phi}_x^2 dx + \omega|S_1| \int_\Omega |\widetilde{\phi}| \cdot |\widetilde{\phi}_x\widetilde{c}_x| + \\
&+ \int_\Omega |\Psi(\widetilde{\phi})| \cdot |\widetilde{\phi}_x\widetilde{c}_x| dx + \omega \int_\Omega |\widetilde{\phi}|\widetilde{c}_x^2 dx,
\end{aligned}
$$

where $\Psi(\widetilde{\phi}) = f'(\phi_\infty + \widetilde{\phi}) - f'(\phi_\infty)$. Using the fact that the function $\widehat{H}(\phi^* - \phi)$ coincides with the Heaviside function at the equilibrium and $\alpha(\phi, c)$, $\beta(\phi, c)$ are C^1 functions we have

$$
\vec{H}(\widetilde{U}) = \begin{pmatrix} \gamma_1 \frac{1}{c^*}\widetilde{\phi}\widetilde{c} \\ -d\widetilde{\phi}\widetilde{c} \end{pmatrix}
$$

and the integral I_4 can be estimated by

$$
\begin{aligned}
I_4 &\leq \frac{\gamma_1}{c^*}|S_1| \int_\Omega \widetilde{\phi}^2\widetilde{c} dx + d \int_\Omega \widetilde{\phi}^2\widetilde{c} dx + \\
&+ \frac{\gamma_1}{c^*} \int_\Omega \widetilde{\phi}\widetilde{c}^2 dx + d|S_2| \int_\Omega \widetilde{\phi}\widetilde{c}^2 dx.
\end{aligned}
$$

From now on we denote all positive constants depending on the parameters of the system as $\widetilde{\mathcal{C}}$ and small parameters as η.

Using the Sobolev inequality for a function $u \in H_0^1([0,1])$ and continuation principle we obtain

$$
\forall t \geq 0 \qquad ||\widetilde{U}(t)||_{L^\infty} \leq \widetilde{\mathcal{C}}||\widetilde{U}(t)||_{H^1} \leq \widetilde{\mathcal{C}}\eta. \tag{2.4.2}
$$

Moreover as a consequence of the continuity of the function Ψ and the condition $\Psi(0) = 0$ we have

$$\exists \;\; \widetilde{a}(\Psi, \eta) : \;\;\; ||\Psi(\widetilde{\phi})||_{L^\infty} \leq \widetilde{a} \;\;\;\;\; \forall \;\; t \geq 0 \tag{2.4.3}$$

with $\widetilde{\phi}$ being a small perturbation from the equilibrium. Using the above inequalities and the fact that S_1, S_2 are constant and bounded we estimate I_2 and I_4

$$
\begin{aligned}
I_2 &\leq \widetilde{\mathcal{C}}||F(\widetilde{\phi})||_{L^\infty} \int_\Omega \widetilde{\phi}_x^2 dx + \widetilde{\mathcal{C}}||\widetilde{\phi}||_{L^\infty} \int_\Omega \left(\widetilde{\phi}_x^2 + \widetilde{c}_x^2 \right) dx + \\
&+ \;\; ||F(\widetilde{\phi})||_{L^\infty} \int_\Omega \left(\widetilde{\phi}_x^2 + \widetilde{c}_x^2 \right) dx + \widetilde{\mathcal{C}}||\widetilde{\phi}||_{L^\infty} \int_\Omega \widetilde{c}_x^2 dx \leq \\
&\leq \;\; \widetilde{\mathcal{C}}\eta \int_\Omega \left(\widetilde{\phi}_x^2 + \widetilde{c}_x^2 \right) dx, \\
I_4 &\leq \widetilde{\mathcal{C}}||\widetilde{c}||_{L^\infty} \int_\Omega \widetilde{\phi}^2 dx + \widetilde{\mathcal{C}}||\widetilde{\phi}||_{L^\infty} \int_\Omega \widetilde{c}^2 dx \leq \\
&\leq \;\; \widetilde{\mathcal{C}}\eta \int_\Omega \left(\widetilde{\phi}^2 + \widetilde{c}^2 \right) dx.
\end{aligned}
$$

Summing four integrals we obtain

$$\frac{d}{dt} E_1(t) \leq \left(\widetilde{\mathcal{C}}\eta - \min\left(S\mathbf{D}(U_\infty) \right) \right) \int_\Omega |\widetilde{U}_x|^2 dx + \left(\widetilde{\mathcal{C}}\eta + \mathrm{pos}\left(S\mathbf{R} \right) \right) \int_\Omega |\widetilde{U}|^2 dx.$$

Next we define energies E_2 and E_3 as

$$
\begin{aligned}
E_2(t) &= \frac{1}{2} \int_\Omega \widetilde{U}_x \cdot S\widetilde{U}_x dx, \\
E_3(t) &= \frac{1}{2} \int_\Omega \widetilde{U}_{xx} \cdot S\widetilde{U}_{xx} dx
\end{aligned}
$$

and estimate their time derivatives using the same method as for E_1.

$$
\begin{aligned}
\frac{d}{dt} E_2(t) &= -\int_\Omega \widetilde{U}_{xx} \cdot S\mathbf{D}(U_\infty)\widetilde{U}_{xx} dx + \\
&- \int_\Omega \widetilde{U}_{xx} \cdot S\left[\mathbf{D}(U_\infty + \widetilde{U}) - \mathbf{D}(U_\infty) \right]_x \widetilde{U}_x dx + \\
&- \int_\Omega \widetilde{U}_{xx} \cdot S\left[\mathbf{D}(U_\infty + \widetilde{U}) - \mathbf{D}(U_\infty) \right] \widetilde{U}_{xx} dx + \int_\Omega \widetilde{U}_x \cdot S\mathbf{R}\widetilde{U}_x dx + \\
&+ \int_\Omega \widetilde{U}_x \cdot S\left[\vec{H}(\widetilde{U}) \right]_x dx, \\
\frac{d}{dt} E_3(t) &= -\int_\Omega \widetilde{U}_{xxx} \cdot S\mathbf{D}(U_\infty)\widetilde{U}_{xxx} dx + \\
&- \int_\Omega \widetilde{U}_{xxx} \cdot S\left[\mathbf{D}(U_\infty + \widetilde{U}) - \mathbf{D}(U_\infty) \right]_{xx} \widetilde{U}_x dx + \\
&- 2\int_\Omega \widetilde{U}_{xxx} \cdot S\left[\mathbf{D}(U_\infty + \widetilde{U}) - \mathbf{D}(U_\infty) \right]_x \widetilde{U}_{xx} dx + \\
&- \int_\Omega \widetilde{U}_{xxx} \cdot S\left[\mathbf{D}(U_\infty + \widetilde{U}) - \mathbf{D}(U_\infty) \right] \widetilde{U}_{xxx} dx + \\
&+ \int_\Omega \widetilde{U}_{xx} \cdot S\mathbf{R}\widetilde{U}_{xx} dx + \int_\Omega \widetilde{U}_{xx} \cdot S\left[\vec{H}(\widetilde{U}) \right]_{xx} dx.
\end{aligned}
$$

Rewriting all terms componentwise and using the smallness of the L_∞ norm of $\Psi(\phi)$, $\widetilde{U}$ and $\widetilde{U}_x$ we find that

$$
\begin{aligned}
\frac{d}{dt}E_2 &\leq \left(\widetilde{\mathcal{C}}\eta + \mathrm{pos}(S\mathbf{R})\right)\int_\Omega \left|\widetilde{U}_x\right|^2 dx + \\
&\quad + \left(\widetilde{\mathcal{C}}\eta - |\min(S\mathbf{D}(U_\infty))|\right)\int_\Omega \left|\widetilde{U}_{xx}\right|^2 dx,
\end{aligned}
$$

$$
\begin{aligned}
\frac{d}{dt}E_3 &\leq \widetilde{\mathcal{C}}\eta \int_\Omega \left|\widetilde{U}_x\right|^2 dx + \left(\widetilde{\mathcal{C}}\eta + \mathrm{pos}(S\mathbf{R})\right)\int_\Omega \left|\widetilde{U}_{xx}\right|^2 dx + \\
&\quad + \left(\widetilde{\mathcal{C}}\eta - |\min(S\mathbf{D}(U_\infty))|\right)\int_\Omega \left|\widetilde{U}_{xxx}\right|^2 dx,
\end{aligned}
$$

The sum of all three energies $E(t)$ is

$$
\begin{aligned}
\frac{d}{dt}E(t) &\leq \left(\widetilde{\mathcal{C}}\eta + \mathrm{pos}(S\mathbf{R})\right)||\widetilde{U}||_{L^2}^2 + \left(3\widetilde{\mathcal{C}}\eta + \mathrm{pos}(S\mathbf{R}) - |\min(S\mathbf{D}(U_\infty))|\right)||\widetilde{U}_x||_{L^2}^2 + \\
&\quad + \left(2\widetilde{\mathcal{C}}\eta + \mathrm{pos}(S\mathbf{R}) - |\min(S\mathbf{D}(U_\infty))|\right)||\widetilde{U}_{xx}||_{L^2}^2 + \\
&\quad + \left(\widetilde{\mathcal{C}}\eta - |\min(S\mathbf{D}(U_\infty))|\right)||\widetilde{U}_{xxx}||_{L^2}^2.
\end{aligned}
$$

Using Poincaré inequality with a constant $C(\Omega)$ we compensate the first, positive term and obtain

$$
\begin{aligned}
\frac{d}{dt}E(t) &\leq \left(\widetilde{\mathcal{C}}\eta + \mathrm{pos}(S\mathbf{R}) - \frac{|\min(S\mathbf{D}(U_\infty))|}{2C(\Omega)}\right)||\widetilde{U}||_{L^2}^2 + \\
&\quad + \left(3\widetilde{\mathcal{C}}\eta + \mathrm{pos}(S\mathbf{R}) - \frac{|\min(S\mathbf{D}(U_\infty))|}{2}\right)||\widetilde{U}_x||_{L^2}^2 + \\
&\quad + \left(2\widetilde{\mathcal{C}}\eta + \mathrm{pos}(S\mathbf{R}) - |\min(S\mathbf{D}(U_\infty))|\right)||\widetilde{U}_{xx}||_{L^2}^2 + \\
&\quad + \left(\widetilde{\mathcal{C}}\eta - |\min(S\mathbf{D}(U_\infty))|\right)||\widetilde{U}_{xxx}||_{L^2}^2 \\
&\leq \left(3\widetilde{\mathcal{C}}\eta + \mathrm{pos}(S\mathbf{R}) - \frac{|\min(S\mathbf{D}(U_\infty))|}{2C(\Omega)}\right)\|\widetilde{U}\|_{H^2}^2 + \\
&\quad + \left(\widetilde{\mathcal{C}}\eta - |\min(S\mathbf{D}(U_\infty))|\right)||\widetilde{U}_{xxx}||_{L^2}^2. \quad\quad (2.4.4)
\end{aligned}
$$

Supposing that η can be arbitrary small, we assume

$$
M = \widetilde{\mathcal{C}}\eta + \mathrm{pos}(S\mathbf{R}) - \frac{|\min(S\mathbf{D}(U_\infty))|}{2} < 0,
$$

where $\widetilde{\mathcal{C}}$ is the maximum of the previous constants. Under this assumption the last term in (2.4.4) is negative, so we estimate it by zero. Then, using the relation (2.3.4), we obtain

$$
\frac{d}{dt}E(t) \leq -\frac{2}{\min(S)}|M|E(t).
$$

From the Gronwall's lemma and the explicit form of $\widetilde{U}$ we get

$$
||U - U_\infty||_{H^2(\Omega)} \leq \sqrt{\frac{\max(S)}{\min(S)}}||U_0 - U_\infty||_{H^2(\Omega)}e^{-\frac{M}{\min(S)}t},
$$

Denoting $C_1 = \sqrt{\frac{\max(S)}{\min(S)}}$ and $C_2 = \frac{\mathcal{M}}{\min(S)}$ we obtain the result stated in the theorem, which proves the convergence of the solution U to the constant, stationary state U_∞ as $t \to \infty$.

2.5   Conclusion

The mathematical model that we presented is a system of non linear partial differential equation of reaction-diffusion type with cross diffusion terms. It describes the evolution of a density of tumour cells, which depends on the availability of an essential nutrient. It is assumed that cells move due to non linear diffusion and chemotaxis towards higher concentration of the nutrient. The model develops on the basis of two main observations for tumour cells. First, they grow and proliferate only under specific conditions. There exist threshold values of nutrient concentration and cells density, which puts cells in quiescent stage. Second, the death of tumour cells occurs as a result of insufficient amount of nutrient and apoptosis. The nutrient is assumed to diffuse linearly in the tissue, where it is consumed. Its concentration is being augmented due to the presence of chemical substances released by tumour cells and decreased by external, pharmacological, factors.

The results that we presented concern asymptotic behaviour of a one dimensional, non linear model. We proved a theorem of convergence of solutions to constant, stationary states in H^2 norm. As a main tool we used the classical symmetrization method. Our non linear stability result is proven via energy Sobolev estimates and holds for small perturbations of initial data from the constant states. The geometrical structure of the diffusion and reaction matrices after linearisation excludes their simultaneous symmetrization in such a way to produce two negative definite quadratic forms. It was the main, technical difficulty in the computation.

Theoretical studies of biological phenomena can verify existing hypothesis or indicate other processes that produce the observed results. Studies of the asymptotic behaviour of solutions of mathematical models of tumour growth can be informative while planning a treatment of a cancer. Its suspension depends on the strength of drugs and efficiency of their delivery in the tissue. Numerical simulations of specific treatment solutions can give essential information before applying them to the human organism. Our work shows that under specific conditions on the system parameters, the solutions converge asymptotically to the stationary states, which can be associated with tumour suspension. The results are limited to the case of initial datum being a small perturbation from the equilibrium, however can serve as a model for an early stage of tumour growth with introduced treatment.

From the modelling point of view, a suggestive improvement to the present model, would be using more complicated death terms representing pharmacological treatment. Also, considering a regulating effect of the blood network in the first phase of treatment, has a significant meaning in the view of new anti angiogenesis drugs. As a future work asymptotic behaviour of two dimensional system is considered. The next step would be obtaining the stability results without the constraints on the initial datum.

BACKGROUND ON NUMERICAL METHODS

3.1 Introduction

Mathematical analysis of chemotaxis models is still limited to special cases. The existing results are obtained assuming for example small, regular initial data, absence of vacuum states or describe only what happens with solutions for long times. Even so well-known systems such as compressible Euler equations have still many open problems. For example how the solution changes near the vacuum and how it becomes the canonical kind of behaviour after finite time. Also important is to study the nonlinear stability of travelling wave solutions and answer what the large time bahaviour of the solutions is. Is there always a time asymptotic equivalence between Euler equations with damping and the porous medium equation when vacuum occurs. This motivates us to use numerical simulations in order to get a better insight into the behaviour of complex systems.

In this chapter we focus our attention on numerical methods to approximate advection-reaction-diffusion systems. Usually each mathematical model needs an individual numerical treatment in order to reflect all its physical features. We are going to present a brief overview of the methods used for parabolic and hyperbolic models of chemotaxis. In particular, we are going to describe schemes adapted to treat nonlinear, cross diffusion terms, coupling between equations, vacuum and influence of sources, which presence can lead to non constant stationary solutions.

The main objective is to present different space discretizations of partial differential equations. The resulting semi-discrete system, which is an ordinary differential equation, has to be then integrated in time using explicit methods depending only on the previous times or implicit, which involve also states at actual time. A simultaneous presence of for example diffusion and advection, which are characterized by respectively high and low stiffness, requires the use of splitting techniques between explicit and implicit treatment to avoid restrictive time steps. We are not going to focus much on this aspect, but rather on the space discretization techniques based on the finite difference and finite volume approach.

The finite difference methods involve an approximation of partial derivatives by finite differences. Upwind and centered discretizations are among the most common ones that form a scheme. A special attention is given to conservative form of schemes, which if monotone,

are L^∞ stable and total variation diminishing, but are at most of the first order. Higher order schemes can be obtained via the flux-limiter approach and are called high resolution schemes. They combine a first order in space, monotone scheme with higher order one in such a way that in smooth regions the scheme has higher order, keeping the numerical viscosity low, while near discontinuities the flux-limiter switch it to the lower one to avoid oscillations. These time of schemes are very efficient for purely transport problems and can be used in the more advanced methods for advection-diffusion systems. One of such methods involves the relaxation techniques and is based on a discrete-kinetic approximation of the problem. As a result the nonlinearities are shifted from the derivatives into the source term and implies that a only diagonal system of linear transport equations has to be solved. This is an explicit method, but choosing suitably the order of the discrete approximation and low viscosity high resolution scheme for the linear problem it is possible to construct very accurate scheme, which can be also easily extended to higher dimensions.

On the other hand, finite volume methods are based on the integral formulation of a partial differential equation defined for so called control volumes. In one dimension the solution can be approximated by a function that is constant at each of these cells and has a discontinuity in the form of a jump at their boundaries, where the Riemann problem can be defined. The Godunov type schemes are based on this approach. The numerical flux functions, defining the finite volume scheme, are obtained by solving the above Riemann problem for each control volume. The exact solution are rarely available and require many computational iterations and approximations, called approximate Riemann solvers, are used instead. Roe's method, HLL, HLLC or Suliciu are among the most common solvers. They vary in accuracy and complexity. For example, Roe's approach needs a special matrix, called Roe's matrix, in order to linearize the flux. Constructing a solver we can assume the structure of the solution to the Riemann problem in order to avoid verifying all the possibilities. In particular, for HLL solver it is considered that only two rarefaction wave are present, while in HLLC a contact discontinuity is added. However, this approached require estimates of the wave speeds in order to get the approximate solution of the Riemann problem. On the other hand, Suliciu solver is based on the relaxation approximation such that all the fields of the new, approximate system are linearly degenerate and the exact solution to the Riemann problem can be easily found.

The above methods concern only homogeneous systems, however, usually real, physical phenomena imply that in the model the source terms are present. They can describe reaction processes such as production or degradation, friction in the momentum balance equations, chemotaxis in the hyperbolic models, topography in the shallow water equations or forces. Their numerical approximation very often is not a trivial task due to high stiffness in the case of reactions and friction or some geometric properties characteristic for chemotaxis and topography. What is more, the balance between the internal forces and the sources can result in non constant stationary solutions and simple, pointwise methods are unable to capture them. As the effect of high stiffness can be approximated accurately by implicit discretizations, preserving the non-constant steady states is not so simple. To obtain this goal the fluxes and the sources have to be treated at the same time level in order to preserve a discrete version of stationary equations. This lead to the so called well-balanced schemes, which by special reconstruction of the interface variables are able to approximate accurately equilibria.

Parabolic and hyperbolic models of chemotaxis, which are the core of the thesis, involve cross diffusion with nonlinear, degenerate terms, coupling between parabolic and hyperbolic

equations, reaction parts describing birth, growth and death very often endowed with threshold quantities, and sources involving space derivatives thus with geometric structure. In the further chapters we foccus our attention on numerical approximation and analysis of these problems. This is why, at first we give a brief description of the available methods that can be used to obtain this goal.

This chapter is organized as follows. In the beginning we present a short introduction to finite difference method focusing on conservative schemes, flux limiter approach, basic implicit-explicit splitting and more advanced schemes based on relaxation techniques. Sections 3.3 and 3.4 are devoted to numerical methods for balance laws using finite volume approach. In the former we present an extension of scalar schemes to systems and the Godunov-type schemes for homogeneous problems, while in the later we focus on the approximation of the source terms. In the end we describe the influence and numerical treatment of boundary conditions.

3.2 Finite differences methods

Finite difference method for a scalar, one dimensional, advection-diffusion problem

$$u_t + f(u)_x = d(u)_{xx}, \qquad \text{for} \quad (x,t) \in [0,L] \times [0,T] \tag{3.2.1}$$

is based on the approximation of partial derivatives by finite differences. In order to construct a numerical scheme we at first have to discretize a space-time plane. In the simplest case we define an uniform grid on $[0,L] \times [0,T]$ by elements (x_i, t^n), $0 \leq i \leq s, 0 \leq n \leq N$. Denoting by $\Delta x, \Delta t$ space and time discretization steps respectively, the grid points are defined as $(x_i, t^n) = ((i-1)\Delta x, n\Delta t)$ for integers $i = 1, 2, ..., s$ and $n = 0, 1, ..., N$ such that $(x_1, t^0) = (0,0)$ and $(x_s, t^N) = (L,T)$. For any function $u = u(x,t)$ defined on the grid we denote by u_i^n to be an approximation of u at node x_i at time step t^n.

Having constructed a numerical domain for the problem (3.2.1) we can define finite difference approximating partial derivatives. There are many methods to do this. The most common for a linear case, where $f(u) = au$ and $d(u) = du$, $d \geq 0$, are

I-order forward upwind difference: $\quad \dfrac{\partial u}{\partial x} \approx \dfrac{u_i - u_{i-1}}{\Delta x}$

I-order backward upwind difference: $\quad \dfrac{\partial u}{\partial x} \approx \dfrac{u_{i+1} - u_i}{\Delta x}$

II-order centered difference: $\quad \dfrac{\partial u}{\partial x} \approx \dfrac{u_{i+1} - u_{i-1}}{\Delta x}$

$$\dfrac{\partial^2 u}{\partial x^2} \approx \dfrac{u_{i+1} - 2u_i + u_{i-1}}{\Delta x^2}$$

A semi-discrete form of a scheme contains finite differences replacing only spatial derivatives that is for example

$$\frac{d}{dt} u_i(t) + \frac{a}{\Delta x} \left(u_i(t) - u_{i-1}(t) \right) = \frac{d}{\Delta x^2} \left(u_{i+1}(t) - 2u_i(t) + u_{i-1}(t) \right), \quad a > 0.$$

To obtain a fully discrete scheme we need to define the finite difference for the time deriva-
tive and determine when the spatial ones are calculated. We have to choose between explicit
approximation, depending only on the states at time steps up to t^n, or implicit discretization,
in which finite differences are calculated up to time t^{n+1}. The difference between the two
approaches is visible when we deal with stiff terms in diffusion or damping. These kinds of
processes are approximated better if treated implicitly. The explicit method requires a strong
condition on the time step, which in the case of diffusion is of order Δx^2.

3.2.1   Conservative schemes

Let us focus our attention on explicit, one step in time methods for the problem (3.2.1). A
general $(2k + 1)$- points finite difference scheme can be presented as

$$u_i^{n+1} = H\left(u_{i-k}^n, \ldots, u_{i+k}^n\right), \qquad \forall i \in I, \tag{3.2.2}$$

where $I = \{i : x_i \in [0, L]\}$. In many problems the unknown u describes a physical quantity
a function of which is conserved in time. For example if we consider $u(x, t)$ to be a density
of gas closed in a container, or cells of bacteria moving in a bounded area without possibility
to leave it, the quantity to be preserved is the total mass $M = \int_{Omega} u(x, t) dx$ of particles
or cells. We want the numerical approximation to conserve it also. One of the methods is to
consider schemes in a conservative form

$$u_i^{n+1} = u_i^n - \frac{\Delta t}{\Delta x}\{f_{i+\frac{1}{2}}^n - f_{i-\frac{1}{2}}^n\}, \tag{3.2.3}$$

where function $f_{i+1/2}$ is defined using numerical flux functions $\mathcal{F}, \mathcal{D}$

$$f_{i+\frac{1}{2}}^n = \mathcal{F}(u_{i-k+1}^n, ..., u_{i+k}^n) - \frac{1}{\Delta x}[\mathcal{D}(u_{i-k+2}^n, ..., u_{i+k}^n) - \mathcal{D}(u_{i-k+1}^n, ..., u_{i+k-1}^n)]. \tag{3.2.4}$$

A scheme of the form (3.2.2) can be put in conservative form if and only if for each vector
$u = (u_i)_{i \in I} \in L^1(I)$ such that $H(u) \in L^1(I)$ holds

$$\sum_{i \in I} H(u_{i-k}, ..., u_{i+k}) = \sum_{i \in I} u_i.$$

Moreover, the conservative scheme (3.2.3) with a numerical flux function (3.2.4) is consistent
with the equation (3.2.1) if for all functions u

$$\begin{aligned}
\mathcal{F}(u, ..., u) &= f(u), \\
\mathcal{D}(u, ..., u) &= d(u).
\end{aligned} \tag{3.2.5}$$

For a 3-points scheme, corresponding to $k = 1$ in (3.2.2), for the problem (3.2.1) the flux
function $\mathcal{D}(u)$ coincides with $d(u)$ in the second order centered scheme. The numerical flux
functions $\mathcal{F}(u, v)$ for the transport part for the basic schemes are

- Upwind scheme:

$$\begin{aligned}
\mathcal{F}(u, v) &= f(u) & \text{if} & & f'(u) > 0 \\
\mathcal{F}(u, v) &= f(v) & \text{if} & & f'(u) < 0
\end{aligned}$$

- Lax-Friedrichs scheme:

$$\mathcal{F}(u,v) = \frac{1}{2}(f(u) + f(v)) + \frac{\Delta x}{2\Delta t}(u - v)$$

- Lax-Wendroff scheme:

$$\mathcal{F}(u,v) = \frac{1}{2}(f(u) + f(v)) - \frac{\Delta t}{2\Delta x}C(u,v)(f(v) - f(u)),$$

where $C(u,v)$ is a consistent approximation of the Jacobian of f.

An important class of numerical schemes are monotone schemes, which satisfy

$$\frac{\partial H_i}{\partial u_j} \geq 0, \qquad j = i-1, i, i+1, \quad i,j \in I. \tag{3.2.6}$$

Assuming $f'(u) \geq 0$, the function H for the upwind scheme is

$$H_i = u_i - \frac{\Delta t}{\Delta x}(f(u_i) - f(u_{i-1})) + \frac{\Delta t}{\Delta x^2}(d(u_{i+1}) - 2d(u_i) + d(u_{i-1})). \tag{3.2.7}$$

Then the monotonicity condition takes the form

$$\begin{aligned} \frac{\Delta t}{\Delta x}f'(u_{i-1}) + \frac{\Delta t}{\Delta x^2}d'(u_{i-1}) &\geq 0 \\ 1 - \frac{\Delta t}{\Delta x}f'(u_i) - 2\frac{\Delta t}{\Delta x^2}d'(u_i) &\geq 0 \qquad \forall i \in I, \\ \frac{\Delta t}{\Delta x^2}d'(u_{i+1}) &\geq 0 \end{aligned} \tag{3.2.8}$$

yielding the L^∞ stability of the scheme under the following CFL condition

$$\Delta t \leq \frac{\Delta x^2}{\Delta x \max_{|u| \leq ||u_0||_\infty} |f'(u)| + 2\max_{|u| \leq ||u_0||_\infty} d'(u)}. \tag{3.2.9}$$

A monotone scheme, if can be put in a conservative form, is L^∞ stable and Total Variation Diminishing (TVD) that is

$$TV(u^{n+1}) \leq TV(u^n), \quad \text{where} \quad TV(u) = \sum_{i \in I}|u_{i+1} - u_i|. \tag{3.2.10}$$

TVD schemes don't create new oscillations in the approximate solution. Harten in [55] showed that they converge in L^∞ to the correct weak solutions of the transport equation. However, conservative, consistent and monotone schemes such that the function H is $\mathcal{C}^3$ are at most of a first order. Constructing a second order, TVD scheme is not an easy task. In the next section we present an approach based on the flux-limiter functions, which transforms a 3-points, first order scheme into a 5-points, second order one.

3.2.2 High resolution schemes: the flux-limiter approach

Another approach to deal with the problem (3.2.1) are so-called high resolution schemes. They combine a first order in space, monotone scheme with order higher than one. Using flux-limiters functions, these schemes are at least of second order accurate in the smooth regions and switch to a first order near discontinuities. This is motivated by the fact that a first order scheme is stable near discontinuities, but is characterized by a high numerical viscosity. On the other hand, a higher order scheme will be less diffusive but in non-smooth regions can produce oscillations. In this section we are going to give a brief description of this method. For a more detailed presentation we send to [45], [76], [63].

Let us consider a general, semi-discrete system $u'(t) = F(u)$, where F denotes space discretization of a differential space operator. We can write a second order scheme as a sum of a low order one and a correction. However, a high order scheme produces oscillations near discontinuities, so by limiting the correction $(F_H - F_L)$ we can control them thus

$$F_H = F_L + \varphi(\theta)(F_H - F_L), \tag{3.2.11}$$

where the function $\varphi(\theta)$ equals one in smooth regions and zero near discontinuities. The parameter θ measures the "smoothness" of solutions. For example, we can take θ as a ratio between successive differences of the solution. Then, if $\theta > 0$ the function is smooth, whereas $\theta < 0$ signifies the presence of oscillations.

In particular, for a homogeneous, linear equation

$$u_t + au_x = 0, \qquad a > 0, \tag{3.2.12}$$

3-points explicit, consistent scheme can be put in the following form

$$u_i^{n+1} = M(u^n) = u_i^n - a\frac{\Delta t}{2\Delta x}(u_{i+1}^n - u_{i-1}^n) + \frac{q}{2}(u_{i+1}^n - 2u_i^n + u_{i-1}^n). \tag{3.2.13}$$

It is monotone under the condition

$$a\frac{\Delta t}{\Delta x} \leq q \leq 1 \tag{3.2.14}$$

and becomes the upwind scheme for $q = a\frac{\Delta t}{\Delta x}$. Let us choose, following Sweby [112], as a high-order scheme the second order Lax-Wendroff scheme. It is obtained from (3.2.13) taking $q = (a\Delta t/\Delta x)^2$. Denoting by $\lambda = \Delta t/\Delta x$ and rewriting it in the form (3.2.11) we get

$$
\begin{aligned}
u_i^{n+1} = LW(u^n) &= u_i^n - a\frac{\lambda}{2}(u_{i+1}^n - u_{i-1}^n) + \frac{(a\lambda)^2}{2}(u_{i+1}^n - 2u_i^n + u_{i-1}^n) \\
&= M(u^n) - \frac{q - (a\lambda)^2}{2}(u_{i+1}^n - 2u_i^n + u_{i-1}^n) \\
&= M(u^n) - \frac{q - (a\lambda)^2}{2}(\triangle_{i+1/2}u^n - \triangle_{i-1/2}u^n). \tag{3.2.15}
\end{aligned}
$$

Now let us introduce a flux-limiter function to control the second order correction obtaining the following approximation

$$u_i^{n+1} = FL(u^n) = M(u^n) - \frac{q - (a\lambda)^2}{2}(\varphi_{i+1/2}^n\triangle_{i+1/2}u^n - \varphi_{i-1/2}^n\triangle_{i-1/2}u^n). \tag{3.2.16}$$

The limiters $\phi^n_{i+1/2}$ and $\phi^n_{i-1/2}$ depend on the ratio between successive differences via a function ϕ that is

$$\varphi^n_{i+1/2} = \varphi\left(\frac{\triangle_{i-1/2}u^n}{\triangle_{i+1/2}u^n}\right) \tag{3.2.17}$$

where ϕ satisfies

$$\begin{cases} \varphi(r) = 0 & \text{for} \quad r \leq 0 \\ 0 \leq \varphi(r) \leq \min(\frac{2r}{|\lambda|\nu}, \frac{2}{1-|\lambda|\nu}) & \text{for} \quad r > 0 \end{cases} \tag{3.2.18}$$

to guarantee that the scheme is TVD. At Figure 3.1 there are some examples of flux-limiter function φ:

- Minmod: $\varphi(r) = \max\{0, \min\{r, 1\}\}$

- Modified Minmod: $\varphi(r) = \max\{0, \min\{\frac{2r}{\lambda\nu}, \frac{2}{1-\lambda\nu}\}\}$

- Superbee di Roe: $\varphi(r) = \max\{0, \min\{\frac{2r}{\lambda\nu}, 1\}, \min\{r, \frac{2}{1-\lambda\nu}\}\}$

- van Leer: $\varphi(r) = \frac{2r}{1+r}$

Taking the upwind method for a general, linear, transport problem (3.2.12) with $a \in \mathbb{R}$ as the monotone, first order scheme the equation (3.2.16) becomes

$$\begin{aligned} u^{n+1}_i &= u^n_i - a\frac{\lambda}{2}(\triangle_{i+1/2}u^n + \triangle_{i-1/2}u^n) \\ &+ |a|\frac{\lambda}{2}\left(\psi_{i+1/2}\triangle_{i+1/2}u^n - \psi_{i-1/2}\triangle_{i-1/2}u^n\right), \end{aligned} \tag{3.2.19a}$$

where

$$\psi_{i\pm1/2} = 1 - (1 - |a|\lambda)\varphi(r^{n,i\pm1/2}_{sgn(a)}) \tag{3.2.19b}$$

and

$$r^{i+1/2}_+ = \frac{\Delta_{i-1/2}u}{\Delta_{i+1/2}u}, \quad r^{i+1/2}_- = \frac{\Delta_{i+3/2}u}{\Delta_{i+1/2}u}. \tag{3.2.19c}$$
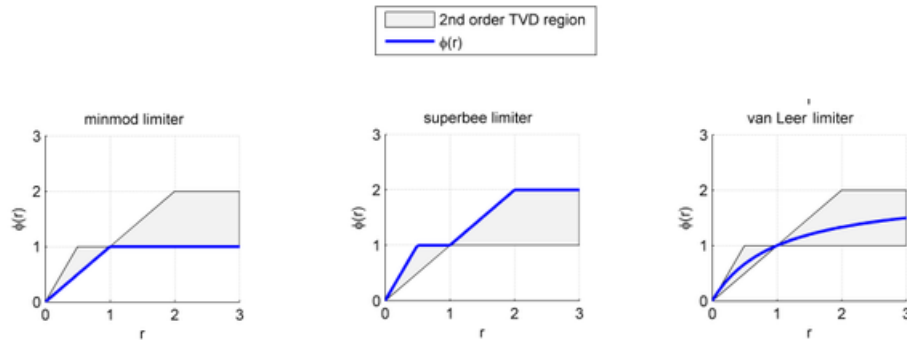

Figure 3.1: Examples of flux-limiter functions ϕ.

3.2.3 θ-method

In the previous section we presented fully explicit, conservative schemes. However, explicit methods give good results only when applied to non-stiff terms such as advection. The presence of processes characterized by a high stiffness requires much smaller time step to assure stability. In the case of diffusion it is of order Δx^2. An application of implicit methods weakens this condition. For the problem (3.2.1) instead of treating all the terms explicitly or implicitly we can split the derivative operators and treat different terms with different methods. The simplest approximation with an explicit-implicit splitting is the θ- scheme. For a semi-discrete problem we split the operator F in the following way

$$u'(t)_i = F_i = (F_1)_i + (F_2)_i, \tag{3.2.20}$$

where F_1 and F_2 are space discretization of non-stiff and stiff terms respectively. Then the θ-scheme has the form

$$u_i^{n+1} = u_i^n + \Delta t (F_1)_i^n + \Delta t (1 - \theta)(F_2)_i^n + \Delta t \theta (F_2)_i^{n+1}, \tag{3.2.21}$$

where the parameter $\theta \in [0, 1]$. If $\theta = 0$ the scheme reduces to the explicit method, while using $\theta = 1$ we get fully implicit scheme. For $\theta = 1/2$ the scheme is called Crank-Nicholson scheme.

The advantage of the above approach is that by mixing explicit-implicit discretization we can treat stiff and non-stiff terms in an optimal way. However, dependence of the finite differences for the space derivatives on the actual state results in the increase of computational complexity. More precisely, if we deal with nonlinear diffusion at each time step we have to solve a system of nonlinear equations, which can be very expensive computationally.

3.2.4 Advanced explicit schemes based of the relaxation technique

In this section we describe numerical schemes based on a discrete, kinetic approximation of systems of conservation laws introduced by Aregba-Driollet and Natalini in [6]. When we deal with nonlinear transport-diffusion problem, the main advantage of this approach is shifting the nonlinearities from the derivatives into a source term. It results in solving only a system of linear, transport problems in order to find a solution at time step t^{n+1}, which reduces the computational complexity. We are going to present the basic ideas of the method on a scalar, D-dimensional equation.

Let us consider

$$u_t + \sum_{d=1}^{D} (A_d(u))_{x_d} = \Delta[B(u)], \qquad (x, t) \in \mathbb{R}^D \times [0, \infty), \tag{3.2.22}$$

where $A(u), B(u)$ are Lipschitz continuous functions such that for every vector $\xi \in \mathbb{R}^D$ the matrix $\sum_{d=1}^{D} \xi_d A_d'(u)$ has real eigenvalues and is diagonalizable and the real parts of the eigenvalues of $B'(u)$ are nonnegative. The scheme for the problem (3.2.22) is based on the discrete BGK approximation. It is composed of a sequence of diagonal, semilinear equations of the form

$$\partial_t f^\epsilon + \sum_{d=1}^{D} \Gamma_d \partial_{x_d} f^\epsilon = \frac{1}{\epsilon} \left(M(u^\epsilon) - f^\epsilon \right) \qquad \epsilon > 0. \tag{3.2.23}$$

For $f \in \mathbb{R}^{N+N'}$ it can be split in the following way

$$\begin{cases} \partial_t f_l^\epsilon + \sum_{d=1}^{D} \lambda_{ld} \partial_{x_d} f_l^\epsilon = \frac{1}{\epsilon} \left(M_l(u^\epsilon) - f_l^\epsilon \right), & 1 \le l \le N, \\ \partial_t f_m^\epsilon + + \sum_{d=1}^{D} \gamma^\epsilon \sigma_{md} \partial_{x_d} f_m^\epsilon = \frac{1}{\epsilon} \left(\frac{B(u^\epsilon)}{N'\theta^2} - f_m^\epsilon \right), & N+1 \le m \le N'+N, \end{cases} \tag{3.2.24}$$

where

$$u^\epsilon(x,t) = \sum_{l=1}^{N+N'} f_l^\epsilon(x,t) \tag{3.2.25}$$

and $\epsilon > 0$, $\lambda_{ld} \in \mathbb{R}$, $\gamma^\epsilon = \mu + \frac{\theta\sqrt{N'}}{\sqrt{\epsilon}}$ where $\mu \ge 0$, $\theta > 0$, $N' \ge D+1$ are parameters. The set $\sigma_{N+1}, ..., \sigma_{N+N'}$ is an orthonormal family such that $\sum_{m=N+1}^{N+N'} \sigma_m = 0$.
Equations (3.2.22) and (3.2.24) are linked together by the compatibility conditions

$$\sum_{l=1}^{N} M_l(u) = u - \frac{B(u)}{\theta^2} \tag{3.2.26a}$$

$$\sum_{l=1}^{N} \lambda_{ld} M_l(u) = A_d(u) \qquad d = 1, ..., D. \tag{3.2.26b}$$

The monotonicity of the Maxwellian functions $M(u)$ assures the stability of the scheme. Taking $N = 2D$ and velocities parallel to the axes

$$\lambda_{jd} = \delta_{jd} \lambda_{md}, \quad \lambda_{D+j,d} = \delta_{jd} \lambda_{pd} \qquad j = 1, ..., D \quad d = 1, ..., D \tag{3.2.27}$$

with $\lambda_{md} < \lambda_{pd}$, to be chosen, we can define the Maxwellian functions as

$$\begin{aligned} M_d(u) &= \frac{1}{\lambda_{pd} - \lambda_{md}} \left(\frac{\lambda_{pd}}{D} \left(u - \frac{B(u)}{\theta^2} \right) - A_d(u) \right), \\ M_{D+d}(u) &= \frac{1}{\lambda_{pd} - \lambda_{md}} \left(-\frac{\lambda_{md}}{D} \left(u - \frac{B(u)}{\theta^2} \right) + A_d(u) \right). \end{aligned} \tag{3.2.28}$$

Let us give more details for the one dimensional problem. Numerical approximation of the solution u to (3.2.22) at time step t^{n+1} consists of two steps, which are the result of the splitting between transport processes and the source in (3.2.24). More precisely, at first we solve a homogeneous system of linear equations

$$\partial_t \vec{f}^\epsilon + \Gamma^\epsilon \partial_x \vec{f}^\epsilon = 0, \tag{3.2.29}$$

where

$$\vec{f}^\epsilon = [f_1^\epsilon, ... f_N^\epsilon, f_{N+1}^\epsilon, ..., f_{N+N'}^\epsilon]^T \tag{3.2.30}$$

and

$$\Gamma^\epsilon = [\lambda_1, ..., \lambda_N, \gamma^\epsilon \sigma_{N+1}, ..., \gamma^\epsilon \sigma_{N+N'}]^T. \tag{3.2.31}$$

with the initial condition $\vec{f}^{\epsilon,0}$

$$f_l^{\epsilon,0} = M_l(u^0) \qquad \text{for} \quad 1 \leq l \leq N, \tag{3.2.32}$$

$$f_m^{\epsilon,0} = \frac{B(u^0)}{N'\theta^2} \qquad \text{for} \quad N+1 \leq m \leq N+N'. \tag{3.2.33}$$

The above, homogeneous system is diagonal and can be solved one by one by any explicit method such as simple upwind scheme. However, to diminish artificial viscosity and increase accuracy high resolution schemes are better. Then we project the result onto the equilibrium that is

$$u^{n+1} = u^{n+1/2} = \sum_{k=1}^{N+N'} f_k^{\epsilon,n+1/2}, \tag{3.2.34}$$

which corresponds to the fractional method for the source term in (3.2.24).

The authors of [6] derived general stability conditions based on the suitable choice of the parameters $\theta, \lambda, \mu, \epsilon$. They are derived from the monotonicity conditions for the Maxwellian functions and in one space dimension have the form

$$\lambda_m \left(1 - \frac{B'(u)}{\theta^2}\right) < A'(u) < \lambda_p \left(1 - \frac{B'(u)}{\theta^2}\right). \tag{3.2.35}$$

To find the suitable constraints on the parameters they choose at first a parameter $\alpha \in]0,1[$ such that

$$0 \leq \alpha \leq 1 - \frac{B'(u)}{\theta^2} \quad \text{yielding} \quad \theta^2 = \frac{\sup_u |B'(u)|}{1 - \alpha}. \tag{3.2.36}$$

Then, taking for example $\lambda_m = -\lambda_p = \lambda$ we get

$$\lambda > \frac{\sup_u |A'(u)|}{\alpha}. \tag{3.2.37}$$

The CFL condition is the minimum of the two hyperbolic conditions for each part of the homogeneous system (3.2.24)

$$\Delta t \leq \min \left\{ \frac{\Delta x}{\lambda}, \frac{\Delta x}{\frac{\mu}{\sqrt{2}} + \frac{\theta}{\sqrt{\epsilon}}} \right\}, \tag{3.2.38}$$

where ϵ, for a three point scheme, is such that

$$\left(\frac{\mu}{\sqrt{2}} + \frac{\theta}{\sqrt{\epsilon}}\right) \frac{\Delta x}{2\theta^2} = 1. \tag{3.2.39}$$

The resulting numerical scheme is TVD and converges to weak solution for the pure advection problem. Moreover, for scalar equation it converges to the entropy solution.

3.3   Systems of conservation laws

We presented numerical methods for scalar, advection-diffusion equations. We considered a one dimensional Cauchy problem

$$\begin{cases} u_t + f(u)_x = 0 & x \in \mathbb{R}, t > 0 \\ u(x,0) = u_0(x) & x \in \mathbb{R} \end{cases} \qquad (3.3.1)$$

and a general, conservative (2k+1)-points scheme on an uniform grid with the mesh size Δx

$$u_i^{n+1} + \frac{\Delta t}{\Delta x}(f_{i+1/2}^n - f_{i-1/2}^n) = 0, \qquad i \in \mathbb{Z}, n \geq 0. \qquad (3.3.2a)$$

Numerical fluxes $f_{i+1/2}$ were defined by a numerical flux function $\mathcal{F} : \mathbb{R}^{2k} \to \mathbb{R}$

$$f_{i+1/2} = \mathcal{F}(u_{i-k+1}, \ldots, u_{i+k}) \qquad (3.3.2b)$$

consistent with (3.3.1) if

$$\forall u \in \mathbb{R} \quad \mathcal{F}(u, \ldots, u) = f(u).$$

Now we are going to describe numerical methods for systems of conservation laws of the form

$$\begin{cases} U_t + \mathrm{div}\,(F(U)) = 0 & x \in \mathbb{R}^d, t > 0 \\ U(x,0) = U_0(x) & x \in \mathbb{R}^d \end{cases}, \qquad (3.3.3)$$

where $U \in \Omega \subset \mathbb{R}^p$ is a p-component vector and $F : \Omega \to \mathbb{R}^p$ is a smooth function. We assume that the system is hyperbolic, so all the eigenvalues of the Jacobian of F are real. However, a strict hyperbolicity is not always the case as the eigenvalues can vanish like in the case of Euler equations for isentropic gas dynamics with nonlinear pressure at the vacuum.

To approximate correctly the behaviour of solutions to (3.3.3) numerical schemes have to reflect all the features of physical phenomena underlying a mathematical model. Preserving non negativity of the solutions is indispensable because usually the quantities being approximated are densities, concentrations or energies. Suitable stability conditions have to be applied in order to avoid oscillations. It is also required to capture accurately shocks and satisfy entropy inequalities to assure that only admissible discontinuities are taken into account. Modelling many physical phenomena concerns also evolution into a vacuum. A system can become degenerate at the free boundary giving rise to mathematical and numerical difficulties. A lot of methods work well under the assumption of strict positiveness of unknown variables and in this case cannot approximate correctly the behaviour at the interface. What is more, in the presence of source terms the system can exhibit non-constant stationary solutions. Their preservation is not a trivial problem especially if they have some geometric properties coming for example from the presence of spatial derivatives.

We are going to present numerical methods for the one dimensional problem (3.3.3) aiming to preserve all the above features by a numerical scheme. In the finite differences framework it is possible to extend scalar $(2k + 1)$-points schemes, however, the procedure is not always straightforward. Another, highly accurate approach are Godunov-type schemes with the Riemann problem as the basic tool. In simple cases it is possible to find its exact solution, while in more complicated, efficient approximations are available. We will focus our attention especially on those that are suitable for the isentropic gas dynamics system with friction and can treat the vacuum.

In Section 3.3.1 we present some extensions of the scalar3-point schemes to systems. We describe the upwind and Lax-Wendroff approach. In Section 3.3.2 we focus on Roe's and Flux-vector splitting method with application to the isentropic gas dynamics system. Section 3.3.3 is devoted to Godunov-type schemes. For the most common approximate Riemann solvers such as Roe's, HLL/HLLC, Suliciu relaxation solver details are given.

3.3.1 Extension of scalar 3-point schemes to systems

At first let us consider a system of one dimensional conservation laws

$$\begin{cases} U_t + F(U)_x = 0 & x \in \mathbb{R}, t > 0 \\ U(x,0) = U_0(x) & x \in \mathbb{R} \end{cases} \tag{3.3.4}$$

where $U = (u_1, \ldots, u_p)^T$ and let us generalize the Lax-Wendroff scheme under the assumption that the flux function F is homogeneous of degree one. It means that

$$\forall \quad \mu \in \mathbb{R} \quad F(\mu u) = \mu F(u) \tag{3.3.5a}$$

and using the Euler's identity

$$F(U) = J_F(U)U. \tag{3.3.5b}$$

Proceeding as in the scalar case we expand U_i^{n+1} in Taylor series around state U_i^n

$$U_i^{n+1} = U_i^n + U_t|_{x_i}\Delta t + \frac{1}{2}U_{tt}|_{x_i}\Delta t^2 + O(\Delta t^3).$$

Using (3.3.4) the time derivatives are

$$\begin{aligned} U_t &= -F(U)_x, \\ U_{tt} &= -(F(U)_x)_t = -(F(U)_t)_x = -(J_F(U)U_t)_x = (J_F(U)F(U)_x)_x. \end{aligned}$$

Applying centered differences for spatial derivatives we obtain Lax-Wendroff scheme for system (3.3.4) in the following form

$$\begin{aligned} U_i^{n+1} = U_i^n &- \frac{\Delta t}{2\Delta x}\left(F_{i+1}^n - F_{i-1}^n\right) \\ &+ \frac{\Delta t^2}{2\Delta x^2}\left[A_{i+1/2}^n\left(F_{i+1}^n - F_i^n\right) - A_{i-1/2}^n\left(F_i^n - F_{i-1}^n\right)\right], \end{aligned} \tag{3.3.6}$$

where matrix $A_{i+1/2}^n$ can be the Jacobian calculated at some average state or the Roe's linearization matrix.

Definition 1. *A matrix $A(U, V)$ is Roe's linearization matrix if a mapping $(U, V) \to A(U, V)$ from $\Omega \times \Omega$ into the set of $p \times p$ matrices satisfies:*

$$\begin{cases} F(V) - F(U) = A(U, V)(V - U) \\ A(U, U) = F(U) \end{cases} \tag{3.3.7}$$

and $A(U, V)$ has real eigenvalues and a corresponding set of eigenvectors forms a basis in $\mathbb{R}^n$.

As we can see, generalization of the Lax-Wendroff scheme to systems is straightforward thanks to centered discretization of space derivatives. It is not the case for upwind schemes, where upwinding of fluxes depends on the sign of the wave velocities. Under the same assumption of the homogenenity of the flux to build an upwind-type scheme we can use the spectral decomposition of J_F to split it into positive and negative definite matrices. Let us denote by $R(U)$

a matrix, which columns are the right eigenvectors of J_F, and take $\Lambda(U) = \text{diag}\left(\lambda_k(U)\right)$, where λ_k are eigenvalues of J_F. Then we can decompose it in the following way

$$J_F(U) = J_F^+(U) + J_F^-(U), \tag{3.3.8a}$$

where

$$J_F^{\pm} = R(U)\Lambda^{\pm}(U)R^{-1}(U). \tag{3.3.8b}$$

and

$$\Lambda^{\pm} = \text{diag}\left(\lambda_k^{\pm}\right) \quad \text{such that} \quad \Lambda = \Lambda^+ + \Lambda^-. \tag{3.3.8c}$$

where

$$\lambda_k^+ = \max(0, \lambda_k) \quad \text{and} \quad \lambda_k^- = \max(0, \lambda_k). \tag{3.3.8d}$$

Introducing a new variable $w = R^{-1}U$ we obtain a diagonal system

$$w_t + (\Lambda^+ + \Lambda^-)w_x = 0,$$

which can be solved using scalar upwind schemes. Then going back to the original variable we get

$$U_i^{n+1} = U_i^n - \frac{\Delta t}{\Delta x}\left[J_F^+(U_i^n)\cdot(U_{i+1}^n - U_i^n) + J_F^-(U_i^n)\cdot(U_i^n - U_{i-1}^n)\right]. \tag{3.3.9}$$

In a nonlinear case we would like to obtain a similar decomposition of the flux that is

$$F(U) = F^+(U) + F^-(U) \tag{3.3.10}$$

with the assumption that the Jacobians of F^+ and F^- have positive and negative eigenvalues respectively, so that we can upwind the fluxes correctly. Assuming we have found such splitting by defining a numerical flux function as

$$\mathcal{F}(U, V) = F^+(U) + F^-(V)$$

we obtain the following 3-point numerical scheme

$$U_i^{n+1} = U_i^n - \frac{\Delta t}{\Delta x}\left[F^+\left(U_i^n\right) - F^+\left(U_{i-1}^n\right)\right] - \frac{\Delta t}{\Delta x}\left[F^-\left(U_{i+1}^n\right) - F^-\left(U_i^n\right)\right]. \tag{3.3.11}$$

For a general flux function F finding a suitable, natural splitting is not trivial. If F satisfies homogenity condition (3.3.5) we get a decomposition proposed by Steger and Warming [111]

$$F^+ = J_F^+U, \quad F^- = J_F^-U \tag{3.3.12}$$

such that $F = F^+ + F^-$ to guarantee consistency and the matrices J_F^+, J_F^-, defined by (3.3.8), are respectively strictly positive and negative. However, the above decomposition is not continuous at sonic points. To solved that problem Van Leer in [119] required additional conditions on the fluxes $F^{\pm}$:

- Continuity of $F^{\pm}$ and $dF^{\pm}/dU$ with

$$\begin{aligned} F^+ &= F \quad \text{for Mach numbers M} > 1 \\ F^- &= F \quad \text{for Mach numbers M} < -1 \end{aligned}$$

- Symmetry
$$F^+(M) = \pm F^-(-M) \quad \text{if} \quad F(M) = \pm F(-M)$$

  for all quantities, apart from the velocity u, constant.

- $F^\pm$ is a polynomial of the lowest possible degree in u

- $dF^\pm/dU$ has a vanishing eigenvalue for $|M| < 1$

The continuity of $dF^\pm/dU$ is not satisfied by the Stager-Warming decomposition and leads to oscillations in degeneracy regions. The presence of the vanishing eigenvalue assures the right sign of eigenvalues of the Jacobians, while the polynomial structure make the splitting unique.

3.3.2 Isentropic gas dynamics

Roe's linearization

We look for a matrix A satisfying (3.3.7) for the flux function F

$$F(U) = \begin{bmatrix} p \\ \frac{p^2}{\rho} + \varepsilon\rho^\gamma \end{bmatrix}, \qquad \varepsilon > 0, \gamma \geq 1 \tag{3.3.13}$$

where $U = [\rho, \quad p]^T$ is a vector of unknowns. In the original work of Roe [103] this matrix is the Jacobian of the flux F calculated at some averaged state, called Roe-averaged state. The derivation is based on a specific change of variables $W \to U(W)$ such that

$$\text{if} \quad G(W) = F(U(W)) \quad \text{then} \quad \begin{matrix} U(W), G(W) \text{ are homogeneous} \\ \text{quadratic functions of W.} \end{matrix} \tag{3.3.14}$$

and the averaging at the level of the new variables.
    For the flux (3.3.13) the Jacobian has the form

$$J_F(U) = \begin{bmatrix} 0 & 1 \\ -u^2 + \varepsilon\gamma\rho^{\gamma-1} & 2u \end{bmatrix}, \tag{3.3.15}$$

where $u = p/\rho$ is the velocity. The new variable is

$$Z = \rho^{-\frac{1}{2}}U \quad \Rightarrow \quad Z = \begin{bmatrix} \rho^{\frac{1}{2}} \\ \rho^{\frac{1}{2}}u \end{bmatrix}. \tag{3.3.16}$$

To verify the property (3.3.14) let us rewrite vector U and flux F in terms of Z thus we get

$$U(Z) = \begin{bmatrix} z_1^2 \\ z_1 z_2 \end{bmatrix}, \quad F(U(Z)) = \begin{bmatrix} z_1 z_2 \\ z_2^2 + \varepsilon z_1^{2\gamma} \end{bmatrix}.$$

From the Definition 1 the Roe's matrix satisfies

$$[F(U)] = A[U],$$

where $[U] = U_L - U_R$, so to find A we look for two matrices B, C such that

$$[U] = B[Z], \tag{3.3.17}$$
$$[F(U)] = C[Z]. \tag{3.3.18}$$

Then $A = CB^{-1}$. The condition (3.3.17) is equivalent to

$$\left[\begin{array}{c} z_{1L}^2 - z_{1R}^2 \\ z_{1L}z_{2L} - z_{1R}z_{2R} \end{array} \right] = \left[\begin{array}{cc} b_1 & b_2 \\ b_3 & b_4 \end{array} \right] \left[\begin{array}{c} z_{1L} - z_{1R} \\ z_{2L} - z_{2R} \end{array} \right].$$

Equality of the vectors yields

$$b_1(z_{1L} - z_{1R}) + b_2(z_{2L} - z_{2R}) = (z_{1L} - z_{1R})(z_{1L} + z_{1R}),$$
$$b_3(z_{1L} - z_{1R}) + b_4(z_{2L} - z_{2R}) = z_{1L}z_{2L} - z_{1R}z_{2R},$$

which implies

$$B = \left[\begin{array}{cc} z_{1L} + z_{1R} & 0 \\ \frac{1}{2}(z_{2L} + z_{2R}) & \frac{1}{2}(z_{1L} + z_{1R}) \end{array} \right]. \tag{3.3.19}$$

The condition (3.3.18) on the other hand is

$$\left[\begin{array}{c} z_{1L}z_{2L} - z_{1R}z_{2R} \\ z_{2L}^2 + \varepsilon z_{1L}^{2\gamma} - z_{2R}^2 - \varepsilon z_{1R}^{2\gamma} \end{array} \right] = \left[\begin{array}{cc} c_1 & c_2 \\ c_3 & c_4 \end{array} \right] \left[\begin{array}{c} z_{1L} - z_{1R} \\ z_{2L} - z_{2R} \end{array} \right]$$

and gives

$$c_1(z_{1L} - z_{1R}) + c_2(z_{2L} - z_{2R}) = z_{1L}z_{2L} - z_{1R}z_{2R},$$
$$c_3(z_{1L} - z_{1R}) + c_4(z_{2L} - z_{2R}) = (z_{2L} - z_{2R})(z_{2L} + z_{2R}) + \varepsilon(z_{1L}^{2\gamma} - z_{1R}^{2\gamma}),$$

which is solved by the matrix C of the following form

$$C = \left[\begin{array}{cc} \frac{1}{2}(z_{2L} + z_{2R}) & \frac{1}{2}(z_{1L} + z_{1R}) \\ \varepsilon \dfrac{z_{1L}^{2\gamma} - z_{1R}^{2\gamma}}{z_{1L} - z_{1R}} & z_{2L} + z_{2R} \end{array} \right]. \tag{3.3.20}$$

Defining the average state

$$\overline{Z} = \frac{1}{2}(Z_L + Z_R) \tag{3.3.21}$$

and using the definition $A = CB^{-1}$ we get the Roe's matrix

$$A(U_L, U_R) = \left[\begin{array}{cc} 0 & 1 \\ \varepsilon\overline{\rho} - \overline{u}^2 & 2\overline{u} \end{array} \right], \tag{3.3.22}$$

where

$$\overline{\rho} = \frac{\rho_L^\gamma - \rho_R^\gamma}{\rho_L - \rho_R} \tag{3.3.23}$$

is the Roe-averaged density and

$$\overline{u} = \frac{\rho_L u_L \sqrt{\rho_R} + \rho_R u_R \sqrt{\rho_L}}{\sqrt{\rho_L \rho_R}(\sqrt{\rho_L} + \sqrt{\rho_R})} \tag{3.3.24}$$

is the Roe-averaged velocity.

Flux-vector splitting

We look for a splitting of

$$F(U) = \begin{pmatrix} \rho u \\ \rho u^2 + \varepsilon \rho^\gamma \end{pmatrix} \tag{3.3.25}$$

where $U = (\rho \quad \rho u)^T$ in the form

$$F(U) = F^+(U) + F^-(U)$$

such that the Jacobians J_{F^+}, J_{F^-} have respectively positive and negative eigenvalues. In this way we distinguish between forward and backward-moving waves. Following Steger and Warming approach we take

$$F^\pm = J_{F^\pm} \cdot U,$$

where

$$J_{F^\pm} = \frac{1}{2} R \cdot \text{diag} \left(\lambda_i \pm |\lambda_i| \right) \cdot R^{-1},$$

with λ_i eigenvalues of the Jacobian of F and R composed of its eigenvectors. Using the explicit form of the eigenvalues $\lambda_\pm = u \pm c$, where $c = \sqrt{P'(\rho)}$ is the speed of sound, we obtain

$$F^\pm = \begin{pmatrix} \rho u \pm \frac{1}{2}\rho(|u+c| + |u-c|) \\ \rho(u^2 + c^2) \pm |u+c|(u+c) \pm |u-c|(u-c) \end{pmatrix}.$$

However, as was pointed before, in this method $dF^\pm/dU$ are discontinuous at sonic points and at the vacuum, where eigenvalues coincide and become zero. It leads to oscillations in the numerical solutions. To fix this problem let us observe that the momentum $p = \rho u$ can be written as

$$\rho u = \frac{\rho}{4c}[(u+c)^2 - (u-c)^2],$$

which leads to the natural splitting for the first component of the flux F

$$F_1^\pm = \pm \frac{\rho}{4c}(u \pm c)^2. \tag{3.3.26}$$

Then using the relation $P(\rho) = \rho c^2/\gamma$ and the equality

$$c^2 = \frac{1}{2}[(u+c)^2 + (u-c)^2] - u^2$$

we obtain

$$F_2 = \frac{\rho u}{4c}[(u+c)^2 - (u-c)^2] + \frac{\rho}{\gamma}\left(\frac{1}{2}[(u+c)^2 + (u-c)^2] - u^2 \right).$$

Preserving the consistency we can decomposed the flux into

$$F_2^\pm = F_1^\pm \frac{(\gamma - 1)u \pm 2c}{\gamma}. \tag{3.3.27}$$

3.3.3 Godunov type schemes: approximate Riemann solvers

Finite difference method (FDM) is based on the approximation of the space derivatives at each node of the grid,however, the resulting numerical scheme is not always conservative. This property can be easily preserved using schemes based on the finite volume method (FVM). In this framework we divide a domain Ω into N control volumes Ω_i such that

$$\Omega = \bigcup_{i=1}^{N} \Omega_i, \quad \text{with } \Omega_i \cap \Omega_j = \emptyset \text{ if } i \neq j$$

and define cell averages as

$$\overline{U}_i(t) = \frac{1}{|\Omega_i|} \int_{\Omega_i} U(x,t)dx.$$

In one space dimension it means to consider cells $C_i = [x_{i-1/2}, x_{i+1/2})$, which are centered at nodes x_i or $C_i = [x_{i-1}, x_i)$ centered at $x_{i-1/2}$. They are called respectively vertex centered and cell centered finite volumes.

Let us consider vertex centered cells. A solution at time $t > 0$ to a general system of conservation laws

$$U_t + F(U)_x = 0, \tag{3.3.28}$$

is given by

$$U(x,t) = U(x,0) - \int_0^t F(U)_x ds. \tag{3.3.29}$$

Assuming the flux function is regular enough and integrating the above equation over the cell C_i we obtain the formula for the cells averages of the solution at time t

$$\overline{U}_i(t) = \overline{U}_i(0) - \frac{1}{\Delta x_i} \left(\int_0^t F_{i+1/2}dt - \int_0^t F_{i-1/2}dt \right), \tag{3.3.30}$$

where $\Delta x_i = x_{i+1/2} - x_{i-1/2}$. Discretization of time leads to

$$\overline{U}_i^{n+1} = \overline{U}_i^n - \frac{\Delta t}{\Delta x_i} \left(\mathcal{F}_{i+1/2} - \mathcal{F}_{i-1/2} \right) \tag{3.3.31a}$$

with

$$\mathcal{F}_{i+1/2} = \int_{t^n}^{t^{n+1}} F(U_{i+1/2}(t))dt. \tag{3.3.31b}$$

being a numerical flux function consistent with the flux $F(U)$.

To complete the scheme we need to find the numerical flux functions $\mathcal{F}_{i+1/2}$ and give the interpretation of the averages $\overline{U}$. In [46] Godunov proposed to consider a solution to (3.3.28) in the form of a piecewise constant function, which values at nodes x_i correspond to the averages over the cell C_i. This assumption generates a sequence of Riemann problems in each interval (x_{i-1}, x_i) that is

$$U_t + F(U)_x = 0 \quad \text{in } (x_{i-1}, x_i) \times \left(t^n, t^{n+1}\right) \tag{3.3.32a}$$

with the initial condition

$$U^n = \begin{cases} U_i^n & \text{if } x > x_{i-1/2} \\ U_{i-1}^n & \text{if } x < x_{i-1/2} \end{cases} \tag{3.3.32b}$$

Its exact solution is given by a self-similar form

$$U^{n+1}(x) = \mathcal{R}\left(\frac{x - x_{i-1/2}}{\Delta t}; U_{i-1}, U_i\right),$$ (3.3.33)

which connects the left and right states at the cell boundary $x_{i-1/2}$ in the time interval (t^n, t^{n+1}). It gives us a solution at the cell boundaries that we can use to calculate the fluxes F in (3.3.31b). Unfortunately solving a Riemann problem (3.3.32) at each cell boundary at each time step is very expensive computationally. In order to simplify the choice we can use approximate Riemann solver instead of the exact ones. In other words we assume a priori a specific structure of the wave pattern for the Riemann problem and limit in this way the number of possible configurations. In the literature there are two types of approximate Riemann solvers. For an approximate *state* Riemann solver we construct the interface values $U_{i+1/2}$ and then the fluxes using (3.3.31b). In an approximate *flux* Riemann solvers we approximate the fluxes directly avoiding the intermediate state, when the solutions of U at the cell boundaries is calculated.

Now we are going to present the most common approximate Riemann solvers, for which the wave structure of Riemann problem consist of a finite number $m > 0$ of discontinuities. To simplify the notation let us consider two states and a Riemann problem in the form

$$\begin{cases} U_t + F(U)_x = 0 \\ U(x, 0) = \begin{cases} U_L & x < 0 \\ U_R & x > 0 \end{cases} \end{cases}$$ (3.3.34)

Denoting by

$$-\infty = \sigma_0 < \sigma_1 < \cdots < \sigma_m < \sigma_{m+1} = \infty$$

speeds of the discontinuities and by

$$U_L = U_0, U_1, \ldots, U_{m-1}, U_m = U_R.$$

the intermediate states separated by them, the self-similar solution joining U_L with U_R at time t is

$$\mathcal{R}\left(x/t; U_L, U_R\right) = \begin{cases} U_L & x/t < \sigma_1 \\ U_1 & \sigma_1 < x/t < \sigma_2 \\ \vdots & \\ U_k & \sigma_k < x/t < \sigma_{k+1} \\ \vdots & \\ U_{m-1} & \sigma_{m-1} < x/t < \sigma_m \\ U_R & \sigma_m < x/t \end{cases}.$$

This type of solvers are called simple solvers.

From the numerical point of view we are interested in the solution at point $x = 0$ that is

$$U_0 = U(0, t) = \mathcal{R}(0; U_L, U_R),$$

which corresponds to finding the values of interface states $U_{i+1/2}$. In fact, to obtain a numerical scheme a flux at $x = 0$

$$\mathcal{F}_0 = F\left(\mathcal{R}(0; U_L, U_R)\right),$$

is needed. Because the wave structure of the Riemann problem consist of m intermediate states, it is equivalent to constructing intermediate fluxes

$$F_L = F_0, F_1, \ldots, F_{m-1}, F_m = F_R.$$

This goal is obtained using the Rankine-Hugoniot conditions across the discontinuities. More precisely

$$F_{k+1} - F_k = \sigma_{k+1} \left(U_{k+1} - U_k \right),$$

and by iterations

$$
\begin{aligned}
F_k &= F_L + \sum_{\sigma_k < 0} \sigma_k (U_k - U_{k-1}) \\
&= F_R - \sum_{\sigma_k > 0} \sigma_k (U_k - U_{k-1}).
\end{aligned}
$$

Roe's method

An exact Riemann solver is easy to find for systems of linear conservation laws. Taking advantage of this property Roe in [103] constructed an approximate Riemann solver for (3.3.34) solving exactly its approximation in the form

$$
\begin{cases}
U_t + A U_x = 0 \\
U(x, 0) = \begin{cases} U_L & x < 0 \\ U_R & x > 0 \end{cases}
\end{cases}
\tag{3.3.35}
$$

The matrix $A = A(U_L, U_R)$ is Roe's matrix with a complete set of eigenvalues $\sigma_k = \sigma_k(U_L, U_R)$ and the corresponding eigenvectors $\xi_k = \xi_k(U_L, U_R)$ for $k = 1, \ldots, m$. Moreover it is assumed that there exists an integer $k_0 > 1$ such that $\sigma_{k_0} < 0 < \sigma_{k_0+1}$. In this case to find the numerical flux function $\mathcal{F}_0$ for the system (3.3.34) we can separate the influence of waves with positive and negative velocities. Integrating (3.3.34) between extreme intervals $[\sigma_1 T, 0] \times [0, T]$ and $[0, \sigma_m T] \times [0, T]$, or equivalently using the Rankine-Hugoniot conditions, we obtain

$$F_0^- = F_L - \sigma_1 U_L - \frac{1}{T} \int_{T\sigma_1}^0 U(x, T) dx$$

$$F_0^+ = F_R - \sigma_m U_R + \frac{1}{T} \int_0^{T\sigma_m} U(x, T) dx$$

(3.3.36)

Approximate Riemann solver of Roe is based on an approximation of the integrals in (3.3.36) using the exact Riemann solver $\mathcal{R}(x/T; U_L, U_R)$ for (3.3.35). More precisely we approximate

$$\frac{1}{T} \int_{T\sigma_1}^0 U(x, T) dx = \frac{1}{T} \int_{T\sigma_1}^0 \mathcal{R}(\frac{x}{T}; U_L, U_R) dx = A U_L A \mathcal{R}(0^-; U_L, U_R) - \sigma_1 U_L$$

$$\frac{1}{T} \int_0^{T\sigma_m} U(x, T) dx = \frac{1}{T} \int_0^{T\sigma_m} \mathcal{R}(\frac{x}{T}; U_L, U_R) dx = A \mathcal{R}(0^+; U_L, U_R) - A U_R + \sigma_m U_R$$

(3.3.37)

where the second equality is a result of the Rankine-Hugoniot condition applied to (3.3.35). Self-similar Riemann solutions $\mathcal{R}(0^+; U_L, U_R)$. $\mathcal{R}(0^-; U_L, U_R)$ are averages on the intervals $[x_L = \sigma_1 T, 0], [0, x_R = \sigma_m T]$ respectively of the solution to the problem (3.3.35) at time T

$$\mathcal{R}(0^-; U_L, U_R) = -\frac{1}{\sigma_1 T} \int_{T\sigma_1}^0 U(x, T) dx$$

$$\mathcal{R}(0^+; U_L, U_R) = \frac{1}{\sigma_m T} \int_0^{T\sigma_m} U(x, T) dx \tag{3.3.38}$$

To find these averages we integrate (3.3.35) between $[\sigma_1 T, 0] \times [0, T]$ and $[0, \sigma_m T] \times [0, T]$, as before, thus get

$$\int_{T\sigma_1}^0 U(x, T) dx = -T\sigma_1 U_L - TA(U_0^- - U_L)$$

$$\int_0^{T\sigma_m} U(x, T) dx = T\sigma_m U_R + TA(U_0^+ - U_R) \tag{3.3.39}$$

Projecting $\Delta U = U_R - U_L$ onto the right eigenvectors

$$U_R - U_L = \sum_{k=1}^m \alpha_k \xi_k, \quad \text{for } \alpha_k \geq 0, \tag{3.3.40}$$

and making use of the eigenvalue problem $A\xi_k = \sigma_k \xi_k$ we get

$$\mathcal{R}(0^-; U_L, U_R) = U_L + \sum_{k=1}^{k_0} \widetilde{\alpha_k^1} \xi_k, \quad \text{where } \widetilde{\alpha}_k^1 = \frac{\sigma_k}{\sigma_1} \alpha_k. \tag{3.3.41a}$$

or

$$\mathcal{R}(0^+; U_L, U_R) = U_R - \sum_{k=k_0+1}^m \widetilde{\alpha_k^m} \xi_k, \quad \text{where } \widetilde{\alpha}_k^m = \frac{\sigma_k}{\sigma_m} \alpha_k. \tag{3.3.41b}$$

Inserting $\mathcal{R}(0^\pm; U_L, U_R)$ in (3.3.36) and (3.3.39) yields

$$F_0^- = F_L + \sum_{k=1}^{k_0} \widetilde{\alpha}_k^1 \sigma_k \xi_k$$

$$F_0^+ = F_R - \sum_{k_0+1}^m \widetilde{\alpha}_k^m \sigma_k \xi_k$$

The flux function $\mathcal{F}_0$ can be taken as an arithmetic mean that is

$$\mathcal{F}_0^{Roe} = \frac{1}{2}(F_L + F_R) - \frac{1}{2} \sum_{k=1}^m \widetilde{\alpha}_k |\sigma_k| \xi_k, \tag{3.3.42}$$

To obtain numerical fluxes we need explicit forms of eigenvalues and eigenvectors of the matrix A and the parameters $\widetilde{\alpha}_k$. Originally Roe found the structure of the eigenproblem for the matrix A directly, as we showed previously for the isothermal gas dynamics equations, and the

coefficients α_k from the relation (3.3.40). A different approach is due to Roe and Pike [105], in which the explicit calculation of the matrix A is avoided. The method is based on the assumption that the system is hyperbolic and it is possible to find the analytical expressions for σ_k and ξ_k, while $\widetilde{\alpha}_k$ are sought from the extra linearization around a reference state $\hat{U}$ such that $|U_{L,R} - \hat{U}| \sim \Delta x^2$.

The linearized approximate Riemann solver is an example of a simple solver. It contains only discontinuous jumps in the wave pattern of the Riemann problem, which means that only character of contact discontinuities and shocks can be approximated correctly. Transonic and sonic rarefaction waves carry continuous change in flow variables and spread in time so their gradients tend to decay. Numerical approximations based on linearization can produce discontinuities in the rarefaction waves, which are unphysical and lead to the violation of the entropy condition. Entropy fix methods, presented in general case by Harten and Hyman in [56], modify Roe's solver such that the resulting scheme is entropy satisfying.

HLL/HLLC solvers

A simple approximate Riemann solver that converges to weak solutions and satisfies entropy condition was introduced in 1983 by Harten, Lax and Leer [57]. It assumes that the solution consists of three constant states separated by two waves with velocities σ_L and σ_R corresponding respectively to the slowest and fastest signal speed. However, even if based on this solver we can construct an efficient numerical scheme, due to the two-wave configuration, it gives correct results only for hyperbolic systems consisting of two equations such as isentropic gas dynamics system in one space dimension. It causes a failure of the approximation at contact surfaces, shear waves of material interfaces. In order to fix this problem an additional wave with speed σ^*, a contact discontinuity, was introduced leading to the HLLC solver. The structures of the solvers are presented at Figure 3.2. However, both of the solvers are obtained under the assumption that the wave speeds $\sigma_L, \sigma^*, \sigma_R$ are known and to construct a scheme they have to be estimated at first.

Let us focus now on the derivation of the intermediate flux in the HLL solver F^{HLL}. We integrate the conservation law (3.3.34) in the control volume $[x_L, x_R] \times [0, T]$ such that $x_L \leq T\sigma_L$ and $x_R \geq T\sigma_R$

$$\int_{x_L}^{x_R} U(x,T)dx = \int_{x_L}^{x_R} U(x,0)dx + \int_0^T F(U(x_L,t))dt - \int_0^T F(U(x_R,t))dt. \quad (3.3.43)$$

Evaluating the integrals we obtain

$$\int_{T\sigma_L}^{T\sigma_R} U(x,T)dx + (T\sigma_L - x_L)U_L + (x_R - T\sigma_R)U_R = x_R U_R - x_L U_L + T(F_L - F_R), \quad (3.3.44)$$

where we used the fact that in the intervals $[x_L, T\sigma_L]$ and $[T\sigma_R, x_R]$ the solution $U(x,T)$ is given by the initial data. Dividing the both sides of (3.3.43) by $T(\sigma_R - \sigma_L)$ we get

$$\frac{1}{T(\sigma_R - \sigma_L)} \int_{T\sigma_L}^{T\sigma_R} U(x,T)dx = \frac{\sigma_R U_R - \sigma_L U_L + F_L - F_R}{\sigma_R - \sigma_L}.$$
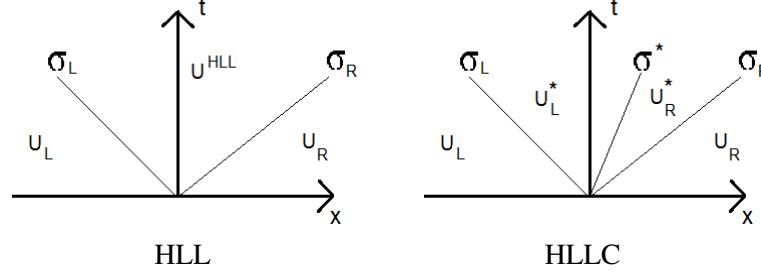
Figure 3.2: Structure of the wave pattern in the HLL and HLLC approximate Riemann solvers.

The left hand side is an integral average in $[\sigma_L T, \sigma_R T]$ of the exact solution at time T and can be associated with the middle state U^{HLL} yielding

$$U^{HLL} = \frac{\sigma_R U_R - \sigma_L U_L + F_L - F_R}{\sigma_R - \sigma_L}. \tag{3.3.45}$$

To find the flux F^{HLL} we use Rankine-Hugoniot conditions across the two waves and the above formula for the intermediate state U^{HLL} obtaining

$$F^{HLL} = \frac{\sigma_R F_L - \sigma_L F_R + \sigma_L \sigma_R (U_R - U_L)}{\sigma_R - \sigma_L} \tag{3.3.46}$$

It leads to the numerical flux function $\mathcal{F}_{i+1/2}$ of the form

$$\mathcal{F}_{i+1/2}^{HLL} = \begin{cases} F_L & 0 \geq \sigma_L \\ \frac{\sigma_R F_L - \sigma_L F_R + \sigma_L \sigma_R (U_R - U_L)}{\sigma_R - \sigma_L} & \sigma_L \leq 0 \leq \sigma_R \\ F_R & \sigma_R \leq 0 \end{cases} . \tag{3.3.47}$$

Remark 4. *To define the HLL approximate Riemann solver we need estimates of σ_L, σ_R to calculate the flux. To simplify it we can assume that the waves have equal speeds and travel in opposite directions. That is why we take $\sigma_+ = \sigma > 0$ for the positive wave and then $\sigma_- = -\sigma$ for the negative one. Substituting these values into the flux F^{HLL} we obtain so called Rusanov flux*

$$F^{Rusanov} = \frac{1}{2}(F_L + F_R) - \frac{\sigma}{2}(U_R - U_L).$$

The HLL approximate Riemann solver is very simple, satisfies entropy inequalities and gives good approximations in the presence of sonic rarefactions. However, the lack of the middle wave in the structure of the solution results in high diffusivity for waves corresponding to multiple eigenvalues so at contact discontinuities, shear waves and material interfaces.

In [113] the authors added a missing wave, the contact wave, which divides the intermediate region between σ_L and σ_R into two sub regions with states U_L^* and U_R^*. The resulting HLLC approximate Riemann solver, where C stands for "contact", has numerical flux function of the form

$$\mathcal{F}_{i+1/2}^{HLLC} = \begin{cases} F_L & 0 \geq \sigma_L \\ F_L^* & \sigma_L \leq 0 \leq \sigma^* \\ F_R^* & \sigma^* \leq 0 \leq \sigma_R \\ F_R & \sigma_R \leq 0 \end{cases} . \tag{3.3.48}$$

The intermediate fluxes F_L^*, F_R^* have to be found from the Rankine-Hugoniot conditions, but the intermediate states U_L^*, U_R^* are also unknown so we have more unknowns than equations and need to impose additional conditions. Let us consider, as an example, the one dimensional Euler system

$$U_t + F(U)_x = 0 \tag{3.3.49a}$$

where

$$U = \begin{pmatrix} \rho \\ \rho u \\ E \end{pmatrix} \quad \text{and} \quad \begin{pmatrix} \rho u \\ \rho u^2 + P \\ u(E + P) \end{pmatrix}. \tag{3.3.49b}$$

It can be assumed that velocity u and pressure P are constant across the central wave

$$\begin{aligned} u_L^* = u_R^* = u^* = \sigma^* \\ P_L^* = P_R^* = P^* \end{aligned} \tag{3.3.50}$$

Then using the explicit form of the fluxes F_L^*, F_R^* from the Rankine-Hugoniot conditions and the assumptions (3.3.50) we obtain

$$U_K^* = \rho_K \frac{\sigma_K - u_K}{\sigma_K - \sigma^*} \left[\begin{array}{c} 1 \\ \sigma^* \\ \frac{E_k}{\rho_K} + (\sigma^* - u_K)\left[\sigma^* + \frac{P_K}{\rho_K(\sigma_K - u_K)}\right] \end{array} \right], \quad \text{K=L,R} \tag{3.3.51}$$

which determine also the intermediate fluxes.

As was already mentioned the HLL and HLLC approximate Riemann solvers assume that the wave velocities $\sigma_L, \sigma^*, \sigma_R$ and the pressure P^* are given. In order to construct a numerical scheme first we have to estimate them. There are two families of methods to find their values. They are divided into direct and pressure-velocity estimates methods. In the former the wave speed is obtained using only data values. For example:

- Bounds for minimum and maximum values

$$\sigma_L = \min\{u_L - c_L, u_R - c_R\}, \quad \sigma_R = \max\{u_L + c_L, u_R + c_R\}$$

  where $c = \sqrt{P'(\rho)}$ is the sound speed.

- Estimates based on Roe's averages

$$\sigma_L = \widetilde{u} - \widetilde{c}, \quad \sigma_L = \widetilde{u} + \widetilde{c}$$

where $\widetilde{\rho}$, $\widetilde{u}$ are averaged Roe's density and velocity. In the case $P(\rho) = \varepsilon \rho^\gamma$ they are given by (3.3.23), (3.3.24).

The later method uses also the pressure and velocity at the middle states, which still have to be found. For a more detailed description we send to [114].

Suliciu Relaxation solver for Euler equations

An exact Riemann solver is easy to find when we deal with a linear system of conservation laws. Another case for which it is not expensive computationally is when a system has only linearly degenerate eigenvalues. For the isentropic gas dynamics equations Suliciu in [**?**] introduced a relaxation system consisting of only linearly degenerate fields. The same as for the approximate solver of Roe, we find an exact Riemann solver of the relaxation system. As it approximates the original problem we obtain in this its approximate Riemann solver. Moreover it can be adopted to treat the vacuum in the following sense. We say that an approximate Riemann solver can resolve vacuum if for two values U_L, U_R, from which only one is zero, under positive CFL condition bigger it gives a nonnegative density and finite speed of propagation. In fact, when both states equal zero there is no problem as we can take $\mathcal{R} = 0$ in (3.3.33). We are going to present the Suliciu relaxation system for isentropic gad dynamics system following [17].

A relaxation approximation of a conservation law

$$U_t + F(U)_x = 0, \qquad U \in \mathbb{R}^p \tag{3.3.52}$$

is a system

$$f_t + \mathcal{A}(f)_x = 0, \qquad f \in \mathbb{R}^q, q > p \tag{3.3.53}$$

and a linear operator $\mathcal{L} : \mathbb{R}^q - \mathbb{R}^p$ such that

$$\forall U \in \mathbb{R}^p \exists M(U) \in \mathbb{R}^q : \left\{ \begin{array}{l} \mathcal{L}(M(U)) = U \\ \mathcal{L}(\mathcal{A}(M(U))) = F(U) \end{array} \right. , \tag{3.3.54}$$

where $M(U)$ is a Maxwellian equilibrium. The above conditions are compatibility conditions linking the two systems. Solving the approximate problem, the solution

$$U \equiv \mathcal{L}f$$

should be an approximation of the solution to the original one. The construction of an approximate Riemann solver for (3.3.52) is based on the following proposition.

Proposition 1. *Let $\mathcal{R}(x/t; f_L, f_R)$ be an approximate Riemann solver for the relaxation system (3.3.53). Then*

$$R(x/t; U_L, U_R) = \mathcal{L}\mathcal{R}\left(x/t; M(U_L), M(U_R)\right)$$

is an approximate Riemann solver for (3.3.52)

When the relaxation system has all eigenvalues linearly degenerate, the solver $\mathcal{R}$ is exact. Let us start with a derivation of Suliciu relaxation system for

$$\left\{ \begin{array}{l} \rho_t + (\rho u)_x = 0 \\ (\rho u)_t + (\rho u^2 + P(\rho))_x = 0 \end{array} \right.$$

Multiplying the first equation by $P(\rho)$ and by $\rho P'(\rho)$, summing the two new relation, we obtain the equation for the pressure in conservative form

$$(\rho P(\rho))_t + (\rho u P(\rho))_x + \rho^2 P'(\rho)u_x = 0.$$

Introducing a new variable π equal to $P(\rho)$ and denoting by a constant $c^2 = \rho^2 P'(\rho)$ yields a relaxation system with unknown vector $f = (\rho, \rho u, \rho \pi)$

$$\begin{cases} \rho_t + (\rho u)_x = 0 \\ (\rho u)_t + (\rho u^2 + \pi)_x = 0 \\ (\rho \pi)_t + (\rho u \pi)_x + c^2 u_x = 0 \end{cases} . \qquad (3.3.55)$$

The solution to the original system is given by

$$U = \mathcal{L}(f_1, f_2, f_3) = (f_1, f_2).$$

while the Maxwellians are

$$M(\rho, \rho u) = (\rho, \rho u, \rho P(\rho)).$$

The eigenvalues of (3.3.55) have the form

$$\sigma_1 = u - \frac{c}{\rho}, \quad \sigma_2 = u, \quad \sigma_3 = u + \frac{c}{\rho}$$

and are all linearly degenerate leading to only contact discontinuities in the wave pattern. However, the suitable choice of the parameter c is crucial in order to preserve the positiveness of the density.

Unfortunately the above approach cannot treat the vacuum in the sense explained before. To see this, let us take $\rho_L = 0$ and $\rho_R > 0$. Then, since the extreme eigenvalues are $u_L - c/\rho_L$, $u_R + c/\rho_R$, unless $c \to 0$ the propagation speed would tend to infinity. But the relation $c^2 = \rho_R^2 P'(\rho_R)$ implies that c cannot be zero because we assumed $\rho_R > 0$. In order to adopt the method to treat the vacuum states parameter c is chosen to be non-constant and satisfies

$$c_t + u c_x = 0.$$

Multiplying (3.3.3) by ρ and using the continuity equation for ρ we can transform it into the conservative form. The resulting relaxation system has the form

$$\begin{cases} \rho_t + (\rho u)_x = 0 \\ (\rho u)_t + (\rho u^2 + \pi)_x = 0 \\ (\rho \pi)_t + (\rho u \pi)_x + c^2 u_x = 0 \\ (\rho c)_t + (\rho u c)_x = 0 \end{cases} , \qquad (3.3.56)$$

where again all eigenvalues linearly degenerate. A wave pattern of the Riemann solver is presented at Figure 3.3, where the wave speeds equal

$$\sigma_1 = u_L - \frac{c_L}{\rho_L}, \quad \sigma_2 = u_L^* = u_R^*, \quad \sigma_3 = u_R + \frac{c_R}{\rho_R}$$

with $c_L^* = c_L$, $c_R^* = c_R$. The intermediate fluxes are

$$F_L^* = \begin{pmatrix} \rho_L^* u_L^* \\ \rho_L^* (u_L^*)^2 + \pi_L^* \end{pmatrix}, \qquad F_R^* = \begin{pmatrix} \rho_R^* u_R^* \\ \rho_R^* (u_R^*)^2 + \pi_R^* \end{pmatrix} \qquad (3.3.57)$$
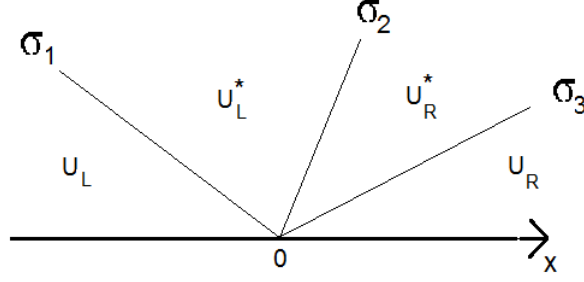
Figure 3.3: Structure of the wave pattern in the Suliciu approximate Riemann solver.

and the intermediate states are obtained from the jump relations across the discontinuities

$$u_L^* = u_R^* = \frac{c_L u_L + c_R u_R + \pi_L - \pi_R}{c_L + c_R},$$

$$\pi_L^* = \pi_R^* = \frac{c_R \pi_L + c_L \pi_R - c_L c_R (u_R - u_L)}{c_L + c_R},$$

$$\frac{1}{\rho_L^*} = \frac{1}{\rho_L} + \frac{c_R(u_R - u_L) + \pi_L - \pi_R}{c_L(c_L + c_R)},$$

$$\frac{1}{\rho_R^*} = \frac{1}{\rho_R} + \frac{c_L(u_R - u_L) + \pi_R - \pi_L}{c_R(c_L + c_R)}.$$

(3.3.58)

The positiveness of ρ_L^*, ρ_R^* is assured by the suitable choice of c_L, c_R stated in the following proposition.

Proposition 2. *Let (3.3.58) holds. If c_L, c_R are such that $\rho_L, \rho_R, \rho_L^*, \rho_R^*$ are positive and satisfy*

$$\begin{array}{ll} \forall \quad \rho \in [\rho_L, \rho_L^*], & \rho^2 P'(\rho) \le c_L^2 \\ \forall \quad \rho \in [\rho_R, \rho_R^*], & \rho^2 P'(\rho) \le c_R^2 \end{array}$$

then the approximate Riemann solver preserves positiveness of density and is entropy satisfying.

It is a sub characteristic condition assuring that the eigenvalues of the original system, to be solved, lay between the eigenvalues of the relaxation system. A possible choice for c_L, c_R is

$$\text{if } P_R - P_L \ge 0, \quad \begin{cases} \dfrac{c_L}{\rho_L} = \sqrt{P'(\rho_L)} + \alpha \left(\dfrac{P_R - P_L}{\rho_R \sqrt{P'(\rho_R)}} + u_L - u_R \right)_+, \\[4mm] \dfrac{c_R}{\rho_R} = \sqrt{P'(\rho_R)} + \alpha \left(\dfrac{P_L - P_R}{c_L} + u_L - u_R \right)_+, \end{cases}$$

(3.3.59)

$$\text{if } P_R - P_L \le 0, \quad \begin{cases} \dfrac{c_R}{\rho_R} = \sqrt{P'(\rho_R)} + \alpha \left(\dfrac{P_L - P_R}{\rho_L \sqrt{P'(\rho_L)}} + u_L - u_R \right)_+, \\[4mm] \dfrac{c_L}{\rho_L} = \sqrt{P'(\rho_L)} + \alpha \left(\dfrac{P_R - P_L}{c_R} + u_L - u_R \right)_+. \end{cases}$$

obtained under assumptions

$$\forall \quad \rho > 0, \qquad \frac{d}{d\rho}\left(\rho\sqrt{P'(\rho)}\right) > 0$$
$$\rho\sqrt{P'(\rho)} \to 0 \quad \text{as} \quad \rho \to \infty$$
$$\frac{d}{d\rho}\left(\rho\sqrt{P'(\rho)}\right) \le \alpha\sqrt{P'(\rho)}, \quad \text{for some constant } \alpha \ge 1$$

3.4 Approximation of the source term

In the previous sections we presented finite differences and finite volumes schemes to approximate homogeneous systems of conservation laws. There are many efficient and accurate methods for this kind of problems. However, models originating in real problems hardly are homogeneous. In hyperbolic systems processes like friction, stresses, gravity or chemotaxis forces are introduced via source terms. Moreover, in many physical problems source terms have specific mathematical properties and imply constraints on numerical approximations. One of the issue we have to face with during a construction of a numerical scheme is stability in the stiff regimes, where the characteristic time step of the source part is much smaller than of the convective part. As an example we can mention very high friction term in Euler equations. Another constraint comes from geometrical character of the source, that is when it has a structure similar to the transport term. The specific balance between internal forces and the source terms leads to non constant stationary solutions. It is highly desirable that numerical schemes preserve these states. What is more important, solutions of hyperbolic models very often have parabolic asymptotics and preserving them in the long time limit under suitable convergence of the boundary fluxes is often required. It is well known that splitting techniques, like fractional steps of ODE methods, don't have the desired properties, unless used on very fine meshes.

3.4.1 Upwinding the sources

At first it was observed by Roe [104] that in the numerical approximation of balance laws the source term should be upwinded in the same way as the physical flux. To justify this he considered a scalar Cauchy problem

$$\begin{cases} u_t + a u_x = s(u), & a = constant > 0 \\ u(x,0) = u_0(x) \end{cases}.$$

The general solution is

$$u(x,t) = u_0(x - at) + \frac{1}{a}\int_{x-at}^{x} s(u(x,t))dx$$

and on a discrete level on a regular grid at time t^{n+1}

$$u(i\Delta x, (n+1)\Delta t) = u((i-\nu)\Delta x, n\Delta t) + \frac{1}{a}\int_{(i-\nu)\Delta x}^{i\Delta x} s(u(x))dx,$$

where $\nu = a\Delta t/\Delta x$ is the Courant number. The integral term has an upwind domain of dependence. The lower limit of integration doesn't need to be an integer. Assuming $\nu \le 1$ it is

contained between the nodes $(i-1)\Delta x$ and $i\Delta x$. To obtain the numerical scheme we still need an accurate approximation of the integral. Following Roe, for a (2k+1)-points support scheme, it can approximated as

$$\frac{1}{a} \int_{(i-\nu)\Delta x}^{i\Delta x} s(u(x))dx = \Delta t \sum_{j=-k}^{k} \alpha_k s_{i+j} + O(\Delta x, \Delta t),$$

with a consistency condition $\sum_{i=-k}^{k} \alpha_i = 1$.

The concept of treating source terms in the same way as the convective part was generalized to systems of conservation laws with sources

$$U_t + F(U)_x = S(U). \tag{3.4.1}$$

In the finite volume formalism a semi discrete scheme for the above system can be put in the following form

$$\Delta x \frac{d}{dt} U_i(t) + \left(F_{i+1/2} - F_{i-1/2}\right) = S_i. \tag{3.4.2}$$

The fluxes $F_{i+1/2}$ are approximated by any consistent numerical flux function for a homogeneous problem. The idea is to discretize the source term at interfaces in the same way as the flux. In other words, to upwind it by introducing a numerical source function $\mathcal{S}$ such that

$$S_i = \mathcal{S}_{i-1/2}^+ + \mathcal{S}_{i+1/2}^-. \tag{3.4.3}$$

The term $\mathcal{S}_{i+1/2}^-$ is the contribution of waves coming from the right boundary of the cell $\mathcal{C}_i$ if they have non positive velocity, so moving towards the cell, while the term $\mathcal{S}_{i-1/2}^+$ represents the waves with nonnegative velocities coming from the left boundary.

In [98], [69], [18] the authors presented a general formalism for the Upwind Interface Source Method (USI), which is based on this kind of splitting of the source term. In the finite volume formalism decomposition (3.4.3) gives the average value of the source over the cell $\mathcal{C}_i = [x_{i-1/2}, x_{i+1/2})$

$$\mathcal{S}_{i-1/2}^+ + \mathcal{S}_{i+1/2}^- \sim \int_{\mathcal{C}_i} S(u)dx. \tag{3.4.4}$$

so the average between the nodes x_i and x_{i+1} can be associated with

$$\mathcal{S}_{i+1/2}^+ + \mathcal{S}_{i+1/2}^- \sim \int_{x_i}^{x_{i+1/2}} S(u)dx + \int_{x_{i+1/2}}^{x_{i+1}} S(u)dx. \tag{3.4.5}$$

In [98] the authors gave the rigorous definition of the consistency of the scheme (3.4.2), (3.4.3) with (3.4.1).

Definition 2. *A numerical scheme (3.4.2), (3.4.3) is consistent with (3.4.1) if*

$$\mathcal{F}(U, U) = F(U) \tag{3.4.6}$$

and

$$\lim_{\Delta x \to 0} \frac{\mathcal{S}^+(U, U, \Delta x) + \mathcal{S}^-(U, U, \Delta x)}{\Delta x} = S(U) \tag{3.4.7}$$

locally uniformly in U.

Moreover, they proved the Lax-Wendroff convergence theorem under the above conditions.

3.4.2 Well-balancing

The presence of source terms leads to non constant stationary solutions. It is a result of the balance between internal forces and reactions. In many physical problems these steady states are very important and their correct numerical approximation is essential. When dealing with a homogeneous case we are equipped with a fundamental tool which is the Riemann problem used to obtain a Godunov type scheme. In a non homogeneous system we could solve approximately a generalized Riemann problem, however, this approach is usually very complicated. In [50] Greenberg and LeRoux presented an original approach to treat the sources in a Godunov type scheme for

$$u_t + f(u)_x + a_x(x)u = 0,$$

where f is a smooth function such that $f(0) = 0$, $f'(0) = 0$, $f'' > 0$ and $a(x)$ is a smooth, nonnegative function. The idea was to get rid of the error coming from the treatment of the convective and reactive part at different time stages. They introduced the notion of well-balanced scheme, that is a scheme preserving some discrete version of stationary equation.

More precisely, let us consider a one dimensional balance law

$$u_t + f(u)_x = s(u). \tag{3.4.8}$$

Instead of solving the above equation we introduce an augmented problem

$$\begin{cases} u_t + f(u)_x = s(u)a_x \\ a_t = 0 \end{cases}, \tag{3.4.9}$$

where the function $x \to a(x)$ is in $C^1(\mathbb{R})$ and such that $a_x = 1$. As long as $f'(u) \geq \alpha > 0$ this system can be solved in the framework of Greenberg and LeRoux that is

$$u^{n+1} = u_i^n - \frac{\Delta t}{\Delta x}(f(u_i) - f(u^*)), \tag{3.4.10}$$

with u^* calculated from a stationary relation $f(u)_x = s(u)a_x$. Introducing a function ϕ such that

$$\phi'(u) = \frac{f'(u)}{s(u)}$$

the state u^* is defined as follows

$$\begin{array}{ll} \phi(u^*) - \phi(u_{i-1}) = \Delta x & \text{if } s(u_{i-1}) \neq 0 \\ u^* = u_{i-1} & \text{if } s(u_{i-1}) = 0 \end{array}.$$

Treating $a(x)$ as a smooth function is computationally very expensive as the solution depends on the specific form of generalized Riemann solvers. Instead the function $a(x)$ is localized on grid points and becomes piecewise constant over the cells. We will denote it by $a^{\Delta x}$. The condition $a_x = 1$ at a discrete level is satisfied for $a_i^{\Delta x} = i\Delta x$. But this approximation creates difficulties. Solutions to hyperbolic system are likely to be discontinuous, so the source $s(u)a_x^{\Delta x}$ can be seen as a "Heaviside×Dirac" product. The precise meaning of such non conservative terms is crucial for the notion of weak solutions and was studied for example in [24], [75], [29]. In the latter one Dal Maso, LeFloch and Murat defined non-conservative products as Borel measures on a family of locally Lipschitz paths. The solution of the Riemann

problem between states U_L and U_R is obtained choosing a suitable path. In this framework, the well-balancing property is achieved by taking as a path the integral curve of the steady state equation starting at the state U_L. In other words, we join U_L and U_R through a middle point lying on the mentioned integral curve.

Let us now present a generalization of the Greenberg- LeRoux approach to systems

$$U_t + F(U)_x = S(U) \tag{3.4.11}$$

As before we introduce an augmented problem

$$\begin{cases} U_t + F(U)_x = S(U)a^{\Delta x} \\ a_t^{\Delta x} = 0 \end{cases} . \tag{3.4.12}$$

A general numerical scheme approximating it can be put in the form

$$\begin{cases} U_i^{n+1} = U_i^n - \frac{\Delta t}{\Delta x}\left(F_{i+1/2}^- - F_{i-1/2}^+ \right) \\ (a^{\Delta x})_i^{n+1} = (a^{\Delta x})_i^n \end{cases} \tag{3.4.13}$$

where $F_{i+1/2}^\pm$ are defined using the negative and positive numerical fluxes

$$F_{i+1/2}^- = F^-(U_i, U_{i+1}), \quad F_{i+1/2}^+ = F^+(U_i, U_{i+1}). \tag{3.4.14}$$

If the flux function $F(U)$ doesn't have critical points, it is possible to find states $U_{i+1/2}^+$ and $U_{i+1/2}^-$ solving

$$F(U_{i+1/2}^-) - F(U_i) = S(U_i, U_{i+1})\Delta a^{\Delta x}$$
$$F(U_{i+1}) - F(U_{i+1/2}^+) = S(U_i, U_{i+1})\Delta a^{\Delta x} \tag{3.4.15}$$

where $S(U_i, U_{i+1})$ is some consistent approximation of the source term and

$$\Delta a^{\Delta x} = a_{i+1}^{\Delta x} - a_i^{\Delta x} = \Delta x$$

. Then defining the negative and positive numerical flux by

$$F^-(U_i, U_{i+1}) = \mathcal{F}(U_i, U_{i+1/2}^-), \quad F^+(U_i, U_{i+1}) = \mathcal{F}(U_{i+1/2}^+, U_i), \tag{3.4.16}$$

where $\mathcal{F}$ is any consistent C^1 numerical flux for a homogeneous problem, the scheme (3.4.13), (3.4.14), (3.4.15) and (3.4.16) is well-balanced and consistent with the original system (3.4.11).

The solution at the center of a cell C_i at time step t^{n+1} depends on the solution of two Riemann problems at the boundaries of the cell. At the right boundary at $x_{i+1/2}$ we solve a Riemann problem with left and right states U_i and U_{i+1} respectively, and at the left boundary a Riemann problem is solved to connect U_{i-1} and U_i. Moreover, the well balancing property is assured by choosing the middle points $U_{i+1/2}^-, U_{i+1/2}^+$ laying on the integral curve of the steady state equation as shown at Figure 3.4.
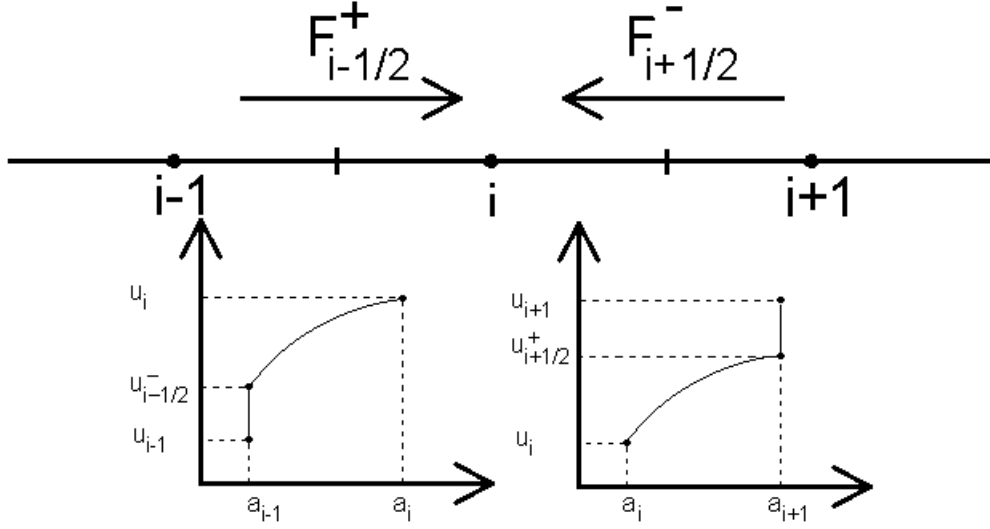
Figure 3.4: Riemann problems at the boundaries of the cell C_i for system (3.4.12).

A well-balanced scheme can be also defined in the framework of USI method. Assuming the states $U_{i+1/2}^-, U_{i+1/2}^+$ solve (3.4.15) we define

$$
\begin{aligned}
F^-(U_i, U_{i+1}) &= \mathcal{F}(U_{i+1/2}^-, U_{i+1/2}^+) - F(U_{i+1/2}^-) + F(U_i) \\
F^+(U_i, U_{i+1}) &= \mathcal{F}(U_{i+1/2}^-, U_{i+1/2}^+) - F(U_{i+1/2}^+) + F(U_{i+1})
\end{aligned}
\tag{3.4.17}
$$

As before $\mathcal{F}$ denotes an approximate Riemann solver for a homogeneous system. Using (3.4.17) the scheme (3.4.13) can be written in the following form

$$
U_i^{n+1} = U_i^n - \frac{\Delta t}{\Delta x}(F_{i+1/2} - F_{i-1/2}) + \Delta t S_i,
$$

where $F_{i+1/2} = \mathcal{F}(U_{i+1/2}^-, U_{i+1/2}^+)$ and

$$
S_i = \frac{1}{\Delta x}(F(U_{i+1/2}^-) - F(U_i) + F(U_i) - F(U_{i-1/2}^+)).
$$

The finite volume formalism implies

$$
\begin{aligned}
\frac{1}{\Delta x}(F(U_{i+1/2}^-) - F(U_i)) &= \frac{1}{\Delta x}\int_{x_i}^{x_{i+1/2}} F(U)_x dx = \frac{1}{\Delta x}\int_{x_i}^{x_{i+1/2}} S(U)a_x dx = \mathcal{S}_{i+1/2}^- \\
\frac{1}{\Delta x}(F(U_i) - F(U_{i-1/2}^+)) &= \frac{1}{\Delta x}\int_{x_{i-1/2}}^{x_i} F(U)_x dx = \frac{1}{\Delta x}\int_{x_{i-1/2}}^{x_i} S(U)a_x dx = \mathcal{S}_{i-1/2}^+
\end{aligned}
$$

The above relations describe the source flux flowing through the right and left boundaries of a cell towards its center.

Construction of a well-balanced numerical scheme (3.4.13), (3.4.15), (3.4.16) involves finding an approximate Riemann solver of a homogeneous problem and solving in general non-linear equations for interface values. Based on the Dal Maso, LeFloch and Murat interpretation

of non-conservative products Gosse in [48] used a generalized Roe's linearization to obtain a well-balanced scheme. The advantage of this method comes from the fact that solving (3.4.15) is avoided. In the same framework Gosse in [47] extended the well-balancing idea to a flux-splitting methods. To solve a homogeneous problem he used an upwind type scheme instead of a Riemann solver, however, the interface states are needed in order to preserve numerically steady states. In general we can use any approximate Riemann solver presented in the previous sections. The difficulties appear when we require well-balancing for all steady states. Solving nonlinear system (3.4.15) becomes particularly difficult from mathematical and numerical point of view if $F(U)$ has sonic points or if we deal with vacuum states. To simplify it in [14] a so called hydrostatic reconstruction was introduced. It is based on the assumption that steady states to be preserved are "at rest".

Non conservative product and a family of paths

The theory developed in [29] gives a precise meaning of non conservative products as Borel measures on a family of locally Lipschitz paths Φ. Following the article we present the precise definitions. Let us consider a $N \times N$ hyperbolic system

$$U_t + A(U)U_x = 0, \tag{3.4.18}$$

where $U \in [BV(\mathbf{R})]^N$ and $U \to A(U)$ is a smooth locally bounded map.

Definition 3. *A path Φ in $\Omega \subset \mathbb{R}^N$ is a family of smooth maps $[0,1] \times \Omega \times \Omega \to \Omega$ satisfying:*

- $\Phi(0; U_L, U_R) = U_L$ *and* $\Phi(1; U_L, U_R) = U_R$

- $\forall \mathcal{V}$ *bounded in* Ω, $\exists k$ *such that* $\forall s \in [0,1]$, $\forall (U_L, U_R) \in \mathcal{V}$
  $\left| \frac{\partial \Phi}{\partial s}(s; U_L, U_R) \right| \leq k |U_L - U_R|$

- $\forall \mathcal{V}$ *bounded in* Ω, $\exists K$ *such that* $\forall s \in [0,1]$, $\forall (U_L^i, U_R^i)_{i=1,2} \in \mathcal{V}$
  $\left| \frac{\partial \Phi}{\partial s}(s; U_L^1, U_R^1) - \frac{\partial \Phi}{\partial s}(s; U_L^2, U_R^2) \right| \leq K \left\{ \left| U_L^1 - U_L^2 \right| + \left| U_R^1 - U_R^2 \right| \right\}$

In the following theorem non conservative products are defined as Borel measures μ constructed on a family of paths Φ and denoted by $[A(U)U_x]_\Phi$.

Theorem 4. *(Dal Maso, LeFloch, Murat) Let $U \in BV(]a,b[, \mathbb{R}^N)$ and $A : \mathbb{R}^N \times]a,b[\to \mathbb{R}^N$ a locally bounded function, i.e.*

$$\forall X \in \mathbb{R}^N \text{ bounded}, \exists C > 0 \text{ such that } \forall U \in X, \forall x \in]a,b[, |A(U,x)| \leq C.$$

There exists a unique Borel measure μ on $]a,b[$ characterized by the following properties:

- *If $x \to U(x)$ is continuous on an open set $B \subset]a,b[$*

$$\mu(B) = \int_B A(U,x)\frac{\partial U}{\partial x} = \int_B A(U(x),x)\frac{\partial U(x)}{\partial x}dx$$

- *If $x_0 \in]a,b[$ is a discontinuity point of $x \to U(x)$, then*

$$\mu(x_0) = \left\{ \int_0^1 A\left(\Phi(s; U(x_0), U(x_0^+)), x_0\right) \frac{\partial \Phi}{\partial s}\left(\Phi(s; U(x_0), U(x_0^+)), x_0\right) ds \right\} \cdot \delta(x_0)$$

where $\delta(x_0)$ denotes the Dirac mass at the point x_0.

Having the notion of non-conservative products, the definition of weak solution to (3.4.18) in the space of BV function can be given.

Definition 4. *Let Φ be a family of paths in the sens of Definition 3. A function $U \in [L^\infty \cap BV_{Loc}(\mathbb{R} \times \mathbb{R})^N]$ is a weak solution of system (3.4.18) if it satisfies $U_t + [A(U)U_x]_\Phi = 0$ as a Borel measure on $\mathbb{R} \times \mathbb{R}^+$.*

The above framework allows us to use the structure of Riemann problem for systems that have genuinely nonlinear and linearly degenerate fields. The generalized Rankin-Hugoniot condition

$$\int_0^1 \left(\sigma \cdot Id - A\left(\Phi(s; U^-, U^+)\right)\right) \frac{\partial \Phi}{\partial s}\left(\Phi(s; U^-, U^+)\right) ds = 0, \tag{3.4.19}$$

depending on the choice of path Φ, describes how to treat discontinuities travelling with speed σ. When the conservative form of the system is available the classical Rankin-Hugoniot condition is recovered.

Let us come back to the scalar balance law

$$u_t + f(u)_x - s(u) = 0. \tag{3.4.20}$$

and its augmented system

$$\begin{cases} u_t + f(u)_x - s(u)a_x^{\Delta x} = 0 \\ a_t^{\Delta x} = 0 \end{cases} \tag{3.4.21}$$

with $a^{\Delta x} = i\Delta x$ for $x \in [x_{i-1/2}, x_{i+1/2}[$ and a locally Lipschitz map $u \to \frac{s(u)}{f'(u)}$ locally Lipschitz in order to exclude resonant regimes. To construct a Godunov type scheme for the augmented problem we need to solve a Riemann problem for each cell boundary. In other words, knowing $a_L^{\Delta x}$, $a_R^{\Delta x}$, we need to join each state u_L with the state u_R. It can be done through a family of paths Φ such that

$$[0,1] \ni s \to \Phi\left(s; \begin{pmatrix} u_L \\ a_L^{\Delta x} \end{pmatrix}, \begin{pmatrix} u_R \\ a_R^{\Delta x} \end{pmatrix}\right) = \begin{pmatrix} u^*(s\Delta x) \\ a^*(s\Delta x) \end{pmatrix}. \tag{3.4.22}$$

It satisfies the assumptions from Definition 3 if $u^*(\Delta x) = u_R$. So starting from a state u_L, we choose $s \in (0,1)$ and get a middle state u^* through which we arrive to the state u^R. The choice of the path, middle state, is crucial for the right determination of the speed of discontinuities. Usually it is based on physical background of the problem. To obtain a well-balanced scheme the states u^* and a^* should lie on the integral curves of the stationary equations starting from (u_L, a_L)

$$\begin{cases} a^* = a_L^{\Delta x} + (a_R^{\Delta x} - a_L^{\Delta x})/\Delta x \\ u^* \text{ is a solution of } f(u^*)_x = s(u^*)a_x^*, u^*(0) = u_L \end{cases} \tag{3.4.23}$$

The above construction can be generalized to N dimensional systems

$$\begin{cases} U_t + F(U)_x = S(U)a_x^{\Delta x} \\ a_t^{\Delta x} = 0 \end{cases} \tag{3.4.24}$$

at least when $F'(U)$ is invertible, so away from sonic points. The family of paths can be defined as in scalar case

$$[0,1] \ni s \to \Phi\left(s; \begin{pmatrix} U_L \\ a_L^{\Delta x} \end{pmatrix}, \begin{pmatrix} U_R \\ a_R^{\Delta x} \end{pmatrix}\right) = \begin{pmatrix} U^*(s\Delta x) \\ a^*(s\Delta x) \end{pmatrix} \tag{3.4.25}$$

where a^* is defined as before and U^* is the solution to

$$\begin{cases} F(U^*)_x = S(U^*)a_x^* \\ U^*(0) = U_L \end{cases} \tag{3.4.26}$$

Generalized Roe's method

The first method to construct a well-balanced scheme in the above framework that we are going to describe is the generalized Roe's method. It is based on the approximation of the augmented system (3.4.12) with the Riemann initial data using the generalized Roe's matrix A_Φ introduced in [115]. Denoting by $W = \begin{pmatrix} U & a^{\Delta x} \end{pmatrix}^T$ the unknown vector and W_L, W_R the left and right states it can be put in the form

$$A_\Phi(W_L, W_R) = \left(R \cdot \text{diag}(\lambda_i) \cdot R^{-1} \right)(W_L, W_R), \tag{3.4.27}$$

where λ_i, $i = 1, ...N$ is a complete set of real eigenvalues and R is a matrix composed of the corresponding right eigenvectors. It has to be consistent with the system (3.4.12) so

$$\forall W \quad A_\Phi(W, W) = A(W)$$

and with the generalized Rankine-Hugoniot condition that is

$$\int_0^1 A\left(\Phi(s; W_L, W_R)\right) \frac{\partial \Phi}{\partial s}(s; W_L, W_R)\, ds = A_\Phi(W_L, W_R)(W_R - W_L).$$

If we define

$$A_\Phi^\pm(W_L, W_R) = \frac{1}{2}\left(R \cdot \text{diag}(\lambda_i \pm |\lambda_i|) \cdot R^{-1} \right)(W_L, W_R).$$

then a numerical scheme for (3.4.12) can be put in the following form

$$\begin{aligned} W_i^{n+1} &= W_i^n - \frac{\Delta t}{\Delta x}\left\{ A_\Phi^+(W_{i-1}^n, W_i^n)(W_i^n - W_{i-1}^n) \right. \\ &\quad + \left. A_\Phi^-(W_i^n, W_{i+1}^n)(W_{i+1}^n - W_i^n) \right\}. \end{aligned} \tag{3.4.28}$$

What remains is to define the matrix A_Φ. In [48] Gosse proposed

$$A_\Phi(W_L, W_R) = \begin{pmatrix} A(W_L, W_R) & -S_\Phi(W_L, W_R) \\ 0 & 0 \end{pmatrix}$$

where $A(W_L, W_R)$ is the usual Roe's matrix for the homogeneous problem and S_Φ is such that

$$S_\Phi(W_L, W_R)(a_R^{\Delta x} - a_L^{\Delta x}) = [S(U)a_x^{\Delta x}]_\Phi.$$

Evaluating (3.4.28) we obtain the scheme

$$\begin{aligned} U_i^{n+1} &= U_i^n - \frac{\Delta t}{\Delta x}\left(F_{i+1/2}^{Roe} - F_{i-1/2}^{Roe} \right) \\ &\quad + \Delta t \left(\Pi_{i+1/2}^- S_\Phi(U_i^n, U_{i+1}^n) + \Pi_{i-1/2}^+ S_\Phi(U_{i-1}^n, U_i^n) \right), \tag{3.4.29} \\ a_i^{n+1} &= a_i^n, \tag{3.4.30} \end{aligned}$$

where

$$F_{i+1/2}^{Roe} = \frac{1}{2}\left(F_{i+1} + F_i\right) - \frac{1}{2}|A(U_i^n, U_{i+1}^n)|(U_{i+1}^n - U_i^n)$$

is the Roe's classical flux with $A(U_L, U_R)$ Roe's matrix. The matrices $\Pi^{\pm}$ are projectors on the positive and negative eigenvalues λ_i, $i = 1, ..., N$ of A. Denoting by r the matrix composed of eigenvectors of A, we have $\Pi^+ = r \cdot diag(\epsilon_i^+) \cdot r^{-1}$ with $\epsilon_i^+ = 1$ if $\lambda_i > 0$ and $\epsilon_i^+ = 0$ otherwise.

To complete the definition of the scheme a suitable approximation of S_Φ along the path Φ is needed. For the first order approximation we can consider the average value of the source at the left and right state

$$S_\Phi = \frac{1}{2}(S(U_L) + S(U_R)).$$

Flux vector splitting

Another method to reduce the complexity coming from the presence of the source term was suggested in [47]. It is based on the splitting the flux

$$F = F^+ + F^-$$

such that the Jacobians of F^+, F^- have positive and negative eigenvalues respectively. For a homogeneous problem we can obtain an upwind type scheme in the form

$$U_i^{n+1} = U_i^n - \frac{\Delta t}{\Delta x}\left[F^+(U_i^n) - F^+(U_{i-1}^n) + F^-(U_{i+1}^n) - F^-(U_i^n)\right].$$

It can be also derived by solving two Riemann problems for the positive and negative fluxes at the right and left boundaries of the cell and then taking the average of the solutions. In the non homogeneous case the Riemann problems are modified in order to treat the sources in the generalized jump relations. At each time step we need to solve

$$\begin{cases} U_t^+ + F^+(U^+) = 0, & \text{for } x \in [x_{i-1/2}, x_i) \\ U^+(x, t^n) = \begin{cases} U_{i-1/2}^+ & \text{for } x \leq x_{i-1/2} \\ U_i^n & \text{for } x > x_{i-1/2} \end{cases} \\ F^+(U_{i-1/2}^+) - F^+(U_{i-1}^n) = [S^+(U)a_x^{\Delta x}]_\Phi \end{cases}$$

and

$$\begin{cases} U_t^- + F^-(U^-) = 0, & \text{for } x \in [x_i, x_{i+1/2}), \\ U^-(x, t^n) = \begin{cases} U_i^n & \text{for } x < x_{i+1/2} \\ U_{i+1/2}^- & \text{for } x \geq x_{i+1/2} \end{cases} \\ F^-(U_{i+1/2}^-) - F^-(U_{i+1}^n) = [S^-(U)a_x^{\Delta x}]_\Phi \end{cases},$$

where $S^{\pm}(U) = J_{F^\pm}(U) \cdot J_F^{-1}(U) \cdot S(U)$. It leads to the following numerical scheme

$$U_i^{n+1} = U_i^n - \frac{\Delta t}{\Delta x}\left[F^+(U_i^n) - F^+(U_{i-1/2}^+) + F^-(U_{i+1/2}^-) - F^-(U_i^n)\right]$$

with

$$U_{i-1/2}^+ = U^+(\Delta x) \text{ with } U^+ \text{ solution to } \begin{cases} F(U^+)_x = S(U^+)a_x \\ U^+(0) = U_{i-1}^n \end{cases}$$

and

$$U_{i+1/2}^- = U^-(-\Delta x) \text{ with } U^- \text{ solution to } \begin{cases} F(U^-)_x = S(U^-)a_x \\ U^-(0) = U_{i+1}^n \end{cases}.$$

3.5 Boundary conditions

Whether we describe phenomena on bounded domains like vasculogenesis experiments or various kinds of flows, where the domain is often thought to be infinite, numerical approximation of mathematical models based on partial differential equations always need to be supplemented with boundary conditions. Unless we can choose periodic boundary conditions, it is always a source of difficulties. However, in many cases specific behaviour at the boundary is essential and has to be reproduced with high accuracy.

Let us consider a one dimensional case. A uniform grid of an interval $[0, L]$ consists of points x_i, $i = 1, ..., s$ such that $x_1 = 0$ and $x_s = L$. To find an approximate solution at time t^{n+1} we need consistent formulas for solutions at these points and very often also values at artificial points x_0 and x_{s+1}, which are defined according to prescribed boundary conditions.

Dirichlet boundary conditions

When the mathematical model is endowed with Dirichlet boundary conditions the values at $x_1 = 0$ and $x_s = L$ are fixed. Then the solution at artificial nodes for a first order approximation can be defined as a linear combination of the values at other nodes that is

$$\rho_0 = 2\rho_1 - \rho_2, \qquad \rho_{s+1} = 2\rho_s - \rho_{s-1}. \tag{3.5.1}$$

Homogeneous Neumann boundary conditions

Neumann boundary conditions are more delicate to implement. They describe inflow/outflow processes and very often are connected with non constant stationary solutions. Moreover, when we deal with no-flux boundary conditions a numerical scheme has to conserve the total mass. For the Dirichlet boundary conditions the values at $x_1 = 0$ and $x_s = L$ were fixed. Now they have to satisfy

$$\rho_x|_{x_1} = \rho_x|_{x_s} = 0. \tag{3.5.2}$$

The first order approximation can be obtained by taking values of ρ at x_1 and x_s as

$$\rho_1 = \rho_2, \qquad \rho_s = \rho_{s-1}. \tag{3.5.3}$$

To derive a second order approximation let us consider Taylor expansion of ρ_2, ρ_3 at node x_1

$$\rho_i = \rho_1 + (i-1)\Delta x \rho_x|_{x_1} + (i-1)\Delta x^2 \frac{1}{2!}\rho_{xx}|_{x_1} + O(\Delta x^3), \quad i = 2, 3 \tag{3.5.4}$$

Then a linear combination of ρ_1, ρ_2, ρ_3 has a form

$$\begin{aligned} \rho_1 + a\rho_2 + b\rho_3 &= (a+b)\rho_1 + (a+2b)\Delta x \rho_x|_{x_1} + \\ &+ \frac{1}{2}(a+4b)\Delta x^2 \rho_{xx}|_{x_1} + O(\Delta x^3). \end{aligned} \tag{3.5.5}$$

The first space derivative of ρ at point x_1 is

$$\rho_x = \frac{a\rho_2 + b\rho_3}{(a + 2b)\Delta x} - \frac{a + b}{(a + 2b)\Delta x}\rho_1 - \frac{(a + 4b)\Delta x}{2(a + 2b)}\rho_{xx} \tag{3.5.6}$$

Applying boundary condition $\rho_x = 0$ the above equality is satisfied, in order to have a 2nd order condition, if

$$\begin{cases} a + b = 1 \\ a + 4b = 0 \\ \rho_1 = a\rho_2 + b\rho_3 \end{cases} \tag{3.5.7}$$

Solving this system and analogical one for $\rho_{s-2}, \rho_{s-1}, \rho_s$ in the second order approximation of homogeneous Neumann boundary conditions the values at the boundary nodes are

$$\begin{aligned} \rho_1 &= \tfrac{4}{3}\rho_2 - \tfrac{1}{3}\rho_3 \\ \rho_s &= \tfrac{4}{3}\rho_{s-1} - \tfrac{1}{3}\rho_{s-2} \end{aligned} \tag{3.5.8}$$

Mass conservation

Let us consider a general one dimensional advection-diffusion problem

$$\rho_t + A(\rho)_x = B(\rho)_{xx} \tag{3.5.9}$$

with homogeneous Neumann boundary conditions. Its numerical approximation in the simples case of a relaxation scheme can be put in the following form

$$\begin{aligned} \rho_i^{n+1} &= \rho_i^n + \lambda\frac{\Delta t}{2\Delta x}\left(\rho_{i-1}^n - 2\rho_i^n + \rho_{i+1}^n\right) \\ &+ \left(1 - \frac{\lambda}{\beta}\right)\frac{\Delta t}{\Delta x^2}\left(B_{i-1}^n - 2B_i^n + B_{i+1}^n\right) \\ &- \frac{\Delta t}{2\Delta x}\left(A_{i+1}^n - A_{i-1}^n\right) \end{aligned} \tag{3.5.10}$$

where λ, β are positive parameters. If we calculate the solution at the boundary points using the first or second order discrete approximation of the total mass of the system M

$$M = \left(\frac{\rho_1(t)}{2} + \sum_{i=2}^{s-1}\rho_i(t) + \frac{\rho_s(t)}{2}\right)\Delta x \tag{3.5.11}$$

will change in time. To see it let us assume the first order approximation $\rho_1 = \rho_2$ and $\rho_s = \rho_{s-1}$. Using the scheme (3.5.10) the mass difference at time t^n and t^{n+1} is

$$\begin{aligned} M^{n+1} - M^n &= \frac{\lambda\Delta t}{4}\left(\rho_1^n - \rho_2^n + \rho_s^n - \rho_{s-1}^n\right) \\ &+ \frac{1}{2}\left(1 - \frac{\lambda}{\beta}\right)\frac{\Delta t}{\Delta x}\left(B_1^n - B_2^n + B_s^n - B_{s-1}^n\right) \\ &+ \frac{\Delta t}{4}\left(A_2^n + 3A_1^n - A_{s-1}^n - 3A_s^n\right) \end{aligned}$$

The presence of the transport part causes that $M^{n+1} \neq M^n$. In order to avoid it the boundary values are to be defined at each time step in such a way that the difference of the mass becomes zero. Rewriting again $M^{n+1} - M^n$ but using the scheme (3.5.10) only for nodes $i = 2, ..., s-1$ we obtain

$$
\begin{aligned}
M^{n+1} - M^n \; = \; & \frac{\Delta x \Delta t}{2} \left[\frac{1}{\Delta t}(\rho_1^{n+1} - \rho_1^n) + \frac{\lambda}{\Delta x}(\rho_1^n - \rho_2^n) \right. \\
& \left. + \frac{2\left(1 - \frac{\lambda}{\beta}\right)}{\Delta x^2}(B_1^n - B_2^n) + \frac{1}{\Delta x}(A_1^n + A_2^n) \right] \\
& + \frac{\Delta x \Delta t}{2} \left[\frac{1}{\Delta t}(\rho_s^{n+1} - \rho_s^n) + \frac{\lambda}{\Delta x}(\rho_s^n - \rho_{s-1}^n) \right. \\
& \left. + \frac{2\left(1 - \frac{\lambda}{\beta}\right)}{\Delta x^2}(B_s^n - B_{s-1}^n) - \frac{1}{\Delta x}(A_s^n + A_{s-1}^n) \right].
\end{aligned}
$$

Requiring the terms in the brackets to vanish the boundary values ρ_1^{n+1} and ρ_s^{n+1} should be

$$
\begin{aligned}
\rho_1^{n+1} \; = \; & \left(1 - \lambda\frac{\Delta t}{\Delta x}\right)\rho_1^n - 2\left(1 - \frac{\lambda}{\beta}\right)\frac{\Delta t}{\Delta x^2}P_1^n - \frac{\Delta t}{\Delta x}A_1^n \\
& + \lambda\frac{\Delta t}{\Delta x}\rho_2^n + 2\left(1 - \frac{\lambda}{\beta}\right)\frac{\Delta t}{\Delta x^2}P_2^n - \frac{\Delta t}{\Delta x}A_2^n && (3.5.12) \\
\rho_s^{n+1} \; = \; & \left(1 - \lambda\frac{\Delta t}{\Delta x}\right)\rho_s^n - 2\left(1 - \frac{\lambda}{\beta}\right)\frac{\Delta t}{\Delta x^2}P_s^n + \frac{\Delta t}{\Delta x}A_s^n \\
& + \lambda\frac{\Delta t}{\Delta x}\rho_{s-1}^n + 2\left(1 - \frac{\lambda}{\beta}\right)\frac{\Delta t}{\Delta x^2}P_{s-1}^n + \frac{\Delta t}{\Delta x}A_{s-1}^n && (3.5.13)
\end{aligned}
$$

In this way we define the boundary conditions dynamically assuring the conservation of the total mass. The same method can be used for any kind of finite difference scheme, as the values ρ_1^{n+1} and ρ_s^{n+1} appear always in a linear form.

In numerical schemes based on finite volume method this kind of problem is not present. The outflow flux at the right boundary of a cell C_i is an inflow at the left boundary for a cell C_{i+1}. So taking zero inflow for the cell C_1 and zero outflow for C_s the total mass is automatically preserved .

NUMERICAL APPROXIMATION: PARABOLIC MODELS WITH NONLINEAR DIFFUSION AND CHEMOTAXIS

4.1 Introduction

In this chapter we focus on the numerical study of reaction-diffusion-advection systems. In particular, we are interested in models containing nonlinear diffusion, chemotaxis and production-degradation terms. We consider simple, two components systems of the form

$$\begin{cases} \rho_t = P(\rho)_{xx} - (\chi\rho\phi_x)_x - d_1\rho + r_1(\rho,\phi) \\ \phi_t = D\phi_{xx} - d_2\phi + r_2(\rho,\phi) \end{cases}. \tag{4.1.1}$$

The positive constants d_1, d_2 are first order degradation rates, while r_1, r_2 are non-stiff reaction function. The nonlinear diffusion is of porous medium type

$$P(\rho) = \varepsilon\rho^\gamma, \qquad , \varepsilon > 0, \gamma > 1. \tag{4.1.2}$$

The mathematical theory concerning this kind of systems is presented in Chapter 1 and 2. From a numerical point of view, the complexity of the model comes from the presence of nonlinearities leading to a free boundary problem and a strong coupling between the two equations. Moreover, chemotaxis can produce steep fronts, where oscillations may occur. Additionally a balance between internal forces and sources can lead to non constant steady states. Their preservation, as was explained in the previous chapter, is not a trivial task. Another difficulty arises for problems defined on bounded domains. Prescribing boundary conditions such that flow/outflow or the total mass are preserved is not always straightforward.

The aim of this chapter is to present numerical schemes, which can deal with all the mentioned features. In particular, an important aspect that we are going to focus on is an accurate approximation of the free boundary. Parabolic models are long time asymptotics of many hyperbolic systems and a correct numerical approximation of a position of the boundary for both problems is essential to study the convergence of the solutions.

Because of the presence of stiff and non-stiff terms the first approach is to use the Imex splitting methods, in which diffusion and stiff reactions can be treated implicitly, while advection explicitly. However, in the case of nonlinear diffusion this method requires a solution at each time step of a system of nonlinear equations, which is very expensive computationally. The explicit methods based on the discrete, kinetic approximation move the nonlinearities from the space derivatives into the source terms resulting in a system of only linear transport equations to solve. The efficiency of such schemes is much higher but the numerical diffusivity has greater influence on the solution and is undesirable in the study of free boundary problems.

We approximate a one dimensional model and extend the schemes to two dimensions using the Peaceman-Rachford splitting. Having constructed the numerical schemes we compare them with a special attention to the accuracy near the vacuum. In particular we consider the porous medium equation, which numerical approximation can be compared with Barenblatt self-similar solution. Other examples we are going to study contain chemotaxis. More precisely we consider a tumour angiogenesis model (4.3.11) and a Keller-Segel type system (4.3.17).

The chapter is organized as follows. In the Section 4.2 we describe the Imex and explicit schemes for model (4.1.1). We present the modifications for different boundary conditions. Section 4.3 is devoted to the numerical simulations of parabolic models. At first the comparison of the presented numerical schemes is preformed. Then the behaviour of chemotaxis model is studied numerically.

4.2 Numerical schemes

In this section we are going to present numerical schemes based on finite difference method. In particular, we consider the Imex and explicit method on an uniform grid with the mesh size Δx. In one dimension on an interval $[0, L]$ we define nodes x_i, $i = 1, ..., s$ such that $x_1 = 0$ and $x_s = L$. We denote by u_i^n an approximation of a function $u(x, t)$ at node x_i at time t^n and for any function $f(u)$ we denote $f(u_i^n) = f_i^n$ for simplicity. This notation is going to be used throughout the chapter.

4.2.1 Splitting schemes

Let us consider advection-diffusion-reaction problem. From the numerical point of view the system contains stiff and non-stiff terms. In the stiff part, which should be treated implicitly, we can include diffusion and first order decays. For the non-stiff part, like advection, explicit treatment is more suitable for simplicity of computations. For this reason it is suggested to use the θ-schemes. It is especially efficient when we deal with linear terms, because then the only numerical difficulty lies in solving a linear system of equations. This is the case for example for the evolution equation of the concentration of chemoattractant, which we are going to approximate at first. The resulting scheme will be used also in the hyperbolic model of chemotaxis. Then we will generalize the Imex scheme to non linear diffusion.

Concentration of chemoattractant

Let us present now description of the numerical scheme for the parabolic equation describing the evolution of the concentration of the chemoattractant of the system (4.1.1). It consists of linear diffusion and two reaction terms, one of which is stiff. Due to the presence of stiffness parts we use the Cran-Nicholson scheme. Diffusion and stiff reaction $-d_2\phi$ is treated implicitly in time, whereas the reaction $r_2(\rho, \phi)$ explicitly. Moreover, diffusion is going to be discretized by a centered difference in space, while the sources by pointwise approximation. To construct the scheme let us denote by Φ^n a vector containing the approximation of the concentration of chemoattractant ϕ at internal nodes x_i at time t^n

$$\Phi^n = (\phi_2^n, ..., \phi_{s-1}^n)^T.$$

Then the Crank-Nicholson scheme takes the form

$$\Phi^{n+1} = \left[\left(1 + \frac{1}{2}d_2\Delta t\right)\mathbb{I} + \frac{D\Delta t}{2\Delta x^2}\mathbb{M}\right]^{-1}\left[\left(\left(1 - \frac{1}{2}d_2\Delta t\right)\mathbb{I} - \frac{D\Delta t}{2\Delta x^2}\mathbb{M}\right)\Phi^n + \Delta t R_2^n\right], \quad (4.2.1)$$

where $\mathbb{I}$ is the identity matrix and $(R_2)_i^n = r_2(\rho_i^n, \phi_i^n)$. The matrix $\mathbb{M}$ is a diffusion matrix and takes into account the boundary conditions. For the first order approximation of the homogeneous Neumann boundary conditions we have

$$\mathbb{M}_{N1} = \begin{pmatrix} 1 & -1 & 0 & \cdots & 0 \\ -1 & 2 & -1 & \ddots & \vdots \\ 0 & \ddots & \ddots & \ddots & 0 \\ \vdots & \ddots & -1 & 2 & -1 \\ 0 & \ldots & 0 & -1 & 1 \end{pmatrix}$$

with

$$\phi_1^{n+1} = \phi_2^{n+1}, \qquad \phi_s^{n+1} = \phi_{s-1}^{n+1}$$

and the second order is obtained using

$$\mathbb{M}_{N2} = \begin{pmatrix} \frac{2}{3} & -\frac{2}{3} & 0 & \cdots & 0 \\ -1 & 2 & -1 & \ddots & \vdots \\ 0 & \ddots & \ddots & \ddots & 0 \\ \vdots & \ddots & -1 & 2 & -1 \\ 0 & \ldots & 0 & -\frac{2}{3} & \frac{2}{3} \end{pmatrix}$$

with

$$\phi_1^{n+1} = \frac{4}{3}\phi_2^{n+1} - \frac{1}{3}\phi_3^{n+1}, \qquad \phi_s^{n+1} = \frac{4}{3}\phi_{s-1}^{n+1} - \frac{1}{3}\phi_{s-2}^{n+1}$$

In the case of homogeneous Dirichlet boundary conditions the diffusion matrix is

$$\mathbb{M}_D = \begin{pmatrix} 2 & -1 & 0 & \cdots & 0 \\ -1 & 2 & -1 & \ddots & \vdots \\ 0 & \ddots & \ddots & \ddots & 0 \\ \vdots & \ddots & -1 & 2 & -1 \\ 0 & \ldots & 0 & -1 & 2 \end{pmatrix}.$$

When we deal with non homogeneous, but constant, Dirichlet boundary conditions

$$\phi(0,t) = \gamma_1, \qquad \phi(L,t) = \gamma_2$$

to find the solution Φ^{n+1} to the formula (4.2.1) we need to add a vector $\vec{B} \in \mathbb{R}^{s-2}$

$$\vec{B} = \left(\frac{D\Delta t}{\Delta x^2}\gamma_1, 0, 0, ..., 0, 0, \frac{D\Delta t}{\Delta x^2}\gamma_2 \right)^T,$$

which contains the boundary values, in the following way

$$\Phi^{n+1} = \left[\left(1 + \frac{1}{2}d_2\Delta t \right) \mathbb{I} + \frac{D\Delta t}{2\Delta x^2}\mathbb{M}_D \right]^{-1} \left[\left(\left(1 - \frac{1}{2}d_2\Delta t \right) \mathbb{I} - \frac{D\Delta t}{2\Delta x^2}\mathbb{M}_D \right) \Phi^n + \Delta t R_2^n + \vec{B} \right].$$

(4.2.2)

The constant boundary conditions imply $\phi_1^{n+1} = \gamma_1$, $\phi_s^{n+1} = \gamma_2$.

Density of cells

Now we are going to present the Crank-Nicholson scheme for the equation describing time evolution of the density of cells that is

$$\rho_t = P(\rho)_{xx} - (\chi\rho\phi_x)_x - d_1\rho + r_1(\rho,\phi) \tag{4.2.3}$$

We apply the same splitting method as for the concentration ϕ that is diffusion and stiff reaction term are treated implicitly, while chemotaxis and the non-stiff source explicitly. However, we have to notice that in this case the presence of nonlinear diffusion complicated the scheme. The system of linear equations in the previous case is replaced by nonlinear one. It has to be solved at each time iteration, which increases computational cost. We are going to use Newton method. It requires calculation of a Jacobian for a $s-2$-dimensional vector not only at each time iteration but also at each iteration inside Newton method until reaching the desired accuracy.

To construct the scheme for (4.2.3) we need at first space discretization of the diffusion and advection terms. We are going to use conservative, second order, centered discretizations. The approximation for diffusion is given at node x_i by

$$P(\rho)_{xx}\Big|_{x_i} \approx \frac{1}{\Delta x^2} \left(P(\rho_{i-1}) - 2P(\rho_i) + P(\rho_{i+1}) \right), \tag{4.2.4}$$

while for the chemotaxis is of the form

$$-\chi(\rho\phi_x)_x\Big|_{x_i} \approx -\frac{\chi}{\Delta x} \left[(\rho\phi_x)_{i+1/2} - (\rho\phi_x)_{i-1/2} \right].$$

In the later, different approximations at the interface nodes $x_{i+1/2}$ lead to different schemes such as

- Upwind: I^{st} order

$$\rho_{i+1/2} = \rho_i, \qquad \phi_x|_{x_{i+1/2}} = \frac{1}{\Delta x} \left(\phi_{i+1} - \phi_i \right)$$

- Centered: IInd order

$$\rho_{i+1/2} = \frac{1}{2}\left(\rho_{i+1} + \rho_i\right), \qquad \phi_x|_{x_{i+1/2}} = \frac{1}{\Delta x}\left(\phi_{i+1} - \phi_i\right)$$

- Upwind- biased: IInd order (IIIrd order with respect to the average cell volume)

$$(\rho\phi_x)_{i+1/2} = \frac{1}{6\Delta x}\left[(-\rho_{i-1} + 5\rho_i + 2\rho_{i+1})\max\{0, \phi_{i+1} - \phi_i\}\right.$$

$$+ \left.(2\rho_i + 5\rho_{i+1} - \rho_{i+2})\min\{0, \phi_{i+1} - \phi_i\}\right]$$

Choosing centered differences we obtain

$$-\chi(\rho\phi_x)_x\Big|_{x_i} \approx -\frac{\chi}{2\Delta x^2}\left[(\rho_i + \rho_{i+1})(\phi_{i+1} - \phi_i) - (\rho_{i-1} + \rho_i)(\phi_i - \phi_{i-1})\right]. \qquad (4.2.5)$$

Introducing vectors $H, G \in \mathbb{R}^s$ such that

$$H_i(\rho) = \frac{1}{\Delta x^2}\left(P(\rho_{i-1}) - 2P(\rho_i) + P(\rho_{i+1})\right) - d_1\rho_i$$

$$G_i(\rho, \phi) = -\frac{\chi}{2\Delta x^2}\left[(\rho_i + \rho_{i+1})(\phi_{i+1} - \phi_i) - (\rho_{i-1} + \rho_i)(\phi_i - \phi_{i-1})\right]$$
$$+ r_1(\rho_i, \phi_i)$$

the Crank-Nicholson scheme for (4.2.3) takes the form

$$\rho_i^{n+1} = \rho_i^n + \frac{1}{2}\Delta t\left(H_i^{n+1} + H_i^n\right) + \Delta t G_i^n. \qquad (4.2.6)$$

As mentioned before the presence of non linear stiff terms requires at each time step the solution of a system of nonlinear equations. Let us define for every vector $q \in \mathbb{R}^{s-2}$ a function

$$F(q) := q - \frac{1}{2}\Delta t H(q) - f(\rho^n), \qquad (4.2.7)$$

where

$$f(\rho^n) = \rho^n + \frac{1}{2}\Delta t H^n + \Delta t G^n \qquad (4.2.8)$$

To solve

$$F(q) = 0, \qquad (4.2.9)$$

which corresponds to finding ρ^{n+1} at internal nodes, we use Newton's method initialized with $q = \rho^n$ and with tolerance Δx. It requires a computation of the Jacobian of F at each iteration. In the case of Neumann boundary conditions we assume J_F is $(s-2) \times (s-2)$ matrix, which can be decomposed in the following way

$$J_F = \begin{pmatrix} J_{1,1} & \dots & J_{1,s-2} \\ \vdots & J^{\text{int}} & \vdots \\ J_{s-2,1} & \dots & J_{s-2,s-2} \end{pmatrix}, \qquad (4.2.10)$$

where $J^{\text{int}} \in \mathcal{M}_{(s-4)\times(s-2)}$ and by J_1, J_{s-2} we denote $(s-2)$-dimensional vectors being the first and last row of the matrix J_F. The elements of the internal part J^{int} equal

$$
\begin{aligned}
J^{\text{int}}_{i,i-1} &= -\frac{\Delta t}{2\Delta x^2}P'(q_{i-1}), \\
J^{\text{int}}_{i,i} &= 1 - \frac{1}{2}\Delta t d_1 + \frac{\Delta t}{\Delta x^2}P'(q_i), \\
J^{\text{int}}_{i,i+1} &= -\frac{\Delta t}{2\Delta x^2}P'(q_{i+1}),
\end{aligned}
$$

The vectors J_1, J_{s-2} contain the information about the homogeneous Neumann boundary conditions and differ for the first and second order approximation. Let $\sigma = 1$ if $k = 1$ and $\sigma = 2$ for $k = s - 2$. The first order approximation yields

$$
\begin{aligned}
(J_k)_{k,k} &= 1 - \frac{1}{2}\Delta t d_1 + \frac{\Delta t}{2\Delta x^2}P'(q_k), \\
(J_k)_{k,k-(-1)^\sigma} &= -\frac{\Delta t}{2\Delta x^2}P'(q_{k-(-1)^\sigma}),
\end{aligned}
$$

and the second

$$
\begin{aligned}
(J_k)_{k,k} &= 1 - \frac{1}{2}\Delta t d_1 - \frac{\Delta t}{2\Delta x^2}\left[\frac{4}{3}P'\left(\frac{4}{3}q_k - \frac{1}{3}q_{k-(-1)^\sigma}\right) - 2P'(q_k)\right], \\
(J_k)_{k,k-(-1)^\sigma} &= -\frac{\Delta t}{2\Delta x^2}\left[-\frac{1}{3}P'\left(\frac{4}{3}q_k - \frac{1}{3}q_{k-(-1)^\sigma}\right) + P'(q_{k-(-1)^\sigma})\right].
\end{aligned}
$$

Two dimensional problem: the Peaceman-Rachford method

The extension to two space dimensions of the above implicit-explicit scheme for the concentration ϕ is obtained for example using the Peaceman-Rachford splitting, which is an example of ADI (Alternating Direction Iteration) method. For a general semi-discrete scheme

$$
\phi'(t) = F_1(\phi(t)) + F_2(\phi(t)), \tag{4.2.11}
$$

where F_1, F_2 are space discretizations of the diffusion and stiff reaction terms in the directions x and y respectively, the Peaceman-Rachford method reads

$$
\begin{aligned}
\phi^{n+1/2} &= \phi^n + \frac{1}{2}\Delta t F_1(\phi^n) + \frac{1}{2}\Delta t F_2(\phi^{n+1/2}) \\
\phi^{n+1} &= \phi^n + \frac{1}{2}\Delta t F_2(\phi^{n+1/2}) + \frac{1}{2}\Delta t F_1(\phi^{n+1})
\end{aligned}. \tag{4.2.12}
$$

The non-stiff source terms are treated explictly within the framework of the IMEX scheme.

4.2.2 Explicit scheme

Numerical approximation of an advection-reaction-diffusion equation, in which all the stiff terms are linear, is accurately done by the implicit-explicit splitting schemes. This is the case of the time evolution equation for the concentration ϕ and we do not study other methods for this problem. On the other hand, we pointed out that to find the density ρ at time t^{n+1} we

have to solve a system of nonlinear equations. In order to avoid it we are going to consider an explicit scheme for

$$\rho_t = P(\rho)_{xx} - \chi(\rho\phi_x)_x - d_1\rho + r_1(\rho, \phi). \qquad (4.2.13)$$

We solve the homogeneous part and the sources separately. For the former we use an advanced, explicit scheme based on the discrete, kinetic approximation. The two reaction terms are approximated in space by a centered discretization. They do not have a geometric character, so well-balancing is not needed, but the first order decay $-d_1\rho$ is stiff so is integrated implicitly in time, while the remaining term explicitly.

Let us now focus on the approximation of the homogeneous system. The approach based on the relaxation technique allows us to remove the nonlinearities from the derivatives leading to only linear transport equations to solve. A special attention, however, has to be paid to the accurate choice of the velocities of the kinetic approximation in order to find correctly the exact position of the free boundary.

Denoting by $A(\rho, \phi) = \chi(\rho\phi_x)$ the chemotaxis term, the homogeneous part of the equation (4.2.13) can be written as

$$\rho_t + A(\rho, \phi)_x = P(\rho)_{xx}. \qquad (4.2.14)$$

In order to obtain a numerical scheme we use the diffusive BGK approximation with two velocities $N = N' = 2$

$$\begin{cases} \partial_t f_k + \lambda_k \partial_x f_k = \frac{1}{\epsilon}(M_k(\rho) - f_k) & \text{if} \quad k = 1, 2 \\ \partial_t f_k + \beta_k \partial_x f_k = \frac{1}{\epsilon}(M_k(\rho) - f_k) & \text{if} \quad k = 3, 4 \end{cases} \qquad (4.2.15)$$

with the Maxwellian functions, introduced in Chapter 3, Section 3.2.4, as follows

$$\begin{aligned} M_1 &= \frac{1}{2\lambda}\left(\lambda\left(\rho - \frac{P(\rho)}{\theta^2}\right) + A(\rho, \phi)\right), \\ M_2 &= \frac{1}{2\lambda}\left(\lambda\left(\rho - \frac{P(\rho)}{\theta^2}\right) - A(\rho, \phi)\right), \\ M_3 &= M_4 = \frac{P(\rho)}{2\theta^2}. \end{aligned}$$

We choose the speeds of propagation to be equal in both directions

$$\lambda_1 = \lambda >, \lambda_2 = -\lambda. \qquad (4.2.16)$$

The parameters λ and $\beta_m = \gamma\sigma_m$, where $\sigma_{3,4} = \pm 1/\sqrt{2}$, and γ, θ will be precised later. To find the approximate value of ρ at time t^{n+1} we treat the homogeneous part of the problem (4.2.15) and the source at different steps. At first we solve in time interval $[t^n, t^{n+1}]$ a system of linear transport equations

$$\vec{f}_t + \Gamma\vec{f}_x = 0, \qquad \Gamma = \text{diag}(\lambda_1, \lambda_2, \beta_1, \beta_2) \qquad (4.2.17)$$

with the initial condition $f_k^n = M_k(\rho^n, \phi^n)$. Following the theory introduced in the Section 3.2 let us denote

$$\psi_{i\pm 1/2}(f_k) = 1 - (1 - |\lambda|\frac{\Delta t}{\Delta x})\varphi(r_{sgn(\lambda_k)}^{i\pm 1/2}(f_k)), \qquad (4.2.18)$$

where $\varphi(r)$ is a limier function and

$$r_+^{i+1/2}(f_k) = \frac{\triangle_{i-1/2}f_k}{\triangle_{i+1/2}f_k} \quad r_-^{i+1/2}(f_k) = \frac{\triangle_{i+3/2}f_k}{\triangle_{i+1/2}f_k}$$

$$r_+^{i-1/2}(f_k) = \frac{\triangle_{i-3/2}f_k}{\triangle_{i-1/2}f_k} \quad r_-^{i-1/2}(f_k) = \frac{\triangle_{i+1/2}f_k}{\triangle_{i-1/2}f_k} \tag{4.2.19}$$

We approximate (4.2.17) using a high resolution method for the first two components and the upwind scheme for the remaining ones corresponding to the diffusion process. We obtain

$$
\begin{aligned}
f_1^{n+1/2,i} &= f_1^{n,i} - \lambda\frac{\Delta t}{\Delta x}\left(\triangle_{i+1/2}f_1^n + \triangle_{i-1/2}f_1^n\right) \\
&+ |\lambda|\frac{\Delta t}{\Delta x}\left[\psi_{i+1/2}(f_1^n)\triangle_{i+1/2}f_1^n - \psi_{i-1/2}(f_1^n)\triangle_{i-1/2}f_1^n\right], \\
f_2^{n+1/2,i} &= f_2^{n,i} + \lambda\frac{\Delta t}{\Delta x}(\triangle_{i+1/2}f_2^n + \triangle_{i-1/2}f_2^n) \\
&+ |\lambda|\frac{\Delta t}{\Delta x}\left[\psi_{i+1/2}(f_2^n)\triangle_{i+1/2}f_2^n - \psi_{i-1/2}(f_2^n)\triangle_{i-1/2}f_2^n\right], \\
f_3^{n+1/2,i} &= f_3^{n,i} - \frac{\gamma}{\sqrt{2}}\frac{\Delta t}{\Delta x}(f_3^{n,i} - f_3^{n,i-1}), \\
f_4^{n+1/2,i} &= f_4^{n,i} + \frac{\gamma}{\sqrt{2}}\frac{\Delta t}{\Delta x}(f_4^{n,i+1} - f_4^{n,i}).
\end{aligned}
$$

Treatment of the source term $\frac{1}{\epsilon}\left(M_k(\rho,\phi) - f_k\right)$ implies solving an ODE. In this case it is equivalent to the projection of the solution $\rho^{n+1/2}$ onto the equilibrium yielding

$$\rho^{n+1} = \rho^{n+1/2} = \sum_{k=1}^{4} f_k^{n+1/2}. \tag{4.2.20}$$

It can be seen as a fractional step method for the source term instead of the well-balanced approach.

To complete the scheme we have to define the parameters γ and λ. The choice of λ has to assure the monotonicity of the Maxwellian functions that is it has to satisfy the condition

$$|A'(\rho_i,\phi_i)| \leq \lambda\left(1 - \frac{P'(\rho_i)}{\theta^2}\right), \quad \forall \quad i = 1,...,s. \tag{4.2.21}$$

At first we choose $\alpha \in (0,1)$ such that

$$\forall \quad i = 1,...,s \quad 0 < \alpha \leq 1 - \frac{P'(\rho_i)}{\theta^2}. \tag{4.2.22}$$

It leads to the following values of θ^{n+1} and λ^{n+1} at each time step

$$\theta^{n+1} = \max_i\sqrt{\frac{P'(\rho_i^n)}{1-\alpha}}, \quad \lambda^{n+1} = \max_i(\chi\,(\phi_x)_i^n), \quad \gamma^{n+1} = 2\theta^2/\Delta x \tag{4.2.23}$$

To guarantee stability of the scheme the CFL condition has to be such that the transport problems for f_k, $k = 1,...,4$ are stable. It gives a restriction on time step of the form

$$\Delta t \leq \min\left\{\frac{\Delta x}{\lambda}, \frac{(\Delta x)^2}{\sqrt{2}\theta^2}\right\}. \tag{4.2.24}$$

4.3 Simulations

In this section we study numerically parabolic models using the schemes presented in the first part of the chapter. We consider the porous medium equation, which describes the nonlinear diffusion that increases with higher densities, and two parabolic, chemotaxis models: tumour angiogenesis model introduced in [25] and a Keller-Segel type system. The aggregation phenomena are well described by this kind of models, however, it is well known that linear diffusion for example in Keller-Segel type models can leads to a pointwise blow-up in finite time in space dimensions higher than one. The use of density dependent function as a diffusive coefficient produces a volume filling effect that guarantees a global existence of solutions. In fact, for the angiogenesis model we study the traveling waves, not aggregation phenomena, and only linear diffusion is taken into account, while for the Keller-Segel model we consider also nonlinear diffusion of the porous medium type.

The main aim is to compare the accuracy of numerical methods in approximating the interface between the region, where density ρ is strictly positive and the region, where it vanishes. These results are needed for the later study, in which we analyze numerically convergence of the hyperbolic models to their parabolic asymptotics. In particular, we are interested in propagation into vacuum and evolution of the free boundary, so its accurate approximation is essential.

4.3.1 Porous medium equation

The first example that we consider is a one dimensional model of flow in a porous medium. The reason why we start with this model is that we know its exact solution. It allows us to compare carefully the implicit scheme from Section 4.2.1 with the explicit one based on the relaxation technique presented in Section 4.2.2 for this particular equation.

Denoting by ρ the density of gas its evolution is described by

$$\begin{cases} \rho_t = P(\rho)_{xx} & (x,t) \in [0,L] \times [0,T] \\ \rho(x,0) = \rho_0(x) & x \in [0,L] \\ \rho(x,t) = 0 & (x,t) \in \{0,L\} \times [0,T] \end{cases} \qquad (4.3.1)$$

where the nonlinear diffusion is given by

$$P(\rho) = \varepsilon \rho^\gamma, \qquad \epsilon > 0, \gamma \geq 1. \qquad (4.3.2)$$

We study convergence of solutions to the trivial equilibrium in the L^2 and L^∞ norms. This behaviour can be quantified by a rate of convergence Γ such that

$$||\rho(x,t)||_{L^p} \sim t^{-\Gamma}, \quad \text{as} \quad t \to \infty. \qquad (4.3.3)$$

To obtain Γ numerically using the equation (4.3.3) we consider the ratio of L^p norms at two successive time steps

$$\frac{||\rho^{n+1}||_{L^p}}{||\rho^n||_{L^p}} = \left(\frac{t^{n+1}}{t^n}\right)^{-\Gamma}. \qquad (4.3.4)$$

Taking the logarithm we obtain

$$\Gamma = -\ln\left(\frac{||\rho^{n+1}||_{L^p}}{||\rho^n||_{L^p}}\right)\left[\ln\left(\frac{t^{n+1}}{t^n}\right)\right]^{-1}. \qquad (4.3.5)$$

In case of the porous medium equation (4.3.1) on an unbounded domain as a reference solution we can take the self-similar Barenblatt solution, which for $\gamma > 1$, has the form

$$B(x,t) = t^{-\frac{1}{\gamma+1}} \left[1 - \frac{\gamma-1}{2\gamma(\gamma+1)} \frac{(x/\sqrt{\varepsilon})^2}{t^{2/(\gamma+1)}} \right]_+^{\frac{1}{\gamma-1}}. \tag{4.3.6}$$

Its norms can be calculated explicitly

$$\begin{aligned}
||B(x,t)||_{L^\infty} &= \max(B(x,t)) \\
||B(x,t)||_{L^2}^2 &= \int_{-\infty}^{\infty} |B(x,t)|^2 dx \\
&= t^{-\frac{2}{\gamma+1}} \int_{x_-}^{x^+} \left(1 - \frac{\gamma-1}{2\gamma(\gamma+1)} \frac{(x/\sqrt{\varepsilon})^2}{t^{2/(\gamma+1)}} \right)^{\frac{2}{\gamma-1}} dx, \tag{4.3.7}
\end{aligned}$$

where

$$x_\pm = \pm \sqrt{\frac{2\varepsilon\gamma(\gamma+1)}{\gamma-1}} t^{\frac{1}{\gamma+1}}. \tag{4.3.8}$$

are positions of the left and right free boundaries. Computing the integral we obtain the following convergence rates of solutions to the trivial equilibrium

$$||B(x,t)||_{L^2} \sim t^{-\frac{1}{2(\gamma+1)}} \tag{4.3.9}$$

and

$$||B(x,t)||_{L^\infty} \sim t^{-\frac{1}{\gamma+1}}. \tag{4.3.10}$$

when $t \to \infty$ for all $\gamma > 1$.

In the first test we consider an interval $[-15, 15]$ and the Barenblatt solution (4.3.6) at time $T_0 = 1$ as initial datum. We perform simulations for different exponents of the diffusion function $P(\rho)$ that is $\gamma = 2, 3, 4, 5, 6$ using space step $\Delta x = 0.1$ for both schemes. Figure 4.1 and 4.2 present the rate of convergence in respectively L^2 and L^∞ norms as a function of time. The asymptotic decay with rate Γ is valid only for large times. The time evolution of the numerically obtained L^2 and L^∞ norms of ρ are shown at Figure 4.3. We compare them with the norms of the Barenblatt solution. It is easy to see that the numerical results are in high agreement with the reference values.

Let us now compare the implicit and explicit schemes. At first we consider the values of the rate of convergence. We compare with the exact rates the average value of Γ^n after $t^n = 35$. The results are presented in Table 4.1. They are in agreement with the theoretical rates of Barenblatt solution up to the order 10^{-3}. However, we have to notice that the implicit scheme produces oscillations. They decrease for smaller mesh size, but can influence the results.

If we compare directly the L^2 and L^∞ norms of the numerical solution with those of Barenblatt solution we see that the implicit scheme performs better. Figure 4.3 presents decays of $||\rho||_{L^2}, ||\rho||_{L^\infty}$ for the quadratic diffusion function $P(\rho) = \rho^2$. The time evolution of the L^∞ norm is similar for both methods and in a good agreement with the theory, however, in the case of the L^2 norm the implicit scheme gives much better results. The same better performance of the implicit scheme is observed for the approximation in the proximity of the free boundary. Figure 4.4 shows density profiles at time $T = 50$ for $\gamma = 2$ and $\gamma = 6$. They are compared

with the Barenblatt solution. We see that the explicit scheme produces very big error at the interface due to the numerical viscosity, while implicit one is able to capture the location of the front correctly.

To sum up, the implicit scheme gives better approximation than the explicit method, especially near the interfaces between the region, where the density ρ is strictly positive and the region where it vanishes. However, the price for treating the nonlinearities implicitly is paid in higher computational complexity. The Jacobian matrix present in Newton method to solve a system of nonlinear equations requires a lot of memory. Moreover, more operations per time iteration are needed, which increases the total time of simulation. What is more, as we will see, low numerical viscosity will be a drawback in the case of steep, traveling fronts in the solution, where spurious oscillations can appear. In this case, an explicit method with suitable limited diffusion will give better results.

γ	$||\rho_{Imex}||_{L^2}$	$||\rho_{Rel}||_{L^2}$	$||B||_{L^2}$	γ	$||\rho_{Imex}||_{L^\infty}$	$||\rho_{Rel}||_{L^\infty}$	$||B||_{L^\infty}$
2	0.1632	0.1619	0.1667	2	0.3266	0.3237	0.3333
3	0.1224	0.1229	0.1250	3	0.2450	0.2446	0.2500
4	0.0980	0.1004	0.1000	4	0.1961	0.1975	0.2000
5	0.0818	0.0856	0.0833	5	0.1634	0.1661	0.1667
6	0.0696	0.0752	0.0714	6	0.1401	0.1436	0.1429

Table 4.1: Rate of convergence to the trivial equilibrium in the L^2, L^∞ norms for different values of the nonlinear diffusion coefficient γ. The results are compared with the theoretical values for the porous medium equation given by Barenblatt solution.

4.3.2 Angiogenesis model

For the second test we consider a model of angiogenesis introduced in [25]. Denoting by ρ the density of endothelial cell and by ϕ the tumour angiogenesis factor (TAF), which is a chemotattractant, the one dimensional system has the form

$$\begin{cases} \rho_t = (\varepsilon\rho^\gamma)_{xx} - (\chi\rho\phi_x)_x + a_1\rho(1-\rho)\max(0, \phi - \phi^*) - b_1\rho \\ \phi_t = D\phi_{xx} - \frac{a_2\rho\phi}{c+\phi} - b_2\phi \end{cases} \qquad (4.3.11)$$

It describes migration of cells via diffusion and due to a response to the chemotactic stimulus, their proliferation and degradation with constant rate b_1. The proliferation is given by a logistic type growth, with a_1 being a maximal mitotic rate. Moreover the growth occurs only if the concentration of the TAF is above the threshold value ϕ^*. The chemoattractant, released by the tumour and stimulating the growth of blood vessels, diffuses in the sourrounding tissue, decays naturally at constant rate b_2 and is lost, according to the Michaelis-Menten law, due to the cells proliferation at the capillary sprout tips.

We assume that a tumour is located at the boundary $x = 0$ and the blood vessel at $x = L$. Initially the concentration of TAF is given by a function $c_0(x)$ such that $c_0(0) = c_{max}$. It remains constant at the boundary of the tumour and decays to zero near the blood vessel

leading to the following boundary conditions

$$c(0, t) = c_{max}, \qquad c(L, t) = 0. \tag{4.3.12}$$

The density of endothelial cells is assumed to be concentrated initially at the blood vessel and remains constant there. The model was build in order to study the progress of the sprout tips of endothelial cells through the tissue until reaching the tumour at $x = 0$, when additional processes have to be taken into account, so the left boundary conditions can be taken as

$$\rho(0, t) = 0 \quad \text{or} \quad \rho_x(0, t) = 0. \tag{4.3.13}$$

Following the original article we study the model defined on an interval $[0, 1]$ with the following values of the parameters

$$\varepsilon = 10^{-3}, \chi = 0.75, a_1 = 100, \phi^* = 0.2, b_1 = 4, a_2 = 10, c = 1, b_2 = 1.$$

We consider two distinct values of diffusivity constant for TAF that is $D = 10^{-3}$ and $D = 1$. Slower diffusion of the chemoattractant leads to a stronger chemotaxis effect and produces steeper gradients in the density profile. We will see that in that case it is much more difficult to obtain accurate numerical approximations. All simulations are performed with initial data of the form

$$\rho(x, 0) = \begin{cases} \rho_0 & \text{if} \quad x = L \\ 0 & \text{elsewhere} \end{cases}, \qquad c(x, 0) = \cos\left(\frac{\pi x}{2}\right) \tag{4.3.14}$$

and the boundary conditions

$$\begin{cases} \rho(0, t) = 0 \\ \rho(L, t) = 1 \end{cases}, \qquad \begin{cases} \phi(0, t) = 1 \\ \phi(L, t) = 0 \end{cases}. \tag{4.3.15}$$

As before we want to compare implicit and explicit method, however, now instead of the fully implicit scheme we use θ-Imex scheme with $\theta = 1/2$ and the CFL condition

$$\Delta t = 0.3 \frac{\Delta x}{\lambda}, \tag{4.3.16}$$

where $\lambda = \chi \max_i \left(\rho_i^0 \frac{\phi_{i+1}^0 - \phi_{i-1}^0}{2\Delta x} \right)$. For the explicit scheme based on the discrete, kinetic approximation from Section 4.2.2 we use the minmod limiter function, introduced in Section 3.2.1), in the solution of the transport problem and take the time step according to (4.2.23) and (4.2.24) with $\alpha = 0.95$. The tests are performed on an uniform grid with space step $\Delta x = 0.01$ up to the maximal time T=0.7, after which the front of cells reaches the tumour at $x = 0$ and additional processes should be taken into account in the model. The results are compared with the reference solution obtained using the fully explicit scheme on a fine grid with $\Delta x = 0.5 \cdot 10^{-3}$.

At first we study the case of $D = 1$. Figure 4.5 presents density at different times obtained by the θ-scheme and the explicit scheme and compared with the reference solution. We observe that both schemes have advantages and disadvantages. The implicit approach, as was already mentioned, produces oscillations in the region where ρ_x changes rapidly. They are visible at time $t = 0.1$. Diminishing the time step solves this problem, however, then the

approximation of the speed of the density front is incorrect as shown at Figure 4.6. We observe that for $\Delta t = 0.5\Delta x/\lambda$ the front is too slow with respect to the reference value. On the contrary, diminishing the time step numerical viscosity becomes higher and the solution at the interface with vacuum is too diffusive. For the explicit scheme we observe the same effect. Due to higher numerical viscosity the approximation is better near steep gradient, but is too diffusive at the free boundary leading to the wrong approximation of the location of the moving front.

When we consider $D = 10^{-3}$ both schemes give inaccurate results with the space step $\Delta x = 10^{-2}$ as we can see at Figure 4.7. As in the previous test, the Imex scheme cannot deal with high gradients of the density. We can observe oscillations at the front of the density profile, which are much steeper than in the previous test. The explicit scheme with minmod limiter smooths the oscillations near sharp edges, but at the same time is not capable of capturing accurately the position of the free boundary. Changing the limiter to the Superbee of Roe from Section 3.2.1, which corresponds to the upper limit of the TVD region and is the less diffusive limiter, improves the accuracy as observed at Figure 4.8. First of all there are no spurious oscillations, which means that the amount of numerical viscosity is large enough, but it is not too large as the front is sharper. The error in the approximation of the location of the free boundary is much smaller than for the scheme with the minmod limiter.

4.3.3 Keller-Segel type model for chemotaxis with nonlinear diffusion of the porous medium type

In the previous numerical tests we compared the Imex splitting scheme and the explicit, relaxation method. We observed that for the porous medium equation fully implicit treatment gives better result, because the explicit one is characterized by higher numerical diffusivity and is incapable of capturing the position of the free boundary accurately. However, it performs better when dealing with advection-diffusion problems containing steep, traveling fronts. On the angiogenesis example we saw that Imex scheme produces spurious oscillations, while the explicit method with flux-limiter functions approximates correctly the position and the height of the front.

Having in mind those results from now on time evolution of the density ρ of all parabolic models of chemotaxis will be approximated by the explicit scheme. In this section we are going to test it in two dimensions on the Keller-Segel type model of the form

$$\begin{cases} \rho_t = \Delta\left(\varepsilon\rho^\gamma\right) - \chi\mathrm{div}\left(\rho\nabla\phi\right) \\ \phi_t = \Delta\phi + a\rho - b\phi \end{cases} \tag{4.3.17}$$

where ε, χ, a and b are positive constants. The system is defined on a square $[-L, L] \times [-L, L]$ domain with homogeneous Neumann boundary conditions. We consider linear and nonlinear diffusion for the density ρ.

It is well known that if $\gamma = 1$ and the initial mass is bigger than the threshold value M^* the model has no global solution. The solution blow-up in finite, positive time. The presence of density dependent diffusivity function, $\gamma > 1$, prevents the density from exploding. We consider two initial data with different mass of the form

1. Global solution:

$$\begin{cases} \rho_0(x) = e^{-100(x^2+y^2)} \\ \phi_0(x) = 0.5 \cdot e^{-500(x^2+y^2)} \end{cases}$$

2. Blow-up:

$$\begin{cases} \rho_0(x) = 1000 \cdot e^{-100(x^2+y^2)} \\ \phi_0(x) = 500 \cdot e^{-50(x^2+y^2)} \end{cases}$$

Figure 4.9 presents the results at time $t = 0.002$ for all the system parameters equal to one in the case when the diffusion of the first component is given by the linear law. We observe that the first initial datum with the total mass smaller than the threshold one leads to a decay of solution. After t=0.002 the maximum of the density decreases from 1 to $\max(\rho(0,0,0.002)) = 0.18$. While the initial datum with much bigger mass results in concentration of the particles at the center of the domain forming a Dirac delta type distribution. On the other hand, Figure 4.10 shows the profile of the density for the quadratic diffusion function $P(\rho) = \rho^2$ and the initial distribution with the total mass higher than the threshold value. The solution is global in time as predicts the theory for the chemotaxis models with density limited diffusion. This example shows that the scheme we have chosen is able to reproduce the blow-up in the case of linear diffusion and its avoidance for the nonlinear one.
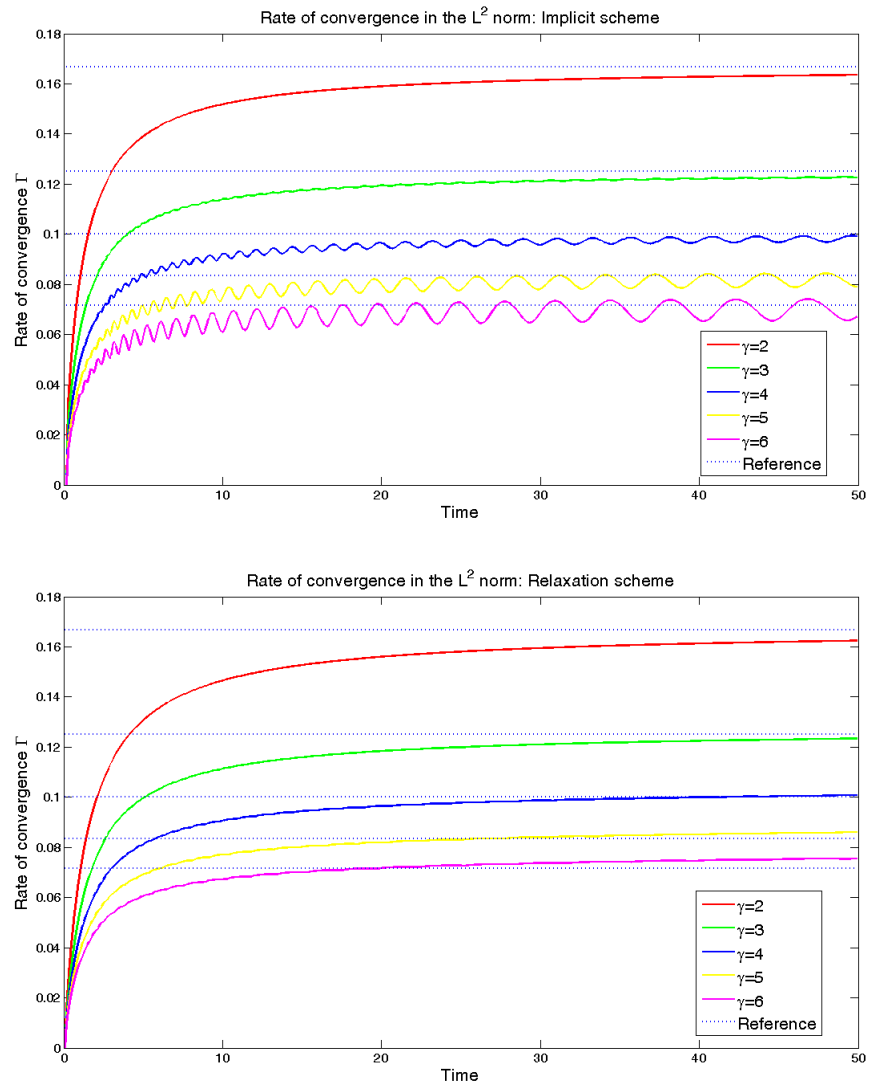
Figure 4.1: Time evolution of the rate of convergence to the trivial equilibrium in L^2 norm obtained using the fully implicit scheme (upper) and the relaxation method (lower). Results are displayed for different values of the exponent γ in the diffusion function $P(\rho) = \rho^\gamma$.
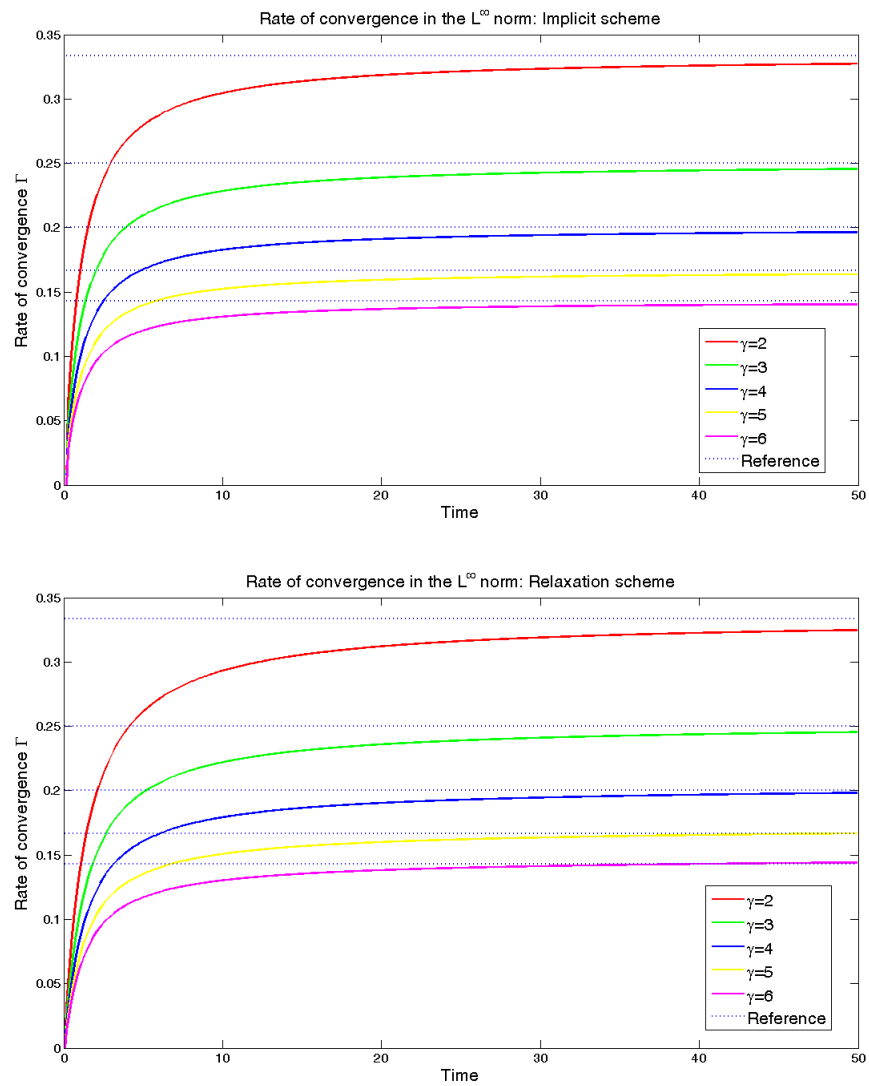
Figure 4.2: Time evolution of the rate of convergence to the trivial equilibrium in L^∞ norm obtained using the fully implicit scheme (upper) and the relaxation method (lower). Results are displayed for different values of the exponent γ in the diffusion function $P(\rho) = \rho^\gamma$
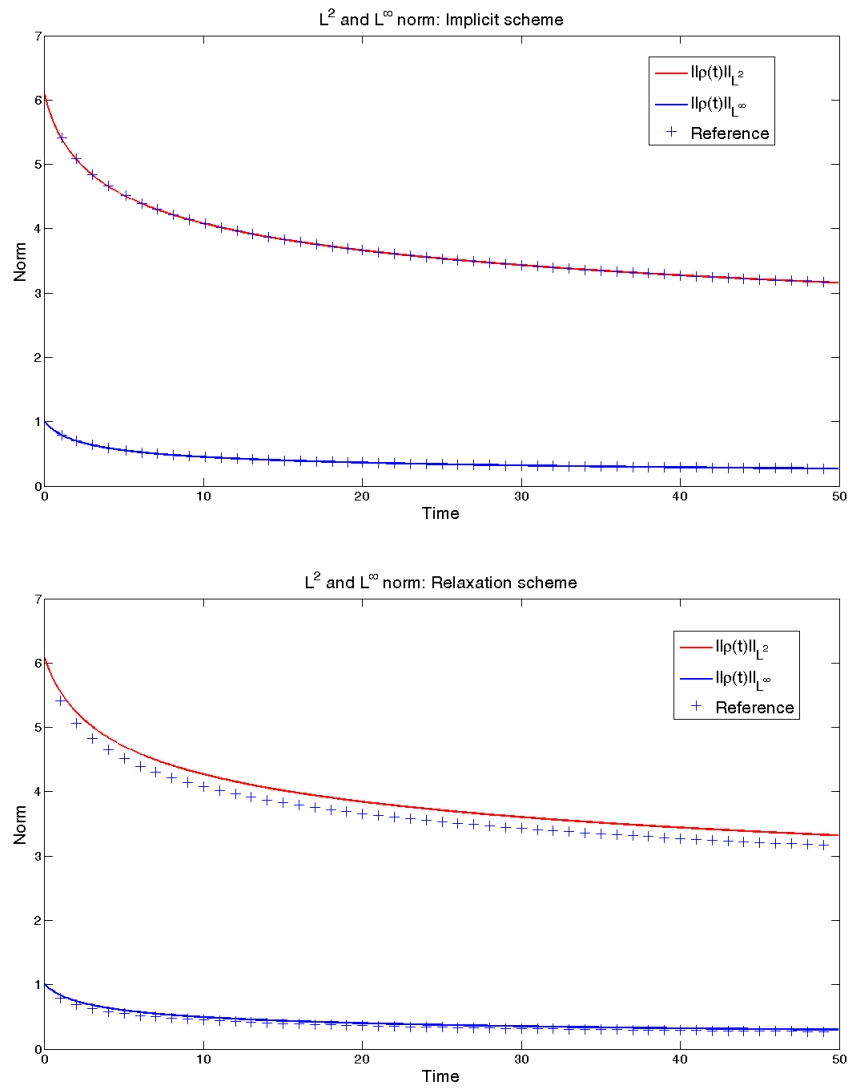
Figure 4.3: Time evolution of $||\rho(t)||_{L^2}$ and $||\rho(t)||_{L^\infty}$ norms for the quadratic diffusion $P(\rho) = \rho^2$ obtained using the Implicit (upper) and Relaxation (lower) schemes. The results are compared with the Barenblatt solution (+).
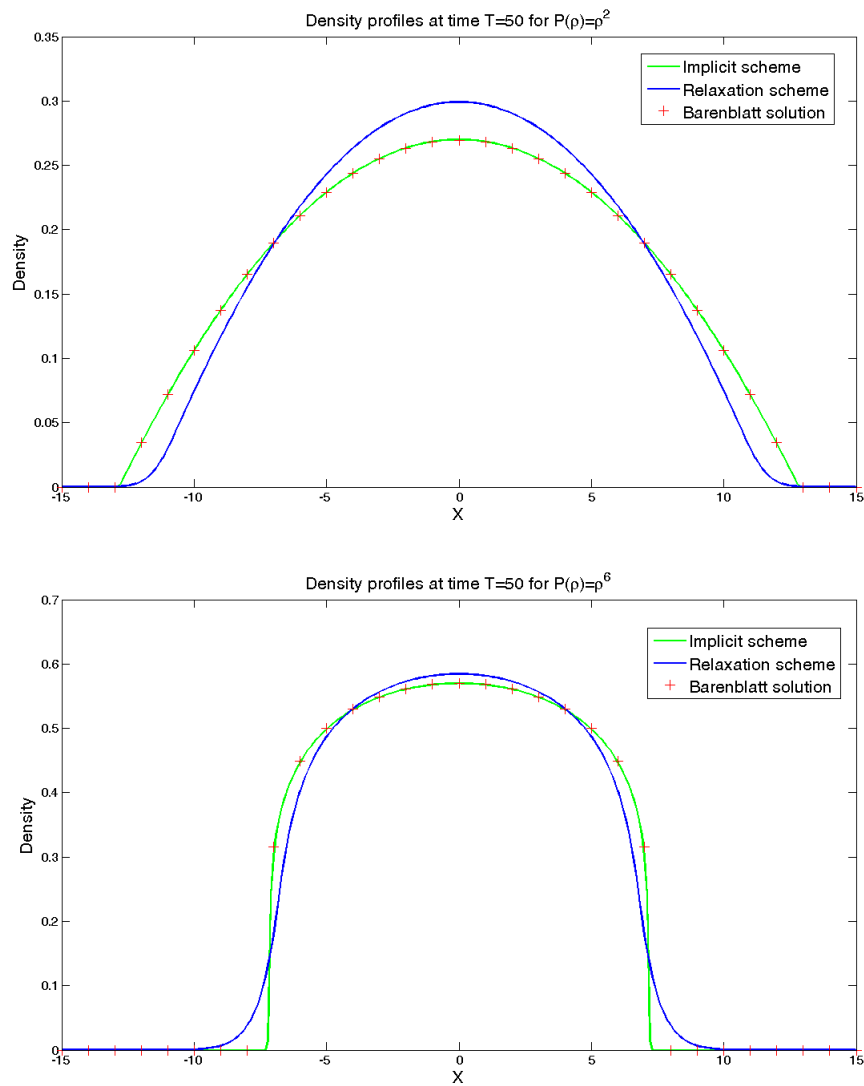
Figure 4.4: Comparison of density profiles at time $T = 50$ obtained by Implicit and Relaxation schemes for the diffusion functions $P(\rho) = \rho^2$ (upper) and $P(\rho) = \rho^6$ (lower). The results are compared with the Barenblatt solution (+).
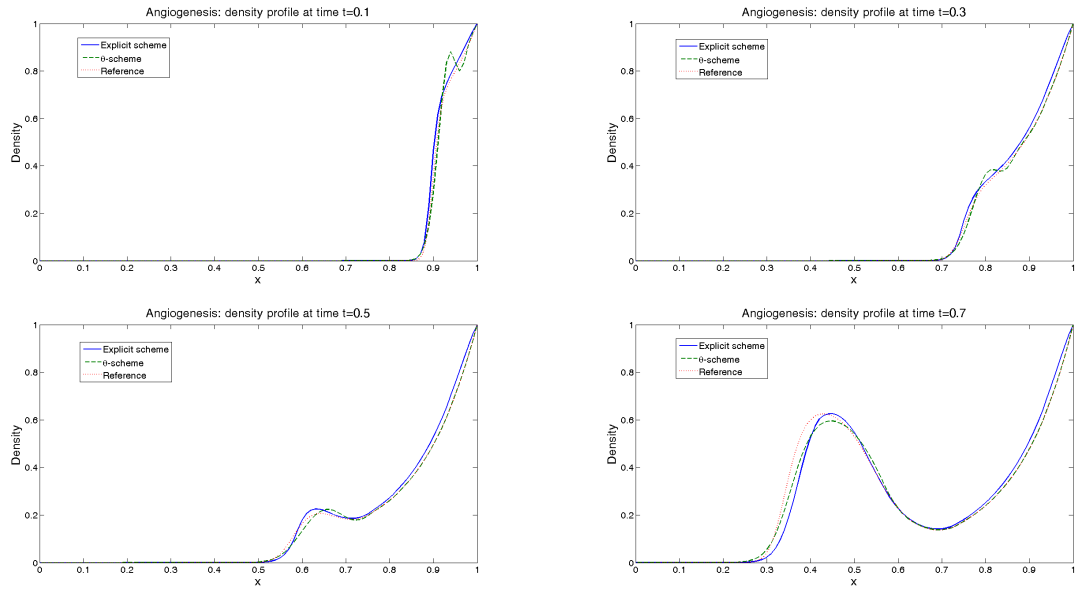
Figure 4.5: Angiogenesis model with $D = 1$: density profiles at times $t = 0.1, 0.3, 0.5, 0.7$ obtained using the θ-scheme and the explicit scheme. The results are compared with the reference solution.
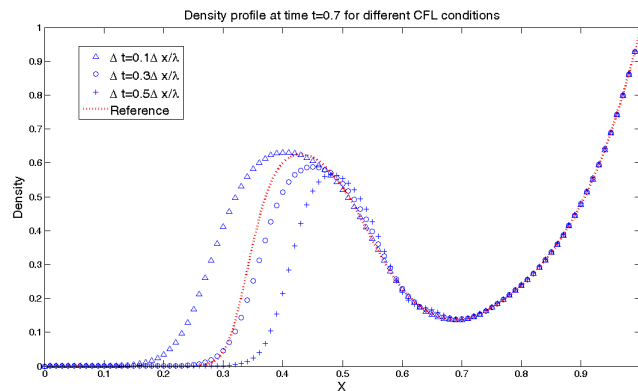
Figure 4.6: Comparison of the density profiles for $D = 1$ at time $t = 0.7$ for different CFL conditions in the θ-Imex scheme.
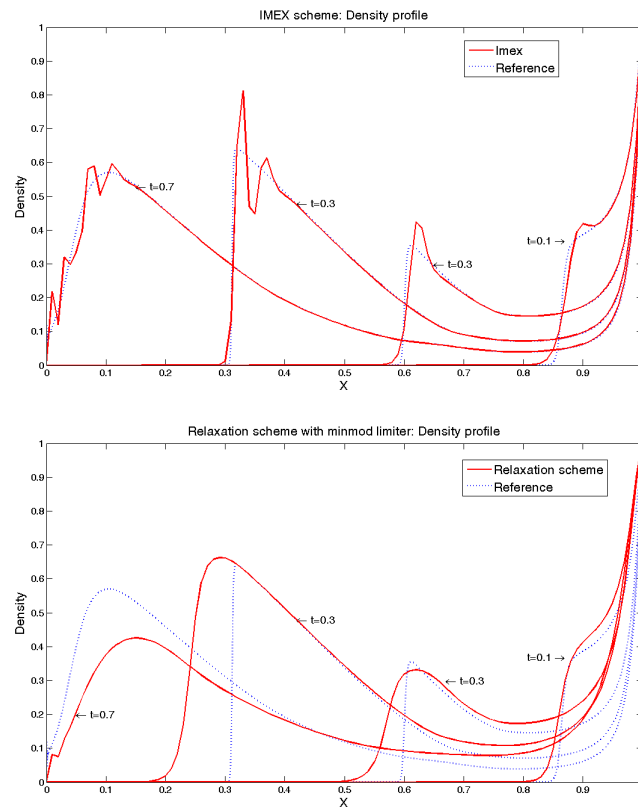
Figure 4.7: Density of endothelial cells profiles in the case of small diffusivity TAF $D = 0.001$. Comparison between Imex and Relaxation with minmod limiter schemes.
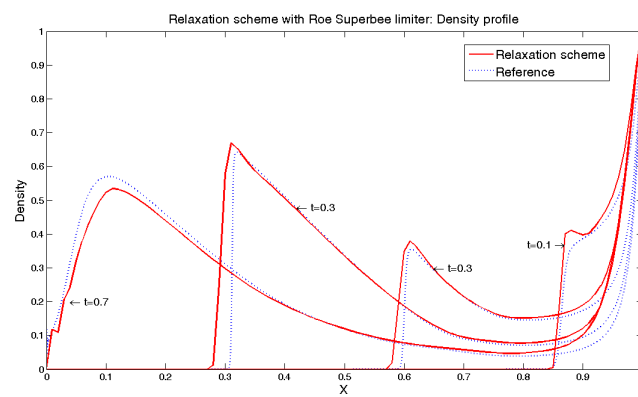
Figure 4.8: Density of endothelial cells profiles in the case of small diffusivity TAF $D = 0.001$ obtained using the Relaxation scheme with Roe Superbee limiter.
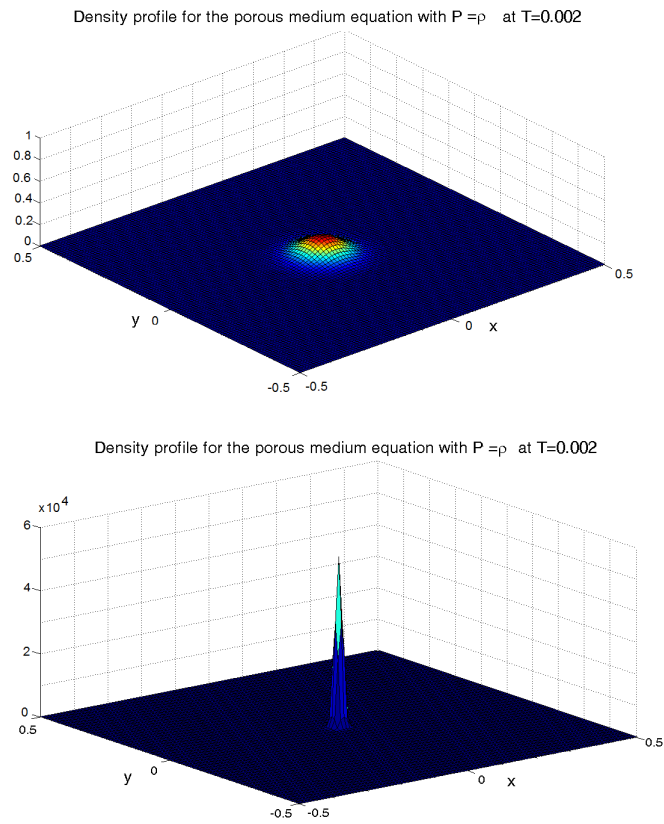
Figure 4.9: Decay to the constant equilibrium (upper) and Blow-up (lower) of the solution to the Keller-Segel type model of chemotaxis with linear diffusion function $P(\rho) = \rho$ at time $t = 0.002$.
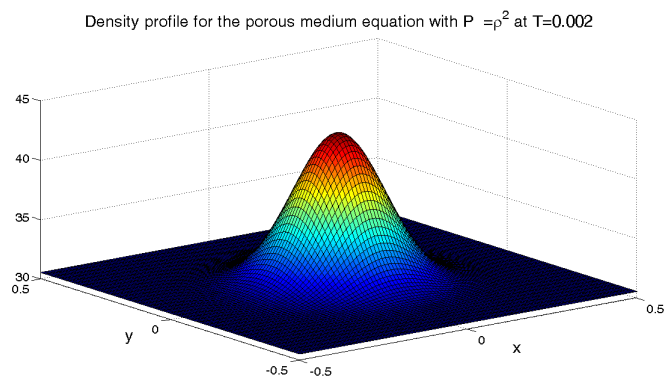
Figure 4.10: Decay to the constant equilibrium of the solution to the Keller-Segel type model of chemotaxis with nonlinear diffusion function $P(\rho) = \rho^2$ at time $t = 0.002$.

NUMERICAL STUDY OF 1D EULER EQUATIONS FOR ISENTROPIC GAS DYNAMICS WITH DAMPING

5.1 Introduction

Despite the fact that it has been more than two hundred years since the first publication by Euler in "Memoires de l'Academie des sciences de Berlin" of the equations describing the flow of a compressible fluid, there are still many questions without answer and many to be asked. In this chapter we focus on the isentropic gas dynamics system with friction in one space dimension

$$\begin{cases} \rho_t + (\rho u)_x = 0, \\ (\rho u)_t + \left(\rho u^2 + P(\rho)\right)_x = -\alpha\rho u, \end{cases} \tag{5.1.1}$$

where ρ is density of gas and u its velocity. The pressure term $P(\rho)$ is defined by a constitutive law for polytropic gases

$$P(\rho) = \varepsilon\rho^\gamma \tag{5.1.2}$$

with $\varepsilon > 0$ and the adiabatic constant $\gamma \geq 1$.

From the point of view of the mathematical analysis, this is a hyperbolic system with eigenvalues

$$\lambda_1 = u - c \qquad \text{and} \qquad \lambda_2 = u + c, \tag{5.1.3}$$

where c is the speed of sound defined by

$$c = \sqrt{P'(\rho)}. \tag{5.1.4}$$

Depending on the velocity, the flow can be classified into three different types: subsonic, sonic and supersonic. The first and the last ones correspond respectively to the flow speed lower and higher than the speed of sound. The sonic flow appears when $|u| = c$ and implies that one of the eigenvalues becomes zero. The situation complicates in the presence of vacuum states, at which density vanishes. In this case both of the eigenvalues are zero and the system becomes degenerate.

The evolution of a compressible gas into the vacuum is one of the topics that has attracted a great attention in the recent years. From the biological point of view, it is not only reasonable, but also essential to consider areas where cells can be absent. Moreover, study of the evolution of an interface between these two zones plays an important role in determining a progression of a tumour or a biofilm for example. It motivates us to study the behaviour of solutions to (5.1.1) with the initial data having compact support.

The presence of vacuum creates new form of singularity and the initial regularity of solution is lost. To the previous list of features (interaction of the nonlinear convective term and dissipation due to damping), we need to add the resonance with vacuum. In this case the eigenvalues coincide and become zero. At this moment the system is no longer symmetrizable with regular coefficients. It prevents us from using standard theories leaving only few mathematical tools to our disposal. Moreover, in [78] the physical vacuum boundary condition was conjectured. It implies a special regularity at the interface and additionally complicates the problem.

Our knowledge of the behaviour of solutions to the compressible Euler equations in the presence of vacuum is still measly due to the limited mathematical theory that we can apply to this kind of systems. It motivates us to approach the problem numerically in order to understand better phenomena that so far were studied only in special cases. More precisely, we are going to explore the behaviour of density ρ in three different processes. At first we are going to study the waiting time phenomenon. If the mass distribution near the free boundary is small enough, the front will remain stationary for finite, positive time. It is quite well understood for the porous medium equation, however, even for that problem the exact waiting times are known only in special cases. Usually only lower and upper bounds are available. For the isentropic gas dynamics no rigorous results are known. Another feature of the solutions to the compressible Euler equation that we are going to study is the regularity of ρ near the interface. In [78] the so called physical boundary condition was conjectured, which implies that the pressure has a bounded, non zero effect on the interface. Under this condition the existence theory is still an open problem. Recently some local well-posedness results were obtained, however, how the regularity changes with time for general initial data is still only a guess. Together with the above phenomena we are going to study the long time behaviour of the problem. In particular, there is a conjecture which states that, as $t \to \infty$, the density ρ obeys the porous medium equation and the velocity is given by the Darcy's law (see [61],[62]).

This chapter is organized as follows. In Section 5.2.1 we present the existing results concerning the waiting time phenomena and well-posedness of solutions under the physical boundary condition. Then, in Section 5.3 we describe numerical methods that we use to approximated the system (5.1.1). Finally Section 5.4 is devoted tot he numerical simulations. Numerical estimates of the waiting times and comparison with the porous medium equation are presented, the behaviour of the solutions under the physical boundary condition is investigated and the asymptotic convergence of the hyperbolic system to the porous medium equation is analyzed.

5.2   Existing mathematical theory.

In this section we present existing mathematical theory concerning behaviour of the degenerate parabolic problem and the isentropic gas dynamics system with damping in the presence of vacuum. In particular, we describe the results on the waiting time phenomena for the porous

medium equation. Details on the existence and estimates of the waiting time are given, as these results are going to be used later in numerical analyses of the hyperbolic model. Then we present existing mathematical theory on the canonical behaviour near free boundary of solutions to the isentropic gas dynamics system with friction. Recent results on local existence theory obtained by [65] and [28] are described.

5.2.1   Waiting time phenomenon

Now let us focus on the parabolic equations with degenerate diffusion, such as the porous medium equation. They are characterized by a finite speed of propagation [94]. It implies that if we choose the initial density with compact support, then at any later time $t > 0$ the support will be compact. It implies the occurrence of the free boundary separating the region,where the density is strictly positive and the region where it vanishes. The most studied degenerate parabolic equation is the porous medium equation

$$\rho_t = P(\rho)_{xx}. \tag{5.2.1}$$

It is endowed with a self-similar, Barenblatt solution

$$B(x,t) = t^{-\frac{1}{\Gamma+1}} \left[1 - \frac{\gamma-1}{2\gamma(\gamma+1)} \frac{(x/\sqrt{\varepsilon})^2}{t^{2/(\gamma+1)}} \right]_+^{\frac{1}{\gamma-1}}, \tag{5.2.2}$$

for which the free boundary $\xi(t)$ is given by

$$\xi_B^2(t) = \frac{2\varepsilon\gamma(\gamma+1)}{\gamma-1} t^{\frac{2}{\gamma+1}}. \tag{5.2.3}$$

In general, if we introduce a positivity set

$$\Omega(t) = \{x \in \mathbf{R} : \quad \rho(x,t) > 0\}, \tag{5.2.4}$$

where $\Omega_0 = \Omega(0)$, the free boundary $\xi(t)$ can be defined as its boundary.

In [72] it is shown the interface $\xi(t)$ is either strictly monotone or initially stationary . The later case corresponds to the so called waiting time phenomenon. Basically it means that for certain initial distributions of the mass, the free boundary can remain motionless for finite, positive time t^*, called the waiting time, then starts to move and never stops.

Existence of the positive waiting time

The existence of the waiting time phenomenon is related to the initial mass distribution close to the free boundary. If the density is sufficiently smooth near the interface then the pressure exerted on it is not large enough to cause its movement. As a consequence, the particles redistribute and accumulate near the boundary until the force at the front is sufficient to set the interface in motion. The first results on the existence of positive waiting times are due to Knerr in [72], where he described the phenomenon in terms of the pressure $v = \rho^{\gamma-1}$ near the boundary. More precisely, for $\text{supp}(\rho_0) = [a_1, a_2]$, assuming the boundary at $x = a_1$ to be fixed, he showed that

$$\begin{aligned} &\text{if} \quad \forall x \in \mathcal{N}_{a_2} \quad v_0(x) \le C(a_2 - x)^2 &&\text{then} \quad t^* > 0 \\ &\text{if} \quad \forall x \in \mathcal{N}_{a_2} \quad v_0(x) \ge C(a_2 - x)^\alpha \quad \alpha < 2 &&\text{then} \quad t^* = 0 \end{aligned}$$

where $\mathcal{N}_{a_2}$ is the neighbourhood of a_2. Then, Vazquez in [120] studied the growth rate of the mass in the proximity of the free boundary and gave a necessary and sufficient condition for the existence of the waiting time. More precisely, he considered an initial value problem for the porous medium equation on $Q_T = \mathbf{R} \times [0, T]$ under the assumption that $\rho_0(x)$ is a non negative Borel measure in $\mathbf{R}$ such that $\rho_0(x) \not\equiv 0$, $\rho_0(x) = 0$ for $x > 0$ and

$$\sup_{R \geq 1} R^{-\frac{\gamma+1}{\gamma-1}} \int_{|x| \leq R} d\rho_0(x) < \infty.$$

The above inequality corresponds to the growth conditions and assures the existence of weak solutions on Q_T. In this setting it was proven that

$$\exists t^* > 0 \quad \Longleftrightarrow \quad \limsup_{x \to 0} |x|^{-\frac{\gamma+1}{\gamma-1}} \int_{(x,0]} d\rho_0(x) < \infty.$$

Estimates of the waiting time

As the existence of a positive waiting time can be deduced from the local distribution of density, the precise estimates of its length are not so straightforward. Despite the great importance of the application, the exact values of t^* are given only in special cases. For example Aronson in [9] considered an initial profile of the form

$$\rho_0^{\gamma-1} = \begin{cases} \cos^2(x) & \frac{\pi}{2} \leq x \leq \frac{\pi}{2} \\ 0 & \text{otherwise} \end{cases}$$

and obtained

$$t^* = \frac{\gamma - 1}{2\gamma(\gamma + 1)}. \tag{5.2.5}$$

Usually only lower and upper bounds are available. What is more important, its length can depend on the local behaviour of ρ_0 near the interface or on the global distribution of mass. More precisely, in [10] the waiting time phenomenon was studied for an initial datum of the form

$$\begin{cases} \rho_0^{\gamma-1} = \alpha|x - \xi|^2 + O\left((x - \xi)^2\right) & \text{near } x = \xi \\ \rho_0^{\gamma-1} \leq \beta|x - \xi|^2 & \text{everywhere} \end{cases}.$$

and the following bounds were obtained

$$\frac{1}{2(\gamma + 1)\beta} \leq t^* \leq \frac{1}{2(\gamma + 1)\alpha}. \tag{5.2.6}$$

Additionally, the authors defined a function

$$t^*(x) := \frac{\gamma}{2(\gamma + 2)} \frac{(x - \xi)^2}{\rho_0^\gamma}, \tag{5.2.7}$$

for a general, initial datum ρ_0

$$\begin{cases} \rho_0 = \alpha|x - \xi|^q & \text{near } x = \xi \\ \rho_0 \leq \beta|x - \xi|^q & \text{everywhere} \end{cases},$$

The limit $x \to \xi$ for any initial data indicates with which situation we are dealing. In particular, when $\lim_{x \to \xi} t^*(x) = 0$ the interface starts to move immediately, while if $\lim_{x \to \xi} t^*(x)$ is finite and non vanishing the waiting time is bounded by (5.2.6) and depends locally on the initial date. Finally, in the case $\lim_{x \to \xi} t^*(x) = \infty$ the length of the waiting time has to be determined from the global distribution of the mass. It is an open problem how to estimate the waiting time in this case.

An important bound of t^*, based on the mass distribution near the interface was obtained by Vázquez [120]. Assuming that initially the free boundary ξ is localized at $x = 0$ and $\rho_0(x) = 0$ for $x > 0$ he proved

$$B = \sup_{x<0} |x|^{-\frac{\gamma+1}{\gamma-1}} \int_{(x,0]} \rho_0(x)dx < \infty \Rightarrow \frac{T_\gamma}{B^{\gamma-1}} \leq t^* \leq \frac{\theta_\gamma}{B^{\gamma-1}},$$

and

$$A = \liminf_{x \to 0} |x|^{-\frac{\gamma+1}{\gamma-1}} \int_{(x,0]} \rho_0(x)dx > 0 \Rightarrow t^* \leq \frac{T_\gamma}{A^{\gamma-1}}$$

where

$$T_\gamma = \left(\frac{\gamma-1}{\gamma+1}\right)^\gamma \frac{1}{2\gamma}, \quad \text{and} \quad \theta_\gamma = \frac{\gamma-1}{2\gamma(\gamma+1)} E_\beta \left(\frac{\gamma}{\gamma-1}, \frac{1}{2}\right)^{\gamma-1}$$

$E_\beta(x, y)$ is the Euler beta function.

Recently Perazzo and Gratton presented in [97] a numerical study of waiting times. Using numerical estimates of t^* for the power log type initial profiles

$$\rho_\alpha^0(x) = \begin{cases} 0 & \text{if} \quad x < 0 \\ (1+\alpha q)x^{\alpha q} & \text{if} \quad 0 \leq x \leq 1 \end{cases}, \tag{5.2.8}$$

where $q = 2/\gamma$, $\alpha \geq 0$ they introduced a method to derive bounds on waiting times for general initial mass distributions $\rho^0(x)$. They showed that if it is possible to find profiles $\rho_{\alpha_1}^0(x), \rho_{\alpha_2}^0(x)$ of the form (5.2.8) and constants $k_1, k_2 > 0$ such that

$$\forall x \leq 1 \quad \int_{-\infty}^x k_1 \rho_{\alpha_1}^0(x)dx \leq \int_{-\infty}^x \rho^0(x)dx \leq \int_{-\infty}^x k_2 \rho_{\alpha_2}^0(x)dx$$

then

$$\frac{t^*(\alpha_2)}{k_2^\gamma} \leq t^* \leq \frac{t^*(\alpha_1)}{k_1^\gamma}. \tag{5.2.9}$$

Regularity of the interface

One of the first works on the regularity of the interface ξ showed that it consists of Lipschitz curves and is continuously differentiable function for $t > t^*$ [20], [72]. This result was improved independently by Aronson and Vázquez in [12] and by Höllig and Kreiss in [60]. They proved that in fact the free boundary is a C^∞ function after the waiting time. Real analyticity of $\xi(t)$ was shown in [4]. Moreover, analysis in [9],[11], [72], [121] showed that

$$\xi'(t) = -\left(\frac{\gamma\rho^{\gamma-1}}{\gamma-1}\right)_x (\xi(t), t) \quad \text{and} \quad \xi''(t) \geq -\frac{\gamma}{(\gamma+1)t}\xi'(t).$$

Knerr and Aronson in [72], [9], [8] studied the evolution of the interface in terms of a pressure variable $v = \rho^{\gamma-1}$ and obtained bounds on $|v_x|$ for $t > t^*$. However, the major development in the study of the regularity of $\xi(t)$ is due to Kath and Cohen [68] who described, for $\gamma << 2$, the appearance of corner layers, where v_x changes significantly withing Δx and becomes a corner shocks at $t = t^*$ indicating discontinuous jumps in v_x. Arbitrary $\gamma > 1$ was studied later in [74]. In [10] examples of initial data, for which the interface is a continuously differentiable function at $t = t^*$ were presented, but later works of Aronson, Caffareli and Vázquez [11] showed that it is not always the case and the free boundary can start to move abruptly. They gave a sufficient condition for smoothness of the interface at $t = t^*$ and conjectured that Lipschitz continuity is optimal.

A study of regularity of the interface in higher dimensions is much more complicated. For N-dimensional porous medium equation Caffarelli, Wolanski and Vázquez [19] showed, under the assumption that at $t = 0$ the boundary starts to move at every point, that the interface is described by a Lipschitz function. In [21] they extended the result proving that in fact it is a $C^{1,\alpha}$ surface. However, no proofs were given for the pressure variable. This goal was achieved in [30], [31]. Under special conditions on the initial pressure v_0 a C^∞ smoothness was obtained for the pressure v up to the boundary for all times.

5.2.2 Physical boundary condition

In the second part of this section we focus our attention on the evolution into vacuum of the isentropic gas described by the Euler equations with damping. In fact, there is a significant difference in the behaviour for the compressible Euler system with and without friction if the initial datum contains vacuum. In the later case, the authors in [77] showed that any shock wave vanishes at the vacuum and singular behaviour corresponds to a centered rarefaction wave. It means that the density ρ is regular at the free boundary. On the other hand, solutions to the isentropic gas dynamics system with damping converge asymptotically to the porous medium equation, for which is known that the boundary has a canonical singular behaviour.

The compressible Euler equation with damping (5.1.1) in a nonconservative form in terms of the speed of sound c and the velocity u are

$$\begin{cases} \left(c^2\right)_t + \left(c^2\right)_x u + (\gamma - 1)c^2 u_x = 0 \\ u_t + u u_x + (\gamma - 1)^{-1}\left(c^2\right)_x = -u \end{cases}.$$ (5.2.10)

The function

$$i = \frac{1}{\gamma - 1}c^2,$$

is the enthalpy and its space derivative represents the effect of the pressure on the particle paths $x(t)$. In [78] it was conjectured that near the boundary Γ defined as

$$\Gamma = \overline{\{(x,t) : \rho(x,t) > 0\}} \cap \overline{\{(x,t) : \rho(x,t) = 0\}}$$

the enthalpy at any point x is proportional to the distance from the interface that is

$$i \sim \eta(x,t) \cdot |\xi(t) - x|$$

for some function $\eta(x,t)$ differentiable up to Γ. As a consequence, at Γ the pressure i_x has a bounded, non zero effect on the interface. It can be stated as

$$0 < \left| \frac{\partial c^2}{\partial x} \right| < \infty. \tag{5.2.11}$$

A vacuum boundary that satisfies the above condition is called **physical**. Using the explicit form of the sound speed it implies that the density behaves like

$$\rho(x,t) \sim |\xi(t) - x|^{\frac{1}{\gamma-1}}$$

near the boundary.

In the case of the porous medium equation the behaviour under the conditions (5.2.11) is well understood and the global existence of solutions has been proven. In [79] it was shown that for compressible Euler equations with damping regular solutions will not be global in time if the initial data has a compact support. The authors also proved local existence for ρ smooth enough such that the energy and characteristic method can be applied. However, this techniques cannot be used under the physical boundary conditions.

Well posedness under the physical vacuum condition

The existence theory for solutions featuring the physical boundary conditions for the compressible Euler equations is still far from being complete. Despite the importance of the problem only few results on the local well-posedness of the problem are available. It is caused by the difficulties coming from the structure of the system in the presence of vacuum. When density vanishes the eigenvalues of different families coincide, the characteristic curves are reflected tangentially at Γ and the problem is no more strictly hyperbolic. Moreover, the physical boundary condition implies additional constrains on the regularity of ρ such that the system cannot be symmetrizable with regular coefficient and the classical theory cannot be used.

In order to find rigorous proofs of the existence theory, new techniques have to be found out. In [125], the authors used a special transformation introduced in [80] to prove the local well-posedness of the compressible Euler equations with physical boundary for an initial condition being a perturbation of a planar wave solution.The transformation of variables was done in the Lagrangian coordinates and allowed to capture the singularity and symmetrize the system. Then, for the system reformulated in the new variable, they used a small perturbation of a linear unbounded solution as an initial data proving the existence and uniqueness of solutions.

The first, general well-posedness result was presented recently by Jang and Masmoudi [65]. Introducing special energy spaces, to overcome analytical difficulties coming from the physical boundary condition, they proved in the new framework the local in time existence and uniqueness of solutions. For a detailed description of the approach we refer to the article. Here we are going to present the reformulation of the problem in the new spaces and state the main result.

The problem was studied in one dimension assuming that one of the free boundaries, at $x = b$, is fixed, while the second is described by a function $a(t)$ that satisfies the physical boundary condition

$$\begin{cases} u(t,b) = 0, \\ \rho(t, a(t)) = 0, \\ 0 < \frac{\partial}{\partial x} \rho^{\gamma-1} \big|_{x=a(t)} < \infty \end{cases}.$$

The symmetrized system (5.1.1), with the pressure given by (5.1.2), in the Lagrangian coordinates can be written as

$$\begin{cases} \phi_t + \mu u_y = 0 \\ u_t + \mu \phi_y = -u \end{cases}, \qquad (5.2.12)$$

where

$$\phi = \frac{2\sqrt{\varepsilon\gamma}}{\gamma - 1}\rho^{\frac{\gamma-1}{2}}, \qquad \mu = \sqrt{\varepsilon\gamma}\rho^{\frac{\gamma-1}{2}}.$$

The new variable

$$y = \int_{a(t)}^{x} \rho(t, z)dz, \qquad a(t) \le x \le b$$

corresponds to a Lagrangian coordinate transformation. The free boundary in this setting corresponds to $y = 0$ and the physical boundary condition is equivalent to $\rho \sim y^{\frac{1}{\gamma}}$ for $y \sim 0$, but the propagation speed of the system (5.2.12) is still degenerate. To overcome it the authors introduced a new variable

$$\xi = \frac{2\gamma}{\gamma - 1}y^{\frac{\gamma-1}{2\gamma}}$$

and setting $k = \frac{1}{2}\frac{\gamma+1}{\gamma-1}$ they obtained the following system

$$\begin{cases} \phi_t + \left(\frac{\phi}{\xi}\right)^{2k} u_\xi = 0 \\ u_t + \left(\frac{\phi}{\xi}\right)^{2k} \phi_\xi = 0 \end{cases}. \qquad (5.2.13)$$

Inserting the physical boundary condition $\rho \sim y^{\frac{1}{\gamma}}$ into the definition of ϕ and using the new transformation from y to ξ yields for $y \sim 0$

$$\phi \sim y^{\frac{\gamma-1}{2\gamma}} \qquad \rightarrow \qquad \phi_\xi = y^{\frac{\gamma-1}{2\gamma}}\phi_y \sim 1.$$

It implies that $\phi \sim \xi$ at the free boundary, so the propagation speed of the system (5.2.13) in no longer degenerate. However, the standard energy estimates cannot be used, because the behaviour of solutions differs in the region where ρ is strictly positive and on the boundary.

The authors of [65] introduced new operators

$$V(f) \equiv \frac{1}{\xi^k}\partial_\xi\left[\frac{\phi^{2k}}{\xi^k}f\right], \quad V^*(g) \equiv -\frac{\phi^{2k}}{\xi^k}\partial_\xi\left[\frac{1}{\xi^k}g\right]$$

for $f, g \in L^2_\xi[0, 1]$ and defined appropriate function spaces $X^{k,s}$, $Y^{k,s}$ and norms $||f||^2_{X^{k,s}}$, $||g||^2_{Y^{k,s}}$. In this framework the system (5.2.13) becomes

$$\begin{cases} \partial_t\left(\xi^k\phi\right) - V^*\left(\xi^k u\right) = 0 \\ \partial_t\left(\xi^k u\right) + \frac{1}{2k+1}V\left(\xi^k\phi\right) = 0 \end{cases}, \qquad (5.2.14)$$

with $\phi(t, 0) = 0$ and $u(t, 1) = 0$ as boundary conditions. For the energy functional of the form

$$\begin{aligned} \mathcal{E}^{k,s}(\phi, u) &\equiv \frac{1}{2k+1}||\xi^k\phi||^2_{L^2_\xi} + ||\xi^k u||^2_{L^2_\xi} \\ &+ \frac{1}{(2k+1)^2}||V\left(\xi^k\phi\right)||^2_{X^{k,s-1}} + ||V^*\left(\xi^k u\right)||^2_{Y^{k,s-1}}. \end{aligned}$$

where $s = \lceil k \rceil + 3$ with $\lceil k \rceil = \min\{n \in \mathbb{Z} : k \le n\}$ the following result was proved.

Theorem 5 (Jang-Masmoudi). *Fix k, where $\frac{1}{2} < k < \infty$. Suppose initial data ϕ_0 and u_0 satisfy the following conditions:*

$$
\begin{aligned}
&(i) \quad \mathcal{E}^{k,\lceil k \rceil +3}(\phi_0, u_0) < \infty \\
&(ii) \quad \frac{1}{C_0} \leq \frac{\phi_0}{\xi} \leq C_0 \text{ for some } C_0 > 1
\end{aligned}.
$$

There exist a time $T > 0$ only depending on $\mathcal{E}^{k,\lceil k \rceil +3}(\phi_0, u_0)$ and C_0, and a unique solution (ϕ, u) to the reformulated Euler equations (5.2.14) with the boundary conditions $\phi(t,0) = 0$ and $u(t,1) = 0$ on the time interval $[0, T]$ satisfying

$$
\mathcal{E}^{k,\lceil k \rceil +3}(\phi, u) \leq 2\mathcal{E}^{k,\lceil k \rceil +3}(\phi_0, u_0),
$$

and moreover, the vacuum boundary behaviour of ϕ is preserved on that time interval:

$$
\frac{1}{C_0} \leq \frac{\phi}{\xi} \leq 2C_0.
$$

The proof of the above result is based on the energy estimates of V, V^* using the weighted Sobolev norms. Nevertheless the existence and uniqueness of solutions was shown, their regularity cannot be determined directly.

This problem was overcome in [28] by Coutand and Shkoller. In order to establish the local well-posedness of the system (5.1.1) they constructed sufficiently regular solutions, viewed as degenerate viscosity solutions. More precisely, let a position of gas particles at point x at time t be given by a function $\eta(x,t)$ such that

$$
\begin{cases}
\eta_t = u(\eta(x,t),t) & \text{for} \quad t > 0 \\
\eta(x,0) = x
\end{cases}.
$$

Then the compressible Euler equations for $\gamma = 2$ in the Lagrangian coordinates on the interval $I = [0,1]$ are

$$
\begin{cases}
\rho_0 v_t + \left(\rho_0^2/\eta_x^2\right)_x = 0 & \text{in} \quad I \times (0, T] \\
(\eta, v) = (e, u_0) & \text{in} \quad I \times \{t = 0\} \\
\rho_0 = 0 & \text{on} \quad \partial I
\end{cases}, \tag{5.2.15}
$$

where $v = u(\eta(x,t),t)$ is the Lagrangian velocity and $e(x) = x$ denotes the identity map on I. For the above problem higher-order energy functional E(t)

$$
\begin{aligned}
E(t) &= \sum_{s=0}^{4} \|\partial_t^s v(t, \cdot)\|^2_{H^{2-\frac{s}{2}}(I)} + \sum_{s=0}^{2} \|\rho_0 \partial_t^{2s} v(t, \cdot)\|^2_{H^{3-s}(I)} \\
&+ \|\sqrt{\rho_0}\partial_t \partial_x^2 v(t, \cdot)\|^2_{L^2(I)} + \|\sqrt{\rho_0}\partial_t^3 \partial_x v(t, \cdot)\|^2_{L^2(I)}.
\end{aligned}
$$

was considered. Its a priori bounds were obtained in [27] . In this framework Coutand and Shkoller proved the existence and uniqueness of solutions under the physical boundary condition. The main result for $\gamma = 2$ is stated in the following theorem. The generalization to $\gamma > 1$ is also available.

Theorem 6 (Coutand-Shkoller). *Given initial data (ρ_0, u_0) such that the total, initial mass of gas $M_0 < \infty$ and the physical boundary condition holds for ρ_0, there exists a solution to (5.2.15) on $[0, T]$ for $T > 0$ taken sufficiently small, such that*

$$sup_{t \in [0,T]} E(t) \leq 2M_0.$$

Moreover if the initial data satisfies

$$\sum_{s=0}^{3} ||\partial_t^s v(0, \cdot)||_{H^{3-s}(I)}^2 + \sum_{s=0}^{3} ||\rho_0 \partial_t^{2s} v(0, \cdot)||_{H^{4-s}(I)}^2,$$

then the solution is unique.

The method used in the proof is based on degenerate parabolic approximation for (5.2.15) of the form

$$\begin{cases} \rho_0 v_t + \left(\rho_0^2 / \eta_x^2\right)_x = \kappa \left[\rho_0^2 v_x\right]_x & \text{in} \quad I \times (0, T] \\ (\eta, v) = (e, u_0) & \text{in} \quad I \times \{t = 0\} \\ \rho_0 = 0 & \text{on} \quad \partial I \end{cases}, \qquad (5.2.16)$$

for $\kappa > 0$, and on generalized to higher order Hardy inequality. First κ-independent energy estimates for the solution to (5.2.16) are obtained. Then the existence and uniqueness of solutions to compressible Euler equations were defined as the weak limit for $\kappa \to 0$ of the sequences of the solutions to (5.2.16).

5.3 Numerical schemes

Let us now explain how we solve numerically the isentropic gas dynamics system with damping. We employ a finite volume scheme for the homogeneous problem with the explicit time discretization and centered, implicit approximation of the friction term.

System (5.1.1) is an example of a conservation law with source term

$$U_t + F(U)_x = S(U), \qquad (5.3.1a)$$

where

$$U = \begin{pmatrix} \rho \\ \rho u \end{pmatrix}, \quad F(U) = \begin{pmatrix} \rho u \\ \rho u^2 + P(\rho) \end{pmatrix}, \quad S(U) = \begin{pmatrix} 0 \\ -\alpha \rho u \end{pmatrix}. \qquad (5.3.1b)$$

Let us consider an uniform grid on Ω with the mesh size Δx and cells $C_i = [x_{i-1/2}, x_{i+1/2})$ centered at nodes x_i. The non constant time step is denoted by Δt^n and the discretization times are give by $t^n = n \Delta t^n$, $n \in \mathbf{N}$.

For the homogeneous, semi-discrete problem we use the Godunov type scheme with the Suliciu relaxation solver adapted to vacuum as an approximate Riemann solver. This choice if motivated by several factors. First we study an evolution of gas into vacuum and the scheme has to deal with points x_i of the grid such that $\rho_i > 0$ and ρ_{i+1} or ρ_{i-1} vanish. Therefore we analyze the propagation of the free boundary $\xi(t)$. In its proximity ρ_x changes very rapidly and the numerical approximation has to be free of spurious oscillations in that region. The Suliciu solver satisfies the above requirements as it preserves the non negativity of ρ. Additionally

it is characterized by a small artificial diffusion, with respect to other approximate Riemann solvers, and it increases the accuracy near the interface. Numerical viscosity has to be as low as possible in order to approximate the location of the front and to catch the moment when it stars to move.

The time discretization of the homogeneous part of the system is the first-order explicit Euler method with the CFL condition

$$\Delta t^n = 0.9 \frac{\Delta x}{\lambda^n}, \tag{5.3.2}$$

where λ^n is the highest of the wave speeds of the Suliciu solver calculated at each iteration.

The source term in the momentum balance equation is a first order decay. It doesn't have a geometric character so we can use a pointwise approximation in space instead of well-balancing. However, it is characterized by high stiffness and implicit treatment is needed.

Thus the solution at time step t^{n+1} is

$$\begin{cases} \rho_i^{n+1} = \rho_i^n - \frac{\Delta t}{\Delta x} \left(\mathcal{F}^\rho(U_i^n, U_{i+1}^n) - \mathcal{F}^\rho(U_{i-1}^n, U_i^n) \right) \\ (\rho u)_i^{n+1} = \frac{1}{1+\Delta t} \cdot \left[(\rho u)_i^n - \frac{\Delta t}{\Delta x} \left(\mathcal{F}^{\rho u}(U_i^n, U_{i+1}^n) - \mathcal{F}^{\rho u}(U_{i-1}^n, U_i^n) \right) \right] \end{cases}, \tag{5.3.3}$$

where $\mathcal{F} = (\mathcal{F}^\rho, \mathcal{F}^{\rho u})$ is the Suliciu relaxation solver.

In this chapter we will study the behaviour of the isentropic gas dynamics system on the interval $\Omega = [0, L]$ with the initial data in the following form

$$\begin{aligned} \rho(x, 0) &= \begin{cases} g(x) & \text{if} \quad 0 \leq x \leq x_f \\ 0 & \text{if} \quad x_f < x \leq L \end{cases} \\ u(x, 0) &= 0 \end{aligned} \tag{5.3.4}$$

for all $x \in \Omega$, where $g(x) \geq 0$ and $g(0) = 0$.

5.3.1 Detection of the waiting time

To obtain reliable estimates of the waiting time we need a very accurate determination of the moment when the interface ξ stars to move. The accuracy of the approximation depends on the criterion that we employ to decide when it happens. Theoretically for $\xi(0)$, corresponding to the node $x_{i_f} = x_f$ with $\rho_{i_f}^0 > 0$ and $\rho_{i_f+1}^0 = 0$, the waiting time t^* could be defined as

$$t^* = t^n \quad \text{if} \quad \rho_{i_f+1}^n > 0 \text{ and } \rho_{i_f+2}^n = 0.$$

Unfortunately, the numerical diffusion can give misleading information about the movement of the front. We tested several criteria based on observations of the interface and what happens in the region in front of it that is in the interval $[x_f, L]$.

- **Criterion I: Time evolution of the interface ξ**
  The first criterion determining when the front starts to move is based on the study of time evolution of the interface $\xi(t)$ defined as

$$\xi(t) = \max_i \left\{ x_i : \quad \rho_i > \delta_\xi \right\}. \tag{5.3.5}$$

- **Criterion II: Time evolution of mass in** $(x_f, L]$
  The front start to move when the pressure of the particles on the interface is large enough. It is connected with the high values of ρ near $\xi(0)$ and corner layers, where ρ_x is large. The mass in $(x_f, L]$ given by

  $$m = \int_{x_f}^{L} \rho(x)dx$$

  should increase rapidly after the waiting time. The moment when

  $$m(t) > \delta_m$$

  corresponds to the waiting time t^*.

- **Criterion III: Time evolution of** ρ_{i_f+1}
  Another approach is based on the observation of changes in the density value at the first grid point in front of the motionless interface. The criterion is motivated by the same argument as in the previous case and the waiting time is associated with the time when

  $$\rho_{i_f+1} > \delta_\rho.$$

In all cases the waiting time t^* is found directly from the plots $\xi(t)$, $m(t)$, $\rho_{i_f}(t)$, however, due to numerical viscosity the theoretically rapid jumps in practice are smooth. It creates additional difficulty in the approximation of the waiting time and this is the reason why we use the parameters $\delta_\xi, \delta_m, \delta_\rho$. They are the threshold quantities, crossing which indicates the movement of the interface. They should be large enough so that the error coming from the presence of the numerical diffusion is minimized. And yet, they cannot be too large since this would lead to the delay between the effective movement of the interface and our observation. In the following simulation we are going to test the advantages and disadvantages of the three criteria that we presented.

We consider the porous medium equation and the isentropic gas system with $P(\rho) = \rho^2$ and the initial condition such that $\rho(x, 0) = \cos(x)^2$ if $x \leq \pi/2$ and zero otherwise. In the case of the parabolic model the waiting time is given by the theory and equals $t^* = 1/12 = 0.083$, while the reference value for the hyperbolic system is obtained from the plot of the time evolution of the interface calculated on a very fine mesh with size $\Delta x = 10^{-4}$ and equals $t^* = 0.58$. Figure 5.1 and Figure 5.2 present time evolution, for respectively the porous medium equation and the hyperbolic model, of the interface $\xi(t)$, the mass $m(t)$, and the density $\rho_{i_f}(t)$ in the case of two different space steps $\Delta x = 10^{-2}, 10^{-3}$. The parameters δ are: $\delta_\xi = 10^{-16}, \delta_m = 10^{-4}, \delta_\rho = 10^{-3}$. We are going to explain this choice in what follows.

The first observation concerns the Criterion I based on the evolution of the free boundary. We see characteristic "steps", which are a consequence of the definition of ξ. According to it, the front moves from node x_i to x_{i+1} if $\rho_{i+1} > \delta_\xi$. But to achieve this value few time iterations have to pass. So in time interval $\Delta t = t^{n_2} - t^{n_1}$ the interface ξ is motionless. Then, at t^{n_2} it jumps to $\xi(t^{n_2}) = \xi(t^{n_1}) + \Delta x$, which we can observe at the plot. So the larger the space step Δx the more probable is that $t^{n_1} < t^* < t^{n_2}$ and won't be captured correctly. However, comparing the results for $\Delta x = 10^{-2}$ and $\Delta x = 10^{-3}$ we observe that for smaller mesh size the "steps" become much smaller and the estimate of the waiting time is more accurate for both systems, parabolic and hyperbolic. The increase of ξ starts abruptly. On the other hand, the
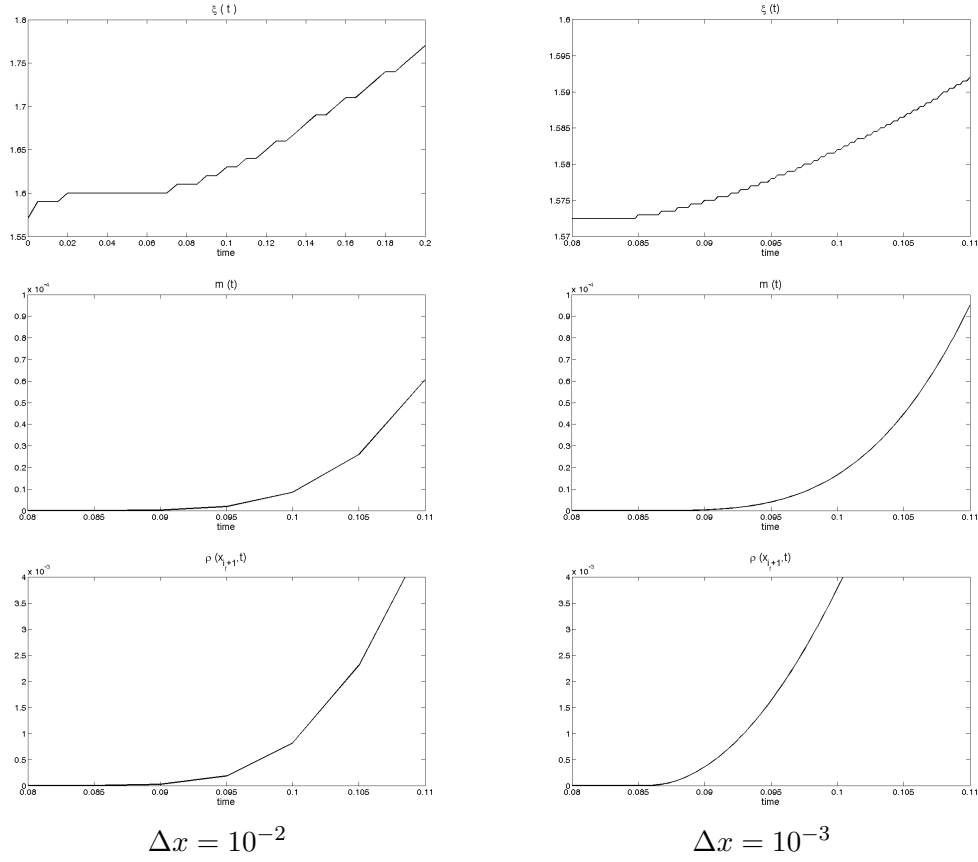
Figure 5.1: Porous medium equation: time evolution of the interface $\xi(t)$, the mass $m(t)$ in $(x_f, L]$ and the value of density $\rho_{i_f+1}(t)$ for the space step $\Delta x = 10^{-2}, 10^{-3}$. Comparison of the criteria determining the waiting time t^*. The exact value is $t^* = 0.083$.

plots of $m(t)$ and $\rho_{i_f}(t)$ are very smooth from the beginning and it is very difficult to determine when the actual movement of the interface starts. This leads to the necessity to introduce the threshold parameters δ.

For the Criterion I we chose the value corresponding to the numerical precision of the program that is $\delta_\xi = 10^{-16}$. Despite the fact that we observe the characteristic "steps", the moment when the interface starts to move is very easy to notice. On the other hand, the smoothness and the increase from the first time iteration of the plots of $m(t)$ and $\rho_{i_f+1}(t)$ makes the choice of the cut off value very difficult. Taking δ_m, δ_ρ of the same order as δ_ξ would lead to $t^* = 0$. The values that we choose in this numerical test $\delta_m = 10^{-4}, \delta_\rho = 10^{-3}$ are motivated by the reference waiting time t^*. As a consequence not knowing at least its approximation, determining when the interface was set in motion using the Criterion II and III is impossible.

To compare in another way the results on the waiting times we introduce a relative error
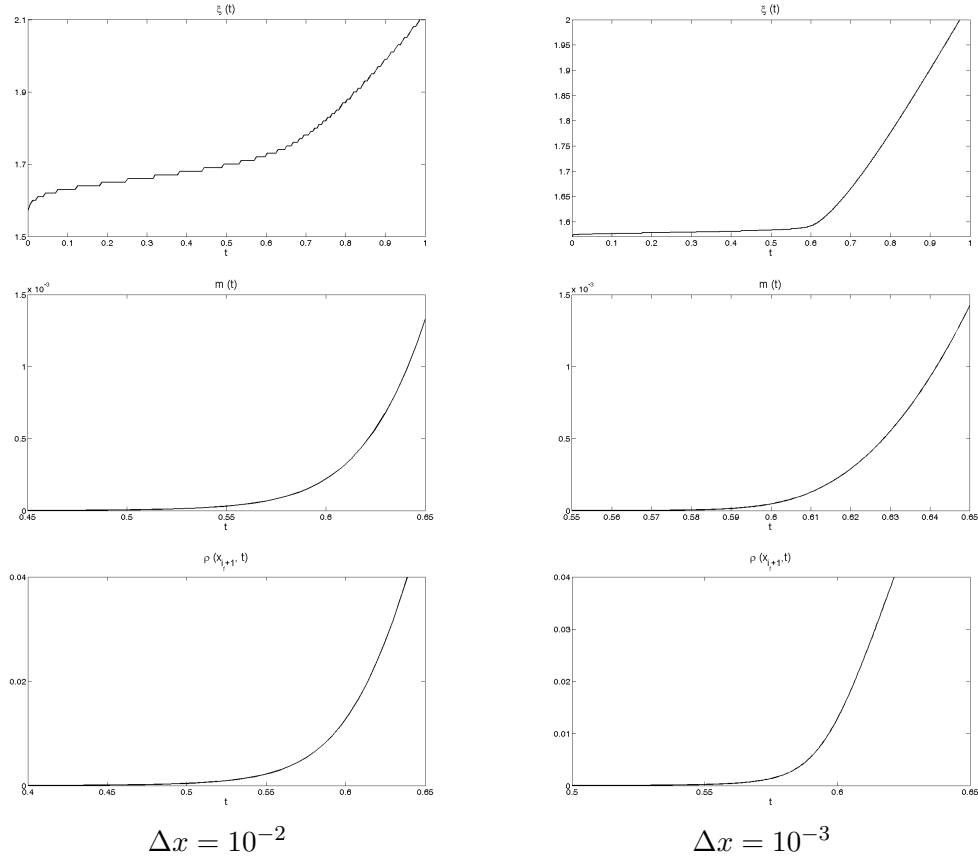
Figure 5.2: Isentropic gas dynamics system with friction: time evolution of the interface $\xi(t)$, the mass $m(t)$ in $(x_f, L]$ and the value of density $\rho_{i_f+1}(t)$ for the space step $\Delta x = 10^{-2}, 10^{-3}$. Comparison of the criteria determining the waiting time t^*. The reference value, estimated on a mesh with $\Delta x = 10^{-4}$, is $t^* = 0.58$.

e_{rel} of numerically estimated t^* with respect to the reference value t^*_{ex}. We define it as

$$e_{rel} = \frac{|t^* - t^*_{ex}|}{t^*_{ex}} \cdot 100\%.$$

Table 5.1 presents the results. We observe that for $\Delta x = 10^{-2}$ the highest error for the parabolic and hyperbolic model corresponds to the Criterion I, but at the same time decreasing the mesh size gives the best improvement. Then for the porous medium equation smaller Δx doesn't decrease much the error in the case of the Criterion II and III. It is due to the fact, that numerical viscosity is already law and only changing the accuracy by taking smaller parameter δ could improve the results. But we cannot know a priori the optimal values of δ_m, δ_ρ. For the isentropic gas dynamics system with friction, the effect of the improvement is much more visible as the difference in the numerical diffusion between $\Delta x = 10^{-2}$ and $\Delta x = 10^{-3}$ is larger.

As a consequence, we say that the Criterion I based on the direct study of the behaviour

Δx	Criterion I	Criterion II	Criterion III
10^{-2}	15.6%	8.4%	5.4%
10^{-3}	2.4%	7.2%	3.6%

PME

Δx	Criterion I	Criterion II	Criterion III
10^{-2}	31%	17.2%	22.4%
10^{-3}	5.2%	0%	8.6%

IG

Table 5.1: Relative errors e_{rel} of the approximation of the waiting time for the porous medium equation (left) and the isentropic gas dynamics system with friction (right). Comparison of the results for different criteria determining the moment when the front starts to move that is based on the time evolution of the interface $\xi(t)$ (Criterion I), the mass $m(t)$ in $(x_f, L]$ (Criterion II) and the value of density $\rho_{i_f+1}(t)$ (Criterion III) and for two space step $\Delta x = 10^{-2}, 10^{-3}$.

of the interface gives the most reliable results of the waiting time. We motivates it by the fact that the actual movement of the free boundary is much more visible on the plot of $\xi(t)$ than on $m(t)$ or $\rho_{i_f+1}(t)$. But, what is more important, we do not need the reference values of the waiting time in order to determine the value of the threshold parameters δ. From now on, in all the simulations we are going to estimate t^* using the Criterion I.

Regularity of solution

In order to study the behaviour of the density near the interface we analyze the parameter α in the relation

$$\rho_i \sim |\xi - x_i|^{\alpha}$$

for nodes x_i in the neighbourhood of ξ^n. The exact location of the interface ξ^n at each time step t^n is not needed and we define its neighbourhood by

$$\mathcal{N}_{\xi^{\Delta x}(t^n)} = \left[\xi^{\Delta x}(t^n - \delta_1, \xi^{\Delta x}(t^n - \delta_2 \right]$$

with positive δ_1, δ_2. Then, to find α, we apply the Least Square Method to

$$\ln (\rho_i^n) = \alpha^n \cdot \ln |\xi^n - x_i| \,.$$

for the set of points (x_i, ρ_i^n), where $x_i \in \mathcal{N}_{\xi^{\Delta x}(t^n)}$.

5.4 Numerical simulations

This section is devoted to the numerical analysis of the isentropic gas dynamics system with damping (5.1.1). The main aim is to give a better insight into the behaviour of the hyperbolic model for the waiting time phenomenon and under the physical boundary condition. In the

previous section we described the processes in the case of the porous medium equation and presented some recent results for the isentropic gas dynamics system. However, as was mentioned, the hyperbolic model becomes degenerate, that is the eigenvalues coincide and become zero, when the vacuum states appear. Then the classical methods cannot be applied. This is the reason why we approach the problem using the numerical analysis.

At first we focus on the waiting time phenomenon and study the dependence on the initial data of the waiting time and the velocity of the interface. More precisely, we consider the isentropic gas dynamics system with the pressure $P(\rho) = \rho^2$ on the bounded interval with the homogeneous Neumann boundary conditions for two different families of initial data. For the first one the behaviour of the free boundary of the porous medium equation depends on the density profile only near the interface, that is locally. For the second family the dependence is global. We study numerically when the interface starts to move, what is its initial velocity and compare the results with the porous medium equation. Then we study the problem (5.1.1) with the general pressure law $P(\rho) = \rho^\gamma$ and give some estimates of the waiting times. We consider different initial data and, as before, compare the behaviour of the parabolic and hyperbolic mode.

In the second part of this section we focus on the analysis of the regularity of density ρ near the interface, when it has been already set in motion. In particular, we study the canonical, singular behaviour of the free boundary characteristic for the porous medium equation. Our aim is to analyze how the regularity changes near the interface and is the physical boundary condition satisfied asymptotically. To obtain this goal we define a parameter α by $\rho \sim |x - \xi(t)|^\alpha$ for points near the interface $\xi(t)$. It characterizes the smoothness of the density ρ. In order to get a better insight in the problem we study the time evolution of this parameter for initial profiles with different regularity near the free boundary.

Dependence of the waiting time on the initial data

We start our analysis from the waiting time phenomenon. In particular, we are going to focus on the dependence on the initial data of the waiting time and the velocity of the interface. It is known [10] that the waiting time t^* for the porous medium equation depends on the initial distribution of the mass. It was pointed out that this dependence can be limited to the region near the free boundary or can concern global profile of the density. In particular, studying the limit $x \to \xi$ of the function

$$t^*(x) = \frac{\gamma - 1}{2(\gamma + 1)} \frac{(x - \xi)^2}{\rho_0^{\gamma-1}(x)} \tag{5.4.1}$$

it is possible to determine with which case we are dealing with. When $\lim_{x \to \xi} t^*(x) = 0$ the interface starts to move immediately, while if $\lim_{x \to \xi} t^*(x)$ is finite and non vanishing the waiting time is bounded and depends locally on the initial date. Finally, in the case $\lim_{x \to \xi} t^*(x) = \infty$ the length of the waiting time has to be determined from the global distribution of the mass.

In the first we are going to study if the same change of dependence holds for the isentropic gas dynamics system with damping. We consider two different profiles with the same total mass and equal initial position of the front

$$\rho(x, 0) = \begin{cases} \cos^2(x) & 0 \le x \le \frac{\pi}{2} \\ 0 & \text{elsewhere} \end{cases}$$

	a) Local dependence	b) Global dependence
$\rho_1(x,0)$	$\begin{cases} \cos^2(x) & 0 \le x \le \frac{\pi}{2} \\ 0 & \text{elsewhere} \end{cases}$	$\begin{cases} 1.75\left(1 - \frac{2x}{\pi}\right)^{2.5} & \le x \le \frac{\pi}{2} \\ 0 & \text{elsewhere} \end{cases}$
$\rho_2(x,0)$	$\begin{cases} 1.2415(1 - 0.4396x)^{2.5} & 0 \le x \le 1 \\ \cos^2(x) & 1 \le x \le \frac{\pi}{2} \\ 0 & \text{elsewhere} \end{cases}$	$\begin{cases} 1.4318\cos^2(x) - 0.2787 & 0 \le x \le 1 \\ 1.75\left(1 - \frac{2x}{\pi}\right)^{2.5} & 1 \le x \le \frac{\pi}{2} \\ 0 & \text{elsewhere} \end{cases}$
$\rho_3(x,0)$	$\begin{cases} 1.1627 & \le x \le 0.5 \\ 0.2919 & 0.5 \le x \le 1 \\ \cos^2(x) & 1 \le x \le \frac{\pi}{2} \\ 0 & \text{elsewhere} \end{cases}$	$\begin{cases} 1.3857 & 0 \le x \le 0.5 \\ 0.1393 & 0.5 \le x \le 1 \\ 1.75\left(1 - \frac{2x}{\pi}\right)^{2.5} & 1 \le x \le \frac{\pi}{2} \\ 0 & \text{elsewhere} \end{cases}$
$\rho_4(x,0)$	$\begin{cases} 0.8041 & \le x \le 0.7 \\ -1.7073x + 1.9992 & 0.7 \le x \le 1 \\ \cos^2(x) & 1 \le x \le \frac{\pi}{2} \\ 0 & \text{elsewhere} \end{cases}$	$\begin{cases} 0.8725 & 0 \le x \le 0.7 \\ -2.444x + 2.5835 & 0.7 \le x \le 1 \\ 1.75\left(1 - \frac{2x}{\pi}\right)^{2.5} & 1 \le x \le \frac{\pi}{2} \\ 0 & \text{elsewhere} \end{cases}$

Table 5.2: Initial densities $\rho(x,0)$ used to study the dependence of the waiting time on the local and global mass distribution.

with $\lim\limits_{x \to \frac{\pi}{2}} t^*(x) = \frac{2}{3}$ and

$$\rho(x,0) = \begin{cases} \frac{7}{4}\left(1 - \frac{2x}{\pi}\right)^{\frac{5}{2}} & 1 \le x \le \frac{\pi}{2} \\ 0 & \text{elsewhere} \end{cases},$$

for which $\lim\limits_{x \to \frac{\pi}{2}} t^*(x) = \infty$. In order to study the dependence of the waiting time t^* on the initial distribution we modify the above initial data. More precisely, the new profiles differ far from the free boundary and remain equal close to it that is

$$\rho(x,0) = \begin{cases} f(x) & \le x \le 1 \\ g(x) & 1 < x \le \frac{\pi}{2} \\ 0 & \text{elsewhere} \end{cases}, \tag{5.4.2a}$$

where

$$g(x) = \cos^2(x) \quad \text{or} \quad g(x) = \frac{7}{4}\left(1 - \frac{2x}{\pi}\right)^{\frac{5}{2}}, \tag{5.4.2b}$$

under the conditions

$$\begin{cases} \int_0^1 f(x)dx = \int_0^1 g(x)dx \\ f(1) = g(1) \end{cases}. \tag{5.4.2c}$$

In particular, Table 5.2 contains all the combinations of the initial data that we use to study the local and global dependence of the waiting time t^*. Figure 5.3 presents the initial data for the two families. We observe that they have different location of the center of the mass. Some
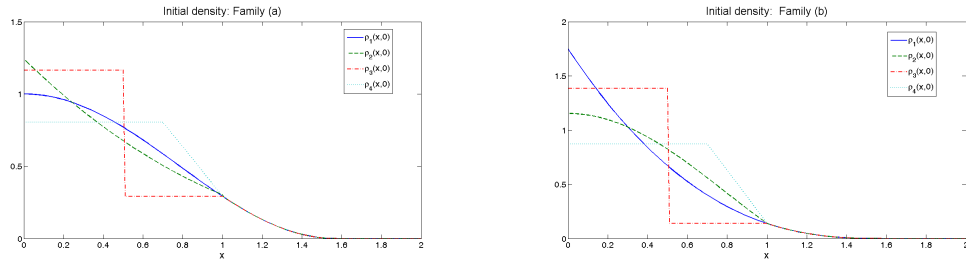
Figure 5.3: Initial densities of the Family (a) (left) and the Family (b) (right).

are moved towards the boundary of the domain, while others towards the interface. Important is, however, that the profiles are unchanged in the region $[1, \frac{\pi}{2}]$. Moreover, the first space derivative of $\rho(x, 0)$ is not continuous everywhere. We are going to analyze how these features influence the waiting time and the initial velocity of the front.

Family (a)

Let us consider at first the family (a), for which the waiting time of the porous medium equation is constant. Figure 5.4 shows the time evolution of the interface $\xi(t)$. We observe that the waiting time remains unchanged as well as for the porous medium equation, confirming the theory, and for the isentropic gas dynamics system.

Asymptotically, for $t \to \infty$, we observe $\xi(t) \sim t^{\frac{1}{3}}$, which corresponds to the behaviour of the interface of Barenblatt solution. Moreover, we see that $\xi(t)$ for different initial data don't converge to the same profile, but it is only due to the differences in the total initial mass, which are of order 10^{-3}. As a result the long time behaviour of the solutions to the isentropic gas dynamics with damping converges to the one given by the porous medium equation. On the other hand the initial behaviour of the interface differs much for the hyperbolic and parabolic model.

To analyze it we assume that in a short time interval $[t^* + \delta t, \bar{t}]$, just after the waiting time, the velocity of the interface increases linearly with time. Then we can approximate its velocity using basic fitting such as the Least Square Method. The results are shown at Figure 5.4. We see that for the porous medium equation the higher concentration of the mass near the free boundary the higher the velocity of the interface. In the case of the isentropic gas evolution we observe only two velocities. One corresponds to the distributions with the center of mass equal or to the left of $\rho_1(x, 0)$. The second, higher, is for $\rho_4(x, 0)$, which the center of mass is on the right of $\rho_1(x, 0)$. The behaviour of the interface for the isentropic gas dynamics system is much more irregular. In order to get a better insight let us consider the same test example but with the initial data of the form

$$\rho(x, 0) = \begin{cases} C & 0 \le x \le \bar{x} \\ \cos(1)^2 & \bar{x} < x \le 1 \\ \cos(x)^2 & 1 < x \le \frac{\pi}{2} \\ 0 & \text{elsewhere} \end{cases} , \tag{5.4.3a}$$
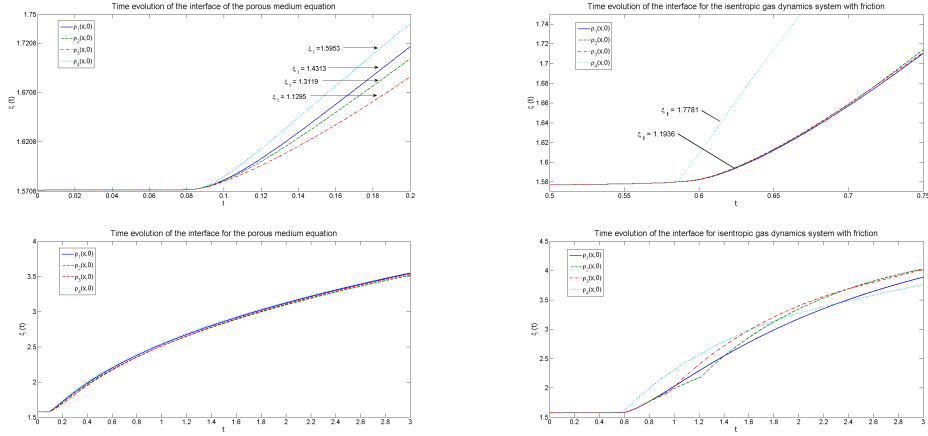
Figure 5.4: Time evolution of the interface for the porous medium equation and the isentropic gas dynamics with damping for the initial data of the Family (a). The upper plots present the behaviour in the proximity of the free boundary, while the lower show the evolution of the interfaces for longer times.

where

$$C = \frac{1}{\bar{x}} \left(\int_0^1 \cos^2(x) dx - \cos^2(1)(1 - \bar{x}) \right) \qquad (5.4.3\text{b})$$

and

$$\bar{x} = \{0.1, 0.2, 0.5, 0.8, 0.9\}. \qquad (5.4.3\text{c})$$

Figure 5.5 presents the initial profiles and the time evolution of the interfaces for the parabolic and hyperbolic models. The results for the porous medium equation are presented just to confirm an agreement with the theory. The waiting times are equal and the velocity changes in a regular way with the position of the mass center. Moreover, the interface $\xi(t)$ is a C^1 function for $t > t^*$ for all the initial data. The initial discontinuities in $\rho^0(x)$ don't influence the behaviour.

The evolution of the hyperbolic model is much more sensitive to the initial distributions. At first we observe that the interface $\xi(t)$ is not continuously differentiable after the waiting time. It is caused by the discontinuities in the initial distributions. They propagate, as the damping of the momentum at the beginning doesn't play a notable role, and produce jumps in the velocity of the interface. Asymptotically they are smoother. Now we analyze the correspondence between the observed behaviour of the interface and the location of the mass center. Let us denote by X_k^C, $k = 1, ..., 5$ the mass centers of the initial distributions ρ_k^0. For the data of the form (5.4.3) they satisfy $X_1^C < X_2^C < X_3^C < X_4^C < X_5^C$. Initial evolution of $\xi(t)$ for ρ_1^0 and ρ_5^0 and for ρ_2^0 and ρ_4^0 is similar. For the first pair the waiting time is much shorter than for all other distributions. Moreover, the interface is set in motion very abruptly, while in all other cases it is continuously differentiable at $t = t^*$. For the profile ρ_1^0 shorter waiting time can bye caused by a very violent increase of the velocity of particles localised at the left boundary of the domain. The velocity not only increases rapidly but also reaches higher

values than for profiles without large gradients of the density. As a result the pressure of the particles reaches the threshold value faster. In the case of ρ_5^0 the mass is distributed closer to the interface and the gradients ρ_x are much smaller so time needed for the reorganization of the particles is shorter. It implies that the front is set in motion earlier, but with lower initial velocity. The second pair has longer waiting times and $\xi(t)$ starts to move smoothly. However, after some time there is a jump of the velocity of the interface, when it becomes discontinuous. Moreover, after that moment the velocity of ξ_2 becomes similar to ξ_1, while of ξ_4 increases to the value of ξ_5. The mass center of the initial profile ρ_3^0 and its shape is the closest to the smooth distribution ρ_6^0 and the behaviours of their interfaces are very similar. So we see that in the case of the isentropic gas dynamics system the dependence on the initial data of the waiting time and the initial velocity of the interface is very non local. What is more, even small changes like between ρ_1^0 and ρ_2^0 or between ρ_4^0 and ρ_5^0 can produce initially very different behaviours. However, asymptotically they converge to the same evolution.

Family (b)

Let us now consider the second family of the initial data, the family (b). For the porous medium equation they lead to the waiting time that depends globally on the profile of the density. The results at Figure 5.6 show that for the parabolic model the closer to the free boundary is the center of mass the shorter is the waiting time, while the velocity remains constant, on the contrary to the previous case. For the isentropic gas dynamics system with damping the dependence on the interface is very similar to the family (a). The initial velocity of the front is the highest for the initial distributions, which mass centers are the farthest from the free boundary that is ρ_3^0 and ρ_1^0. Profiles ρ_2^0 and ρ_4^0 concentrated at the beginning closer to the interface exert smaller pressure on it, so the initial force causing that the front stars to move is smaller and the same happens for the initial velocity. The waiting time is influenced by the location of the mass center and the smoothness of the initial solution. Its length reflects the same features as in the previous case, suggesting that the dependence on the initial data is global for both of the families.

Estimates of the waiting times

Now we are going to study the behaviour of the interface for initial densities given by

$$\rho_0(x) = \begin{cases} g(x) & x \le x^0 \\ 0 & \text{elsewhere} \end{cases}, \tag{5.4.4}$$

where x^0 is the initial location of the free boundary and the function $g(x)$ is strictly positive for $x < x^0$ and $g(x^0) = 0$. In particular, we are going to focus on the waiting time for different initial profiles and different adiabatic coefficients in the constitutive law for the pressure $P(\rho)$.

At first we consider initial data of the form (5.4.4) with the function $g(x) = \cos(x)^{\frac{2}{\gamma-1}}$ and $x^0 = 0.5\pi$, which corresponds to the problem studied by Aronson in [9]. We notice that it changes with the parameter γ, but belongs always the the family (a) from the previous simulations. At Figure 5.9 we show the time evolution of the interface $\xi(t)$ of the porous medium equation and isentropic gas dynamics system for different values of the adiabatic coefficient γ. We see that the higher is the parameter γ the earlier the front is set in motion, however,

γ	Theory	PME	IG
2	0.083	0.086	0.64
3	0.083	0.083	0.65
4	0.075	0.079	0.62
5	0.067	0.072	0.59
6	0.060	0.066	0.56
7	0.054	0.061	0.51
8	0.047	0.056	0.48
9	0.044	0.052	0.44

Table 5.3: Numerical approximations of the waiting times t^* for the porous medium equation (PME) and isentropic gas dynamics system (IG) when the initial data of the form (5.4.4) with the function $g(x) = \cos(x)^{\frac{2}{\gamma-1}}$ and $x^0 = 0.5\pi$. They are compared with the theoretical value for the parabolic model.

.

its initial velocity remains unchanged. Shorter waiting time is the results of the change of the location of the mass center towards the free boundary for higher values of γ. Table 5.3 presents the comparison between the numerical approximation of the waiting times obtained using the criterion I and theoretical values for the porous medium equation.

$$t^*_{th} = \frac{\gamma - 1}{2\gamma(\gamma + 1)}. \tag{5.4.5}$$

We observe a good agreement between the theoretical and numerical results for the parabolic problem. For the hyperbolic model, in comparison to the porous medium equation, the interface remains stationary for much longer time. The values are ten times bigger. However, as shown on Figure 5.8, the dependence of the waiting time on the pressure $P(\rho)$ is similar to the one of porous medium equation. It decreases for higher values of γ.

Let us now consider an initial data that is smooth and doesn't depend on the adiabatic coefficient γ. More precisely, it is of the form (5.4.4) with the function $g(x) = \cos(x)^2$ and $x^0 = 0.5\pi$. Figure 5.9 presents the time evolution of the interface $\xi(t)$ for the parabolic and hyperbolic model. In the case of the latter one the numerical viscosity produces initially some errors for law values of γ, but despite this inaccuracy we can analyze the waiting time. We observe that in this case the behaviour is opposite to the previous example. The initial profile is equal for all pressure functions. The density is law near the front and inreases towards the domain boundary. So the smaller the adiabatic coefficient, the smaller are the differences between the diffusion forces in these two regions. For higher γ the particles near ξ move slower and the whole gas needs more time for the reorganization, so the waiting time is longer. Its approximate values are given in Table 5.4. We observe the increases with γ. Moreover, this increase is much faster for the porous medium equation as we can see at Figure 5.10.

γ	PME	IG
2	0.084	0.53
3	0.035	0.93
4	0.7	1.11
5	1.34	1.32
6	2.38	1.56
7	4.32	1.85
8	7.95	2.27
9	14.57	1.76

Table 5.4: Numerical approximations of the waiting times t^* for the porous medium equation (PME) and isentropic gas dynamics system (IG) when the initial data of the form (5.4.4) is given by the function $g(x) = \cos(x)^2$ and $x^0 = 0.5\pi$.
.

Regularity of the solution near the interface

Mathematical theory concerning well posedness of the compressible Euler equations with friction under physical boundary condition is still far from complete. The same refers to the description of the behaviour of the interface. It is not well understood how the density evolves into the vacuum. Asymptotically phenomena similar to the ones of porous medium equation are expected, but short time dynamics of hyperbolic and parabolic models differs.

In the previous section we studied the waiting time phenomenon occurring for initial densities smooth enough near the interface. The difference between the compressible gas dynamics system and the porous medium equation was manifested by different length of the waiting times and initial velocity of the front. Now we are going to consider a general initial data and study how the regularity of the density near the free boundary changes with time.

The smoothness of the density ρ near the boundary Γ can be quantified by the parameter α in

$$\rho \sim |x(t) - x|^{\alpha}. \tag{5.4.6}$$

The larger α becomes, the smoother the density at the interface is. The physical boundary condition corresponds to the value $\alpha = \frac{1}{\gamma}$. According to this parameter we distinguish four cases with the following expected behaviours:

1. $\alpha \geq \dfrac{2}{\gamma - 1}$: Density is very smooth near the interface. The behaviour of the hyperbolic system is expected to be similar to the porous medium equation. It means that there exists a time T^*, such that for $t < T^*$ the boundary is stationary and α remains constant. At $t = T^*$ the front starts to move and $\alpha \to \frac{1}{\gamma - 1}$ asymptotically.

2. $\dfrac{1}{\gamma - 1} < \alpha < \dfrac{2}{\gamma - 1}$: The concentration of mass at the boundary is large enough in order to have a non zero forcing effect on the interface. It starts to move immediately and $\alpha \to \frac{1}{\gamma - 1}$ with time

3. $\alpha = \dfrac{1}{\gamma - 1}$: Physical boundary. α=constant

4. $0 < \alpha < \dfrac{1}{\gamma - 1}$: Density is not smooth near the boundary and $\alpha \to \frac{1}{\gamma-1}$ asymptotically

We are going to study numerically regularity of the density ρ near the boundary via the bahaviour of the parameter α. In particular, for the system (5.1.1) on an interval $I = [0, L]$, with Dirichlet boundary conditions, we consider the initial data of the form

$$\rho_0(x) = \begin{cases} (1-x)^{\alpha_0} & \text{for} \quad x \leq 1 \\ 0 & \text{for} \quad x > 1 \end{cases}, \qquad u_0(x) = 0 \tag{5.4.7}$$

where

$$\alpha_0 = \left\{ \frac{2}{\gamma - 1}, \frac{3}{2(\gamma - 1)}, \frac{1}{\gamma - 1}, \frac{1}{2(\gamma - 1)} \right\}.$$

This choice corresponds to the four cases presented above. We assume the left boundary at $x = 0$ to be fixed and the only free boundary is given by a nondecreasing function $\xi(t)$.

Figure 5.11 presents time evolution of the coefficient α for different values of the adiabatic exponent γ. For the porous medium equation the results are in agreement with the theory. More precisely, when the initial density is smooth, so $\alpha \geq 2/(\gamma - 1)$ and the initial mass is accumulated far from the interface, we observe the waiting time phenomena. When the boundary starts to move, immediately of after t^*, the parameter $\alpha(t)$ converges monotonically to the value given by the physical boundary condition.

For the isentropic gas dynamics system the convergence is not monotone any more. At some point there is a sudden loss of the regularity of ρ. It is manifested by the oscillations of the parameter α, which decrease for higher values of the exponent γ and for smaller α^0. Asymptotically the velocity is constant in space and the density satisfies the physical boundary condition near the free boundary.

This behaviour can be explained studying the initial distribution of the density of the gas ρ and the momentum equation of the form

$$u_t + \left(\frac{u^2}{2} \right)_x + \frac{1}{\gamma - 1} \left(c^2 \right)_x = -u. \tag{5.4.8}$$

When α is big enough, the solution is smooth near the interface and almost all the mass is concentrated at the left boundary $x = 0$. It results in its violent redistribution. Moreover, near ξ its value and gradient are small so in (5.4.8) the term $(c^2)_x$ can be neglected. The velocity increases rapidly and behaves like the Burger's equation with damping shown at Figure 5.13. When the gas starts to concentrates at the front the pressure on the interface, proportional to the gradient of the density, becomes higher then under the physical boundary condition, on the contrary to the behaviour of the porous medium equation. The initial velocity of the interface for hyperbolic system is larger that for the parabolic equation. At Figure 5.12 we can see, for $\gamma = 2$, that indeed it is like that. The boundary is pushed with much stronger force and after it is set in motion the density relaxes near Γ. Its regularity increases, what we observe by increase of the parameter α. The production term $(c^2)_x$ in (5.4.8) balances the damping $-u$ and the velocity starts to behave like the solution to the Burger's equation converging to it asymptotically as shown at Figure 5.13. Equivalently, it is given by the Darcy's law (1/

$(\gamma - 1)(c^2)_x = -u.$

On the other hand, when the initial condition is with $\alpha^0 \leq 1/(\gamma - 1)$ in the equation for the momentum (5.4.8) the dominant terms are the production $(c^2)_x$ and the damping $-u$. The velocity obeys the Darcy's law, which is a characteristic behaviour of the solution to the porous medium equation.
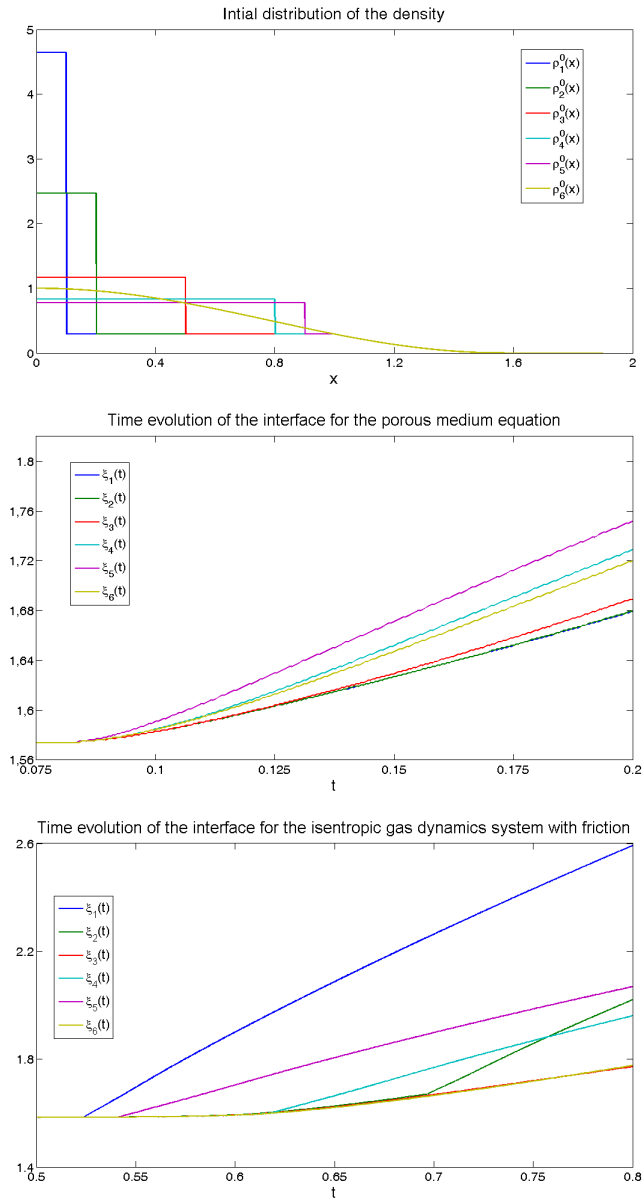
Figure 5.5: Simulation for the initial data of the form (5.4.3). The first figure presents the initial distributions of the density ρ. The next show the time evolution of the interface $\xi(t)$ for the porous medium equation and the isentropic gas dynamics system with damping respectively.
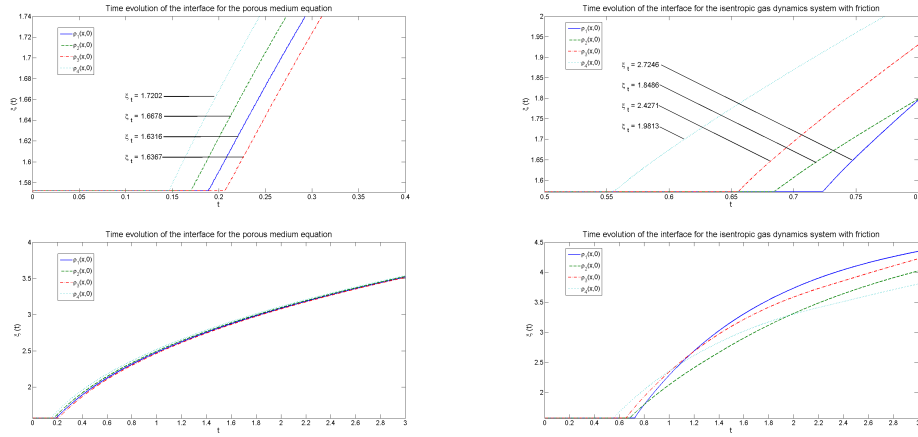
Figure 5.6: Time evolution of the interface for the porous medium equation and the isentropic gas dynamics with damping for the initial data of the Family (b). The upper plots present the behaviour in the proximity of the free boundary, while the lower show the evolution of the interfaces for longer times.
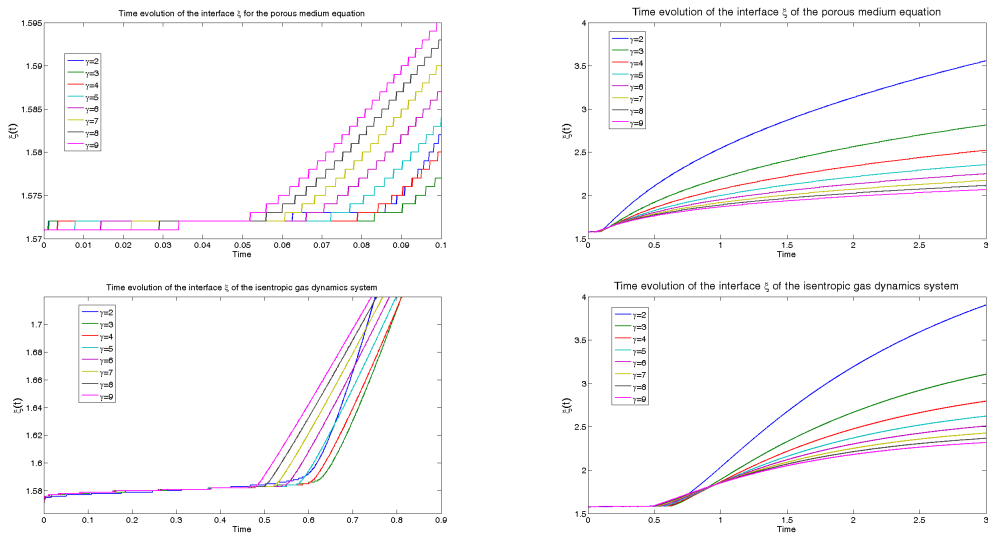
Figure 5.7: Time evolution of the interface $\xi = \xi(t)$ of the porous medium equation (top) and the isentropic gas dynamics system (bottom) when the initial data of the form (5.4.4) with the function $g(x) = \cos(x)^{\frac{2}{\gamma-1}}$ and $x^0 = 0.5\pi$.
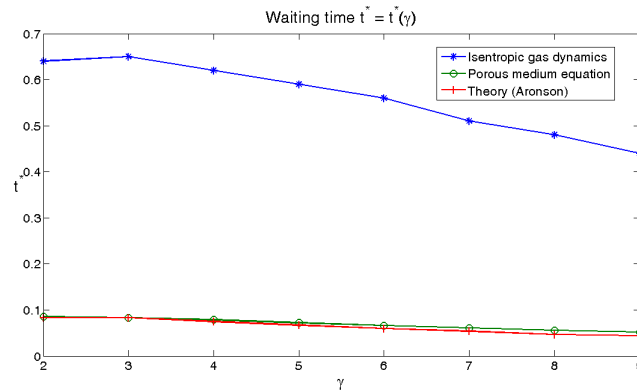
Figure 5.8: Dependence of the waiting times t^* on the adiabatic constant γ for the porous medium equation (-o-) and the isentropic gas dynamics system (-*-) when the initial data of the form (5.4.4) is given by the function $g(x) = \cos(x)^{\frac{2}{\gamma-1}}$ and $x^0 = 0.5\pi$.
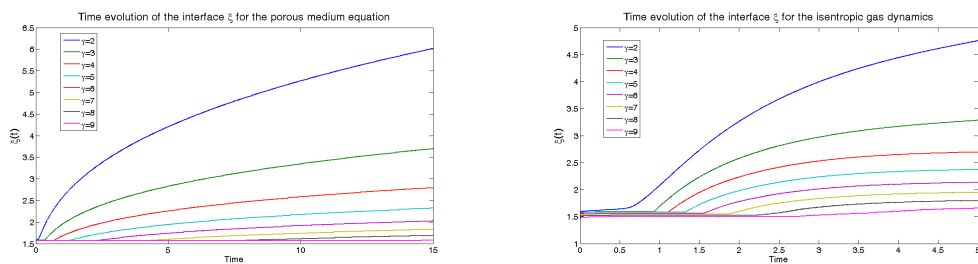
Figure 5.9: Time evolution of the interface $\xi = \xi(t)$ of the porous medium equation (left) and the isentropic gas dynamics system (right) for the initial data of the form (5.4.4) with the function $g(x) = \cos(x)^2$ and $x^0 = 0.5\pi$.
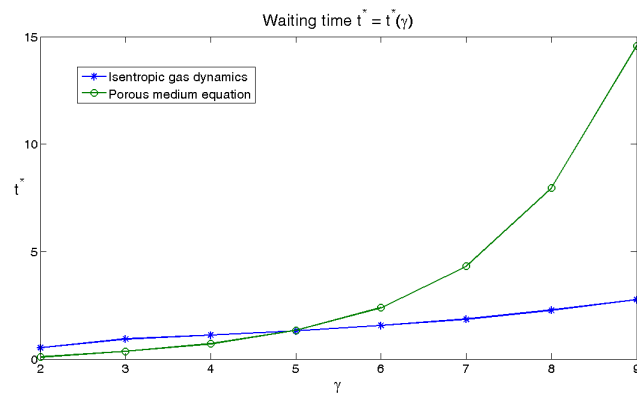
Figure 5.10: Dependence of the waiting times t^* on the adiabatic constant γ for the porous medium equation (-o-) and the isentropic gas dynamics system (-*-) when the initial data of the form (5.4.4) is given by the function $g(x) = \cos(x)^2$ and $x^0 = 0.5\pi$.

Isentropic gas dynamics   Porous medium equation
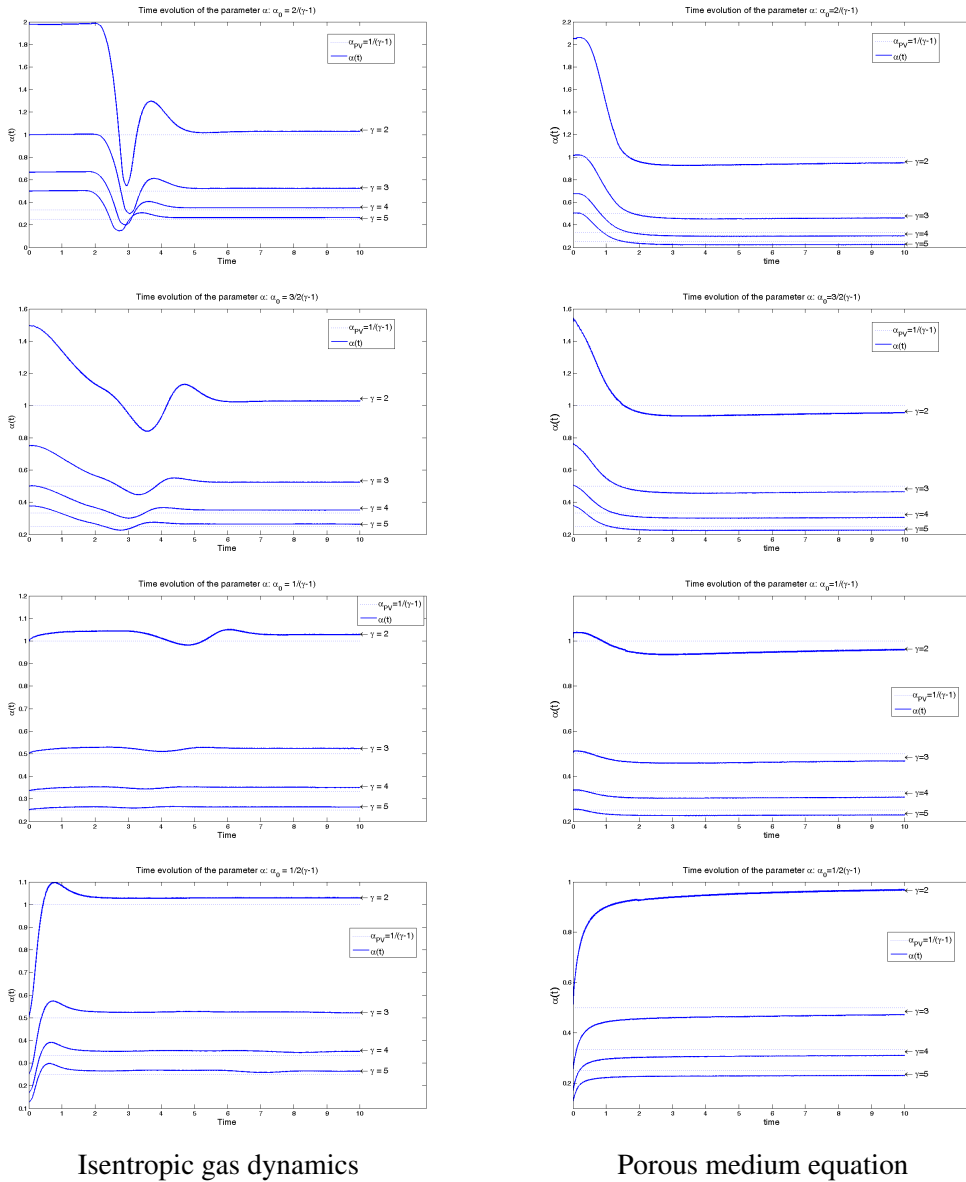
Figure 5.11: Time evolution of the parameter $\alpha(t)$ for the isentropic gas dynamics system and the porous medium equation with the adiabatic coefficient $\gamma = 2, 3, 4, 5$ and initial data $\rho_0 = (4 - x)^{\alpha_0(\gamma)}$ for $x \leq 4$ and $\rho_0 = 0$ elsewhere. $\alpha_0(\gamma) = \{2/(\gamma - 1), 3/2(\gamma - 1), 1/(\gamma - 1), 1/2(\gamma - 1)\}$
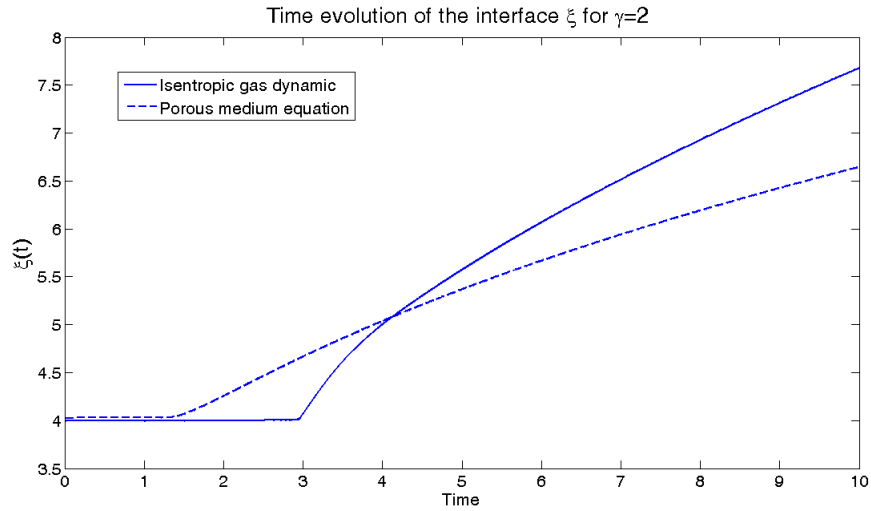
Figure 5.12: Time evolution of the interface $\xi(t)$ for the isentropic gas dynamics system and the porous medium equation with the adiabatic coefficient $\gamma = 2$ and initial data $\rho_0 = (4-x)^2$ for $x \leq 4$ and $\rho_0 = 0$ elsewhere. Comparison of the initial velocity of the front. Steeper gradient of $\xi(t)$ when the boundary is set in motion indicates higher speed.
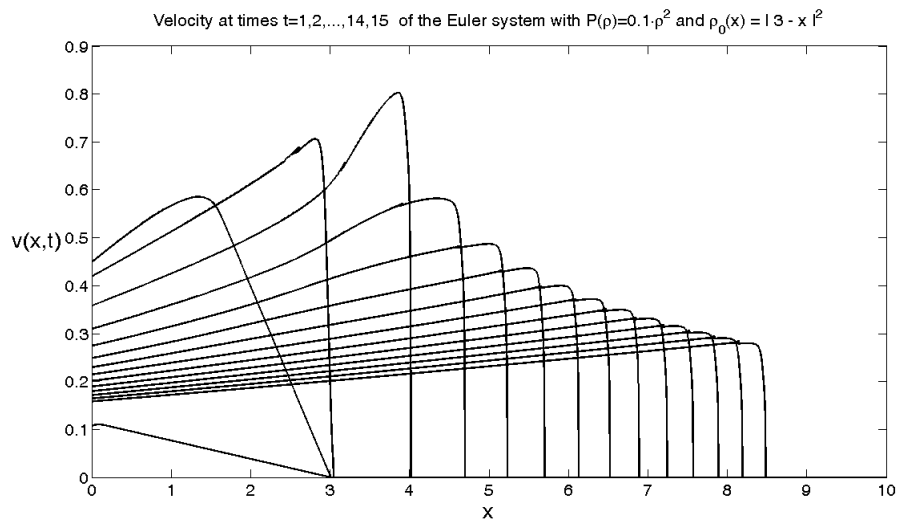
Figure 5.13: Velocity profiles at times $t = 1, 2, ..., 14, 15$ of the isentropic gas dynamics system with the pressure $P(\rho) = 0.1\rho^2$ and initial data $\rho_0 = (3-x)^2$ for $x \leq 3$ and $\rho_0 = 0$ elsewhere.

NUMERICAL APPROXIMATION: SOME HYPERBOLIC MODELS OF CHEMOTAXIS

6.1 Introduction

The aim of this thesis in to investigate some models of chemotaxis from both, analytical and numerical point of view. One of them is the model of vasculogenesis proposed by Gamba et.al. [44]. It describes the evolution of density ρ of endothelial cells, their velocity u and concentration ϕ of chemical substance being a chemoattractant. In one dimension, the system writes as

$$\begin{cases} \rho_t + (\rho u)_x = 0, \\ (\rho u)_t + \left(\rho u^2 + P(\rho)\right)_x = -\alpha\rho u + \chi\rho\phi_x, \\ \phi_t = D\phi_{xx} + a\rho - b\phi, \end{cases} \qquad (6.1.1)$$

where the pressure law is the one for isentropic gases that is

$$P(\rho) = \varepsilon\rho^\gamma, \qquad \gamma \geq 1, \varepsilon > 0. \qquad (6.1.2)$$

The positive parameters D, a, b are respectively diffusion coefficient, production and degradation rates of the chemoattractant, while α measures the friction force and χ the strength of the response of cells to the presence of the chemical substance. The system is endowed with initial data, which can contain vacuum states, and suitable boundary conditions. For the later purpose we denote the flux and the source term by

$$F(U) = \left(\rho u, \rho u^2 + P(\rho)\right), \quad S(U) = \left(0, -\alpha\rho u + \chi\rho\phi_x\right), \qquad (6.1.3)$$

where $U = (\rho, \rho u)$ and $F = (F^\rho, F^{\rho u})$.

Chapter 1 was devoted to the mathematical theory concerning chemotaxis models. Based on the original works of Gamba et.al. we described the derivation of system and its ability to reproduce the experimentally observed phenomena of blood network formation, on the contrary to the parabolic mode. However the analytical results are still limited and many questions are still open. It motivates us to study system (6.1.1) numerically. In order to obtain this goal first we have to construct numerical schemes that can reproduce all of the important features

of the model. Among them there are the conservation of the total mass and the preservation of the non negativity of densities and concentrations. Due to the presence of the source term the system can be endowed with non constant stationary solutions, which are also to be preserved. Moreover, the ability to deal with the vacuum states, which can occur also for strictly positive initial data, is essential.

System (6.1.1) is composed of a hyperbolic and a parabolic part. Despite the strong coupling between them via the reaction terms, we approximate them separately using different methods. The parabolic equation, describing the evolution of the chemoattractant, is solved using the finite difference Crank-Nicholson scheme given by (4.2.1). In this chapter we are going to focus only on the hyperbolic part, in which we "freeze" the potential ϕ_x at each time interval.

At the beginning we present a finite difference, explicit scheme with centered in space discretization of the source term. We show the failure of this approach in two cases. The first one concerns the conservation of the total mass of cells, which is a necessary feature of the model (6.1.1) defined on a bounded domain with no-flux boundary conditions. We are going to show that a standard scheme is unable to preserve this property. The next problem is connected with the approximation of the non constant steady states. More precisely, the scheme that we consider gives inaccurate solution of the momentum, which should vanish under the prescribed no-flux boundary conditions. Instead, we get stabilization of the velocity at values far from zero.

Similar problems are considered in the article of Natalini and Ribot [92], where a dissipative, semilinear, hyperbolic system is analyzed. In this case the large error in the approximation of the velocity is also present, but the mass is conserved for the upwind scheme for both, constant and non constant, steady states. This is guaranteed by defining the boundary conditions in terms of the diagonal variables. In order to obtain correct results for the momentum Natalini and Ribot propose higher order corrections of a standard upwind method obtaining the so called Asymptotically High Order (AHO) scheme. It is characterized by a truncation error computed on every steady state of order two or more. As a result the scheme is increasingly accurate for large times with respect to the asymptotic behaviour and approximates the momentum correctly. However, the above modifications lead to the loss of mass and further modifications of boundary conditions has to be introduced.

In the case of the model (6.1.1) the failure of mass conservation appears for a simple upwind scheme, without any modifications. To overcome this problem we apply the method introduced by Natalini and Ribot in [92] of the modification of the boundary conditions obtaining a scheme, for which the mass difference between two time steps is of order Δx^2. However, the problem with the inaccurate approximation of the momentum is left open for this type of scheme.

In order to obtain a numerical scheme that conserves the total mass and approximates correctly the non constant stationary solutions we use finite volume method based on an approximate Riemann solver for the homogeneous part of the system. The mass is preserved as an immediate result of imposing zero flux condition at control cells lying at the boundary of the domain. To satisfy the second condition we use well-balanced method to treat the source terms. This approach guarantees that the fluxes and sources are treated at the same time level what, as a consequence, leads to the correct approximation of the density and the momentum at equilibria. We introduce a special reconstruction of variables at control cells interfaces us-

ing stationary solutions with constant velocity. For such, semi-discrete scheme we prove the consistency with the original system, the preservation of the non negativity of ρ and the preservation of steady states with constant velocity. Moreover, we give a weak stability conditions for a fully discrete scheme.

The chapter is organized as follows. In Section 6.2 we describe the failure of the finite difference, explicit scheme with centered in space approximation of the source term. Numerical results showing its accuracy and drawbacks are presented. Then, Section 6.3 is devoted to the well-balanced scheme based on finite volume method. Proofs of the scheme properties are given and the CFL condition is stated.

6.2 Failure of the standard, explicit scheme

In this section we are going to present an explicit scheme based on finite difference method for the hyperbolic part of the model (6.1.1). Our aim is to explain, why this approach is incapable of giving a good approximation on bounded domains with no-flux boundary conditions. We show that in the case of non constant stationary solutions it produces an error in the approximation of the momentum and fails to conserve the total, discrete mass defined at each time step t^n using the trapezoidal rule

$$M^n = \left(\frac{\rho_1^n}{2} + \sum_{i=2}^{s-1} \rho_i^n + \frac{\rho_s^n}{2} \right) \Delta x. \qquad (6.2.1)$$

First we describe the above problems in the case of a semilinear, hyperbolic model studied in [92]. Then we focus on the system (6.1.1). We give details on the origins of the loss of mass and propose the modifications preventing from it. In the end we present the problem with the approximation of the momentum. However, so far it is still an open problem.

6.2.1 Semilinear model

Problems with the mass conservation and the correct approximation of the velocity at the non constant steady states were studied by Natalini and Ribot in [92]. They considered a semilinear, dissipative model of chemotaxis of the following form

$$\begin{cases} \rho_t + u_x = 0, \\ u_x + \varepsilon^2 \rho_x = \rho \phi_x - u, \\ \phi_t - D \phi_{xx} = a\rho - b\phi. \end{cases} \qquad (6.2.2)$$

Despite the similarities between the above model and (6.1.1) the problems with the numerical approximation that we consider are not equal. The semilinear system (6.2.2) can be written in diagonal variables

$$w = \frac{1}{2} \left(\rho - \frac{u}{\varepsilon} \right) \quad \text{and} \quad z = \frac{1}{2} \left(\rho + \frac{u}{\varepsilon} \right)$$

with the no-flux boundary conditions of the form

$$w(0,t) = z(0,t) = 0, w(L,t) = z(L,t) = 0, \phi_x(0,t) = \phi_x(L,t) = 0. \qquad (6.2.3)$$

In this setting a standard, upwind scheme conserves the discrete mass (6.2.1). However, a large error in the approximation of the momentum at the non constant steady states. This is due to the presence of the numerical viscosity induced by the upwind scheme for density

$$\rho_i^{n+1} = \rho_i^n - \frac{\Delta t}{2\Delta x}(u_{i+1}^n - u_{i-1}^n) + \frac{\varepsilon \Delta t}{2\Delta x}(\rho_{i+1}^n - 2\rho_i^n + \rho_{i-1}^n). \tag{6.2.4}$$

At the non constant steady state $\rho_i^{n+1} = \rho_i^n$. If the second space derivative of ρ is high, then the space step Δx has to be very small in order to make the velocity u constant.

To improve the accuracy authors of [92] introduce higher order corrections to the upwind scheme. The goal is to obtain truncation error calculated at each steady state of order two or more. As a consequence, the scheme is increasingly accurate with time with respect to the asymptotic behaviour of solutions. This approach was already applied in [7] to dissipative hyperbolic systems and this type of schemes are called the Asymptotically high order (AHO) schemes.

Modification of the upwind scheme increase the accuracy of the approximation at the stationary solutions, but create another problem. Now the upwind discretization of the boundary condition produces a loss of the total mass and further corrections have to be introduced. More precisely, Natalini and Ribot in [92] defined the values of ρ in $x = 0$ and $x = L$ at time step t^{n+1} using the solution at time t^n such that a discrete mass M given by (6.2.1) is exactly preserved in time. As we already mentioned, the problem with mass conservation in the case of the system (6.1.1) is different. We cannot use diagonal variables and the boundary conditions have to be imposed directly on ρ and u. It implies that a standard upwind scheme, without modifications, fails to preserve the mass. We are going to explain why it happens and how to solved this problem.

6.2.2 Quasilinear model

Now let us focus on the model (6.1.1). After a brief description of a standard scheme applied to this system, we give details why it fails to conserve the mass. Then we present a method to modify boundary values in order to improve the accuracy. In the end, using numerical analysis, we explain the problem in the approximation of the momentum.

Numerical scheme

We start with describing a numerical scheme based on finite difference method for the hyperbolic part of the chemotaxis model (6.1.1). The transport part and the sources are to be treated at different time steps. More precisely, first we solve the homogeneous system using a standard method based on the relaxation technique presented in the Chapter 3. Then we integrate in time the reaction terms discretized in space by the centered difference. The chemotaxis part is treated explicitly, while the damping implicitly, because of its high stiffness. The forward Euler method is used yielding the following scheme

$$\begin{cases} U^* = U^n + \Delta t H(U^n), \\ U^{n+1} = U^* + \Delta t \left(0, \quad \chi \rho_1^n \frac{\phi_{i+1}^n - \phi_{i-1}^n}{2\Delta x} - \alpha \rho_i^{n+1} u_i^{n+1}\right). \end{cases} \tag{6.2.5}$$

The function $H(U^n)$ corresponds to the space discretization of the homogeneous system obtained using the BGK approximation with two velocities of equal speed and the opposite sign. In this case the numerical flux function is a Rusanov flux. Now we are going to describe it in details.

Let us denote by the vector $\vec{f}_k = \left(f_k^\rho, f_k^{\rho u} \right)^T$, $k = 1, 2$ the components of the BGK model approximating $U = (\rho, \rho u)$ of the form of linear transport equations

$$\begin{cases} \partial_t \vec{f}_1 + \lambda \partial_x \vec{f}_1 = \frac{1}{\epsilon} \left(\vec{\mathcal{M}}_1(U) - \vec{f}_1 \right) \\ \partial_t \vec{f}_2 - \lambda \partial_x \vec{f}_2 = \frac{1}{\epsilon} \left(\vec{\mathcal{M}}_2(U) - \vec{f}_2 \right) \end{cases}, \qquad (6.2.6)$$

where the local Maxwellian functions are given by

$$\begin{cases} \vec{\mathcal{M}}_1 = \frac{1}{2\lambda}(\lambda U + F(U)), \\ \vec{\mathcal{M}}_2 = \frac{1}{2\lambda}(\lambda U - F(U)). \end{cases} \qquad (6.2.7)$$

In the Chapter 3 we explained how to solve the problem (6.2.6). It is split into a homogeneous system of equations and an ODE corresponding to the time integration of the source part. To obtain $\vec{f}_k^{n+1/2}$, $k = 1, 2$ we solve

$$\partial_t \begin{pmatrix} \vec{f}_1 \\ \vec{f}_2 \end{pmatrix} + \operatorname{diag}(\lambda, \lambda, -\lambda, -\lambda) \partial_x \begin{pmatrix} \vec{f}_1 \\ \vec{f}_2 \end{pmatrix} = 0 \qquad (6.2.8a)$$

in the interval $[t^n, t^{n+1}]$ with the initial states

$$\begin{pmatrix} \vec{f}_1^0 \\ \vec{f}_2^0 \end{pmatrix} = \begin{pmatrix} \vec{\mathcal{M}}_1(U(x, 0)) \\ \vec{\mathcal{M}}_2(U(x, 0)) \end{pmatrix} = \begin{pmatrix} \frac{1}{2\lambda}(\lambda U(x, 0) + F(U(x, 0))) \\ \frac{1}{2\lambda}(\lambda U(x, 0) - F(U(x, 0))) \end{pmatrix}. \qquad (6.2.8b)$$

Adding the source term the solution U at time step t^{n+1} is given by

$$U_i^{n+1} = U_i^{n+1/2} = \vec{f}_1^{i,n+1/2} + \vec{f}_2^{i,n+1/2} + \Delta t \left(0, \quad \chi \rho_1^n \frac{\phi_{i+1}^n - \phi_{i-1}^n}{2\Delta x} - \alpha \rho_i^{n+1} u_i^{n+1} \right). \qquad (6.2.8c)$$

The stability of the scheme guaranteed by the CFL condition of the form

$$\Delta t^{n+1} = 0.9 \frac{\Delta x}{\lambda^n}. \qquad (6.2.9)$$

Mass conservation

Now let us focus on the problem with the mass conservation. The above scheme fails to preserve it and a special care is needed to deal with boundary conditions. In the case of the velocity u and the concentration of the chemoattractant ϕ the choice is clear

$$u_1^n = u_s^n = 0 \quad \text{and} \quad \phi_x|_{x=0} = \phi_x|_{x=L} = 0.$$

The latter can be approximated by the standard first or second order method given by (3.5.3), (3.5.8) respectively. Theoretically for the density ρ we have the same condition as for ϕ and the first idea one would follow is taking for example

$$\rho_1^n = \frac{4}{3}\rho_2^n - \frac{1}{3}\rho_3^n, \quad \rho_s^n = \frac{4}{3}\rho_{s-1}^n - \frac{1}{3}\rho_{s-2}^n.$$

However, this choice leads to a significant loss of mass M at any non constant steady state.

Figure 6.1 presents time evolution of the total mass of the model (6.1.1) with linear pressure $\gamma = 1$, $\alpha = a = b = D = \xi = 1$, $\varepsilon = 100$ and the initial datum of the form

$$\rho_0(x) = \phi_0(x) = 1500 + \sin(4\pi|x - L/4|), \qquad u_0(x) = 0.$$

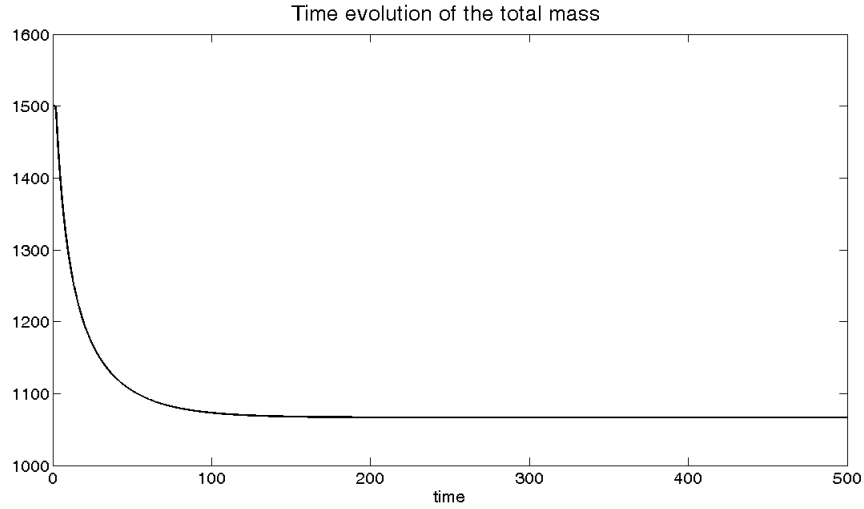We observe rapid, unphysical decrease of the mass and its stabilization with time at a constant

Figure 6.1: Time evolution of the total mass (6.2.1) of the model (6.1.1) with linear pressure $\gamma = 1$, $\alpha = a = b = D = \xi = 1$, $\varepsilon = 100$. The boundary nodes $\rho_1^{n+1}, \rho_s^{n+1}$ are computed using the second order approximation (3.5.8).

value. It is the result of the fact that the system reached a constant solution.

In order to explain why the scheme (6.2.8) is incapable of conserving the total mass let us compute the difference of the discrete mass (6.2.1) at two different time steps. Using the upwind scheme for the system of linear, transport equations (6.2.8a) the density at time step t^{n+1} is given by

$$\rho_i^{n+1} = \rho_i^n + \frac{\lambda \Delta t}{2\Delta x}(\rho_{i+1}^n - 2\rho_i^n + \rho_{i-1}^n) - \frac{\Delta t}{2\Delta x}(p_{i+1}^n - p_{i-1}^n) \qquad (6.2.10)$$

and the mass difference equals

$$\begin{aligned} \Delta M = M^{n+1} - M^n \quad &= \quad \frac{\lambda \Delta t}{4}(\rho_1^n - \rho_2^n + \rho_s^n - \rho_{s-1}^n) \\ &+ \quad \frac{\Delta t}{4}(p_2^n + p_1^n - p_{s-1}^n - p_s^n). \end{aligned} \qquad (6.2.11)$$

Assuming the first order, homogeneous Neumann boundary conditions (3.5.3)

$$\rho_1^n = \rho_2^n, \quad \rho_s^n = \rho_{s-1}^n, \quad \text{and} \quad p_1^n = p_s^n = 0$$

we get

$$\Delta M = \frac{\Delta t}{4}(p_2^n - p_{s-1}^n).$$ (6.2.12)

As a consequence, if the momentum p is approximated incorrectly, it may lead to the loss of mass. In fact, it happens for the model (6.1.1) at non constant steady state. The velocity should vanish under the no-flux boundary conditions, instead the approximation is far from being zero and causes the mass loss. We are going to describe this problem subsequently.

To guarantee the mass preservation at each time step we are going to modify the values ρ_1^{n+1}, ρ_s^{n+1} such that $\Delta M = 0$. In order to find the formulas we calculate again the difference $M^{n+1} - M^n$, but now the numerical solution ρ_i^{n+1} given by (6.2.10) is used only for the internal nodes $i = 2, ..., s-1$ yielding

$$
\begin{aligned}
M^{n+1} - M^n &= \frac{\Delta x \Delta t}{2}\left[\frac{1}{\Delta t}(\rho_1^{n+1} - \rho_1^n) + \frac{\lambda}{\Delta x}(\rho_1^n - \rho_2^n) + \frac{1}{\Delta x}(p_1^n + p_2^n)\right] \\
&+ \frac{\Delta x \Delta t}{2}\left[\frac{1}{\Delta t}(\rho_s^{n+1} - \rho_s^n) + \frac{\lambda}{\Delta x}(\rho_s^n - \rho_{s-1}^n) - \frac{1}{\Delta x}(p_s^n + p_{s-1}^n)\right].
\end{aligned}
$$ (6.2.13)

To satisfy the condition $\Delta M = 0$ the terms in the brackets have to vanish giving

$$
\begin{cases}
\rho_1^{n+1} = \left(1 - \lambda\frac{\Delta t}{\Delta x}\right)\rho_1^n + \lambda\frac{\Delta t}{\Delta x}\rho_2^n - \frac{\Delta t}{\Delta x}(p_1^n + p_2^n), \\
\rho_s^{n+1} = \left(1 - \lambda\frac{\Delta t}{\Delta x}\right)\rho_s^n + \lambda\frac{\Delta t}{\Delta x}\rho_{s-1}^n + \frac{\Delta t}{\Delta x}(p_s^n + p_{s-1}^n).
\end{cases}
$$ (6.2.14)

If we use a high resolution method (3.2.19) for the linear, transport system (6.2.8a) the same approach can be followed. In this case the density at time step t^{n+1} is given by

$$
\begin{aligned}
\rho_i^{n+1} = \rho_i^n &- \frac{\Delta t}{2\Delta x}(p_{i+1}^n - p_{i-1}^n) \\
&+ \lambda\frac{\Delta t}{4\Delta x}\left[\left(\psi_1^{i+1/2,n} + \psi_2^{i+1/2,n}\right)\rho_{i+1}^n + \left(\psi_1^{i-1/2,n} + \psi_2^{i-1/2,n}\right)\rho_{i-1}^n\right. \\
&\left. - \left(\psi_1^{i+1/2,n} + \psi_1^{i-1/2,n} + \psi_2^{i+1/2,n} + \psi_2^{i-1/2,n}\right)\rho_i^n\right] \\
&+ \frac{\Delta t}{4\Delta x}\left[\left(\psi_1^{i+1/2,n} - \psi_2^{i+1/2,n}\right)p_{i+1}^n + \left(\psi_1^{i-1/2,n} - \psi_2^{i-1/2,n}\right)p_{i-1}^n\right. \\
&\left. - \left(\psi_1^{i+1/2,n} + \psi_1^{i-1/2,n} - \psi_2^{i+1/2,n} - \psi_2^{i-1/2,n}\right)p_i^n\right],
\end{aligned}
$$

where

$$
\begin{aligned}
\psi_1^{i+1/2,n} &= 1 - \left(1 - \lambda\frac{\Delta t}{\Delta x}\right)\varphi\left(r_+^{i+1/2}(\mathcal{M}_1^\rho(U^n))\right), \\
\psi_2^{i+1/2,n} &= 1 - \left(1 - \lambda\frac{\Delta t}{\Delta x}\right)\varphi\left(r_-^{i+1/2}(\mathcal{M}_2^\rho(U^n))\right).
\end{aligned}
$$

The function φ is a flux limiter function and $r_{\pm}^{i+1/2}(\mathcal{M}(U))$ are defined by (3.2.19c). Calculating the mass difference between the two time steps and requiring that it vanishes we obtain

$$\rho_1^{n+1} = \rho_1^n - \lambda \frac{\Delta t}{\Delta x} \left[1 - \frac{1}{2} \left(1 - \lambda \frac{\Delta t}{\Delta x} \right) \left(\varphi_1^{3/2} + \varphi_2^{3/2} \right) \right] (\rho_1^n - \rho_2^n)$$
$$- \frac{\Delta t}{\Delta x} \left[1 - \frac{1}{2} \left(1 - \lambda \frac{\Delta t}{\Delta x} \right) \left(\varphi_2^{3/2} - \varphi_1^{3/2} \right) \right] p_2^n, \tag{6.2.15}$$

$$\rho_s^{n+1} = \rho_s^n - \lambda \frac{\Delta t}{\Delta x} \left[1 - \frac{1}{2} \left(1 - \lambda \frac{\Delta t}{\Delta x} \right) \left(\varphi_1^{s-1/2} + \varphi_2^{s-1/2} \right) \right] (\rho_s^n - \rho_{s-1}^n)$$
$$+ \frac{\Delta t}{\Delta x} \left[1 + \frac{1}{2} \left(1 - \lambda \frac{\Delta t}{\Delta x} \right) \left(\varphi_2^{s-1/2} - \varphi_1^{s-1/2} \right) \right] p_{s-1}^n. \tag{6.2.16}$$

To define $r_+^{3/2}, r_-^{s-1/2}$ in the flux limiter function φ we need to approximate values at artificial nodes ρ_0^n, ρ_{s+1}^n and u_0^n, u_{s+1}^n. In particular, taking

$$\rho_0^n = \frac{4}{3}\rho_1^n - \frac{1}{3}\rho_2^n, \quad \rho_{s+1}^n = \frac{4}{3}\rho_s^n - \frac{1}{3}\rho_{s-1}^n,$$

and the rigid wall boundary condition for the velocity

$$u_0^n = -u_2^n, \quad u_{s+1}^n = -u_{s-1}^n,$$

we obtain

$$r_+^{3/2} = \frac{\frac{\lambda}{3}(\rho_2^n - \rho_1^n) + p_2^n}{\lambda(\rho_2^n - \rho_1^n) + p_2^n}, \qquad r_-^{3/2} = \frac{\lambda(\rho_3^n - \rho_2^n) - (p_3^n + p_2^n)}{\lambda(\rho_2^n - \rho_1^n) - (p_2^n + p_1^n)},$$
$$r_+^{s-1/2} = \frac{\lambda(\rho_{s-1}^n - \rho_{s-2}^n) + (p_{s-1}^n + p_{s-2}^n)}{\lambda(\rho_s^n - \rho_{s-1}^n) + (p_s^n + p_{s-1}^n)}, \qquad r_-^{s-1/2} = \frac{\frac{\lambda}{3}(\rho_s^n - \rho_{s-1}^n) + p_{s-1}^n}{\lambda(\rho_s^n - \rho_{s-1}^n) + p_{s-1}^n}.$$

Under the introduced modifications of the boundary states the scheme (6.2.8) conserves the total mass.

Conservation of non-constant steady states

The presence of non constant steady solutions gives rise to problems with the mass conservation caused by the incorrect approximation of the momentum. We already explained that centered discretizations of sources do not balance the internal forces correctly and are not capable of preserving stationary distributions. Even if the density ρ and the concentration of chemoattractant ϕ are approximated with high accuracy, there is a large error in the numerical solution of the momentum.

Figure 6.2 presents stationary solutions of ρ, ϕ and p for the system (6.1.1) with the linear pressure $P(\rho) = \varepsilon\rho$. The residues of the density and the momentum at Figure 6.3 are of order 10^{-10} so the steady state is reached. The total mass is conserved, because we used a scheme (6.2.8) with the modified values at boundaries (6.2.14). However, we observe that there is a large error in the approximation of the momentum. The boundary conditions imply that it should vanish, but we observe that it has a sign and its L^∞ norm is of order 10^3.
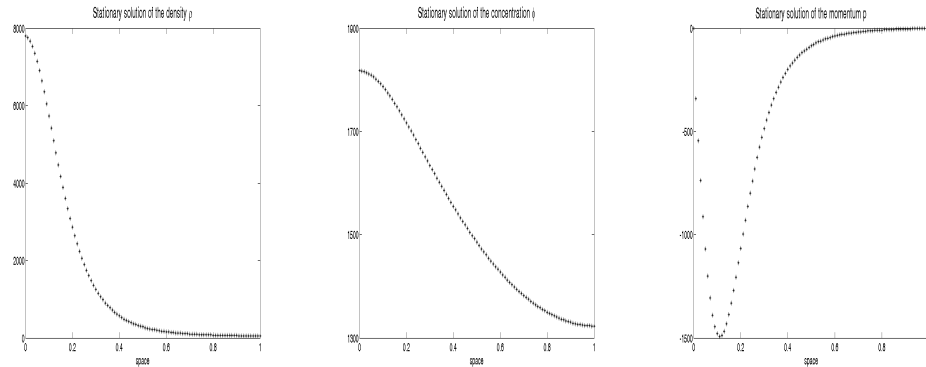
Figure 6.2: Numerical approximation obtained using a finite difference scheme (6.2.8) of stationary solutions of ρ, ϕ and p for the model (6.1.1) with linear pressure $\gamma = 1$, $\alpha = a = b = D = \xi = 1$, $\varepsilon = 100$ and the initial mass equal to 1500.
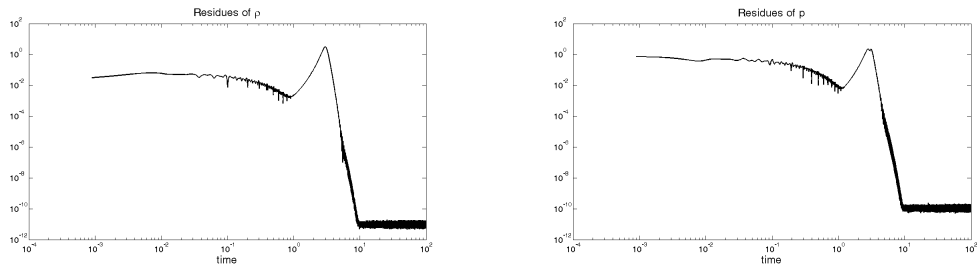

Figure 6.3: Time evolution of residues obtained obtained using a finite difference scheme (6.2.8) of the density ρ (left) and the momentum p (right) for the model (6.1.1) with linear pressure $\gamma = 1$, $\alpha = a = b = D = \xi = 1$, $\varepsilon = 100$ and the initial mass equal to 1500.

Decreasing the artificial diffusion improves the approximation but insignificantly. Figure 6.4 presents the velocity at steady state for the scheme (6.2.8), in which the linear transport system is solved using upwind method or the high resolution scheme with minmod and Superbee of Roe flux-limiters for the linear-transport system. The L^∞ norm of the momentum decreases for less viscous scheme, for example with the Superbee of Roe limiter, however, the error is still unacceptable. Other idea to improve the accuracy would be to follow the approach of the Asymptotic High Order schemes. But the system (6.1.1) and the semilinear one (6.2.2) have different fluxes of the momentum. Moreover, in the quasilinear case, we consider a general, nonlinear pressure function $P(\rho) = \rho^\gamma$, for $\gamma \geq 1$. This implies that the truncation errors, calculated to order higher than one, become nonlinear and finding the conditions to cancel lower order terms complicated. This is the reason why so far we haven't found them to guarantee the higher order of truncation error at steady states. This problem is still open.
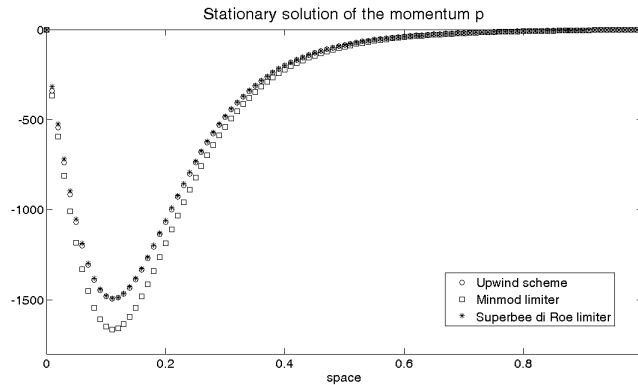
Figure 6.4: Numerical approximation obtained using a finite difference scheme (6.2.8) of the momentum p for the model (6.1.1) with linear pressure $\gamma = 1$, $\alpha = a = b = D = \xi = 1$, $\varepsilon = 100$ and the initial mass equal to 1500. Comparison between different flux limiter functions.

6.3   Well-balanced scheme

The aim of the next chapter is the numerical study of the behaviour of the hyperbolic model of chemotaxis (6.1.1) in one space dimension defined on a bounded interval with no-flux boundary conditions. In particular, we are be interested in the analysis of the non constant stationary solutions. In order to perform such study we need a scheme that can reproduce all the important features of the model. Among them are the conservation of the total mass, the preservation of the non negativity of density and the preservation of the stationary solutions. Moreover, the hyperbolic system can produce vacuum states even for a strictly positive initial datum. This means that an accurate approximation at interface between the region, where $\rho > 0$ and the region, where it vanishes, is essential.

In the previous section we showed that a scheme based on the finite difference method (6.2.8) fails in satisfying all the above properties. We explained why it doesn't conserve the mass at the non constant steady states. Moreover, we performed some numerical simulations to prove that this approach is also unable to approximate correctly the momentum at equilibrium. We managed to solved the problem with the mass preservation by modifying the values of the density at boundary nodes, but we were unable to increase the accuracy of the approximation of the momentum.

The above problems that we encounter using finite difference methods with centered in space approximation of the source term motivated us to look for other approaches. In this section we are going to present a finite volume scheme that satisfies all the essential features, mentioned earlier, of the chemotaxis model. The construction is based on the solution of the Riemann problem defined at each cell interface and using the approximate Riemann solver as a numerical flux function. The total mass is conserved automatically in the finite volume framework, while the well-balancing approach guarantees the correct approximation of the non constant steady states. The well-balanced property is obtained substituting the left and right state of the Riemann problem, which are the cells averages for the homogeneous system, by

the reconstructed variables. The correct reconstruction implies also the preservation of the non negativity of the density if the numerical flux function for the homogeneous problem does it.

First we present a general construction starting from defining the flux functions. Then we give details of the reconstruction and prove the properties of the scheme in a semi-discrete case. In the end we state a weak-stability condition assuring the preservation of non negativity for a fully discrete scheme.

Finite volume scheme

We construct a finite volume scheme using the general theory introduced in Chapter 3. As was already explained, we decouple parabolic and hyperbolic part of the system (6.1.1) freezing the potential ϕ_x at each time interval. The solution ϕ^{n+1} is found using the Crank-Nicholson scheme (4.2.1). Now we focus on the hyperbolic part

$$\begin{cases} \rho_t + (\rho u)_x = 0, \\ (\rho u)_t + \left(\rho u^2 + P(\rho)\right)_x = -\alpha \rho u + \chi \rho \phi_x^n. \end{cases} \tag{6.3.1}$$

The main idea of the method is to build a scheme using the approximate solutions of the Riemann problem posed at each cell boundary. In the case of the homogeneous system it is well known approach leading to Godunov type scheme. But the presence of the source make the problem more difficult. Solving generalized Riemann problem in not trivial. This is the reason why we follow a different approach. The numerical flux function remains the same as in the homogeneous case, for example Suliciu relaxation solver, while the influence of the reaction terms is going to be taken into account via the definition of the left and right states in the Riemann problem. Then, by a special reconstruction we can guarantee the well-balanced property and the preservation of the non negativity of density.

More precisely, denoting $U = (\rho, \rho u)$, a first-order, finite volume semi-discrete scheme on an uniform grid is

$$\frac{d}{dt} U_i + \frac{1}{\Delta x} \left(F_{i+1/2}^- - F_{i-1/2}^+ \right) = 0, \tag{6.3.2a}$$

$$F_{i+1/2}^- = \mathcal{F}^- \left(U_i, U_{i+1}, \Delta\phi_{i+1/2} \right), \quad F_{i+1/2}^+ = \mathcal{F}^+ \left(U_i, U_{i+1}, \Delta\phi_{i+1/2} \right), \tag{6.3.2b}$$

for some left/right numerical fluxes $\mathcal{F}^\pm$, where $\Delta\phi_{i+1/2} = \phi_{i+1} - \phi_i$. We look for them in the following form

$$\mathcal{F}^- \left(U_i, U_{i+1}, \Delta\phi_{i+1/2} \right) = \mathcal{F} \left(U_{i+1/2}^-, U_{i+1/2}^+ \right) - F \left(U_{i+1/2}^- \right) + F(U_i), \tag{6.3.3a}$$

$$\mathcal{F}^+ \left(U_i, U_{i+1}, \Delta\phi_{i+1/2} \right) = \mathcal{F} \left(U_{i+1/2}^-, U_{i+1/2}^+ \right) - F \left(U_{i+1/2}^+ \right) + F(U_{i+1}), \tag{6.3.3b}$$

where $\mathcal{F}$ is any consistent C^1 numerical flux for the homogeneous problem and F is the analytical flux given by (6.1.3). The variables $U_{i+1/2}^\pm$ are reconstructed from the local equilibrium system. The dependence on the gradient of the concentration of the chemoattractant is hidden inside them. Inserting the numerical flux functions (6.3.3) into the scheme (6.3.2) we obtain

$$\Delta x \frac{d}{dt} U_i + \mathcal{F} \left(U_{i+1/2}^-, U_{i+1/2}^+ \right) - \mathcal{F} \left(U_{i-1/2}^-, U_{i-1/2}^+ \right) = S_i \tag{6.3.4a}$$

with

$$S_i = \mathcal{S}_{i+1/2}^- + \mathcal{S}_{i-1/2}^+$$

$$= \begin{pmatrix} 0 \\ F^{\rho u}\left(\rho_{i+1/2}^-\right) - F^{\rho u}(\rho_i) \end{pmatrix} + \begin{pmatrix} 0 \\ F^{\rho u}(\rho_i) - F^{\rho u}\left(\rho_{i+1/2}^+\right) \end{pmatrix}, \qquad (6.3.4\text{b})$$

where $\mathcal{S}_{i+1/2}^\pm$ are numerical source functions.

Reconstruction

In order to complete the construction of the scheme we have to define the variables $U_{i+1/2}^\pm$, which contain all the information about the source term, in such a way that the scheme is consistent, well-balanced and preserves the non negativity of the density. In the case of the system (6.3.1) well balancing means satisfying some discrete version of the equilibrium equations of the form

$$\begin{cases} (\rho u)_x = 0, \\ \left(\rho u^2 + P(\rho)\right)_x = -\alpha \rho u + \chi \rho \phi_x^n. \end{cases} \qquad (6.3.5)$$

Let us rewrite the above system using the internal energy function $e(\rho)$. For a pressure law of isentropic gas dynamics $P(\rho) = \varepsilon \rho^\gamma, \varepsilon > 0, \gamma > 1$ it is defined by

$$e'(\rho) = \frac{P(\rho)}{\rho^2}$$

under the assumption that $e(\rho) + \frac{P(\rho)}{\rho}$ has a finite limit when $\rho \to 0$. In this case the equilibrium system becomes

$$\begin{cases} (\rho u)_x = 0, \\ \left(\frac{1}{2}u^2 + e(\rho) + \frac{P(\rho)}{\rho} - \chi \phi^n\right)_x = -\alpha u. \end{cases} \qquad (6.3.6)$$

Reconstruction of the variables $U_{i+1/2}^\pm$ is based on solving the above system in each half of the cell. More precisely, integrating (6.3.6) between x_i and $x_{i+1/2}^-$ and between $x_{i+1/2}^+$ and x_{i+1} we obtain the equations for $U_{i+1/2}^\pm$. However, finding the solutions in a general case is not always possible. This is due to the fact that the relations are nonlinear, for example they are polynomials of order two or higher. In order to simplify the problem we can request a numerical scheme to preserve only a special class of stationary solutions. Then the reconstruction of the interface variables $U_{i+1/2}^\pm$ is obtained from (6.3.6) under additional constraints. In particular, we can consider constant velocity, which corresponds to the following steady state system

$$\begin{cases} u_x = 0, \\ \left(e(\rho) + \frac{P(\rho)}{\rho} - \chi \phi^n\right)_x = -\alpha u. \end{cases} \qquad (6.3.7)$$

In the case of the velocity equal to zero at the steady state we obtain static equilibria, which lead to the so called hydrostatic reconstruction introduced in [14] for shallow water equations. Our choice of constant, instead of vanishing, velocity is motivated by the presence of the damping term, which in this case is taken into account inside the reconstruction variables. For the hyperbolic model of chemotaxis on bounded domain with no-flux boundary conditions

the hydrostatic reconstruction assures well-balancing for all possible steady states.

To find $U^-_{i+1/2}$ we integrate (6.3.7) between x_i and $x_{i+1/2}$, while to reconstruct $U^+_{i+1/2}$ between $x_{i+1/2}$ and x_{i+1}. From the first equation of (6.3.7) we get

$$u^-_{i+1/2} = u_i \quad \text{and} \quad u^+_{i+1/2} = u_{i+1}. \tag{6.3.8}$$

Now let us focus on the second condition. Under the assumption that $e(\rho) + \frac{P(\rho)}{\rho}$ has a limit for $\rho \to 0$ integration of the second equation of (6.3.7) yields

$$\begin{cases} \left(e(\rho) + \dfrac{P(\rho)}{\rho}\right)\Big|_{x_i}^{x^-_{i+1/2}} = -\alpha \displaystyle\int_{x_i}^{x^-_{i+1/2}} u\,dx + \chi\phi\big|_{x_i}^{x^-_{i+1/2}}, \\[3mm] \left(e(\rho) + \dfrac{P(\rho)}{\rho}\right)\Big|_{x^+_{i+1/2}}^{x_{i+1}} = -\alpha \displaystyle\int_{x^+_{i+1/2}}^{x_{i+1}} u\,dx + \chi\phi\big|_{x^+_{i+1/2}}^{x_{i+1}}. \end{cases} \tag{6.3.9}$$

The integral terms can be approximated using any consistent method. Taken into account that u is constant in each half of the cell we can consider for example

$$-\alpha \int_{x_i}^{x^-_{i+1/2}} u\,dx = -\alpha u_i \frac{\Delta x}{2}, \quad -\alpha \int_{x^+_{i+1/2}}^{x_{i+1}} u\,dx = -\alpha u_{i+1}\frac{\Delta x}{2}$$

or

$$-\alpha \int_{x_i}^{x^-_{i+1/2}} u\,dx = -\alpha \max(0, u_i)\Delta x, \quad -\alpha \int_{x^+_{i+1/2}}^{x_{i+1}} u\,dx = -\alpha \min(0, u_{i+1})\Delta x.$$

We are going to use the second approximation. The choice of the interface values $\phi_{i+1/2}$ is not so flexible if we want the scheme to preserve the non negativity of ρ. For example taking $\phi_{i+1/2} = \frac{1}{2}(\phi_i + \phi_{i+1})$ will lead to the violation of this property. Instead we consider

$$\phi_{i+1/2} = \min(\phi_i, \phi_{i+1}).$$

Summing all the terms we obtain

$$\begin{cases} u^-_{i+1/2} = u_i, \\[2mm] e\left(\rho^-_{i+1/2}\right) + \dfrac{P\left(\rho^-_{i+1/2}\right)}{\left(\rho^-_{i+1/2}\right)} = e(\rho_i) + \dfrac{P(\rho_i)}{\rho_i} - \alpha\max(0, u_i)\Delta x + \chi(\min(\phi_i, \phi_{i+1}) - \phi_i), \end{cases} \tag{6.3.10a}$$

and

$$\begin{cases} u^+_{i+1/2} = u_{i+1}, \\[2mm] e\left(\rho^+_{i+1/2}\right) + \dfrac{P\left(\rho^+_{i+1/2}\right)}{\left(\rho^+_{i+1/2}\right)} = e(\rho_{i+1}) + \dfrac{P(\rho_{i+1})}{\rho_{i+1}} + \alpha\min(0, u_{i+1})\Delta x + \chi(\min(\phi_i, \phi_{i+1}) - \phi_{i+1}). \end{cases} \tag{6.3.10b}$$

In order to simplify the notation we denote $X_+ = \max(0, X)$, $X_- = \min(0, X)$ and introduce a function

$$\Psi(\rho) = \left(e + \frac{P}{\rho}\right)(\rho).$$

It is strictly increasing for $\rho > 0$ and has a finite limit for $\rho \to 0$ so there exists an inverse Ψ^{-1}. Then the reconstruction takes the form

$$\rho^-_{i+1/2} = \Psi\left([\Psi(\rho_i) - \alpha(u_i)_+\Delta x + \chi(\min(\phi_i, \phi_{i+1}) - \phi_i)]_+\right),$$
$$\rho^+_{i+1/2} = \Psi\left([\Psi(\rho_{i+1}) + \alpha(u_{i+1})_-\Delta x + \chi(\min(\phi_i, \phi_{i+1}) - \phi_{i+1})]_+\right),$$

where the positivity-preserving truncations of the leading order densities guarantee the non-negativity of ρ.

As a result we obtain a finite volume scheme, which is well-balanced at the steady states with constant velocity. In the case of the system (6.3.1) these are all possible equilibria. To find the solution at time step t^{n+1}, first we have to find the variables at cells interfaces $U^\pm_{i+1/2}$ using (6.3.7). Then we obtain a finite volume, well-balanced scheme taking (6.3.4), in which numerical flux and source functions are calculated at the reconstructed states. We choose numerical flux function for the homogeneous problem in the form of an approximate Riemann solvers such as HLL or Suliciu.

Properties of the semi-discrete scheme

Now we focus on describing the properties of the constructed scheme. We pointed out that the total mass is conserved automatically in the framework of finite volume, while the consistency with the original system is guaranteed by a correct reconstruction of the variables $U^\pm_{i+1/2}$. It assures also the preservation of the non negativity and the preservation of the steady states. Let us state the above properties in the following theorem.

Theorem 7. *Let $F = (F^\rho, F^{\rho u})^T$ be the analytical flux of the system (6.3.1) and let $\mathcal{F}$ be a consistent, $\mathcal{C}^1$ numerical flux preserving the non negativity of ρ for the homogeneous problem. The finite volume scheme*

$$\Delta x \frac{d}{dt} U_i + \mathcal{F}\left(U^-_{i+1/2}, U^+_{i+1/2}\right) - \mathcal{F}\left(U^-_{i-1/2}, U^+_{i-1/2}\right) = S_i \qquad (6.3.11\text{a})$$

with

$$S_i = \mathcal{S}^-_{i+1/2} + \mathcal{S}^+_{i-1/2}$$
$$= \begin{pmatrix} 0 \\ F^{\rho u}\left(\rho^-_{i+1/2}\right) - F^{\rho u}(\rho_i) \end{pmatrix} + \begin{pmatrix} 0 \\ F^{\rho u}(\rho_i) - F^{\rho u}\left(\rho^+_{i+1/2}\right) \end{pmatrix} \qquad (6.3.11\text{b})$$

and the reconstruction

$$\left(\rho^-_{i+1/2}, u^-_{i+1/2}\right) = \left(\Psi^{-1}\left[\Psi(\rho_i) - \alpha(u_i)_+\Delta x + \chi(\phi_{i+1/2} - \phi_i)\right]_+, u_i\right),$$
$$\left(\rho^+_{i+1/2}, u^+_{i+1/2}\right) = \left(\Psi^{-1}\left[\Psi(\rho_{i+1}) + \alpha(u_{i+1})_-\Delta x + \chi(\phi_{i+1/2} - \phi_{i+1})\right]_+, u_{i+1}\right),$$
$$(6.3.11\text{c})$$

where $\phi_{i+1/2} = \min(\phi_i, \phi_{i+1})$,

i) is consistent with (6.3.1) away from the vacuum
ii) preserves the non negativity of $\rho_i(t)$
iii) preserves the steady states given by (6.3.7).

Proof. In order to prove the consistency of the numerical scheme (6.3.11) with the system (6.3.1) we need to check two properties. The first one concerns consistency with the exact flux, while the second with the source. The former one is obtained using the consistency of the numerical flux function $\mathcal{F}$ for the homogeneous problem, while the latter is based on the criterion given by Perthame and Simeoni in [98]. To make this chapter self-contained we state here the definition that they introduced.

Definition 5. *A numerical scheme (6.3.11) is consistent with (6.3.1) if*

$$\forall i = 1, 2, ..., s \qquad \lim_{U_i, U_{i+1} \to U} \mathcal{F}\left(U^-_{i+1/2}, U^+_{i+1/2}\right) = F(U) + O(\Delta x)$$

and

$$\forall i = 1, 2, ..., s \qquad \lim_{U_i, U_{i+1} \to U} \frac{1}{\Delta x}\left(\mathcal{S}^-_{i+1/2} + \mathcal{S}^+_{i+1/2}\right) = S(U) + O(\Delta x).$$

The specific form of the reconstruction (6.3.11c) restricts the use of the above definition only to states $U = (\rho, \rho u)$ away from vacuum. It is a result of the presence of maxima in the definition of $\rho^\pm_{i+1/2}$. To see this let us consider Taylor expansion of $U^\pm_{i+1/2}$ in the case of for example $\rho^-_{i+1/2}$. The reconstruction has the form

$$\rho^-_{i+1/2} = \Psi^{-1}\left[\Psi(\rho_i) - \alpha(u_i)_+\Delta x + \chi(\phi_{i+1/2} - \phi_i)\right]_+.$$

As $\phi_{i+1} - \phi_i \approx \phi_x \Delta x$ we get

$$\rho^-_{i+1/2} = \Psi^{-1}\left[\Psi(\rho_i) - (\alpha(u_i)_+ - \chi\phi_x)\Delta x)\right]_+.$$

In the limit $\Delta x \to 0$ the expression inside the maximum function remains positive. If ρ_i vanishes this is not always true.

Let us now prove the consistency with the flux away from vacuum. We need to show that

$$\forall i = 1, 2, ..., s \qquad \lim_{U_i, U_{i+1} \to U} \mathcal{F}\left(U^-_{i+1/2}, U^+_{i+1/2}\right) = F(U) + O(\Delta x).$$

The Taylor expansion of $\mathcal{F}\left(U^-_{i+1/2}, U^+_{i+1/2}\right)$ around (U_i, U_{i+1}) is

$$\mathcal{F}\left(U^-_{i+1/2}, U^+_{i+1/2}\right) = \mathcal{F}(U_i, U_{i+1}) + \left.\frac{\partial\mathcal{F}}{\partial U}\right|_{U_i}\left(U^-_{i+1/2} - U_i\right) + \left.\frac{\partial\mathcal{F}}{\partial U}\right|_{U_{i+1}}\left(U_{i+1} - U^+_{i+1/2}\right) + O(\Delta x).$$

From the assumptions in the theorem

$$\forall i = 1, 2, ..., s \qquad \lim_{U_i, U_{i+1} \to U} \mathcal{F}(U_i, U_{i+1}) = F(U)$$

and $\frac{\partial\mathcal{F}}{\partial U} = \mathcal{F}_U(U)$ exists and is continuous. Moreover, the Taylor expansion of $\rho^-_{i+1/2}$ at ρ_i has the form

$$\rho^-_{i+1/2} = \rho_i + \frac{\rho_i}{P'(\rho_i)}\left(-\alpha(u_i)_+\Delta x + \frac{1}{2}\chi\phi_x\Delta x)\right) + O(\Delta x)^2,$$

where we used the property of the inverse function $(f^{-1})'(x) = 1/f'(f^{-1}(x))$. Then

$$
\begin{aligned}
U_{i+1/2}^- - U_i &\approx \left(\frac{\rho_i}{P'(\rho_i)} \left(-\alpha(u_i)_+ + \frac{1}{2}\chi\phi_x \right) \Delta x, \, u_x \Delta x \right), \\
U_{i+1} - U_{i+1/2}^+ &\approx \left(-\frac{\rho_{i+1}}{P'(\rho_{i+1})} \left(\alpha(u_{i+1})_- - \frac{1}{2}\chi\phi_x \right) \Delta x, \, u_x \Delta x \right),
\end{aligned}
$$

so

$$
\lim_{U_i, U_{i+1} \to U} \mathcal{F}\left(U_{i+1/2}^-, U_{i+1/2}^+ \right) = F(U) + \mathcal{F}_U(U) \cdot \left(\begin{array}{c} \frac{\rho}{P'(\rho)}(-\alpha u + \chi\phi_x) \\ 0 \end{array} \right) \Delta x + O(\Delta x^2)
$$

for all $i = 1, 2, ..., s$ if $\rho > 0$, which ends the proof of the consistency with the flux. To prove the consistency with the source term we have to show that

$$
\forall i = 1, 2, ..., s \qquad \lim_{U_i, U_{i+1} \to U} \frac{1}{\Delta x} \left(\mathcal{S}_{i+1/2}^- + \mathcal{S}_{i+1/2}^+ \right) = S(U) + O(\Delta x).
$$

In our case it becomes

$$
\frac{1}{\Delta x} \left(\begin{array}{c} 0 \\ P\left(\rho_{i+1/2}^-\right) - P\left(\rho_{i+1/2}^+\right) \end{array} \right) = \left(\begin{array}{c} 0 \\ -\alpha\rho u + \chi\rho\phi_x \end{array} \right) + O(\Delta x),
$$

whenever $U_i, U_{i+1} \to U$. Let us consider at first the reconstructed density $\rho_{i+1/2}^-$. As before for strictly positive ρ_i and Δx small enough the maxima in the definition can be omitted. Using the Taylor expansion of $\rho_{i+1/2}^-$ the expansion of $P(\rho_{i+1/2}^-)$ at ρ_i yields

$$
P(\rho_{i+1/2}^-) = P(\rho_i) + \rho_i \left(-\alpha(u_i)_+ \Delta x + \frac{1}{2}\chi\phi_x \Delta x \right) + O(\Delta x)^2.
$$

The same calculations for $\rho_{i+1/2}^+$ give

$$
P(\rho_{i+1/2}^+) = P(\rho_{i+1}) + \rho_{i+1} \left(\alpha(u_{i+1})_- \Delta x - \frac{1}{2}\chi\phi_x \Delta x \right) + O(\Delta x)^2.
$$

Therefore

$$
\begin{aligned}
P(\rho_{i+1/2}^-) - P(\rho_{i+1/2}^+) &= P(\rho_i) + \rho_i(-\alpha(u_i)_+ + \frac{1}{2}\chi\phi_x)\Delta x \\
&\quad - P(\rho_{i+1}) - \rho_{i+1}(\alpha(u_i)_- - \frac{1}{2}\chi\phi_x)\Delta x + O(\Delta x)^2 \\
&= (-\alpha\rho u + \chi\rho\phi_x)\,\Delta x + O(\Delta x)^2,
\end{aligned}
$$

whenever $U_i, U_{i+1} \to U$, which proves $i)$.

Now let us prove $ii)$. For a semi-discrete scheme

$$
\Delta x \frac{d}{dt}\rho_i(t) + \mathcal{F}^\rho(U_i, U_{i+1}) - \mathcal{F}^\rho(U_{i-1}, U_i) = 0
$$

the assumption that $\mathcal{F}$ preserves the non negativity of ρ by interface means that whenever $\rho_i(t)$ vanishes the inequality

$$
\mathcal{F}^\rho(U_i, U_{i+1}) - \mathcal{F}^\rho(U_{i-1}, U_i) \le 0
$$

holds for all other choices of parameters. This implies in our case

$$\mathcal{F}^\rho(U^-_{i+1/2}, U^+_{i+1/2}) - \mathcal{F}^\rho(U^-_{i-1/2}, U^+_{i-1/2}) \leq 0,$$

which is satisfied if $U^-_{i+1/2}, U^+_{i+1/2} \to 0$ whenever U_i vanishes. And it is true for the reconstruction we proposed. To see it let us consider at first $\rho^-_{i+1/2}$. Assuming $\phi_i > \phi_{i+1}$ we have

$$\Psi(\rho^-_{i+1/2}) = [\Psi(\rho_i) - \alpha(u_i)_+ \Delta x + \chi(\min(\phi_i, \phi_{i+1}) - \phi_i)]_+$$
$$= [\Psi(\rho_i) - \alpha(u_i)_+ \Delta x - \chi|\phi_{i+1} - \phi_i|]_+ = 0,$$

where the last equality was obtained using the assumption that $\Psi(\rho) \to 0$ when $\rho \to 0$ in the limit $U_i \to 0$. Then $\Psi(\rho^-_{i+1/2}) = 0$ for vanishing U_i implies that $\rho^-_{i+1/2} \to 0$ as $U_i \to 0$. Let us assume now on the contrary that $\phi_i < \phi_{i+1}$. Then in the limit $U_i \to 0$ we get

$$\Psi(\rho^-_{i+1/2}) = [\chi(\phi_i - \phi_i)]_+ = 0.$$

Analogical results can be showed for $\rho^+_{i-1/2}$, which completes the proof of $ii)$.

It remains to prove $iii)$. For any two left and right states U_i, U_{i+1} the steady solution

$$\begin{cases} u_{i+1} = u_i \\ \Psi(\rho_{i+1}) - \chi\phi_{i+1} - \Psi(\rho_i) + \chi\phi_i = -\alpha\left((u_i)_+ + (u_{i+1})_-\right)\Delta x \end{cases}$$

is maintained exactly by the scheme if

$$F^-_{i+1/2} - F^+_{i-1/2} = 0$$

at the equilibrium. Using the explicit formulas for the left and right numerical fluxes the above condition is equivalent to

$$\mathcal{F}(U^-_{i+1/2}, U^+_{i+1/2}) - F(U^-_{i+1/2}) - \mathcal{F}(U^-_{i-1/2}, U^+_{i-1/2}) + F(U^-_{i-1/2}) = 0.$$

Since the numerical flux function $\mathcal{F}$ is consistent to finish the proof we have to show that $U^-_{i+1/2} = U^+_{i+1/2}$ at the steady states. The equality for the velocity is obvious as $u^-_{i+1/2} = u_i = u_{i+1} = u^+_{i+1/2}$. In the case of the density let us consider $\rho^-_{i+1/2}$. From the reconstruction we have

$$\Psi(\rho^-_{i+1/2}) = \left[\Psi(\rho_i) - \alpha(u_i)_+ \Delta x + \chi(\phi_{i+1/2} - \phi_i)\right]_+,$$

while the equilibrium equation for the momentum at nodes x_i and x_{i+1} yields

$$\Psi(\rho_i) = \Psi(\rho_i) - \alpha\left((u_i)_+ + (u_{i+1})_-\right)\Delta x - \chi(\phi_{i+1} - \phi_i).$$

Inserting $\Psi(\rho_i)$ into $\Psi(\rho^-_{i+1/2})$ gives

$$\Psi(\rho^-_{i+1/2}) = \left[\Psi(\rho_{i+1}) + \alpha(u_i)_- \Delta x + \chi(\phi_{i+1/2} - \phi_{i+1})\right]_+ = \Psi(\rho^+_{i+1/2})$$

and implies $\rho^-_{i+1/2} = \rho^+_{i-1/2}$, which completes the proof of $iii)$. $\qquad\square$

Stability of the fully-discrete scheme

The fully discrete scheme (6.3.2) has the form

$$U_i^{n+1} = U_i^n - \frac{\Delta t}{\Delta} \left(\mathcal{F}^-(U_i^n, U_{i+1}^n) - \mathcal{F}^+(U_{i-1}^n, U_i^n) \right), \tag{6.3.12}$$

where the numerical left and right fluxes $\mathcal{F}^\pm$ are defined by (6.3.3). Time integration doesn't influence the consistency and well-balanced property, however, to assure the stability of the scheme we have to precise the CFL condition.

For a finite volume numerical scheme preserving non negativity is a weak stability condition, which we are going to use in order to derive the bounds on the time step. We follow the proof presented in [14]. We first we give a definition of a homogeneous solver preserving non negativity for a fully discrete scheme.

Definition 6. *We say that a solver $\mathcal{F}$ for a homogeneous system preserves the non negativity of ρ by interfaces with a numerical speed $\sigma(U_i, U_{i+1}) \geq 0$ if whenever the CFL condition*

$$\sigma(U_i, U_{i+1})\Delta t \leq \Delta x$$

holds, we have

$$\rho_i - \frac{\Delta t}{\Delta x} \left(\mathcal{F}^\rho(U_i, U_{i+1}) - \rho_i u_i \right) \geq 0,$$

$$\rho_{i+1} - \frac{\Delta t}{\Delta x} \left(\rho_{i+1} u_{i+1} - \mathcal{F}^\rho(U_i, U_{i+1}) \right) \geq 0.$$

The following propositions gives the stability conditions in the non homogeneous case.

Proposition 3. *Let us assume that the homogeneous flux preserves the non negativity of ρ by interfaces. Then the fully discrete scheme*

$$U_i^{n+1} = U_i^n - \frac{\Delta t}{\Delta} \left(\mathcal{F}(U_{i+1/2}^{n,-}, U_{i+1/2}^{n,+}) - \mathcal{F}(U_{i-1/2}^{n,-}, U_{i-1/2}^{n,+}) \right) + \frac{\Delta t}{\Delta x} S_i^n, \tag{6.3.13}$$

with the reconstruction at interfaces given by (6.3.11c) preserves the non negativity of ρ by interfaces, which means than whenever the CFL condition

$$\sigma(U_{i+1/2}^-, U_{i+1/2}^+)\Delta t \leq \Delta x \tag{6.3.14}$$

holds, we have

$$\rho_i - \frac{\Delta t}{\Delta x} \left(\mathcal{F}^\rho(U_{i+1/2}^-, U_{i+1/2}^+) - \rho_i u_i \right) \geq 0,$$
$$\rho_{i+1} - \frac{\Delta t}{\Delta x} \left(\rho_{i+1} u_{i+1} - \mathcal{F}^\rho(U_{i+1/2}^-, U_{i+1/2}^+) \right) \geq 0. \tag{6.3.15}$$

Proof. Assuming the CFL condition (6.3.14) holds and knowing that $\mathcal{F}$ preserves the non negativity for the homogeneous system we have

$$\rho_{i+1/2}^- - \frac{\Delta t}{\Delta x} \left(\mathcal{F}^\rho(U_{i+1/2}^-, U_{i+1/2}^+) - \rho_{i+1/2}^- u_{i+1/2}^- \right) \geq 0,$$

$$\rho_{i+1/2}^+ - \frac{\Delta t}{\Delta x} \left(\rho_{i+1/2}^+ u_{i+1/2}^+ - \mathcal{F}^\rho(U_{i+1/2}^-, U_{i+1/2}^+) \right) \geq 0.$$

It is equivalent to

$$\begin{cases} \left(1 + \dfrac{\Delta t}{\Delta x} u_i\right) \rho_{i+1/2}^- - \dfrac{\Delta t}{\Delta x} \mathcal{F}^\rho(U_{i+1/2}^-, U_{i+1/2}^+) \geq 0, \\ \left(1 - \dfrac{\Delta t}{\Delta x} u_{i+1}\right) \rho_{i+1/2}^+ + \dfrac{\Delta t}{\Delta x} \mathcal{F}^\rho(U_{i+1/2}^-, U_{i+1/2}^+) \geq 0. \end{cases} \tag{6.3.16}$$

From the reconstruction (6.3.11c) we know that $\rho_{i+1/2}^- \leq \rho_i$ and $\rho_{i+1/2}^+ \leq \rho_{i+1}$. So as long as

$$\left(1 + \frac{\Delta t}{\Delta x} u_i\right) \geq 0, \qquad \left(1 - \frac{\Delta t}{\Delta x} u_{i+1}\right) \geq 0$$

the condition (6.3.16) implies that (6.3.15) holds. But $u_i \geq -\frac{\Delta t}{\Delta x}$ and $u_{i+1} \geq \frac{\Delta t}{\Delta x}$ under the CFL condition (6.3.14) since $|u_i| \leq \sigma(U_{i+1/2}^-, U_{i+1/2}^+)$ for all $i = 1, 2, ..., s$, which ends the proof. $\qquad \square$

NUMERICAL STUDY OF SOME HYPERBOLIC MODELS OF CHEMOTAXIS IN 1D

7.1 Introduction

It is well known that aggregation phenomena are precisely explained by Keller-Segel type models. They occur at large time scales and parabolic systems are able to capture the macroscopic behaviour of interacting species. However, this approach fails when spatially complex structures have to be reproduced. This was found out while studying experiments performed by Serini et. al [107] with human vascular, endothelial cells. Randomly seeded on the plain gel substratum, they migrate and aggregate to finally form a complex network seen as the beginning of vascularization that is formation of blood capillaries from the mesoderm. The Patlak-Keller-Segel model cannot explain this process as well as cannot describe the 'run and tumble' movement of, for example, Eusterichia Coli. This is why in recent years there is a tendency to use hyperbolic systems, which correspond to models at the lower, mesoscopic scale. They are able to capture the particular features of the modeled quantity and as a consequence can describe short time behaviour of physical problems.

From the mathematical point of view the formation of a complex system, such as a network of blood capillaries, corresponds to the appearance of the non-constant stationary solutions. The study of the existence, stability and properties of such equilibria, besides being extremely interesting and challenging, is essential for understanding entirely dynamics of non linear systems. This motivates us to study analytically and numerically some models of chemotaxis on bounded domains with no-flux boundary conditions. This setting is chosen on purpose to mimic the experimental environment. In particular, we focus our attention on the hyperbolic model system proposed by Gamba et.al in [44] to describe the vasculogenesis process. It is a simple system, which takes into account only two constituents. It describes the evolution of the density ρ of endothelial cells and a concentration of chemoattractant ϕ and has the form

$$\begin{cases} \rho_t + (\rho u)_x = 0, \\ (\rho u)_t + (\rho u \otimes u + P(\rho))_x = -\alpha \rho u + \chi \rho \phi_x, \\ \phi_t = D\phi_{xx} + a\rho - b\phi. \end{cases} \tag{7.1.1}$$

The pressure law for $P(\rho)$ is given by the constitutive law for isentropic gases

$$P(\rho) = \varepsilon \rho^\gamma, \qquad \varepsilon > 0, \gamma \geq 1. \tag{7.1.2}$$

It models the short range interaction between cells and the fact that they have their own volume and cannot be penetrable by others. The friction term $-\rho u$ describes the adhesion of cells to the structure, while $\chi \rho \phi_x$ directional response to the chemical gradient. This model is connected for large times with the following Keller-Segel model of parabolic type, which writes as

$$\begin{cases} \rho_t = P(\rho)_{xx} - (\chi \rho \phi_x)_x, \\ \phi_t = D\phi_{xx} + a\rho - b\phi. \end{cases} \tag{7.1.3}$$

This chapter is devoted to the study of non constant solutions of the above systems. In particular, we are interested in the non constant equilibria of a characteristic form that is composed of regions, where the density is strictly positive and regions, where it vanishes. It is important to stress that the vacuum states appear also for strictly positive initial datum. This process reflects what is observed in experiments on the behaviour of endothelial cells. Regions with high densities of cells correspond to the location of blood capillaries, while the vacuum states are the empty space between them. Our aim is to characterize this type of equilibria.

In the first section we focus on the analytical description of the form of steady states for the model (7.1.1). We start with a general pressure function $P(\rho)$ and we find solutions of the form of sinus-type bumps separated by vacuum. We explain that it is possible to describe the solutions exactly only in the case of one region with strictly positive density and we provide the formulas for quadratic pressure that is $\gamma = 2$. We show that under special conditions on the system parameters there exists one equilibrium composed of one bump located at the boundary of the domain or at its center. Then we study numerically the properties of the stationary states. First we analyze stability of one bump and the dependence of the numbers of bumps on the length of the domain L and chemosensitivity χ for $\gamma = 2$. We show that there exists a threshold length, below which steady states are only constant, and that increasing the size of the domain new bumps appear. Similar effect is observed when increasing the chemotactic response. However, simulations suggest that for each length there is a maximum number of bumps. After reaching it, no matter how high the chemosensitivity would be it affects only the shape of the bumps but not their number. Then we consider different adiabatic coefficients γ. We show that increasing the cells response to the compression, that is increasing γ, leads to the formation of wider and lower bumps, which can merge together and for γ sufficiently large the equilibrium becomes a constant state. In the end we analyzed the influence of the total mass. Motivated by the experiments, in which at some threshold initial densities transitions between different structures were observed. In the numerical simulation we observe two ways of accommodating new cells. For $\gamma = 2$ they are accumulating always at the same regions that is the number of bumps and their support don't change. Only the maximal density increases for larger initial mass. On the other hand, for $\gamma = 3$, increasing the mass implies thicker bumps. They can join with each other and at some threshold density, constant state is observed.

Our aim in Section 7.3 is to analyze numerically the long time behaviour of solutions and possible convergence to equilibria for $\gamma = 1$. Simulations suggest that we can distinguish at least two types of asymptotic states. In particular, if the effect of the internal pressure is much stronger than the chemotactic force, that is $\varepsilon >> \chi$, the solutions converge asymptotically to constant or sinus-type states. On the other hand, when chemotaxis is dominant we

observe numerically for ρ a comb of Dirac distributions. The second structure of solutions is particular as it contains vacuum. We analyze their nature and the influence of the total mass. The comparison with the results for $\gamma > 1$ is also presented.

In the last part we compare the long time behaviour of the parabolic (7.1.3) and hyperbolic model (7.1.1). It is known that Keller-Segel model can exhibit the so-called spike patterns composed of regions with high densities separated by vacuum. However, as reported by several authors, they are metastable. It means that if there are more than one spike, there is a slow exchange of mass between them. As a consequence, over large times they move towards each other and merge together. We study numerically this type of behaviour. First, we are going to consider a model with logistic chemosensitivity function and linear diffusion. In this case for the parabolic model we observe the existence of metastable peaks with plateaus equal to the maximal density $\rho_{\max}$, above which the chemotactic effect is switched off. The hyperbolic model yields equilibria with several plateaus, which do not move. Moreover, in the limit of large $\rho_{\max}$ we observe solutions composed of Dirac concentrations. Then we consider the models with nonlinear density function $P(\rho) = \varepsilon\rho^2$ and constant chemosensitivity. We analyze the long time behaviour of bumps and compare the asymptotic states with the results of the hyperbolic model. Simulations indicate the metastability in the parabolic case and static equilibria containing several bumps for the hyperbolic system.

7.2   Stationary solutions

The model (7.1.1) was developed in order to describe a process of vasculogenesis that is formation of blood vessels from the mesoderm. In experiments done by Serini et.al [107] it was observed that starting from the randomly seeded cells after some time a network of capillaries appears. Moreover, the initial densities of the cells have a decisive effect on the formation of complex structures. At small densities percolative-like transitions appear, while a smooth transition to a "Swiss cheese" configuration occurs at large ones. More precisely, below the threshold value a connected network breaks down into a disconnected structure and for the initial mass large enough the thickness of the network increases as more cells are accumulated. From the mathematical point of view the formation of a complex system, such as a network of blood capillaries, corresponds to the appearance of the non-constant stationary solutions.

In this section we are going to study these steady states for the system (7.1.1) defined on the interval $[0, L]$ with no-flux boundary conditions. We start the analysis from the mathematical description. In particular, we are interested in the non constant equilibria of a characteristic form that is composed of region, where the density is strictly positive and region, where it vanishes. It is important to stress that the vacuum states appear also for strictly positive initial datum. This process is observed in the experiments behaviour of cells, which movement is directed by the chemotaxis. Our aim is to find explicitly some of these solutions. We focus on the case with quadratic pressure $P(\rho) = \varepsilon\rho^2$ because it is the simplest from the mathematical point of view. We managed to obtain formulas in the presence of only one region with positive density. Moreover, we show that this is the only case, where calculating the equilibrium explicitly is possible.

The second step of our analysis is devoted to the numerical study of the above non constant stationary solutions. However, before we analyze two numerical schemes presented in

the previous chapter. At one side we consider a finite difference scheme (6.2.8) based on the relaxation technique for the homogeneous part of the system (7.1.1) with centered in space approximation of the source terms. We compare it with a finite volume, well-balanced scheme given by (6.3.11) and explain why this method is more suitable for the problem (7.1.1).

Having chosen a scheme, we focus on numerical analysis of stability and dependence on the system parameters of stationary solutions to (7.1.1). In particular, we study how the number of regions, where $\rho > 0$, changes for different lengths of the domain and chemotactic sensitivities. It is essential to understand better the mechanisms leading to the formation of non-constant equilibria. Moreover, we analyze the influence of the initial mass, as its effect was significant in the experiments. The mathematical analysis that we perform concerns only the case of the quadratic pressure that is $\gamma = 2$, but we also study numerically the behaviour of the system (7.1.1) for higher values of γ.

7.2.1 Analytic results

At first we focus on the mathematical study of the steady states of the system

$$\begin{cases} \rho_t + (\rho u)_x = 0, \\ (\rho u)_t + (\rho u^2 + P(\rho))_x = -\alpha \rho u + \chi \rho \phi_x, \\ \phi_t = D\phi_{xx} + a\rho - b\phi, \end{cases} \tag{7.2.1}$$

defined on a bounded interval $\Omega = [0, L]$ and endowed with the homogeneous Neumann boundary conditions

$$\rho_x(0, \cdot) = \rho_x(L, \cdot) = 0, \quad u(0, \cdot) = u(L, \cdot) = 0 \quad \text{and} \quad \phi_x(0, \cdot) = \phi_x(L, \cdot) = 0. \tag{7.2.2}$$

Let us define the total mass M of cells by

$$M = \int_0^L \rho(x, t) dx,$$

which under the no-flux boundary conditions is conserved in time and we treat it as a parameter of the system (7.2.1).

The above problem admits stationary states, which are solutions to the following equilibrium system

$$(\rho u)_x = 0, \tag{7.2.3a}$$

$$\left(\rho u^2 + P(\rho)\right)_x = -\alpha \rho u + \chi \rho \phi_x, \tag{7.2.3b}$$

$$-D\phi_{xx} = a\rho - b\phi. \tag{7.2.3c}$$

The boundary condition for the velocity (7.2.2) implies

$$\rho u = 0.$$

It means that $u = 0$ and the steady states are static or in other words "at rest". Inserting the above result into (7.2.3b) we obtain

$$P(\rho)_x = \chi \rho \phi_x. \tag{7.2.4}$$

Of course this relation is satisfied if the density ρ and the concentration ϕ are constant, but we are interested in the non-constant equilibria. More precisely, we look for the solutions to (7.2.4) of the form

$$\rho = 0 \quad \text{or} \quad \frac{P(\rho)_x}{\rho} = \chi \phi_x$$

with ϕ given by the last equation of system (7.2.3). The above, non trivial relation rewritten for a general pressure of isentropic gases $P(\rho) = \varepsilon \rho^\gamma$, $\varepsilon > 0$, $\gamma > 1$ becomes

$$\frac{\varepsilon \gamma}{\chi(\gamma - 1)} \left(\rho^{\gamma - 1} \right)_x = \phi_x$$

and yields the following solution

$$\rho^{\gamma - 1} = \frac{\chi(\gamma - 1)}{\varepsilon \gamma} \phi + K \tag{7.2.5}$$

for some integration constant $K > 0$. It means that the non-constant steady states may contain region, where density vanishes $\rho = 0$ and those, in which the equation (7.2.5) is satisfied with ϕ given by (7.2.3c). However, no information is given on how many of these zones there are. Let us assume that there exist $p \in \mathbb{N}$ intervals with strictly positive density, which are separated by vacuum. Moreover, let us denote by x_i the boundaries of these intervals such that $x_0 = 0$ and $x_{2p-1} = L$. Then the density at the non-constant steady state can be written as

$$\rho(x) = \sum_{k=1}^{p} \rho_k(x) \Xi_{[x_{2k-2}, x_{2k-1}]}, \tag{7.2.6a}$$

where Ξ is the characteristic function

$$\Xi_A = \begin{cases} 1 & \text{if } x \in A \\ 0 & \text{elsewhere} \end{cases} \tag{7.2.6b}$$

with

$$\rho_k(x)^{\gamma - 1} = \frac{\chi(\gamma - 1)}{\varepsilon \gamma} \phi_k(x) + K_k \quad \text{for} \quad x \in [x_{2k-2}, x_{2k-1}] \tag{7.2.6c}$$

and ϕ_k being the solution to

$$\begin{aligned} -D \left(\phi_k \right)_{xx} &= a \rho_k - b \phi_k \quad \text{for} \quad x \in [x_{2k-2}, x_{2k-1}] \\ & \qquad \qquad \qquad \qquad k = 1, ..., p, \\ -D \left(\phi_k \right)_{xx} &= -b \phi_k \qquad \text{for} \quad x \in [x_{2k-1}, x_{2k}] \\ & \qquad \qquad \qquad \qquad k = 1, ..., p - 1. \end{aligned} \tag{7.2.6d}$$

Moreover, with each interval $[x_{2k-2}, x_{2k-1}]$ we associate a mass M_k with a constrain

$$M = \sum_{k=1}^{p} M_k.$$

Quadratic pressure $P(\rho) = \varepsilon\rho^\gamma$

Solving the partial differential equations (7.2.6d) for a general ρ_k given by (7.2.6c) is a non trivial problem. What is more, as we will see later, the accuracy of the numerical scheme that we presented in the previous chapter, depends strongly on the nonlinearity of the pressure $P(\rho)$. This is why we begin with the simplest case of the quadratic pressure $P(\rho) = \varepsilon\rho^2, \varepsilon > 0$. In this case the relation between ρ_k and ϕ_k given by equation (7.2.6c) becomes linear

$$\rho_k(x) = \frac{\chi}{2\varepsilon}\phi_k + K_k. \tag{7.2.7}$$

Inserting the above solution into the equation (7.2.6d) we obtain

$$-(\phi_k)_{xx} - \left(\frac{a\chi}{2\varepsilon D} - \frac{b}{D}\right)\phi_k = \frac{aK_k}{D}. \tag{7.2.8}$$

For simplification let us denote

$$\alpha = \frac{a\chi}{2\varepsilon D} - \frac{b}{D} \quad \text{and} \quad \beta = \frac{b}{D}.$$

Now, in order to solve (7.2.8), let us assume that $\alpha > 0$. Later we will show that $\alpha < 0$ leads to constant steady states. The solution in the interval $[x_{2k-2}, x_{2k-1}]$, where $\rho > 0$, is

$$\phi_k(x) = C_{4k-3}\cos(\sqrt{\alpha}x) + C_{4k-2}\sin(\sqrt{\alpha}x) - \frac{aK_k}{\alpha D} \tag{7.2.9a}$$

for $k = 1, ..., p$, while in $[x_{2k-1}, x_{2k}]$ for $k = 1, ..., p-1$, where the density vanishes, the equation (7.2.8) yields

$$\phi_k(x) = C_{4k-1}\cosh(\sqrt{\beta}x) + C_{4k}\sinh(\sqrt{\beta}x). \tag{7.2.9b}$$

Inserting the formula (7.2.9a) into (7.2.7) we observe that in the intervals $[x_{2k-2}, x_{2k-1}]$ the density ρ forms a bump of sinus type. This structure of the non-constant steady state is presented at Figure 7.1. To obtain the explicit solutions we need to find $4p - 2$ constants C, the
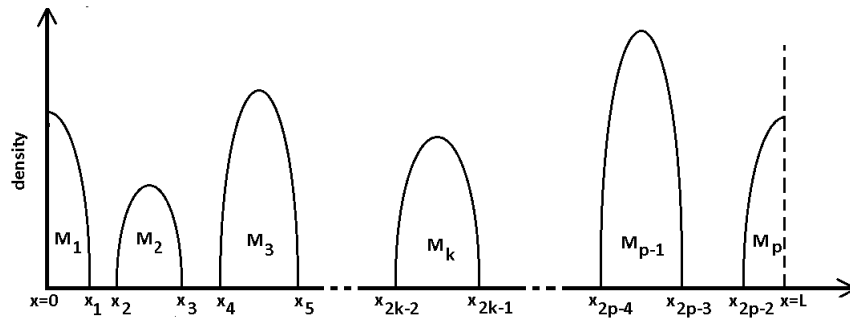
Figure 7.1: Structure of the non-constant steady state of the density ρ.

location of $2p - 2$ interface points x and p integration constants K. It gives $7p - 4$ parameters

to determine. On the other hand, we have two equations coming from the boundary conditions, three equations for each point $x_i, i = 1, 2, ..., 2p - 2$ from the continuity of ϕ and its first and second space derivatives and one equation from the total mass conservation condition. Summing them we get $6p - 3$ conditions, which only in the case of $p = 1$ matches the number of unknowns. The missing $p - 1$ equations are due to the unknown mass distributions among the p bumps. Because of this problem we consider at first the case of one interval with strictly positive density. This corresponds to two situations. We can have one, lateral bump with one region, where the density vanishes, or one bump in the interior of the domain surrounded by the vacuum. Then we will give details of the general solution, $p > 1$, assuming that the masses M_k (or equivalently the constants K_k) are known.

Lateral bump

Let us now focus on the first case, in which we can determine all the constants defining the solution. We assume that the non-constant stationary solution consists of one interval, where the density is strictly positive and one, where it vanishes. Let us denote by $\bar{x} \in (0, L)$ the location of the interface between the two regions. Then the density has the form

$$\rho(x) = \begin{cases} \frac{\chi}{2\varepsilon}\phi(x) + K & x \in [0, \bar{x}] \\ 0 & x \in (\bar{x}, L] \end{cases} \tag{7.2.10}$$

and the concentration ϕ is given by

$$\phi(x) = \begin{cases} C_1 \cos(\sqrt{\alpha}x) + C_2 \sin(\sqrt{\alpha}x) - \frac{aK}{\alpha D} & x \in [0, \bar{x}] \\ C_3 \cosh(\sqrt{\beta}x) + C_4 \sinh(\sqrt{\beta}x) & x \in (\bar{x}, L] \end{cases} \tag{7.2.11}$$

under the assumption $\alpha > 0$. Using the boundary condition for ϕ at $x = 0$ we obtain

$$-\sqrt{\alpha}C_1 \sin(\sqrt{\alpha}0) + \sqrt{\alpha}C_2 \cos(\sqrt{\alpha}0) = 0,$$

which yields $C_2 = 0$, while at $x = L$ we have

$$\sqrt{\beta}C_3 \sinh(\sqrt{\beta}L) + \sqrt{\beta}C_4 \cosh(\sqrt{\beta}L) = 0,$$

implying $C_4 = -C_3 \tanh(\sqrt{\beta}L)$. Denoting $C_2 = C_3/\cosh(\sqrt{\beta}L)$ from now on the concentration ϕ can be written as

$$\phi(x) = \begin{cases} C_1 \cos(\sqrt{\alpha}x) - \frac{aK}{\alpha D} & x \in [0, \bar{x}] \\ C_2 \cosh(\sqrt{\beta}(x - L)) & x \in (\bar{x}, L] \end{cases} . \tag{7.2.12}$$

There are still four parameters to find. The constants C_1, C_2 and $\bar{x}$ are going to be determined from the continuity of the function ϕ, its first and second space derivative at the interface point $\bar{x}$, whereas the constant K is computed from the conservation of the total mass. The continuity conditions yield

$$\begin{aligned} C_1 \cos(\sqrt{\alpha}\bar{x}) - \frac{aK}{\alpha D} &= C_2 \cosh(\sqrt{\beta}(\bar{x} - L)), \\ -\sqrt{\alpha}C_1 \sin(\sqrt{\alpha}\bar{x}) &= \sqrt{\beta}C_2 \sinh(\sqrt{\beta}(\bar{x} - L)), \\ -\alpha C_1 \cos(\sqrt{\alpha}\bar{x}) &= \beta C_2 \cosh(\sqrt{\beta}(\bar{x} - L)). \end{aligned}$$

$$\tag{7.2.13}$$

Solving the above system we obtain

$$
\begin{cases}
C_1 = \dfrac{2\varepsilon\beta K}{\alpha\chi}\cos(\sqrt{\alpha}\bar{x})^{-1}, \\[3mm]
C_2 = -\sqrt{\dfrac{\beta}{\alpha}}\,\dfrac{2\varepsilon K}{\chi}\tan(\sqrt{\alpha}\bar{x})\sinh(\sqrt{\beta}(\bar{x}-L))^{-1},
\end{cases}
\tag{7.2.14}
$$

and the location of the interface $\bar{x}$ is given by the solution to

$$
\sqrt{\dfrac{\beta}{\alpha}}\tan(\sqrt{\alpha}\bar{x}) = \tanh\left(\sqrt{\beta}(\bar{x}-L)\right).
\tag{7.2.15}
$$

To determine whether there exists a solution let us study the function

$$
f(x) = \sqrt{\dfrac{\beta}{\alpha}}\tan(\sqrt{\alpha}x) - \tanh\left(\sqrt{\beta}(x-L)\right).
$$

The function f is not defined for $x = \frac{1}{\sqrt{\alpha}}\left(\frac{\pi}{2}+\pi\mathbb{Z}\right)$ and has a positive derivative elsewhere. If $L \geq \frac{l\pi}{\sqrt{\alpha}}, l \in \mathbb{N}$ there exists a solution $\bar{x}$ in each interval of the form $\frac{1}{\sqrt{\alpha}}\left(]\pi/2,\pi[+\pi\{0,1,...,l-1\}\right)$. As a conclusion, if $L < \frac{\pi}{\sqrt{\alpha}}$, there is no non-constant stationary solution of the form (7.2.10), whereas for $L \geq \frac{\pi}{\sqrt{\alpha}}$, the function $f(x)$ equals zero at $[\sqrt{\alpha}\frac{L}{\pi}]$ points, where $[.]$ denotes the integer part. However, only the smallest of these points gives a function ρ, which is non negative everywhere.

Once the constants C_1, C_2 and $\bar{x}$ have been found, the parameter K is calculated from the mass conservation

$$
M_0 = \int_0^L \rho(x)dx.
$$

Inserting the explicit form of ρ we get

$$
M_0 = \int_0^{\bar{x}}\dfrac{\chi}{2\varepsilon}\phi(x)dx + K\bar{x},
$$

which gives

$$
K = \dfrac{\alpha M_0}{\frac{\beta}{\sqrt{\alpha}}\tan(\sqrt{\alpha}\bar{x}) - \beta\bar{x}}.
\tag{7.2.16}
$$

In the case $\alpha < 0$ the concentration is given by

$$
\phi(x) = \begin{cases}
C_1\cosh(\sqrt{-\alpha}x) - \dfrac{aK}{\alpha D} & x \in [0,\bar{x}] \\[3mm]
C_2\cosh(\sqrt{\beta}(x-L)) & x \in (\bar{x},L]
\end{cases}.
$$

Using, as before, the continuity at $\bar{x}$ of ϕ and its first and second space derivative we obtain the following values of the constants C_1 and C_2

$$
\begin{cases}
C_1 = \dfrac{a\beta K}{\alpha D(\beta-\alpha)}\cosh(\sqrt{-\alpha}\bar{x})^{-1}, \\[3mm]
C_2 = \dfrac{aK}{D(\beta-\alpha)}\sqrt{-\dfrac{\beta}{\alpha}}\tanh(\sqrt{-\beta}\bar{x})\sinh(\sqrt{\beta}(x-L))^{-1}
\end{cases}
$$

and relation for the location of the interface $\bar{x}$ of the form

$$\sqrt{-\frac{\beta}{\alpha}}\tanh(\sqrt{-\alpha}\bar{x}) = \tanh\left(\sqrt{\beta}(\bar{x} - L)\right). \qquad (7.2.17)$$

However, the above equation has no solution for $\bar{x} \in [0, L]$. The left-hand side is negative, whereas the right-hand side is positive.

Let us summarize the above results in the following proposition.

Proposition 4. *Let us consider the system (7.2.1) with $P(\rho) = \varepsilon\rho^2$, total mass M and the stationary solutions of the form (7.2.6). If $\frac{a\chi}{2\varepsilon D} - \frac{b}{D} > 0$ and $L > \frac{\pi}{\sqrt{\alpha}}$ then there exists a unique, positive solution of the form (7.2.10) given by the smallest $\bar{x} \in \frac{1}{\sqrt{\alpha}}]\frac{\pi}{2}, \pi[$ satisfying*

$$\sqrt{\frac{\beta}{\alpha}}\tan(\sqrt{\alpha}\bar{x}) = \tanh(\sqrt{\beta}(\bar{x} - L)) \qquad (7.2.18a)$$

and by the following expressions:

$$on \quad [0, \bar{x}], \quad \phi(x) = \frac{2\varepsilon\beta K}{\alpha\chi}\frac{\cos(\sqrt{\alpha}x)}{\cos(\sqrt{\alpha}\bar{x})} - \frac{aK}{\alpha D}, \quad \rho(x) = \frac{\chi}{2\varepsilon}\phi(x) + K$$

$$on \quad [\bar{x}, L], \quad \phi(x) = \frac{2\varepsilon b K}{\chi}\tan(\sqrt{\beta}L)\frac{\sinh(\sqrt{\beta}(x - L))}{\cosh(\sqrt{\beta}(\bar{x} - L))}, \quad \rho(x) = 0$$

$$(7.2.18b)$$

where K is given by

$$K = \frac{\alpha M}{\frac{\beta}{\sqrt{\alpha}}\tan(\sqrt{\alpha}\bar{x}) - \beta\bar{x}}. \qquad (7.2.18c)$$

Figure 7.2 presents an exact solution of density and concentration for a lateral of system (7.1.1) with $\varepsilon = a = b = D = L = 1$, $\chi = 50$ and the initial mass $M = 1.3183$, where the interface point $\bar{x} = 0.3943$.

Centered bump

The second case with $p = 1$ corresponds to the presence of one interval, where the density is strictly positive, in the interior of the domain. Denoting by $\bar{x}, \bar{y} \in (0, L)$ respectively the left and the right boundary of the interval, such that $\bar{x} < \bar{y}$, the density at the non constant steady state writes as

$$\rho(x) = \begin{cases} 0 & x \in [0, \bar{x}) \\ \frac{\chi}{2\varepsilon}\phi(x) + K & x \in [\bar{x}, \bar{y}] \\ 0 & x \in (\bar{y}, L] \end{cases}. \qquad (7.2.19)$$

We follow the same approach as in the previous case to find the formula for the concentration ϕ. In general it has the form

$$\phi(x) = \begin{cases} C_1\cosh(\sqrt{\beta}x) + C_2\sinh(\sqrt{\beta}x) & x \in [0, \bar{x}) \\ C_3\cos(\sqrt{\alpha}x) + C_4\sin(\sqrt{\alpha}x) - \frac{aK}{\alpha D} & x \in [\bar{x}, \bar{y}] \\ C_5\cosh(\sqrt{\beta}x) + C_6\sinh(\sqrt{\beta}x) & x \in (\bar{y}, L] \end{cases},$$
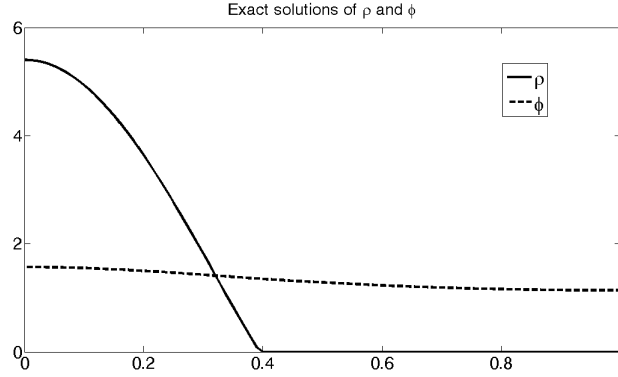
Figure 7.2: Exact solutions of density ρ and concentration ϕ given by (7.2.18) for system (7.1.1) with $\varepsilon = a = b = D = L = 1$, $\chi = 50$, initial mass $M = 1.3183$ and the interface point is $\bar{x} = 0.3943$.

under the assumption $\alpha > 0$. Applying the homogeneous Neumann boundary conditions we get

$$\phi(x) = \begin{cases} C_1 \cosh(\sqrt{\beta}x) & x \in [0, \bar{x}) \\ C_2 \cos(\sqrt{\alpha}x) + C_3 \sin(\sqrt{\alpha}x) - \frac{aK}{\alpha D} & x \in [\bar{x}, \bar{y}] \\ C_4 \cosh(\sqrt{\beta}(x-L)) & x \in (\bar{y}, L] \end{cases} \qquad (7.2.20)$$

Continuity of ϕ, ϕ_x and ϕ_{xx} at the interface points $\bar{x}$, $\bar{y}$ give respectively

$$\begin{cases} C_1 = -\frac{2K\varepsilon}{\chi} \cosh(\sqrt{\beta}\bar{x})^{-1} \\ C_2 = \frac{2K\varepsilon}{\chi} \sqrt{\frac{\beta}{\alpha}} \left(\tanh(\sqrt{\beta}\bar{x}) \sin(\sqrt{\alpha}\bar{x}) + \sqrt{\frac{\beta}{\alpha}} \cos(\sqrt{\alpha}\bar{x}) \right) \\ C_3 = \frac{2K\varepsilon}{\chi} \sqrt{\frac{\beta}{\alpha}} \left(-\tanh(\sqrt{\beta}\bar{x}) \cos(\sqrt{\alpha}\bar{x}) + \sqrt{\frac{\beta}{\alpha}} \sin(\sqrt{\alpha}\bar{x}) \right) \end{cases}$$

and

$$\begin{cases} C_4 = -\frac{2K\varepsilon}{\chi} \cosh(\sqrt{\beta}(\bar{y}-L))^{-1} \\ C_2 = \frac{2K\varepsilon}{\chi} \sqrt{\frac{\beta}{\alpha}} \left(\tanh(\sqrt{\beta}(\bar{y}-L)) \sin(\sqrt{\alpha}\bar{y}) + \sqrt{\frac{\beta}{\alpha}} \cos(\sqrt{\alpha}\bar{y}) \right) \\ C_3 = \frac{2K\varepsilon}{\chi} \sqrt{\frac{\beta}{\alpha}} \left(-\tanh(\sqrt{\beta}(\bar{y}-L)) \cos(\sqrt{\alpha}\bar{y}) + \sqrt{\frac{\beta}{\alpha}} \sin(\sqrt{\alpha}\bar{y}) \right) \end{cases} .$$

Therefore the constants C_2 and C_3 coincide if

$$\tanh(\sqrt{\beta}\bar{x}) \sin(\sqrt{\alpha}\bar{x}) + \sqrt{\frac{\beta}{\alpha}} \cos(\sqrt{\alpha}\bar{x}) = \tanh(\sqrt{\beta}(\bar{y}-L)) \sin(\sqrt{\alpha}\bar{y}) + \sqrt{\frac{\beta}{\alpha}} \cos(\sqrt{\alpha}\bar{y})$$

$$-\tanh(\sqrt{\beta}\bar{x}) \cos(\sqrt{\alpha}\bar{x}) + \sqrt{\frac{\beta}{\alpha}} \sin(\sqrt{\alpha}\bar{x}) = -\tanh(\sqrt{\beta}(\bar{y}-L)) \cos(\sqrt{\alpha}\bar{y}) + \sqrt{\frac{\beta}{\alpha}} \sin(\sqrt{\alpha}\bar{y})$$

yielding the equations for $\bar{x}$ and $\bar{y}$.

Analyzing the existence of solutions $(\bar{x}, \bar{y})$ to the above system and solving it is in general non trivial task . In the case of one lateral bump we found the conditions that guarantee

the existence of $\bar{x}$ giving non negative density everywhere. Nevertheless, due to the nonlinearity of equation (7.2.15), we solve it numerically. For one centered bump we find out that the solution is symmetric. This reduces the above system to one equation and allows us to solve it. However, this trick will not work for higher number of bumps.

In order to see that centered bump is symmetric let us multiply the first one by $\sin(\sqrt{\alpha}x)$ and subtract the second multiplied by $\cos(\sqrt{\alpha}x)$ we obtain

$$\tanh(\sqrt{\beta}\bar{x}) = \tanh(\sqrt{\beta}(\bar{y} - L))\cos(\sqrt{\alpha}(\bar{y} - \bar{x})) - \sqrt{\frac{\beta}{\alpha}}\sin(\sqrt{\alpha}(\bar{y} - \bar{x})). \quad (7.2.21)$$

On the other hand, summing the equations multiplied respectively by $\cos(\sqrt{\alpha}x)$ and $\sin(\sqrt{\alpha}x)$ yields

$$\sqrt{\frac{\beta}{\alpha}} = \tanh(\sqrt{\beta}(\bar{y} - L))\sin(\sqrt{\alpha}(\bar{y} - \bar{x})) + \sqrt{\frac{\beta}{\alpha}}\cos(\sqrt{\alpha}(\bar{y} - \bar{x})).$$

From the above system we get the relation

$$\tanh(\sqrt{\beta}\bar{x}) = \sqrt{\frac{\beta}{\alpha}}\frac{\cos(\sqrt{\alpha}(\bar{y} - \bar{x}) - 1}{\sin(\sqrt{\alpha}(\bar{y} - \bar{x})} = -\tanh(\sqrt{\beta}(\bar{y} - L)),$$

which implies that $\bar{y} = L - \bar{x}$ with $\bar{x} \in]0, L/2[$ satisfying

$$\tanh(\sqrt{\beta}\bar{x}) = \sqrt{\frac{\beta}{\alpha}}\tan(\sqrt{\alpha}(\bar{x} - L/2)). \quad (7.2.22)$$

It means that the centered bump is symmetric. Moreover, the solution for the lateral bump calculated with $L/2$ and $M_0/2$ and symmetrized to be defined on the whole interval $[0, L]$ is equal to the one computed for the centered bump. Therefore, if there are several $\bar{x} \in]0, L/2[$, which are the solutions to the equation (7.2.22), only the largest gives a nonnegative function ρ.

Once we have found the solution $\bar{x}$ to (7.2.22), the constants $C_i, i = 1, 2, 3, 4$ are

$$\begin{cases} C_1 = C_4 = -\dfrac{2K\varepsilon}{\chi}\cosh(\sqrt{\beta}\bar{x})^{-1}, \\[2mm] C_2 = \dfrac{2K\varepsilon\beta}{\chi\alpha}\cos(\sqrt{\alpha}L/2)\cos(\sqrt{\alpha}(\bar{x} - L/2))^{-1}, \\[2mm] C_3 = \dfrac{2K\varepsilon\beta}{\chi\alpha}\sin(\sqrt{\alpha}L/2)\cos(\sqrt{\alpha}(\bar{x} - L/2))^{-1}, \end{cases} \quad (7.2.23)$$

and the parameter K equals

$$K = \frac{M_0\alpha}{(2\bar{x} - L)\beta - 2\sqrt{\beta}\tanh(\sqrt{\beta}\bar{x})}. \quad (7.2.24)$$

Proposition 5. *Let us consider the system (7.2.1) defined on the interval $[0, L]$ with $P(\rho) = \varepsilon\rho^2$, total mass M and the stationary solutions of the form (7.2.6). If $\frac{a\chi}{2\varepsilon D} - \frac{b}{D} > 0$ and $L > \frac{2\pi}{\sqrt{\alpha}}$ then there exists a unique, positive solution of the form (7.2.19) given by the largest $\bar{x} \in \frac{1}{\sqrt{\alpha}}]\frac{\pi}{2}, \pi[$ satisfying*

$$\tanh(\sqrt{\beta}\bar{x}) = \sqrt{\frac{\beta}{\alpha}}\tan(\sqrt{\alpha}(\bar{x} - L/2)). \quad (7.2.25)$$

and by the following expressions:

$$on \qquad [0, \bar{x}], \qquad \phi(x) = -\frac{2\varepsilon K}{\chi} \frac{\cosh(\sqrt{\beta}x)}{\cosh(\sqrt{\beta}\bar{x})}, \quad \rho(x) = 0$$

$$on \quad [\bar{x}, L - \bar{x}], \quad \phi(x) = \frac{2\varepsilon\beta K}{\alpha\chi} \frac{\cos(\sqrt{\alpha}(x - \frac{L}{2}))}{\cos(\sqrt{\alpha}(\bar{x} - \frac{L}{2}))} - \frac{aK}{\alpha D}, \quad \rho(x) = \frac{\chi}{2\varepsilon}\phi(x) + K$$

$$on \qquad [\bar{x}, L], \qquad \phi(x) = -\frac{2\varepsilon K}{\chi} \frac{\cosh(\sqrt{\beta}(x - L))}{\cosh(\sqrt{\beta}\bar{x})}, \quad \rho(x) = 0$$

$$(7.2.26)$$

where K is given by

$$K = \frac{M\alpha}{(2\bar{x} - L)\beta - 2\sqrt{\beta}\tanh(\sqrt{\beta}\bar{x})}. \tag{7.2.27}$$
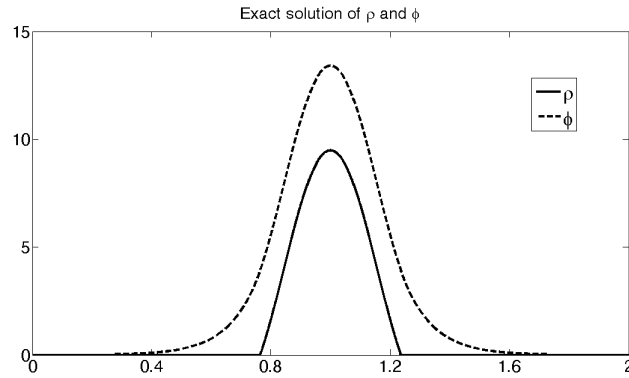
Figure 7.3: Exact solutions of density ρ and concentration ϕ for a centered bump of system (7.1.1) with $\varepsilon = 1$, $a = 20$, $b = 10$, $D = 0.1$, $L = 2$, $\chi = 2$ and the initial mass $M = 2.6366$, where the interface point is $\bar{x} = 0.7644$

Figure 7.3 presents an exact solution of density and concentration for a centered bump of system (7.1.1) with $\varepsilon = 1$, $a = 20$, $b = 10$, $D = 0.1$, $L = 2$, $\chi = 2$ and the initial mass $M = 2.6366$, where the interface point $\bar{x} = 0.7644$.

General non-constant steady state

At the beginning of this section we explained that only in the presence of one interval with non vanishing density it is possible to calculate all the constants in the solution. In other cases we should know the mass M_k of each bump in order to find the constants K. It cannot be determined a priori, but as the later simulations will show, the values of K can be obtained numerically with high accuracy. This is why in the following theorem we present details of a non constant stationary solutions for $p > 1$, $p \in \mathbb{N}$.

Theorem 8. *Let us consider the system (7.2.1) with $P(\rho) = \varepsilon\rho^2, \varepsilon > 0$ and assume that $\frac{a\chi}{2\varepsilon D} - \frac{b}{D} > 0$ and $L > \frac{\pi}{\sqrt{\alpha}}$. Moreover, let us assume that the masses M_k, $k = 1, ..., p$ in each*

region, where $\rho > 0$, are fixed and known. Then the solution of the form

$$\rho(x) = \sum_{k=1}^{p} \rho_k(x) \Xi_{[x_{2k-2}, x_{2k-1}]},$$

where for $x \in [x_{2k-2}, x_{2k-1}]$

$$\rho_k(x) = \frac{\chi}{2\varepsilon} \phi_k(x) + K_k, \qquad K_k > 0,$$

$$\phi_k(x) = C_{4k-3} \cos(\sqrt{\alpha}x) + C_{4k-2} \sin(\sqrt{\alpha}x) - \frac{aK_k}{\alpha D} \quad \text{if} \quad \begin{array}{l} [x_{2k-2}, x_{2k-1}] \\ k = 1, 2, ..., p \end{array}$$

$$\phi_k(x) = C_{4k-1} \cosh(\sqrt{\beta}x) + C_{4k} \sinh(\sqrt{\beta}x) \quad \text{if} \quad \begin{array}{l} [x_{2k-1}, x_{2k}] \\ k = 1, ..., p-1 \end{array}$$

and K_k given by

$$C_{4k-3} \left[\sin(\sqrt{\alpha}x_{2k-1}) - \sin(\sqrt{\alpha}x_{2k-2}) \right] - C_{4k-2} \left[\cos(\sqrt{\alpha}x_{2k-1}) - \cos(\sqrt{\alpha}x_{2k-2}) \right]$$
$$= \frac{2\varepsilon\sqrt{\alpha}}{\chi} \left(M_k - K_k(x_{2k-1} - x_{2k-2}) \left(1 - \frac{a\chi}{2\epsilon\alpha D} \right) \right).$$

is the stationary state of the system (7.2.1) if there exists a solution to

$$C_{4k-3} \cos(\sqrt{\alpha}x_{2k-1}) + C_{4k-2} \sin(\sqrt{\alpha}x_{2k-1}) = \frac{2\varepsilon K_k \beta}{\alpha\chi}, \quad k = 2, 3, ..., p-1$$

$$C_{4k-1} \cosh(\sqrt{\beta}x_{2k}) + C_{4k} \sinh(\sqrt{\beta}x_{2k}) = -\frac{2\varepsilon K_{k+1}\beta}{\alpha\chi} \quad k = 1, 3, ..., p-1$$

$$C_{4p-2} = C_{4p-3} \tan(\sqrt{\alpha}L)$$

where the constants are

$$C_1 = \frac{2\varepsilon K_1 \beta}{\alpha\chi} \cos(\sqrt{\alpha}x_1)^{-1}$$

$$C_2 = 0$$

$$C_3 = \frac{2\varepsilon K_1}{\chi} \left[\sqrt{\frac{\beta}{\alpha}} \tan(\sqrt{\alpha}x_1) \sinh(\sqrt{\beta}x_1) - \cosh(\sqrt{\beta}x_1) \right]$$

$$C_4 = \frac{2\varepsilon K_1}{\chi} \left[-\sqrt{\frac{\beta}{\alpha}} \tan(\sqrt{\alpha}x_1) \cosh(\sqrt{\beta}x_1) + \sinh(\sqrt{\beta}x_1) \right]$$

and the remaining ones defined recurrently in the following way:

for $k = 2, 3, ..., p-1$

$$C_{4k-1} = C_{4k-3} \left[\sqrt{\frac{\alpha}{\beta}} \sin(\sqrt{\alpha}x_{2k-1}) \sinh(\sqrt{\beta}x_{2k-1}) - \frac{\alpha}{\beta} \cos(\sqrt{\alpha}x_{2k-1}) \cosh(\sqrt{\beta}x_{2k-1}) \right]$$
$$+ C_{4k-2} \left[-\sqrt{\frac{\alpha}{\beta}} \cos(\sqrt{\alpha}x_{2k-1}) \sinh(\sqrt{\beta}x_{2k-1}) - \frac{\alpha}{\beta} \sin(\sqrt{\alpha}x_{2k-1}) \cosh(\sqrt{\beta}x_{2k-1}) \right]$$

$$C_{4k} = C_{4k-3} \left[-\sqrt{\frac{\alpha}{\beta}} \sin(\sqrt{\alpha}x_{2k-1}) \cosh(\sqrt{\beta}x_{2k-1}) + \frac{\alpha}{\beta} \cos(\sqrt{\alpha}x_{2k-1}) \sinh(\sqrt{\beta}x_{2k-1}) \right]$$
$$+ C_{4k-2} \left[\sqrt{\frac{\alpha}{\beta}} \cos(\sqrt{\alpha}x_{2k-1}) \cosh(\sqrt{\beta}x_{2k-1}) + \frac{\alpha}{\beta} \sin(\sqrt{\alpha}x_{2k-1}) \sinh(\sqrt{\beta}x_{2k-1}) \right]$$

and for $k = 1, 2, ..., p-1$

$$C_{4k+1} = C_{4k-1}\left[-\sqrt{\frac{\beta}{\alpha}}\sin(\sqrt{\alpha}x_{2k})\sinh(\sqrt{\beta}x_{2k}) - \frac{\beta}{\alpha}\cos(\sqrt{\alpha}x_{2k})\cosh(\sqrt{\beta}x_{2k})\right]$$

$$+ C_{4k}\left[-\sqrt{\frac{\beta}{\alpha}}\sin(\sqrt{\alpha}x_{2k})\cosh(\sqrt{\beta}x_{2k}) - \frac{\beta}{\alpha}\cos(\sqrt{\alpha}x_{2k})\sinh(\sqrt{\beta}x_{2k})\right]$$

$$C_{4k+2} = C_{4k-1}\left[\sqrt{\frac{\beta}{\alpha}}\cos(\sqrt{\alpha}x_{2k})\sinh(\sqrt{\beta}x_{2k}) - \frac{\beta}{\alpha}\sin(\sqrt{\alpha}x_{2k})\cosh(\sqrt{\beta}x_{2k})\right]$$

$$+ C_{4k}\left[\sqrt{\frac{\beta}{\alpha}}\cos(\sqrt{\alpha}x_{2k})\cosh(\sqrt{\beta}x_{2k}) - \frac{\beta}{\alpha}\sin(\sqrt{\alpha}x_{2k})\sinh(\sqrt{\beta}x_{2k})\right]$$

Proof. In order to find the constants C_1, C_2, C_3 and C_4 we proceed as in the case of one lateral bump and obtain the same results. For the remaining unknowns we apply the continuity conditions separately for even and odd points x_i that is x_{2k-1} for $k = 2, 3, ..., p-1$ and x_{2k} for $k = 1, 2, ..., p-1$.

At first let us consider the odd nodes. We define ϕ_L, ϕ_R, which describe the concentration ϕ respectively at the left and at the right side of the interface point x_{2k-1} that is

$$\phi_L(x) = C_{4k-3}\cos(\sqrt{\alpha}x) + C_{4k-2}\sin(\sqrt{\alpha}x) - \frac{aK_k}{\alpha D}$$

$$\phi_R(x) = C_{4k-1}\cosh(\sqrt{\beta}x) + C_{4k}\sinh(\sqrt{\beta}x)$$

The continuity conditions yield

$$C_{4k-3}\cos(\sqrt{\alpha}x_{2k-1}) + C_{4k-2}\sin(\sqrt{\alpha}x_{2k-1}) - \frac{aK_k}{\alpha D}$$
$$= C_{4k-1}\cosh(\sqrt{\beta}x_{2k-1}) + C_{4k}\sinh(\sqrt{\beta}x_{2k-1})$$
$$-\sqrt{\alpha}C_{4k-3}\sin(\sqrt{\alpha}x_{2k-1}) + \sqrt{\alpha}C_{4k-2}\sin(\sqrt{\alpha}x_{2k-1})$$
$$= \sqrt{\beta}C_{4k-1}\sinh(\sqrt{\beta}x_{2k-1}) + \sqrt{\beta}C_{4k}\cosh(\sqrt{\beta}x_{2k-1})$$
$$-\alpha C_{4k-3}\cos(\sqrt{\alpha}x_{2k-1}) - \alpha C_{4k-2}\sin(\sqrt{\alpha}x_{2k-1})$$
$$= \beta C_{4k-1}\cosh(\sqrt{\beta}x_{2k-1}) + \beta C_{4k}\sinh(\sqrt{\beta}x_{2k-1})$$

Solving the above system for unknowns C_{4k-1}, C_{4k} and x_{2k-1} in the case $k = 2, ..., p-1$ we get the recurrent formulas. From the last two equations of the above conditions we obtain

$$C_{4k-1} = C_{4k-3}\left[\sqrt{\frac{\alpha}{\beta}}\sin(\sqrt{\alpha}x_{2k-1})\sinh(\sqrt{\beta}x_{2k-1}) - \frac{\alpha}{\beta}\cos(\sqrt{\alpha}x_{2k-1})\cosh(\sqrt{\beta}x_{2k-1})\right]$$

$$+ C_{4k-2}\left[-\sqrt{\frac{\alpha}{\beta}}\cos(\sqrt{\alpha}x_{2k-1})\sinh(\sqrt{\beta}x_{2k-1}) - \frac{\alpha}{\beta}\sin(\sqrt{\alpha}x_{2k-1})\cosh(\sqrt{\beta}x_{2k-1})\right]$$

$$C_{4k} = C_{4k-3}\left[-\sqrt{\frac{\alpha}{\beta}}\sin(\sqrt{\alpha}x_{2k-1})\cosh(\sqrt{\beta}x_{2k-1}) + \frac{\alpha}{\beta}\cos(\sqrt{\alpha}x_{2k-1})\sinh(\sqrt{\beta}x_{2k-1})\right]$$

$$+ C_{4k-2}\left[\sqrt{\frac{\alpha}{\beta}}\cos(\sqrt{\alpha}x_{2k-1})\cosh(\sqrt{\beta}x_{2k-1}) + \frac{\alpha}{\beta}\sin(\sqrt{\alpha}x_{2k-1})\sinh(\sqrt{\beta}x_{2k-1})\right]$$

while the first one

$$C_{4k-3}\cos(\sqrt{\alpha}x_{2k-1}) + C_{4k-2}\sin(\sqrt{\alpha}x_{2k-1}) = \frac{2\varepsilon K_k\beta}{\alpha\chi}.$$

determines x_{2k-1}, as it depends only on the points preceding it.

Seemingly, at the even points the function ϕ at both sides of x_{2k}, $k = 1, 2, ..., p - 1$ is

$$\phi_L(x) = C_{4k-1} \cosh(\sqrt{\beta}x) + C_{4k} \sinh(\sqrt{\beta}x)$$

$$\phi_R(x) = C_{4k+1} \cos(\sqrt{\alpha}x) + C_{4k+2} \sin(\sqrt{\alpha}x) - \frac{aK_{k+1}}{\alpha D}$$

The continuity conditions give

$$C_{4k+1} \cos(\sqrt{\alpha}x_{2k}) + C_{4k+2} \sin(\sqrt{\alpha}x_{2k}) - \frac{aK_{k+1}}{\alpha D}$$

$$= C_{4k-1} \cosh(\sqrt{\beta}x_{2k}) + C_{4k} \sinh(\sqrt{\beta}x_{2k})$$

$$-\sqrt{\alpha}C_{4k+1} \sin(\sqrt{\alpha}x_{2k}) + \sqrt{\alpha}C_{4k+2} \sin(\sqrt{\alpha}x_{2k})$$

$$= \sqrt{\beta}C_{4k-1} \sinh(\sqrt{\beta}x_{2k}) + \sqrt{\beta}C_{4k} \cosh(\sqrt{\beta}x_{2k})$$

$$-\alpha C_{4k+1} \cos(\sqrt{\alpha}x_{2k}) - \alpha C_{4k+2} \sin(\sqrt{\alpha}x_{2k})$$

$$= \beta C_{4k-1} \cosh(\sqrt{\beta}x_{2k}) + \beta C_{4k} \sinh(\sqrt{\beta}x_{2k})$$

implying

$$C_{4k+1} = C_{4k-1} \left[-\sqrt{\frac{\beta}{\alpha}} \sin(\sqrt{\alpha}x_{2k}) \sinh(\sqrt{\beta}x_{2k}) - \frac{\beta}{\alpha} \cos(\sqrt{\alpha}x_{2k}) \cosh(\sqrt{\beta}x_{2k}) \right]$$

$$+ C_{4k} \left[-\sqrt{\frac{\beta}{\alpha}} \sin(\sqrt{\alpha}x_{2k}) \cosh(\sqrt{\beta}x_{2k}) - \frac{\beta}{\alpha} \cos(\sqrt{\alpha}x_{2k}) \sinh(\sqrt{\beta}x_{2k}) \right]$$

$$C_{4k+2} = C_{4k-1} \left[\sqrt{\frac{\beta}{\alpha}} \cos(\sqrt{\alpha}x_{2k}) \sinh(\sqrt{\beta}x_{2k}) - \frac{\beta}{\alpha} \sin(\sqrt{\alpha}x_{2k}) \cosh(\sqrt{\beta}x_{2k}) \right]$$

$$+ C_{4k} \left[\sqrt{\frac{\beta}{\alpha}} \cos(\sqrt{\alpha}x_{2k}) \cosh(\sqrt{\beta}x_{2k}) - \frac{\beta}{\alpha} \sin(\sqrt{\alpha}x_{2k}) \sinh(\sqrt{\beta}x_{2k}) \right]$$

and

$$C_{4k-1} \cosh(\sqrt{\beta}x_{2k}) + C_{4k} \sinh(\sqrt{\alpha}x_{2k}) = -\frac{2\varepsilon K_{k+1}\beta}{\alpha\chi}.$$

However, now it is a relation not only between x_{2k} and the points preceding but also involves x_{2k+1}.

The last relation, corresponding to x_{2p-1} is obtained from the boundary condition at $x = L$ that is

$$-\sqrt{\alpha}C_{4p-3} \sin(\sqrt{\alpha}L) + \sqrt{\alpha}C_{4p-2} \cos(\sqrt{\alpha}L) = 0 \quad \Rightarrow \quad C_{4p-2} = C_{4p-3} \tan\sqrt{\alpha}L.$$

Having found the constants C and the interface points x we use the masses M_k of the bumps to calculate the integration constants K_k

$$M_k = \int_{x_{2k-2}}^{x_{2k-1}} \rho_k dx = \frac{\chi}{2\varepsilon} \int_{x_{2k-2}}^{x_{2k-1}} \phi_k dx + K_k(x_{2k-1} - x_{2k-2}).$$

Inserting the formula for ϕ_k in the interval $[x_{2k-2}, x_{2k-1}]$ we obtain the condition joining K_k and $K_{k-1}, K_{k-2}, ..., K_1$

$$C_{4k-3} \left[\sin(\sqrt{\alpha}x_{2k-1}) - \sin(\sqrt{\alpha}x_{2k-2}) \right] - C_{4k-2} \left[\cos(\sqrt{\alpha}x_{2k-1}) - \cos(\sqrt{\alpha}x_{2k-2}) \right]$$

$$= \frac{2\varepsilon\sqrt{\alpha}}{\chi} \left(M_k - K_k(x_{2k-1} - x_{2k-2}) \left(1 - \frac{a\chi}{2\epsilon\alpha D} \right) \right).$$

for $k = 1, 2, ..., p$.   □

7.2.2 Simulations

In this section we focus on numerical analysis of stationary solutions of system (7.1.1). In order to do it first we study the accuracy of two different methods to approximate the solutions. We consider an explicit, finite difference scheme (6.2.8) and compare it with a finite volume, well-balanced one given by (6.3.11). Having choses the method, we analyze stability and dependence on the system parameters of stationary solutions to (7.1.1). In particular, for $\gamma = 2$ we study how the number of regions, where $\rho > 0$, changes for different lengths of the domain and chemotactic sensitivities. Then we compare behaviour for different values of adiabatic exponent γ and finally we study the influence of the initial mass comparing the results for $\gamma = 2$ and $\gamma = 3$.

Comparison between different schemes

In the previous chapter we constructed a finite volume scheme, which is well-balanced at the steady states with constant velocity, given by (6.3.11). We proved that it is consistent, keeps density non negative and preserves the steady states. Before studying the behaviour of the hyperbolic system of chemotaxis, we analyze this scheme and compare it with other methods. At first, we are going to verify the accuracy of different approximate Riemann solvers introduced in Section (3.3.3) that are used to solve the homogeneous part of the problem. In particular, we analyze Suliciu relaxation solver adopted to vacuum, HLL solver and Roe method. Then two methods to treat the source term are going to be compared. We consider well-balancing and centered in space approximation in the finite volume scheme. Moreover, we compare the results with a standard finite difference scheme with centered in space approximation of a source described by (6.2.8).

Comparison of approximate Riemann solvers

Let us focus now on the comparison between methods approximating the homogeneous part of the model (7.1.1). For the source term we choose the well-balanced method with the reconstruction at steady states with constant velocity (6.3.11c), which we introduced in the previous chapter. The first simulation is performed for the system (7.2.1) with $\varepsilon = D = a = b = L = 1$, $\chi = 50$, quadratic pressure function and the initial datum of the form

$$\rho_0(x) = 1 + \sin(4\pi|x - L/4|), \quad \phi_0 = 0, \qquad u_0 = 0.$$

Figure 7.4 presents the L^∞ and L^2 numerical errors for $\Delta x = 0.05$ and $\Delta x = 0.01$, where the reference solution is obtained using the finite volume scheme with Suliciu solver and well-balancing reconstruction on the fine grid with mesh size $\Delta x = 10^{-3}$. We observe that all the errors manifest similar behaviour. They oscillate at the beginning and stabilize with time. Moreover, there is no significant difference between the solvers. The HLL and Suliciu perform with the same accuracy in this test, while the error for Roe method is a little higher.

If we increase the adiabatic coefficient γ in the pressure function and take $\gamma = 3$ HLL and Suliciu solvers behave correctly under the CFL condition $\Delta t = 0.9\Delta x/\lambda$, but the Roe

method explodes at the vacuum. The density profiles are presented at Figure 7.5. Changing γ leads to steeper gradients in the solution, with which linearized method of Roe cannot deal with producing oscillations. Values of the adiabatic coefficients higher than 2 cause instabilities also for HLL and Suliciu solvers if we take larger initial mass. Figure 7.6 shows solution of the density for $M = 1000$. We observe that the Suliciu approximate Riemann solver is unable to preserve the positivity, while the standard explicit, finite difference scheme (6.2.8) gives asymptotically a constant steady state and keeps non negativity of ρ.
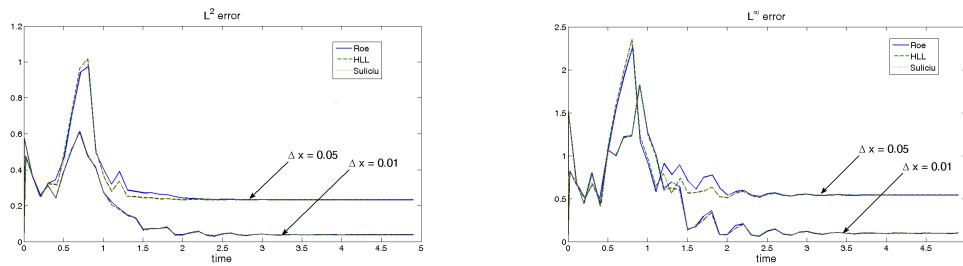
Figure 7.4: Time evolution of L^∞ and L^2 numerical errors of densities ρ for system (7.1.1) in the case $P(\rho) = \varepsilon \rho^2$ and $\varepsilon = D = a = b = L = 1$, $\chi = 50$ approximated using a finite volume, well-balanced scheme (6.3.11). Three different approximate Riemann solvers: Roe method, HLL solver, Suliciu relaxation solver are compared for $\Delta x = 0.05$ and $\Delta x = 0.01$.

| Roe | HLL | Suliciu |
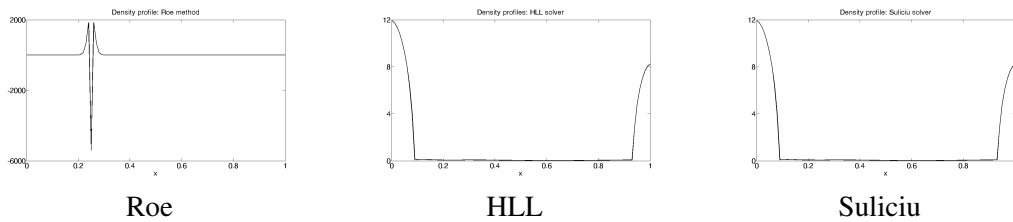
Figure 7.5: Density profiles for system (7.1.1) in the case $P(\rho) = \varepsilon \rho^3$ and $\varepsilon = 1, D = 0.1$, $a = 20$, $b = 10$, $\chi = 10$ approximated using a finite volume, well-balanced scheme (6.3.11). Three different approximate Riemann solvers: Roe method, HLL solver, Suliciu relaxation solver are compared for the total mass $M = 1$.
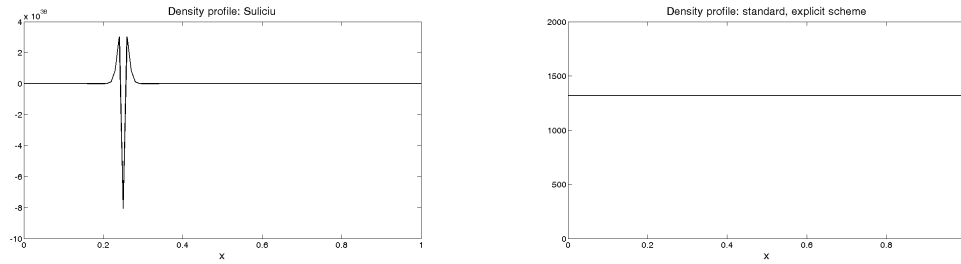
Figure 7.6: Density profiles for system (7.1.1) in the case $P(\rho) = \varepsilon\rho^3$ and $\varepsilon = 1, D = 0.1$, $a = 20$, $b = 10$, $\chi = 10$. Comparison between two schemes: (left) Finite volume method with Suliciu relaxation solver and well-balancing "at rest" (6.3.11); (right) Finite difference scheme based on the relaxation technique with centered in space approximation of the source (6.2.8).

Comparison of the source approximation methods

In the second test, using the same parameters and initial datum, we analyze different methods of approximation of the source term. More precisely, we want to compare well-balancing approach with the centered in space approximation in the case of finite volume scheme. In the comparison we also consider the same centered in space discretization of the source term in the case of finite difference explicit scheme scheme (6.2.8). In the case of the finite volume schemes for the homogeneous part the Suliciu relaxation solver is chosen as the numerical flux function.

At Figure 7.7 we present density profiles in the case $\gamma = 2$ at the steady state obtained on the mesh size $\Delta x = \{0.1, 0.05, 0.01\}$ and compared with the exact stationary solution of the form of one, lateral bump given by (7.2.18). We see that only a scheme with the well-balanced

$\Delta x = 0.1$ $\hspace{3cm}$ $\Delta x = 0.05$ $\hspace{3cm}$ $\Delta x = 0.01$
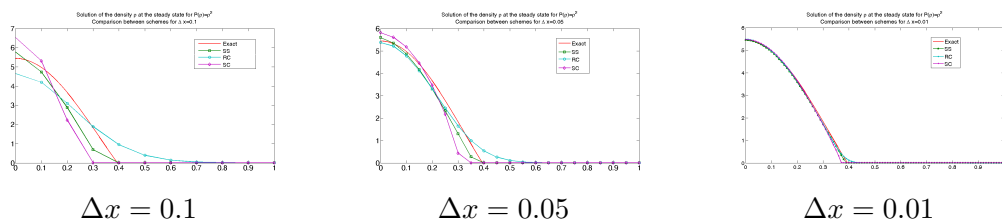
Figure 7.7: Density profiles for system (7.1.1) with $P(\rho) = \rho^2$, total mass $M = 1$ and $\varepsilon = 1, D = 0.1$, $a = 20$, $b = 10$, $\chi = 10$. Comparison for $\Delta x = \{0.1, 0.05, 0.01\}$ between different methods of approximation of a source term: (green) SS - Finite volume method with Suliciu relaxation solver and well-balancing "at rest" (6.3.11); (pink) SC - Finite volume method with the Suliciu relaxation solver and centered in space discretization of the source term, (blue) RC - Finite difference scheme based on the relaxation technique with centered in space approximation of the source (6.2.8). Reference solution (red) is given by the exact solution (7.2.18)

property is able to approximate correctly the location of the interface. Finite difference method is characterized by a very high numerical diffusion, while centered treatment of the source increases unnaturally the chemotaxis effect and leads to too high concentration at the left boundary of the domain. Decreasing the space step we observe that all the schemes converge to the reference solution, but still the finite volume, well-balanced scheme is the most accurate.

Accuracy in the approximation of velocity

Another important aspect of the numerical approximation of system (7.2.1) is the accuracy in the approximation of the velocity. In the case of the homogeneous Neumann boundary conditions the momentum should be zero at the steady state. In Section 6.2 we considered a finite difference, explicit scheme with centered in space discretization of the source term (6.2.8) and showed for $P(\rho) = \rho$ that it is not able to approximate the velocity field at the stationary state. Now we analyze it in the case $P(\rho) = \rho^2$ and compare the results with the approximation obtained by a finite volume, well-balanced scheme (6.3.11).

Figure 7.8 presents the steady states of the density and the momentum for both schemes and, on the right, the residues of the momentum. First we observe that at time $T = 100$ the residues are of order at least 10^{-8} and decreasing, which means that the steady state is reached. Then we see that the approximation of the density is comparable for both schemes, but a finite difference, explicit scheme (6.2.8) produces an error in the momentum profile. Its L^∞ norm is close to one instead of being equal to zero. On the other hand, the momentum obtained using the finite volume, well-balanced method (6.3.11) is of order 10^{-4}, which gives much better accuracy.

Discussion

Numerical comparison that we performed of different schemes approximating the hyperbolic model chemotaxis (7.2.1) shows that the problem of finding an optimal approach is not trivial. We compared finite difference and finite volume schemes, various approximate Riemann solvers for a homogeneous problem and different source approximations. We see that all of the methods have advantages and disadvantages. Finite volume schemes are based on the approximate Riemann solver and are able to capture shocks and discontinuities. As a result the interface between the region, where the density is strictly positive and the region, where it vanishes is approximated with much higher accuracy than in the case of standard, explicit schemes based on finite differences. For the later, at the free boundary the solution is smoothed due to the artificial viscosity. Moreover, schemes based on the finite volume method conserve the total mass automatically, without any additional conditions, but very low numerical viscosity leads to the occurrence of oscillations when steep gradients appear like for example in the case of $\gamma = 3$. Roe solver in unable to preserve the non negativity of the density at low initial masses, while HLL and Suliciu solver fail at larger initial densities. In this case standard, explicit schemes are stable for both, high values of γ and large initial masses. Comparison between different source term approximations leads to the conclusion that the well balanced approach is necessary to obtain correct approximations at the steady states. The centered in space treatment of the chemotaxis term in the model (7.1.1) causes an error in the momentum solution, which do not vanish at the steady states "at rest".
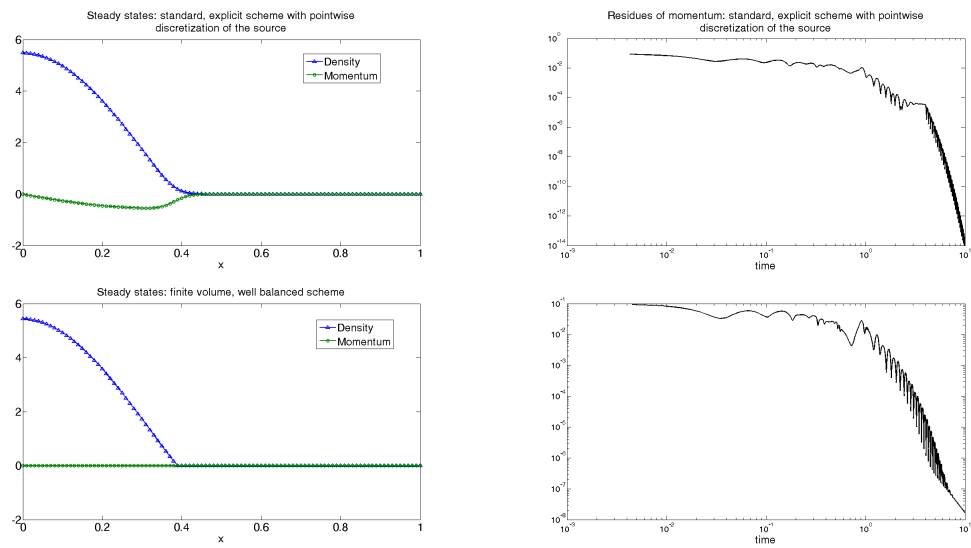
Figure 7.8: On the left: Density and momentum profiles at steady state for system (7.1.1) in the case $P(\rho) = \varepsilon\rho^2$ and $\varepsilon = D = a = b = L = 1$, $\chi = 50$ obtained by: (at the top) a finite difference scheme based on the relaxation technique with centered in space approximation of the source (6.2.8); (at the bottom) a finite volume method with Suliciu relaxation solver and well-balancing (6.3.11). On the right: corresponding residues of the momentum.

Simulations in the following part, in which we study the influence on the asymptotic behaviour of the length of the domain and the chemosensitivity constant are performed for $\gamma = 2$. While studying the behaviour of for higher values of γ the total mass is small enough so that approximate Riemann solvers are free from oscillations. This is the reason why we use the scheme presented in the previous chapter that is based on the finite volume method with Suliciu relaxation solver for the homogeneous part and well-balancing on the steady states with constant velocities (6.3.11). It is the most accurate approach to approximate non constant stationary solutions, especially the velocity at static steady states, and when good approximation at the interface with vacuum is essential.

Stability of non-constant steady states

One of the first problems concerning stationary solutions is their stability or instability. This is the reason why we start our numerical study from the analysis of the stability of the non constant steady state of the form of one, lateral bump. The choice of this form of equilibrium is motivated by the fact that we know the exact solution in this case.

In the study we are going to perturb the exact equilibrium and analyze the stability using the residues. We consider two different types of perturbation of the equilibrium. At first we perturb the location of the interface between the region, where the density is strictly positive, and the vacuum, which also affects the profile of the concentration. Since we choose a perturbation of mass zero it that concerns the solutions on their entire support. In the second

type of perturbation we change only the density profile in a small region. In both cases the velocity remains constant and equal to zero. The perturbations are chosen in such a way that the total mass of the exact solution and the perturbed one are equal. This condition is necessary in order to guarantee that the equilibrium doesn't change. The simulations are performed for the system (7.1.1) with the quadratic pressure function $P(\rho) = \varepsilon\rho^2$ and the following remaining parameters:

$$\varepsilon = D = a = b = L = 1, \quad \chi = 50$$

and the initial data with the mass $M_0 = 1 + \frac{1}{\pi}$. This choice guarantees that the constant $\alpha = \frac{a\chi}{2\varepsilon D} - \frac{b}{D} > 0$ and $L > \pi/\sqrt{\alpha}$ so the non-constant steady states exist. Assuming that the initial datum is non symmetric, this problem is endowed with the equilibrium of the form of one lateral bump given by (7.2.18). The interface $\bar{x}$ between the region, where $\rho > 0$ and the vacuum, is the smallest solution to

$$\sqrt{\frac{\beta}{\alpha}} \tan(\sqrt{\alpha}\bar{x}) = \tanh\left(\sqrt{\beta}(\bar{x} - L)\right). \tag{7.2.28}$$

Let us notice that it is insensitive to the change of the total mass M_0. It means that choosing the perturbation, which produces the initial datum with different masses, doesn't change the interface point of the equilibrium. Only the L^∞ norm of density increases. Solving the above equation numerically we obtain $\bar{x} \approx 0.3943$. In the case of a symmetric initial datum we would have obtained a centered bump as a steady state. We are not going to consider it because we explained that this form of equilibrium can be obtained from the lateral bump by symmetrization of the solution.

Perturbation of the interface

In the first test we consider a perturbation of the position of the interface $\bar{x}$. More precisely, we take the initial data of the form (7.2.18), in which $\bar{x}$ is replaced by $x^* = \bar{x} + \delta$. In order to have a perturbation of the null mass we recalculate the parameter K. The parameter δ is a perturbation parameter and cannot be too large, because the definition (7.2.18) can lead to negative values of the density. We study the stability of solutions for $\delta = -0.05$ and $\delta = 0.1$.

Simulations show that in both cases the perturbed solutions converge to the non-constant steady state given by (7.2.18) with $\bar{x}$. In order to verify that the stationary solution is reached we calculate the residues of the density at each time step t^n

$$R^n = \sqrt{\sum_{i=1}^{s} \left|\rho_i^n - \rho_i^{n-1}\right|^2 \Delta x}.$$

The results are presented at Figure 7.9 for $\delta = 0.1$ and at Figure 7.10 for $\delta = -0.05$. On the left we have the profiles of density, concentration and momentum for the initial data, exact and perturbed solution, while on the right we plot the residues. Initially the residues of density have the values of order 10^{-2}, which suggest that the solution evolves between each time steps. Then, at some point, they decrease rapidly up to the order of 10^{-14} and stabilize at this value suggesting that the solution reached the steady state and does not move any more. We observe that the residues of the concentration are free from oscillations during the convergence process.

The reason may come from the higher regularity of the solution and the fact that it doesn't contain the vacuum. The oscillations of residues after reaching the steady state are probably due to the numerical, systematic errors, as they are periodic, bounded and have similar absolute value. Another error of order 10^{-4} appears in the approximation of the momentum at the steady state. However, it is present in all the simulations so we assume that the steady state is reached. As a consequence, the lateral bump given by (7.2.18) is stable under these kinds of perturbations.
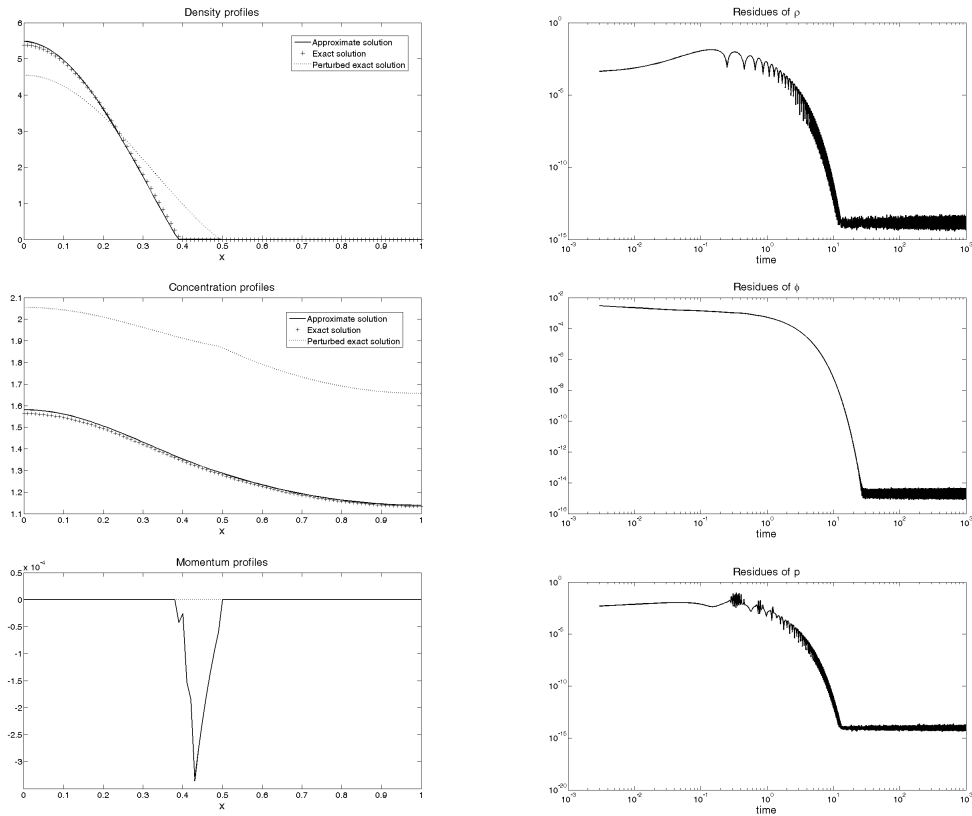
Figure 7.9: On the left: Profiles for system (7.1.1) with $\gamma = 2$ and $\varepsilon = D = a = b = L = 1$, $\chi = 50$ of density, concentration and momentum: (+++) exact solution (7.2.18) with the interface point $\bar{x} = 0.3943$; (...) initial datum being the exact solution (7.2.18) with the interface point $x^* = \bar{x} + 0.1$; (—) approximate solution. On the right: corresponding residues.

Perturbation in the small region

In the second test we introduce a small perturbation to the density profile in (7.2.18) only in small region $[x_1, x_2]$ satisfying $0 < x_1 < x_2 < \bar{x}$ having a jump at $x^* \in (x_1, x_2)$.
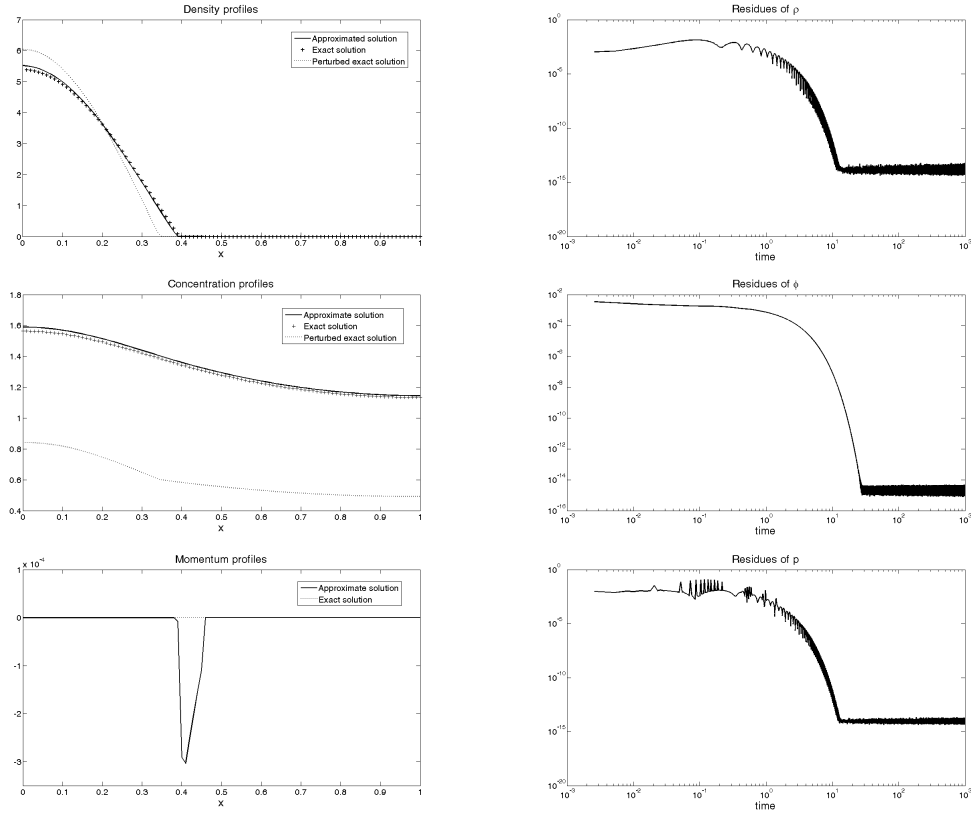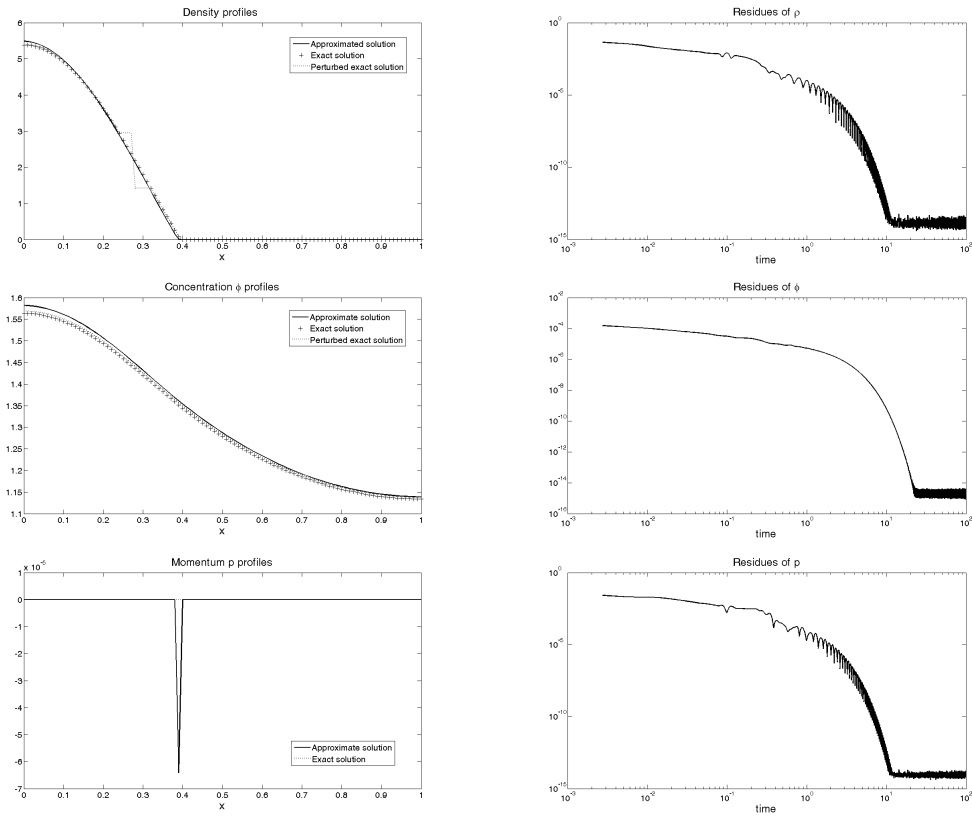
Figure 7.10: On the left: Profiles for system (7.1.1) with $\gamma = 2$ and $\varepsilon = D = a = b = L = 1$, $\quad \chi = 50$ of density, concentration and momentum: (+++) exact solution (7.2.18) with the interface point $\bar{x} = 0.3943$; (...) initial datum being the exact solution (7.2.18) with the interface point $x^* = \bar{x} - 0.05$; (—) approximate solution. On the right: corresponding residues.

More precisely, we choose the initial data in the following form

$$\rho^*(x) = \begin{cases} \frac{\chi}{2\varepsilon}\phi(x) + K & 0 < x \leq x_1 \\ \rho(x_1) & x_1 < x \leq x^* \\ \rho(x_2) & x^* < x \leq x_2 \\ \frac{\chi}{2\varepsilon}\phi(x) + K & x_2 < x \leq \bar{x} \\ 0 & \bar{x} < x \leq L \end{cases}, \qquad (7.2.29)$$

where ϕ, ρ, K are given by (7.2.18) and $\bar{x}$ is defined as previously. To conserve the total mass we choose the location of the jump x^* such that

$$\int_0^{\bar{x}} \rho^*(x)dx = \int_0^{\bar{x}} \rho(x)dx$$

Inserting the explicit formulas of $\rho^*(x), \rho(x)$ we get

$$x^* = \frac{\frac{1}{\sqrt{\alpha}}[\sin(\sqrt{\alpha}x_1) - \sin(\sqrt{\alpha}x_2)] + x_2\cos(\sqrt{\alpha}x_2) - x_1\cos(\sqrt{\alpha}x_1)}{\cos(\sqrt{\alpha}x_2) - \cos(\sqrt{\alpha}x_1)}, \qquad (7.2.30)$$

for arbitrary x_1, x_2 satisfying $0 < x_1 < x_2 \leq \bar{x}$.

The simulation for $[x_1, x_2] = [0.6\bar{x}, 0.8\bar{x}]$ shows that the non-constant steady state (7.2.18) is stable also for these types of perturbation. As before we plot the profiles of density, concentration and momentum and the time evolution of the residues. They are presented at Figure 7.11. We observe that the residues behave similarly as in the previous test. They decrease very fast to the order of 10^{-14} and stabilize.

Figure 7.11: On the left: Profiles for system (7.1.1) with $\gamma = 2$ and $\varepsilon = D = a = b = L = 1$, $\chi = 50$ of density, concentration and momentum: (+++) exact solution (7.2.18) with the interface point $\bar{x} = 0.3943$; ($\ldots$) initial datum in the form (7.2.29) with $[x_1, x_2] = [0.6\bar{x}, 0.8\bar{x}]$ and x^* given by (7.2.30) ; (—) approximate asymptotic state solution. On the right: corresponding residues.

Mechanism of the convergence

In the first test the convergence to the stable steady state (7.2.18) involves moving the interface and redistributing part of the particles towards the left boundary of the domain. It can be seen as the process of transporting the mass from the right to the left of the do-

main. In the second simulation the form and the localization of the perturbation would suggest that the convergence involves only smoothing the irregularities and the redistribution of particles takes place only in the restricted area. To study the character of the convergence to the equilibrium we analyze the time evolution of the density at control points that is at $x = \{0.08, 0.12, 0.16, 0.24, 0.28\}$. In the case of the first type of perturbation we consider $\delta = 0.1$, while for the second test we perturb the solution in the interval $[0.6\bar{x}, 0.8\bar{x}]$. The results are presented at Figure 7.12 and show that in both cases the convergence to equilibrium involves redistribution of the mass in the whole support with similar mechanism. We observe increase of density at points located closer to the left boundary of the domain and decrease near the interface $\bar{x}$. The dragging force responsible for it is chemotaxis. It moves the cells towards the left boundary, because there the concentration of the chemoattractant is higher. However, the density dependent internal pressure pushes the cells back in the direction of the free boundary, where the density is lower. This movement is periodic until achieving the balance between the pressure and the chemotaxis force. We also notice that for the perturbation of the interface the oscillations of density have much bigger amplitude. The maximal increase of the density for the second type of perturbation is ten times smaller. It can be caused by the presence of the smoothing effect of the initial jump. It is motivated by the behaviour of solutions at $x = 0.24$ and $x = 0.28$. From the plot we observe that at $x = 0.24$, where the perturbation stars, the density decreases, but not because the mass moves towards the left boundary as in the case of the first test. It moves in the direction of the interface, as shown by the increase of the value $x = 0.28$. Moreover, as the increase of density near the boundary of the domain and near the interface happen at the same time, it suggests that the smoothing occurs simultaneously with the movement of the cells due to the chemotactic force.
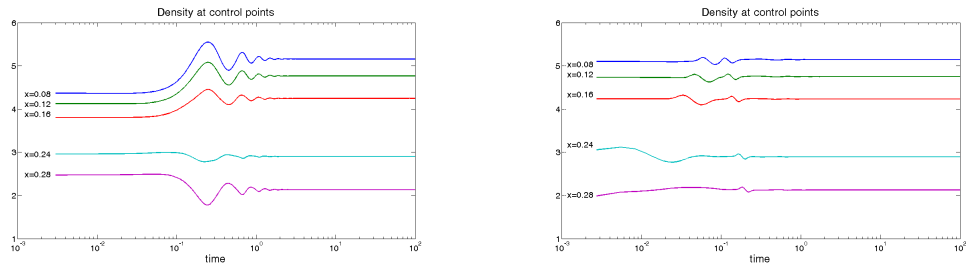

Figure 7.12: Time evolution of the density ρ for system (7.1.1) with $\gamma = 2$ and $\varepsilon = D = a = b = L = 1, \quad \chi = 50$ calculated at the control points $x = \{0.08, 0.12, 0.16, 0.24, 0.28\}$. On the left: initial datum is the exact steady state (7.2.18) with the perturbed interface point $x^* = \bar{x} + 0.1$, where $\bar{x} = 0.3943$. On the right: initial datum is in the form (7.2.29) with $[x_1, x_2] = [0.6\bar{x}, 0.8\bar{x}], \bar{x} = 0.3943$ and x^* given by (7.2.30)

Dependence of the structure of steady states on χ and L.

The form of steady states of the system (7.1.1) depends on its parameters. We showed analytically that if $\alpha \leq 0$ equation (7.2.17) has no solution for $\bar{x} \in [0, L]$ so the only equilibrium is

a constant state. The same situation occurs if $\alpha > 0$ and $L \leq \pi/\sqrt{\alpha}$. On the contrary, for L large enough, with other parameters fixed, we observe non constant stationary solutions. We can describe their shape exactly in the case of one bump and approximately, using numerical methods to find the mass distributions, otherwise. However, we are unable to determine analytically of how many bumps the stationary solution will contain. This motivates us to study the problem numerically. More precisely, we analyze how different parameters influence the number of bumps. In particular, we focus on the dependence on the chemotactic sensitivity χ, length of the domain L in the case $\gamma = 2$. The simulations are performed for the initial data in the following form

$$\rho_0(x) = \xi \cdot [1 + \sin(4\pi|x - 0.25L|)], \qquad \phi_0(x) = u_0(x) = 0 \qquad (7.2.31a)$$

where

$$\xi = \frac{1 + 1/\pi}{L + (1 - \cos(\pi L))/\pi} \qquad (7.2.31b)$$

is the scaling parameter and guarantees that changing the length of the domain keeps the mass constant, equal to the one obtained for $L = 1$.

At first we study the influence of the chemotactic sensitivity χ and the length of the domain L. Figure 7.13 presents density profiles at the steady states in the case of residues of order $10^{-8} - 10^{-10}$. We consider $\chi = \{3, 5, 50, 200\}$ and $L = \{1, 5, 7, 30\}$.

In the case $L = 1$ for $\chi = 3$ and $\chi = 5$ the condition $L > \pi/\sqrt{\alpha}$ is not satisfied and the steady states are constant. Increasing the chemosensitivity implies smaller value of α. As a consequence, for $\chi = 50$, we observe the appearance of a bump. The same process occurs when we enlarge the domain from $L = 1$ to $L = 5$ for $\chi = 3$. The condition $L > \pi/\sqrt{\alpha}$ is satisfied again and a lateral bump is formed. Now let us look what happens when we further increase of the chemotactic force. The stronger it is, the more concentrated are the bumps. It is particularly visible for $L = 7$ and $L = 30$ when we increase χ ten times from $\chi = 5$ to $\chi = 50$. At some point, when there is enough space between the bumps, new one appears. The formation of new intervals with strictly positive density is observed also when we increase the length of the domain making, as before, more free space. However, we consequence that there is a maximum number of bumps that can be formed at least when all other parameters except χ are fixed. It is motivated by the fact that further increase of the chemotactic force (even up to the value 10 000) for $L = 5$ and $L = 7$ doesn't produce new bumps.
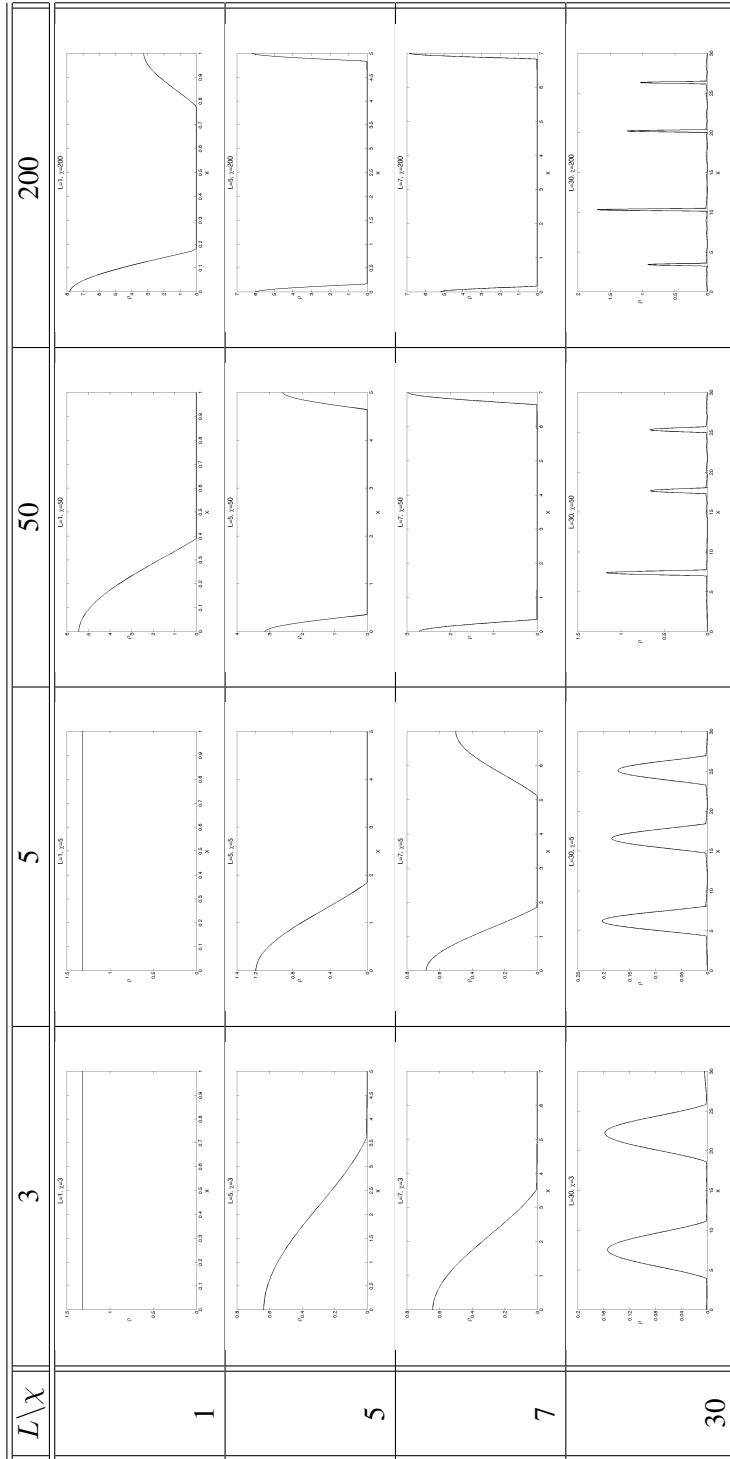
Figure 7.13: The density profiles at the steady states for system (7.1.1) with $P(\rho) = \varepsilon\rho^2$, $\varepsilon = D = a = b = 1$, total mass equal to $M_0 = 1.3183$ and initial datum of the form (7.2.31). Comparison of the structure of equilibria for different values of the chemosensitivity constant (columns) $\chi = \{3, 5, 50, 200\}$ and the length of the domain (rows) $L = \{1, 5, 7, 30\}$.

As a consequence, we see that the free space available to the cells has an essential effect on the formation of non-constant steady states. If it is too small only constant solutions are observed. The minimal length of the domain, at which a bump can appear, depends on the other parameters of the system. So if for example internal pressure between cells is much higher than the external forces caused by chemotaxis the inhomogeneities cannot be formed and we observe constant distributions. This hypothesis is confirmed also by the fact that when we increase the chemotaxis effect the smoothing process is overcome. It makes the movement of cells more oriented towards specific areas and if is strong enough breaks the homogeneity. At this moment a question appears. Is there a conditions joining L and other parameters of the system equivalent to the one for the one bump? In other words, is there a condition determining the number of bumps that can be formed at certain domains. Simulations suggest that there should be, because increasing L always only one new bump appear, however, we did not find any precise formulation for this connection.

Dependence on the adiabatic exponent γ

At the beginning of this chapter we presented a detailed analysis of the stationary solutions in the case of quadratic pressure function $P(\rho)$. We gave the general form of steady states for arbitrary γ, however, it was mentioned that for any other case apart from $\gamma = 2$, finding the exact formulas for density and concentration at equilibrium in non trivial. The reason lies in the nonlinear relation between ρ and ϕ in the equation (7.2.5). Despite this fact, the form of the non constant steady states remains the same that is they are composed of the regions, where density is strictly positive and regions, where it vanishes.

In the following test we consider the model with the following parameters: $\varepsilon = 1, D = 0.1, a = 20, b = 10, \chi = 10$ defined on the interval $[0, 3]$ with the initial datum $\rho_0(x) = 1.5 + \sin(4\pi|x - L/4|)$, $\phi_0(x) = u_0(x) = 0$. We analyze the structure of stationary solutions for different values of the adiabatic coefficient $\gamma = \{2, 3, 4, 5\}$. At Figure 7.14 we present density and concentration profiles at the steady states. We observe that with the increase of the parameter γ the number of bumps decreases until, for $\gamma = 5$, the equilibrium becomes constant. Moreover, in the case of the smallest chemosensitivity, that is for example $\chi = 2$, the constant steady states appear already for $\gamma = 3$. We see that the dependence of the existence of non-constant stationary solutions on the nonlinearity of the pressure function is very strong. In fact, in the case $\gamma = 2$ the parameter $\alpha = \frac{a\chi}{\gamma \varepsilon D} - \frac{b}{d}$ has to be strictly positive to guarantee that the equilibria are non constant. The simulations suggest that similar conditions should hold for higher γ.

Dependence on the initial mass

Variations of the initial mass very often lead to the appearance of different phenomena. For example, the solutions to Keller-Segel model in two space dimensions with linear diffusion blow up in finite time if the initial mass is larger that some threshold value. Other example concerns the experiments on the vasculogenesis process. It was observed that the character of the structure that is formed from randomly seeded cells may differ depending on the number of cells that are used. More precisely, in the experiments performed by Serini et al. [107] a vascular-like network develops if cell density ranges from 100 to 400 cell/mm^2. These values correspond
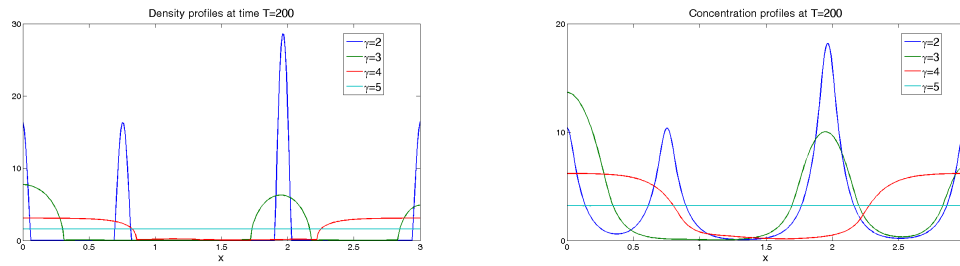
Figure 7.14: Profiles of the density and the concentration at steady states for system (7.1.1) with $\varepsilon = 1, D = 0.1, a = 20, b = 10, \chi = 10$ on the interval $[0, 3]$ with the initial datum $\rho_0(x) = 1.5 + \sin(4\pi|x - L/4|), \phi_0(x) = u_0(x) = 0$. Comparison for different values of the adiabatic coefficient $\gamma = \{2, 3, 4, 5\}$.

to two transitions. The first one, which occurs at the critical density of 100 cell/mm^2, is a percolative transition. Below this value the cells group into disconnected structures. The second threshold value, 400 cell/mm^2, gives rise to thicker chords. Increasing the density further leads to the formation of the so called "Swiss cheese" structure, which is a continuous carpet of cells with holes.

From the mathematical point of view, formation of the vascular-like network can be seen as non constant equilibrium composed of regions, where the density is strictly positive and regions with vacuum. At the beginning of this section we described this form of stationary solutions in one space dimension for the hyperbolic model. We gave details in the case of $P(\rho) = \rho^2$, but explained that how the system chooses the number of bumps is still an open question. We studied the dependence on L, χ and γ, giving a better insight into the mechanisms of the formation of networks. Now we are going to focus our attention on the influence of the initial mass and compare the results with the experimental observations.

$\underline{\gamma = 2}$

Let us start with the quadratic pressure function $P(\rho) = \rho^2$. We showed analytically that in the case of one lateral and central bump the location $\bar{x}$ of the interface remains constant regardless the change of the initial mass. The mass conservation leads to the increase of the L^∞ norm of the density. Natural question arises at this moment. Is it the same when more than one bump is present? We are unable to answer at the analytical level, but Figure 7.15 suggests that yes. It presents the density profiles of the system (7.2.1) with $\varepsilon = 1$, $D = 0.1$, $a = 20$, $b = 10$, $\chi = 10$ for different initial masses of the form $\rho_0(x) = \xi(1 + \sin(4\phi|x - L/4|))$, where $\xi = \{0.1, 1, 5, 10\}$. The stationary solution is composed of four bumps. We observe that their boundaries are the same for all initial masses. Only maximal density of each bump increases. But this is not what the experiments with endothelial cells suggest. It was observed that the thickness of the chords, corresponding to the size of bumps in one dimension, increases. The possible explanation may be that the mechanisms in one and two space dimensions differ, which is difficult to verify. Other possibility is connected with the effect of the internal pressure between cells.
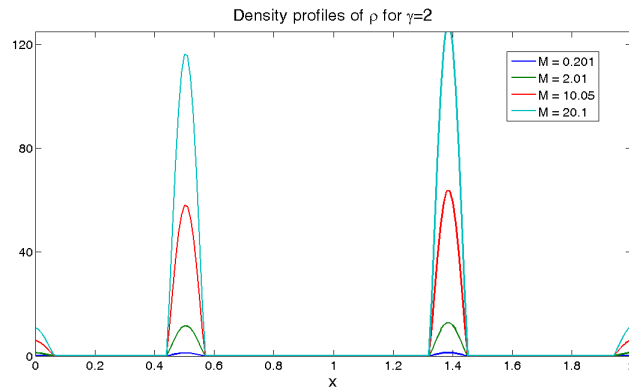
Figure 7.15: Density profiles in the case $P(\rho) = \rho^2$ for system (7.1.1) with $\varepsilon = 1$, $D = 0.1$, $a = 20$, $b = 10$, $\chi = 10$ and initial datum of the form $\rho_0(x) = \xi(1 + \sin(4\phi|x - L/4|))$. Comparison for different initial masses taking $\xi = \{0.1, 1, 5, 10\}$.

$\gamma = 3$

We showed numerically that increasing the chemotactic effect leads to higher maximal densities of the bumps. Moreover, the Keller-Segel model with $\gamma = 1$ produces a pointwise blow-up. The blow-up in the hyperbolic model is not expected, but other question arises. What happens if the quadratic pressure $\gamma = 2$ is to weak to limit the accumulation of cells, which as a consequence would give rise to larger bumps, instead of higher? To verify this, we perform a test
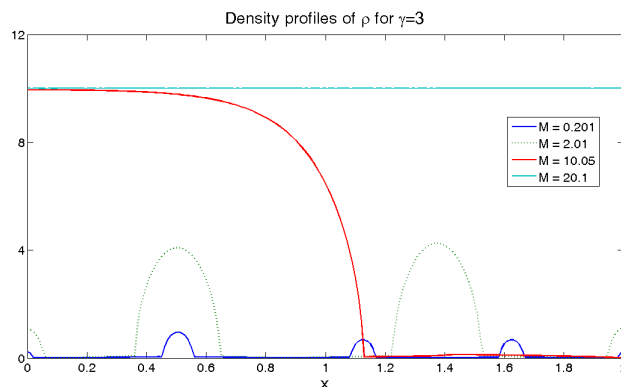

Figure 7.16: Density profiles in the case $P(\rho) = \rho^3$ for system (7.1.1) with $\varepsilon = 1$, $D = 0.1$, $a = 20$, $b = 10$, $\chi = 10$ and initial datum of the form $\rho_0(x) = \xi(1 + \sin(4\phi|x - L/4|))$. Comparison for different initial masses taking $\xi = \{0.1, 1, 5, 10\}$.

with the same parameters as previously, but now we consider $\gamma = 3$. Figure 7.16 presents the

density profiles. The bumps become larger and join together when the initial mass increases. When it is sufficiently large the constant equilibrium appears. So the pressure is strong enough to limit the excessive accumulation of cells.

Discussion

In this test, motivated by the experiments with endothelial cells, we studied the influence of the initial mass on the structure of equilibrium. In two space dimensions the growth of regions, where density is strictly positive, with the increase of the initial mass is suggested by the experiments. Our simulations in one space dimension show that in the case of $P = \rho^2$ the maximal density of bumps changes, while their support remains constant. For $\gamma = 3$ the structure of equilibria reflects the configurations observed in the experiments. Increasing γ further, implies that the constant state appears for lower initial masses.

This test indicates how important is the suitable choice of the adiabatic exponent γ in the modeling phase in order to capture correctly behaviour of the system. Moreover, this type of analysis, performed in two space dimensions, could be used in determining this parameter. As the threshold values of the initial mass can be found from experiments,we might perform simulations for different values of γ, in order to estimate the correct one, which gives rise to transitions and chord lengths in agreement with the experiments.

7.3 Linear vs. Nonlinear pressure

It has been proved that the solutions to Keller-Segel type model with linear diffusion blow up in two space dimensions if the initial mass is large enough. In the case of the hyperbolic system the finite time blow up was proved for symmetric solutions for the model of chemotaxis (7.1.1), in which the parabolic equation for ϕ was substituted by a Poisson type one [82]. However, in general we rather expect shock-type structures and instead of blow-up, wall-concentrations. They were observed in the numerical simulations in two dimensional setting, for example in [38]. We are going to analyze numerically the long time behaviour of the system (7.1.1) with linear pressure, that is $\gamma = 1$ in one space dimension. It poses some interesting and still open questions from the analytical and numerical points of view. For example, we observed numerically that for some choices of parameters the asymptotic states of the system form a comb of Dirac deltas, which are not stationary states because of the presence of vacuum. Moreover, using the finite volume and finite difference schemes, presented in the previous chapter, we were unable to capture the equilibria. Their existence and approximation are still unsolved.

In the previous section we studied the hyperbolic model of chemotaxis with nonlinear pressure function $P(\rho) = \varepsilon \rho^\gamma$ for $\gamma > 1$. We analyzed the behaviour of solutions on bounded intervals with no-flux boundary conditions. In particular, we focused our attention on the non constant steady states in the form of bumps, where the density is strictly positive, separated by vacuum.

Now we devote our study to the same model but with linear pressure that is $\gamma = 1$. In this case the internal pressure between cells depends linearly on their density and the repeling force is independent of it. For the parabolic equation it means the infinite speed of propagation in the absence of chemotaxis. Moreover, as was already mentioned, the solutions may blow-up. But this is not the only difference between the situation when $\gamma > 1$ and $\gamma = 1$. The anal-

ysis of stationary equations on a bounded domain with the homogeneous Neumann boundary conditions shows that linear pressure implies the absence of vacuum at the equilibrium. More precisely, the stationary momentum equation

$$\varepsilon \rho_x = \chi \rho \phi_x$$

yields the non trivial solution for density of the form

$$\rho = K e^{\frac{\chi}{\varepsilon}\phi}, \quad K > 0, \tag{7.3.1}$$

where ϕ is given by the solution to

$$-D\phi_{xx} = a\rho + b\phi.$$

Our aim is to analyze numerically the long time behaviour of solutions and possible convergence to equilibria. Simulations suggest that we can distinguish at least two types of asymptotic states. In particular, if the effect of the internal pressure is much stronger than the chemotactic force, that is $\varepsilon >> \chi$, the solutions converge asymptotically to constant or sinus-type states. On the other hand, when chemotaxis is dominant we observe numerically for ρ a comb of Dirac distributions. In the first case our results correspond to the the behaviour of a semilinear model (6.2.2) studied numerically in [92]. The second structure of solutions is particular as it contains vacuum. We stress that they are not equilibria of the model (7.1.1) with $\gamma = 1$. Now we are going to study these two cases. In particular, the influence of the size of the total mass is considered and confrontation with the results for $\gamma > 1$ is made.

Pressure dominant case: $\varepsilon >> \chi$

At first we are going to study numerically the asymptotic behaviour of solutions to system (7.1.1) when the effect of the internal pressure between cells is much stronger than the chemotaxis forces that is $\varepsilon >> \chi$. We perform simulations for the system with the following parameters $a = b = D = \gamma = L = \chi = 1$ and $\varepsilon = 100$. We are interested in analyzing the dependence of the long time behaviour on the initial mass. As the system preserves the symmetry we consider two types of initial data that is

$$\begin{cases} \rho_0 = \xi + \sin(4\pi|x - L/4|) \\ \phi_0 = \xi + \sin(4\pi|x - L/4|) \\ u_0 = 0 \end{cases}$$

in a non-symmetric case and

$$\begin{cases} \rho_0 = \xi + \sin(4\pi|x - L/2|) \\ \phi_0 = \xi + \sin(4\pi|x - L/2|) \\ u_0 = 0 \end{cases}$$

in a symmetric one, where $\xi > 0$.

In [53], [92] a semillinear model (6.2.2) was studied. In particular, the existence of a threshold mass was proved, below which the steady states are constant. This is why we consider initial profiles with two masses $M = 1135$ and $M = 4100$, for which different

behaviours of the semilinear system were observed. Figure 7.17 presents the asymptotic states of ρ, ϕ and u for symmetric and non symmetric initial profiles with $M = 1135$. We see that in the symmetric case the states are constant, while for non symmetric initial datum the solution converges asymptotically to a strictly positive, non constant distributions. However, for smaller mass also in this case we observe constant asymptotic state. As a result, we see that the amount of mass may be insufficient to induce a chemotactic force strong enough to overtake the diffusive process. Increasing it to $M = 4100$, which is bigger than the threshold value
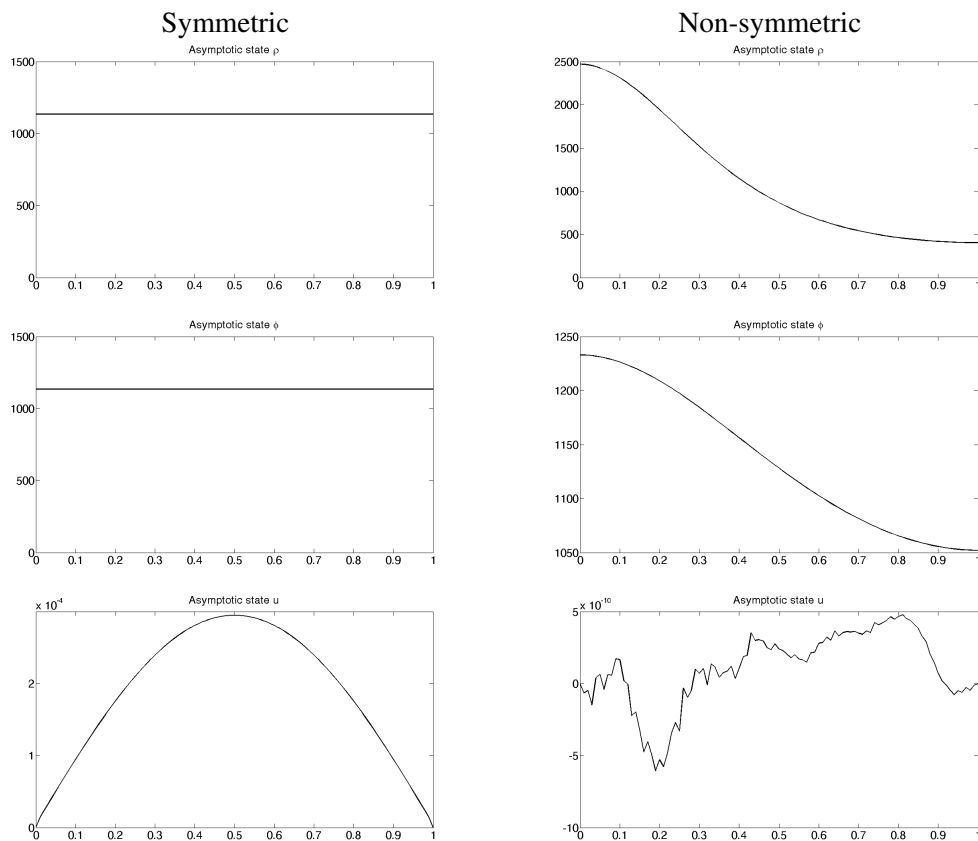

Figure 7.17: Asymptotic states of the density ρ, concentration ϕ and velocity u for system (7.1.1) with the linear pressure function $P(\rho) = \varepsilon\rho$ and $a = b = D = \gamma = L = \chi = 1$ and $\varepsilon = 100$ for the initial mass $M_0 = 1135$. On the left: symmetric initial datum. On the right: non-symmetric initial datum. The velocity u is of order 10^{-4} in the symmetric case and of order 10^{-10} for the non symmetric initial profile.

of the semilinear model, implies the appearance for long times of non constant states for both, symmetric and non symmetric, initial data observed at Figure 7.18. In the case of the former the profile is symmetric, as predicts the theory. For the latter we observe an accumulation of cells at the left boundary.

Linear pressure function $P(\rho) = \varepsilon\rho$ means that the force repealing the cells doesn't
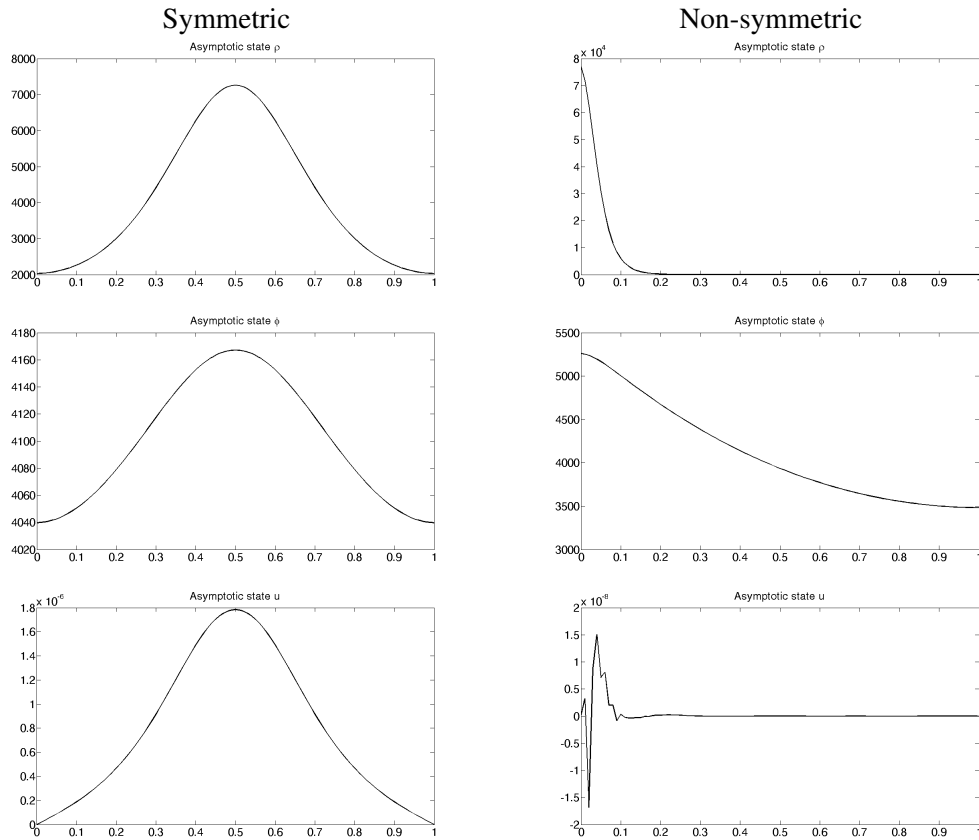
Symmetric   Non-symmetric

Figure 7.18: Asymptotic states of the density ρ, concentration ϕ and velocity u for system (7.1.1) with the linear pressure function $P(\rho) = \varepsilon\rho$ and $a = b = D = \gamma = L = \chi = 1$ and $\varepsilon = 100$ for the initial mass $M_0 = 4100$. On the left: symmetric initial datum. On the right: non-symmetric initial datum. The velocity u is of order 10^{-6} in the symmetric case and of order 10^{-8} for the non symmetric initial profile.

depend on the density. On the other hand, the chemotaxis effect depends on the density and the gradient of chemoattractant concentration, so may change for different total masses of cells and chemical substance. As a consequence of these two features, increasing the initial mass the directed movement due to the chemotaxis may become dominant. We observed the result of such situation in the appearance of non constant states and a stronger accumulation of cells. In the case of $\gamma = 2$ the solutions are constant no matter how big the mass would be. This is because the particular choice of the system parameters used in the simulations $a = b = D = \gamma = L = \chi = 1$ and $\varepsilon = 100$ yields $\alpha = \frac{a\chi}{2\varepsilon D} - \frac{b}{D} < 0$.

Chemotaxis dominant case

Now let us choose the following parameters of the model $\varepsilon = 1$, $a = 20$, $b = 10$, $D = 0.1$ and $\chi = 2$ and analyze the long time behaviour. For $\gamma = 2$ we have $\alpha > 0$ and non constant equi-

libria may occur. At Figure 7.19 we present asymptotic states of density for the initial datum $\rho_0(x) = \xi(1 + \sin(4\pi|x - L/4|))$, $\phi_0(x) = u_0(x) = 0$, where $\xi = \{10, 50, 100\}$. The long time profiles that we obtaine have the form of a comb with peaks, where cells are accumulated.

At first let us verify the nature of these peaks. To do this we study how their maximal
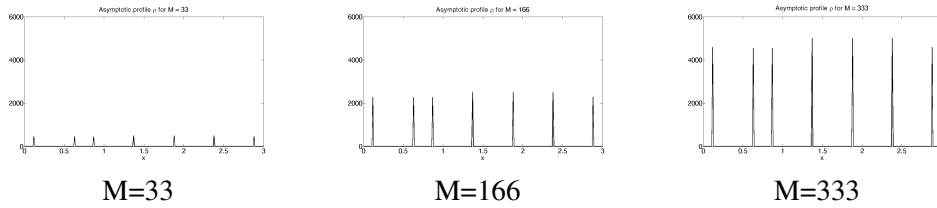

| M=33 | M=166 | M=333 |

Figure 7.19: Asymptotic density profiles for system (7.1.1) with the linear pressure $P(\rho) = \varepsilon\rho$ and $\varepsilon = 1$, $a = 20$, $b = 10$, $D = 0.1$ and $\chi = 2$ for the initial datum given by $\rho_0(x) = \xi(1 + \sin(4\pi|x - L/4|))$, $\phi_0(x) = u_0(x) = 0$. Comparison for different initial masses $\xi = \{10, 50, 100\}$.

values and supports change when we decrease the space step. If they are Dirac delta distributions we should observe the increase of the density and shrinking of the support for smaller Δx. Figure 7.20 shows the density profiles for three different mesh sizes $\Delta x = \{0.05, 0.01, 0.005\}$. We observe the above type behaviour characteristic for Dirac delta. The regions, where the density is strictly positive, become smaller, while the hight if the peaks increases.

Results at Figure 7.19 show that the non constant asymptotic profiles are present for all

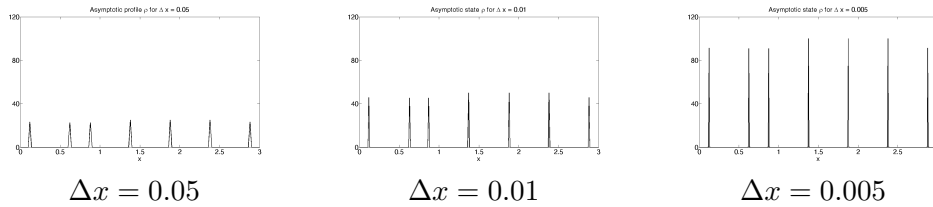| $\Delta x = 0.05$ | $\Delta x = 0.01$ | $\Delta x = 0.005$ |

Figure 7.20: Asymptotic density profiles for system (7.1.1) with the linear pressure $P(\rho) = \varepsilon\rho$ and $\varepsilon = 1$, $a = 20$, $b = 10$, $D = 0.1$ and $\chi = 2$ for the initial datum given by $\rho_0(x) = 1 + \sin(4\pi|x - L/4|)$, $\phi_0(x) = u_0(x) = 0$. Comparison for different sizes of the mesh $\Delta x = \{0.05, 0.01, 0.005\}$.

initial masses, even for much smaller than the threshold values from the previous test. Also increasing the total mass we see stronger accumulation of cells in the same regions of the domain. So we see that this behaviour is similar to the one for $\gamma = 2$. However, we stress that in that case the bumps were stationary solutions. Here, we observe only convergence to some asymptotic states composed of a series of Dirac masses, which are not equilibria of system (7.1.1) in the case $\gamma = 1$. It is due to the fact that for $\gamma = 1$ steady state are given by (7.3.1) and are trivial or strictly positive. The dependence on the initial mass for $\gamma = 1$ and $\gamma = 2$, when the chemotactic effect is strong enough, is ruled by similar mechanisms, however, is completely

different from the behaviour for higher values of γ. In the case $\gamma = 3$ we observed the growth of the regions, where the density is strictly positive and the existence of the threshold mass, above which the equilibria are constant.

7.4 Parabolic vs. Hyperbolic model

Macroscopic, parabolic systems are suitable to model the processes that occur at long time scales. In particular, aggregation phenomena such as for example behaviour of slime mold, are described very well by them. However, they usually fail when a spatially complex structures has to be reproduced. One of such phenomena is vasculogenesis process, in which randomly distributed endothelial cells by migration and interaction between themselves via chemical signals form in time networks corresponding to blood capillaries. The Keller-Segel type models are unable to describe this behaviour as well as cannot explain the so called "run and tumble" movements. Mechanisms of both of these phenomena depend on the processes that occur at smaller scales and parabolic models are unable to capture them. This is why there is a tendency in recent years to use hyperbolic systems, as they describe the movements of entities at lower, mesoscopic level.

In particular, in this chapter we study the hyperbolic system of chemotaxis (7.1.1) constructed to model the vasculogenesis process on bounded domains. We are interested in the existence and stability of non constant stationary solutions in the form of bumps, where density is strictly positive, separated by vacuum states. We compared the regions with high concentrations to the location of blood capillaries and the vacuum to the empty regions between them. Our numerical simulations indicate that asymptotically, under suitable conditions on the system parameters, the solutions converge to states that can be composed of one or several bumps. Moreover, they are stable in the sense that numerically we do not observe any exchange of mass between the bumps and for long times their location remains constant. However, these observations are valid only numerically up to the numerical error and no rigorous results on the stability of such solutions are known.

This section is devoted to the study of the equilibria of the parabolic model (7.1.3) in one space dimension posed on a bounded domain with no-flux boundary conditions and comparison of its behaviour with the hyperbolic system (7.1.1). The research on so called spike patterns for the Keller-Segel type systems was conducted by several authors. The possible existence of small regions with high concentration of reactant has been already introduced by Turing for diffusion systems, however, the appearance of solutions with narrow peaks is even more natural in cross-diffusion systems such as chemotaxis models. In one space dimension the existence and stability of spikes for Keller-Segel type models were analyzed for example in [59], [109], [58], [67], [100]. First, the studies show that there is a difference in the behaviour between a spike located at the boundary and in the interior of the domain. In [59] numerical simulations for a model with volume filling effect indicate that if the initial datum consists of a single spike in the interior it will drift towards the boundary. Authors of [109] considered a logarithmic sensitivity function and proved that the boundary spike is stable under the assumption of smallness of the chemoattractant diffusivity. Moreover, they gave a characterization of the metastable interior spike dynamics. In the limit of large total mass in [67] an equilibrium spike was constructed and under double limit of large mass and large domain it was shown that it will move in time in the direction of the boundary of the domain. Moreover, the authors

showed that starting from two peaks located at each boundary of the domain, asymptotically only one will remain. This type of spikes, which seem to be stable, over long times move slowly towards the boundary or other spike, are called metastable [100]. Now, going back to the vasculogenesis process, the existence of such spikes could explain the incapability of the parabolic model to reproduce the network structures. Motivated by this, we are going to study the problem numerically in order to understand better the dynamics beyond it.

First, we are going to consider a model with logistic chemosensitivity function and linear diffusion. This problem was studied by Dolak and Schmeiser [36] in the case of small diffusivity of the cells and the evolution equation of the chemoattractant given by an elliptic equation. They observed the existence of metastable peaks with plateaus, which correspond to the maximal density above which the chemotactic effect is switched off. Moreover, in the limit of vanishing cells diffusivity their numerical simulations indicated that the equilibria with several plateaus are reached with no further movement. Then we consider models with nonlinear density function $P(\rho) = \varepsilon\rho^2$ and constant chemosensitivity. We are going to analyze the long time behaviour of bumps and compare the asymptotic states with the results of the hyperbolic model.

7.4.1 Logistic Sensitivity function and linear pressure $\gamma = 1$

At first we study the behaviour of solutions to a model of chemotaxis with logistic, density dependent chemosensitive functions. In the parabolic case the system writes as

$$\begin{cases} \rho_t = P(\rho)_{xx} - (\chi(\rho)\rho\phi_x)_x \\ \phi_t = D\phi_x x + a\rho - b\phi \end{cases}, \tag{7.4.1}$$

while in the hyperbolic case it is of the form

$$\begin{cases} \rho_t + (\rho u)_x = 0 \\ (\rho u)_t + \left(\rho u^2 + P(\rho)\right)_x = -\rho u + \chi(\rho)\rho\phi_x \\ \phi_t = D\phi_x x + a\rho - b\phi \end{cases} \tag{7.4.2}$$

where

$$P(\rho) = \varepsilon\rho, \quad \varepsilon > 0, \quad \text{and} \quad \chi(\rho) = \chi\left(1 - \frac{\rho}{\rho_{\max}}\right), \quad \chi > 0. \tag{7.4.3}$$

Parameter $\rho_{\max} > 0$ denotes the maximal density, above which the chemotaxis effect is switched off. For $\rho_{\max} < \infty$ this type of chemosensitivity function reflects the volume filling effect modelling the fact that the cells are impenetrable and exert a repealing forces when compressed. In the second model that we are going to study this mechanism is modelled via the nonlinear function $P(\rho)$.

In the simulation, we take $\varepsilon = 10^{-4}$ and other parameters $\chi = D = a = b = 1$ and consider the threshold density $\rho_{\max} = 5$. As initial datum we take random perturbation from the constant state $\rho = 1$ for the density and absence of the chemical $\phi_0(x) = 0$. The small value of ε is chosen in order to guarantee that the cells reaction to the presence of the chemoattractant is strong enough to influence their movement and direct them towards the higher concentrations of the chemical substance. As a consequence regions with high densities may be formed. In the opposite case, for ε big enough, the random redistributions towards the constant equilibrium

would have prevailed. High values of ρ_{max} also imply stronger chemotactic effect especially in regions of high cells density. In fact, in the limit $\rho_{max} \to \infty$ the comb of Dirac deltas, observed in the previous sections, is expected.

Figure 7.21 presents the density profiles at different times for the parabolic model (7.4.1). We see that starting from the perturbed constant solution inhomogeneities appear. As time

$$T=0 \qquad\qquad\qquad T=10$$
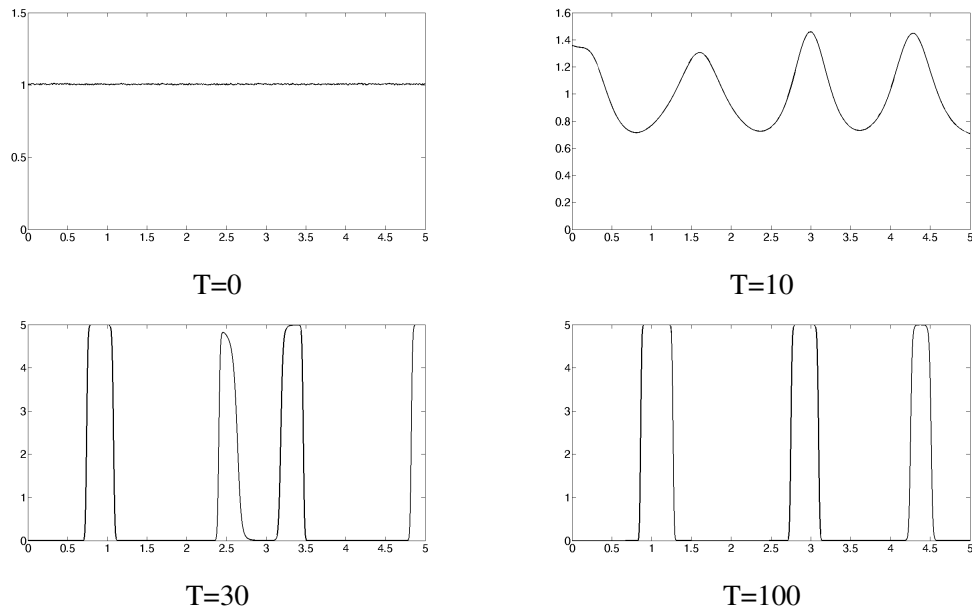
$$T=30 \qquad\qquad\qquad T=100$$

Figure 7.21: Density profiles for the Keller-Segel model (7.4.1) with logistic sensitivity function and $P(\rho) = \varepsilon\rho$ and $\varepsilon = 10^{-4}$, $\chi = D = a = b = 1$, $\rho_{max} = 5$. Comparison at different times $T = \{0, 10, 30, 100\}$

passes they are amplified and form a series of regions, in which density is approximately constant and equal to ρ_{max}, separated by vacuum. Once the pattern is formed, it seems stable for some time. This state is called metastable, because there is a continuous exchange of mass between the regions, where $\rho > 0$. It leads to the slow movement of the peaks towards each other observed at time T=30. When they merge with each other another metastable state occurs. With time we observe other peaks merging with each other. The situation repeats until only one region with strictly positive density is left and it is located at the boundary of the domain. On the other hand, the stationary solution to the hyperbolic model (7.4.2) with the same parameters and initial datum, presented at Figure 7.22, contains several peaks.

The logistic chemosensitive function is the mechanism to prevent overcrowding of cells. The presence of maximal density, at which the chemotactic response is switched off implies that cells cannot accumulated to unnaturally high densities. Both models form solutions composed of series of regions with constant, strictly positive density. The value of such plateaus corresponds to the maximal density ρ_{max}. For the hyperbolic case simulations indicate that these solutions are non-constant stationary solutions. Moreover, the equilibrium may contain more that one region, where density is strictly positive. Increasing the maximal density, at which
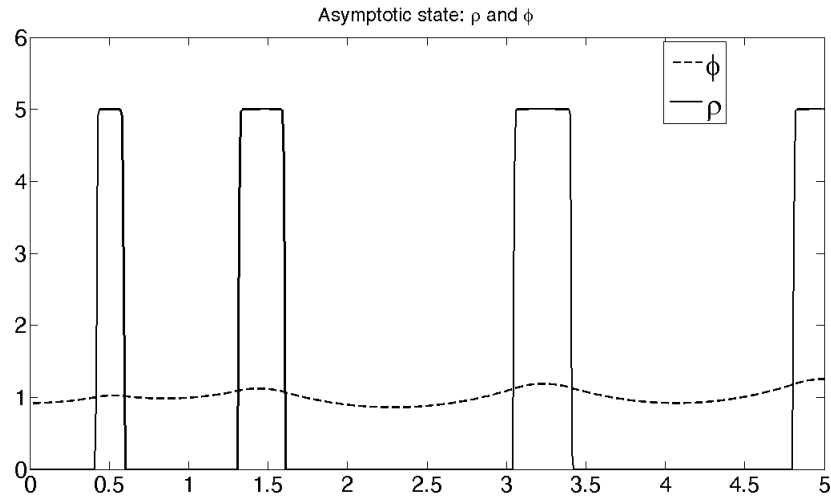
Figure 7.22: Asymptotic sates of density and concentration for the hyperbolic model of chemotaxis (7.4.2) with logistic sensitivity function and $P(\rho) = \varepsilon\rho$ and $\varepsilon = 10^{-4}$, $\chi = D = a = b = 1$, $\rho_{\max} = 5$.

the chemotactic effect is switched off, the size of plateaus becomes smaller, while their value higher. On the contrary, the plateaus of the parabolic model are metastable. After reaching a state with several regions, where $\rho > 0$, the mass exchange at small rates takes place between the zones. As a consequence, over large time the plateaus move towards each other and merge together. The movement stops when only one plateau region is left and is located at the boundary.

7.4.2 Constant sensitivity function and quadratic pressure $\gamma = 2$

Now we focus on models (7.4.1), (7.4.2) with nonlinear pressure function and constant chemosensitivity that is

$$P(\rho) = \varepsilon\rho^2, \quad \varepsilon > 0, \qquad \text{and} \qquad \chi(\rho) = \chi > 0. \qquad (7.4.4)$$

In this case the volume filling phenomenon is located in the function $P(\rho)$. Its nonlinear character implies that the repealing force between cells depends on their density. For the hyperbolic model we showed in the previous section that solutions to this model, under certain conditions on the parameters, reach the non-constant stationary solutions in the form of sinus-type bumps. Moreover, as in the previous example, the equilibrium may contain more that one bump of this type. Let us now analyze the behaviour of the parabolic model and verify if its behaviour follows the same mechanism as in the case of logistic sensitivity function and linear diffusion.

We are going to study convergence of solutions to equilibrium in three cases, for which in the hyperbolic case different numbers of bumps are observed. In particular we consider the following values of the system parameters:

1. Test1: $L = 1$, $\varepsilon = 1$, $a = 20$, $b = 10$, $D = 0.1$, $\chi = 20$

2. Test2: $L = 1$, $\varepsilon = 1$, $a = 1$, $b = 1$, $D = 1$, $\chi = 50$

3. Test3: $L = 2$, $\varepsilon = 1$, $a = 20$, $b = 10$, $D = 0.1$, $\chi = 10$

with the initial datum as is the previous test. Figures 7.23,7.24,7.25 present respectively for the above three tests density profiles at different times for the parabolic and hyperbolic model. We observe that the solutions to the parabolic model behave in the same way as in the previous test. Random perturbation of a constant state evolves in time into a highly inhomogeneous solution, which is composed of characteristic bumps separated by vacuum. However, the localized concentrations are not stable. There is a constant exchange of mass between them. As a consequence, over long times the bumps move towards each other until they merge together and another form of metastable solutions is reached. The situation appears to continue until one bump, located at the boundary, is left.

   In the first test, presented at Figures 7.23, the solution of the parabolic model if formed by two bumps at $T = 0.12$. One is located at the boundary, the second in the interior of the domain. We observe that the latter is attracted by the "more stable" one and moves towards it. Before time $T = 0.6$ they had merged together and an equilibrium was reached. On the other hand, the hyperbolic model at time $T = 1.6$ also contains two bumps, which are located at the same points. However, in this case, the internal one instead of being attracted toward the lateral bump moves in the direction of the other boundary of the domain. As a results two regions with $\rho > 0$ are formed and remain motionless.

   The second set of system parameters leads to the formation of a metastable state composed of two bumps, one at each of the boundaries, as seen at Figure 7.24. As before, in the case of the hyperbolic model this solution is stationary. No further movement is observed. The profiles of density show that this configuration is metastable for the parabolic model. A smaller bump at the right boundary starts to decrease and the mass is transfered to the other one. The equilibrium is reached when only one bump is left.

   In the last test, presented at Figure 7.25, the solution to hyperbolic model converges to an equilibrium composed of four bumps. The evolution of the density for the parabolic model shows the same metastability of bumps as in the previous test. However, now the length of the interval is bigger and the chemotactic sensitivity smaller. It implies that the communication between the bumps is weaker. As a consequence, we observe that the time needed to merge regions with strictly positive density is much longer. In fact, when two bumps are left, the mass exchange is very slow and their effective movement is difficult to observe. Numerical simulation for longer time, shown at Figure 7.26 indicates that the right bump moves very slowly towards the right boundary, while the left one in the opposite direction. As a consequence, a metastable state will be composed of two lateral bumps and, as we have seen in the previous test, after some time they will merge together and form one bump at one of the boundaries. The last, equilibrium state is not shown due to the velocity of the process, which requires very long simulation times.

7.5   Discussion

Parabolic models of Keller-Segel type describe evolution of populations at macroscopic level. They are particularly accurate in aggregation phenomena, in which interactions between individuals lead to directed movement and formation of one, connected mass. On the other hand,

hyperbolic models are based on the mechanisms occurring at mesoscopic scale. As a consequence, they are able to reproduce more complex behaviours such as the formation of networks. An attempt to model the process of vasculogenesis showed that a parabolic system cannot describe the observed results, while hyperbolic approach is successful in it. It motivated many researches in better understanding the difference between the two systems. Moreover, from the mathematical point of view both, aggregation into one solid mass or formation of a complex network, correspond to stationary or asymptotic states. Characterization of such equilibria lies at the base of a better understanding of the mechanism of biological or physical phenomena. In order to give a better insight in the behaviour of the chemotaxis systems, we devoted our study to the long time evolution of solutions on bounded domains with no flux boundary conditions. This setting mimics some experimental environments and allows us to compare the observed results. As a consequence we were able to give some answers on the particular features of the studied models. Our research is focused on the analysis of non constant stationary solutions of a hyperbolic model with nonlinear pressure term of the porous medium type. The equilibria that we study are composed of the region, where density is strictly positive and the region, where it vanishes and may appear also for initial datum that doesn't contain vacuum. In one space dimension they form a so called bumps of high density and we associate them with the location of vascular network chords.

The first objective was to describe their structure. For $\gamma = 2$ we obtained necessary conditions on the existence and explicit formulas in the case of one bump, which can be localized at the boundary or symmetrically at the center of the domain. In the case of more than one region with strictly positive density the formulas are also presented, however, the existence of such solutions is not proved. At the next step we studied these types of non constant steady states numerically. The numerical method, that we constructed in the previous section, is able to preserve stationary solutions and deals with vacuum. It gives us a powerful tool to characterize the behaviour of the models. At first we considered stability of the solutions in the form of one lateral bump. We showed that numerically it is stable under small perturbations and explained that due to the chemotaxis effect the convergence mechanism concerns all particles, even in the case of perturbation localized in a small region. Then we focus on the dependence of the number of bumps on the system parameters. In particular, we considered length of the domain, chemosensitivity constant, adiabatic coefficient and total mass. Simulations suggest that the bumps are formed if they have enough space or the response to the presence of the chemical is strong enough. Increasing the size of the domain or chemosensitivity constant implies formation of new bumps. However, even if not proved, the results might suggest the existence a maximal number of bumps that can form at domain with certain length. Numerical study of the equilibria for different γ shows that the higher the internal force between cells is, the less bumps are formed. In other words, increase of the parameter γ leads to wider bumps with smaller maximum density. When the support of one bump meets another one, they merge together. If γ is big enough, the equilibrium is constant. The last parameter in our study is the total mass. Its significant influence was observed in the experiments on vasculogenesis, where threshold values of initial densities determined transitions between different structures. We compared the reaction of equilibria on the increase of total mass in two cases, $\gamma = 2$ and $\gamma = 3$. We found out that the model with quadratic pressure $\gamma = 2$ doesn't reproduce the experimental results. Increasing initial densities only the height of bumps grows, while their

support and location remains constant. In this case, a so called "Swiss cheese" configuration couldn't be observed. On the other hand, taking $\gamma = 3$ implies stronger repealing forces at higher densities and the unnatural overcrowding is prevented. As a consequence, for higher mass the bumps become wider and lower converging to a constant state for initial density large enough.

The analysis of the model with quadratic pressure is the simplest from the mathematical point of view. This is because in this case the equilibrium relation between the density and concentration is linear, while for $\gamma = 1$ it is exponential and $\gamma > 2$ leads to power type relation. Numerical analysis of the latter case indicated that the behaviour is in agreement with the experimental results. Moreover, simulations for different total mass showed that $\gamma > 2$ is more realistic than in the case of $\gamma = 2$. However, an interesting behaviour is observed also for $\gamma = 1$. Here the internal force between cells doesn't depend on their density and is constant everywhere. It implies that if the chemotaxis effect is much weaker that the diffusive one, for example $\varepsilon >> \chi$, the equilibria are constant. However, on the contrary to the cases with $\gamma > 1$ there is a threshold mass, above which the number of cells is large enough to induce a directed movement and accumulate in some regions. So increasing the initial mass inhomogeneities may occur due to the augmented chemotaxis transport and non constant states are formed. On the other hand, when in the system the chemotaxis process is dominant, solutions converge numerically to some asymptotic states composed of a series of Dirac delta concentrations. We underline that they are not equilibria of the model and their mathematical description and numerical approximation are still open problems.

The last part of our research is devoted to the comparison of the long time behaviour of the parabolic and hyperbolic models. In particular, we focused on the asymptotic convergence to the non constant stationary solutions described previously. Our numerical simulations confirmed the failure of the Keller-Segel type system in describing the formations of complex networks. This is due to the metastability of the solutions composed of more than one bump. More precisely, when at least two regions with strictly positive density are formed, they might be "relatively" stable for long times. However, there is a constant exchange of mass between them. The larger the domain and the weaker the chemotactic response are, the smaller the rate of exchange is. Nevertheless, it leads to a movement of a bump towards other one and merging of them in the end. Then another metastable state is reached and the exchange of mass occurs between remaining bumps. The mechanism repeats until only one bump is present, however, the equilibrium is reached only if the remaining bump is localized at one of the domain boundaries. On the other hand, we observed that the hyperbolic model is endowed with stationary solutions that can be composed of several regions with positive density separated by vacuum.

Analytical and numerical analysis became a very important tool in exploration of complex processes and in discovering new mechanisms that are still hidden to biologists. It gives a better understanding in the process of the formation of complex structures. In this thesis we investigated how different parameters can change the behaviour of solutions of some models of chemotaxis. However, still little is known beyond the analysis we have presented and there are still many open problems:

Modelling

- Similar analysis in two space dimensions in order to confirm the above results. It may happen that new mechanisms will occur, which prevent unnatural behaviours, which we observed, from appearing. On the other hand, adding a space dimension may introduce instabilities leading to blow up of solutions in the cases, when global existence was observed in one dimensional setting.

- Further study of behaviour for very large adiabatic constants γ. It is motivated by the fact that cells have their own volume and cannot be penetrable by others. In fact, the coefficient $\gamma = 2$ is used in the shallow water equations to describe the internal pressure between the molecules of water. It would suggest that in the case of cells this value should be much larger.

- What is the behaviour for very large initial masses, which is observed in tumour growth?

Mathematical analysis

- Analysis of the linear case $\gamma = 1$. Even if not relevant from the biological point of view, it is an interesting mathematical question. The observed numerically asymptotic convergence to states, which contains vacuum so are not equilibria in the case $\gamma = 1$, raises a question about the existence and stability of the steady states.

- For $\gamma = 2$ a rigorous analysis of the existence of more than one bump and stability of steady states is unknown. Especially important would be finding mechanisms and conditions determining how many bumps appear.

- The case $\gamma > 2$ is entirely open for hyperbolic model of chemotaxis (7.1.1) on bounded domains.

- Possibility of a blow-up in finite time for hyperbolic model of chemotaxis (7.1.1). Even if it is not expected, no rigorous proofs are available.

- Mathematical analysis in the presence of vacuum. Degeneracy of the system (7.1.1) in this case makes the classical methods useless and new techniques have to be found out.

Numerical methods

- Numerical methods that would allow us to analyze the behaviour with high accuracy when we deal with very high total mass, steep gradients

- Methods to treat homogeneous Neumann boundary conditions such that the total mass is conserved and errors that can appear at the boundary nodes are not amplified during the evolution.

- Approximation of hyperbolic model of chemotaxis (7.1.1) for large values of γ, which requires more refined well-balancing than for example in the case $\gamma = 2$.

- Approximation of the velocity fields. The error in the case of finite volume, well-balanced schemes, even if small, still exists. New approaches are needed to suitable balance all the terms at steady states.

- Extension of schemes to two dimensions. In one space dimension to construct a finite volume scheme for conservation laws we are equipped with a powerful tool such as Riemann problem, however, its extension to higher dimensions is not trivial.
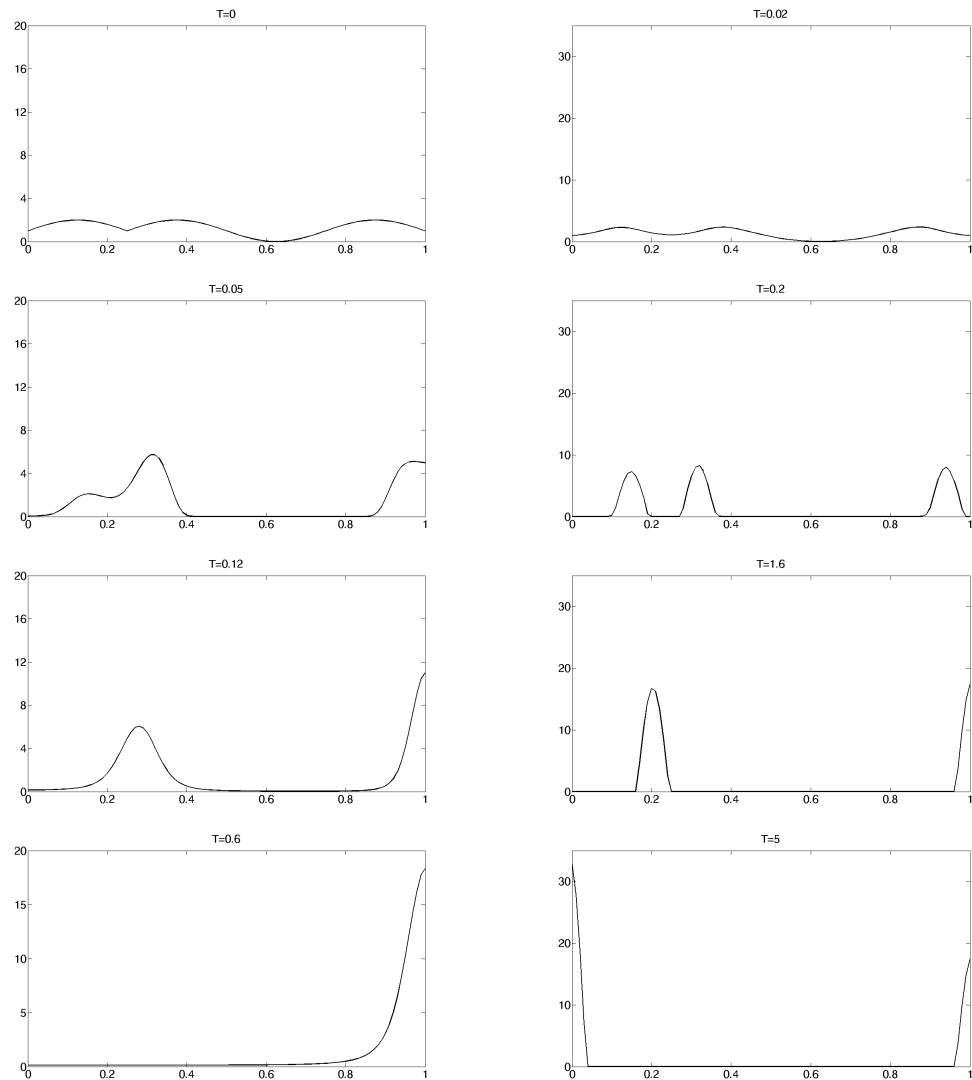
Figure 7.23: TEST 1: Density profiles at different times in the case of quadratic pressure $P(\rho) = \varepsilon\rho^2$ and and constant chemosensitivity of (on the left) parabolic model (7.1.3) and (on the right) hyperbolic model (7.1.1) with $L = 1$, $\varepsilon = 1$, $a = 20$, $b = 10$, $D = 0.1$, $\chi = 20$ and initial datum being a random perturbation of a constant state.
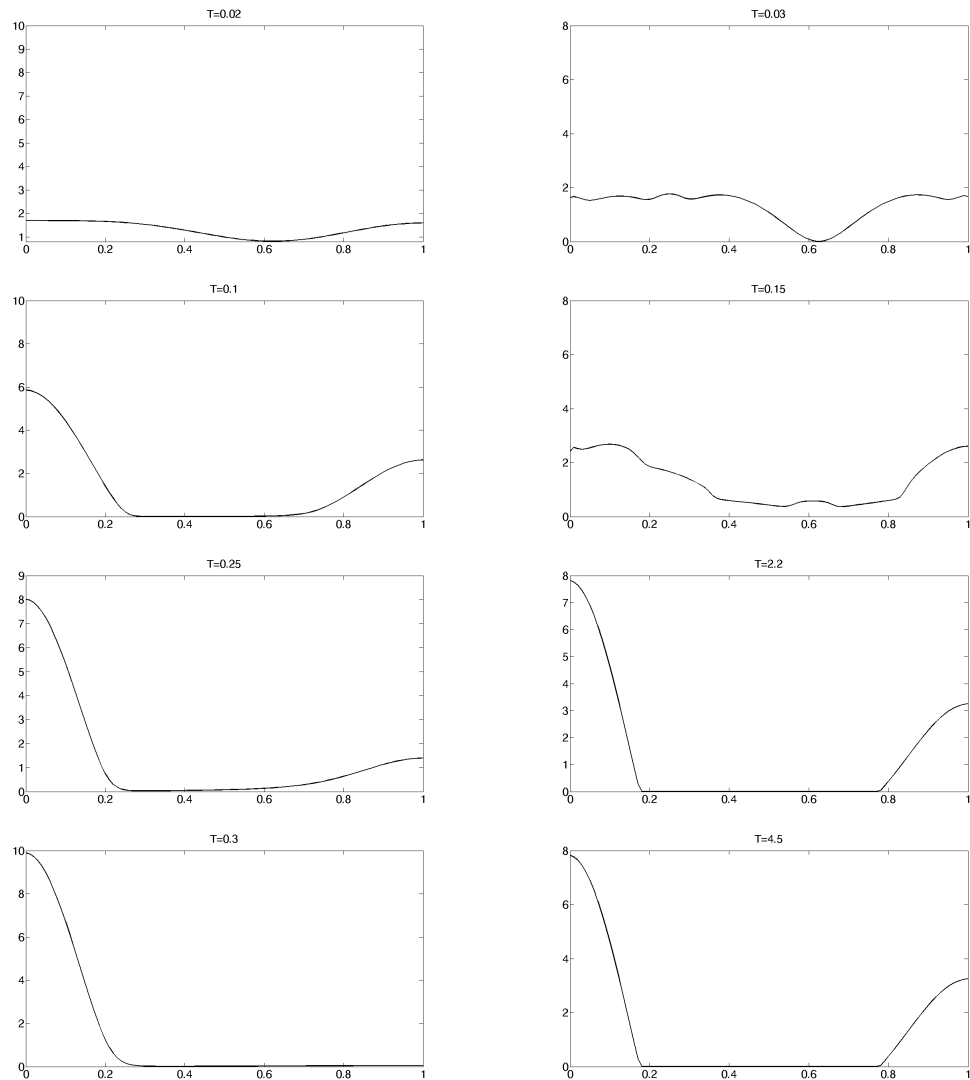
Figure 7.24: TEST 2: Density profiles at different times in the case of quadratic pressure $P(\rho) = \varepsilon \rho^2$ and and constant chemosensitivity of (on the left) parabolic model (7.1.3) and (on the right) hyperbolic model (7.1.1) with $L = 1$, $\varepsilon = 1$, $a = 1$, $b = 1$, $D = 1$, $\chi = 50$ and initial datum being a random perturbation of a constant state.
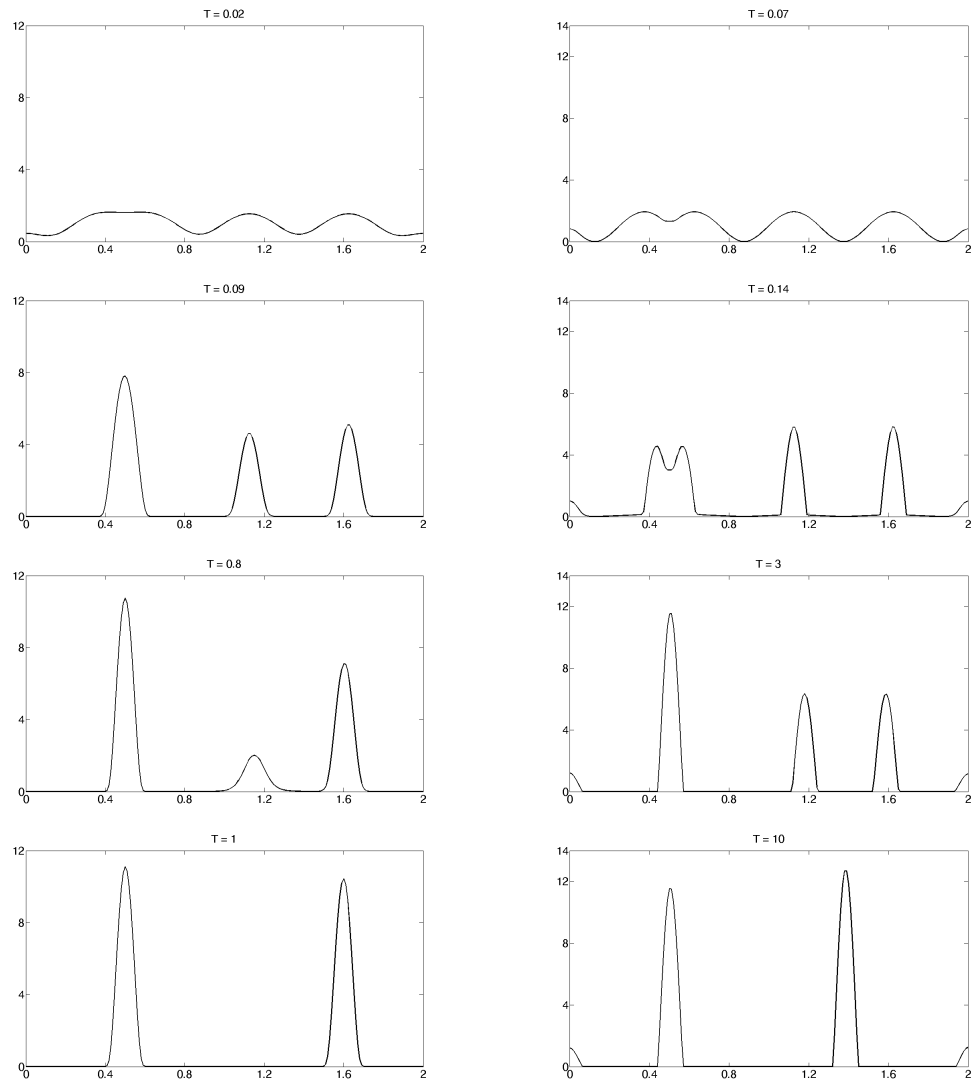
Figure 7.25: TEST 3: Density profiles at different times in the case of quadratic pressure $P(\rho) = \varepsilon \rho^2$ and and constant chemosensitivity of (on the left) parabolic model (7.1.3) and (on the right) hyperbolic model (7.1.1) with $L = 2$, $\varepsilon = 1$, $a = 20$, $b = 10$, $D = 0.1$, $\chi = 10$ and initial datum being a random perturbation of a constant state.

Figure 7.26: TEST 3: Density profiles at $T = 1$ and $T = 25$ in the case of quadratic pressure $P(\rho) = \varepsilon\rho^2$ and and constant chemosensitivity of parabolic model (7.1.3) with $L = 2$, $\varepsilon = 1$, $a = 20$, $b = 10$, $D = 0.1$, $\chi = 10$ and initial datum being a random perturbation of a constant state.
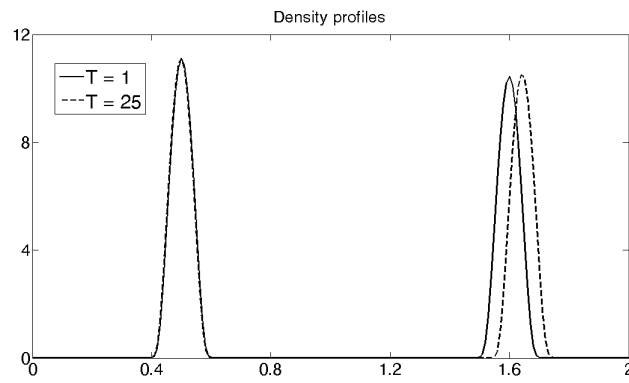
Bibliography

[1] H. Amann. Global existence for semilinear parabolic systems. *J. Reine Angew. Math.*, 360:47–83, 1985.

[2] D. Ambrosi, F. Bussolino, and L. Preziosi. A review of vasculogenesis models. *Journal of Theoretical Medicine*, 6(1):1–19, March 2005.

[3] D. Ambrosi and L. Preziosi. On the closure of mass balance models for tumor growth. *Math. Models Methods Appl. Sci.*, 12(5):737–754, 2002.

[4] Sigurd Angenent. Analyticity of the interface of the porous media equation after the waiting time. *Proc. Amer. Math. Soc.*, 102(2):329–336, 1988.

[5] Robyn P. Araujo and D. L. Sean McElwain. A mixture theory for the genesis of residual stresses in growing tissues. II. Solutions to the biphasic equations for a multicell spheroid. *SIAM J. Appl. Math.*, 66(2):447–467 (electronic), 2005.

[6] D. Aregba-Driollet, R. Natalini, and S. Tang. Explicit diffusive kinetic schemes for nonlinear degenerate parabolic systems. *Math. Comp.*, 73(245):63–94 (electronic), 2004.

[7] Denise Aregba-Driollet, Maya Briani, and Roberto Natalini. Asymptotic high-order schemes for 2×2 dissipative hyperbolic systems. *SIAM J. Numer. Anal.*, 46(2):869–894, 2008.

[8] D. G. Aronson. Regularity properties of flows through porous media: A counterexample. *SIAM J. Appl. Math.*, 19:299–307, 1970.

[9] D. G. Aronson. Regularity properties of flows through porous media: The interface. *Arch. Rational Mech. Anal.*, 37:1–10, 1970.

[10] D. G. Aronson, L. A. Caffarelli, and S. Kamin. How an initially stationary interface begins to move in porous medium flow. *SIAM J. Math. Anal.*, 14(4):639–658, 1983.

[11] D. G. Aronson, L. A. Caffarelli, and Juan Luis Vázquez. Interfaces with a corner point in one-dimensional porous medium flow. *Comm. Pure Appl. Math.*, 38(4):375–404, 1985.

[12] D. G. Aronson and J. L. Vázquez. Eventual C^∞-regularity and concavity for flows in one-dimensional porous media. *Arch. Rational Mech. Anal.*, 99(4):329–348, 1987.

[13] S. Astanin and L. Preziosi. Multiphase modells of tumour growth. *Selected Topics on Cancer Modelling: Genesis - Evolution - Immune Competition - Therapy, Nicola Bellomo, Mark Chaplain, and Elena De Angelis*, 2007.

[14] Emmanuel Audusse, Francois Bouchut, Marie-Odile Bristeau, Rupert Klein, and Benot Perthame. A fast and stable well-balanced scheme with hydrostatic reconstruction for shallow water flows. *SIAM Journal on Scientific Computing*, 25(6):2050, 2004.

[15] N. Bellomo, E. Angelis, and L. Preziosi. Multiscale modelling and mathematical problems related to tumor evolution and medical therapy. *Theoretical Medicine*, 5:111–136, 2004.

[16] N. Bellomo and L. Preziosi. Modelling and mathematical problems related to tumor evolution and its interaction with the immune system. *Math. Comput. Modelling*, 32(3-4):413–452, 2000.

[17] François Bouchut. In *Nonlinear stability of finite volume methods for hyperbolic conservation laws, and well-balanced schemes for sources*, Frontiers in Mathematics. Birkhauser, 2004.

[18] Francois Bouchut, Haythem Ounaissa, and Benoît Perthame. Upwinding of the source term at interfaces for Euler equations with high friction. *Comput. Math. Appl.*, 53(3-4):361–375, 2007.

[19] L. A. Caffarelli, J. L. Vázquez, and N. I. Wolanski. Lipschitz continuity of solutions and interfaces of the N-dimensional porous medium equation. *Indiana Univ. Math. J.*, 36(2):373–401, 1987.

[20] Luis A. Caffarelli and Avner Friedman. Regularity of the free boundary for the one-dimensional flow of gas in a porous medium. *Amer. J. Math.*, 101(6):1193–1218, 1979.

[21] Luis A. Caffarelli and Noemí I. Wolanski. $C^{1,\alpha}$ regularity of the free boundary for the N-dimensional porous media equation. *Comm. Pure Appl. Math.*, 43(7):885–902, 1990.

[22] V. Calvez and J. A. Carrillo. Volume effects in the Keller-Segel model: energy estimates preventing blow-up. *J. Math. Pures Appl. (9)*, 86(2):155–175, 2006.

[23] Vincent Calvez and Jos A. Carrillo. Volume effects in the keller-segel model: energy estimates preventing blow-up, tech. Technical report, 2005.

[24] J.-J. Cauret, J.-F. Colombeau, and A. Y. LeRoux. Discontinuous generalized solutions of nonlinear nonconservative hyperbolic equations. *J. Math. Anal. Appl.*, 139(2):552–573, 1989.

[25] M.A.J. Chaplain and A.M. Stuart. A model mechanism for the chemotactic response of endothelial cells to tumour angiogenesis factor. *IMA J. Math. Appl. Med. Biol.*, 10:149–168, 1993.

[26] E. Conway, D. Hoff, and J. Smoller. Large time behavior of solutions of systems of nonlinear reaction-diffusion equations. *SIAM J. Appl. Math.*, 35(1):1–16, 1978.

[27] Daniel Coutand, Hans Lindblad, and Steve Shkoller. A priori estimates for the free-boundary 3D compressible Euler equations in physical vacuum. *Comm. Math. Phys.*, 296(2):559–587, 2010.

[28] Daniel Coutand and Steve Shkoller. Well-posedness in smooth function spaces for moving-boundary 1-D compressible Euler equations in physical vacuum. *Comm. Pure Appl. Math.*, 64(3):328–366, 2011.

[29] Gianni Dal Maso, Philippe G. Lefloch, and François Murat. Definition and weak stability of nonconservative products. *J. Math. Pures Appl. (9)*, 74(6):483–548, 1995.

[30] P. Daskalopoulos and R. Hamilton. Regularity of the free boundary for the porous medium equation. *J. Amer. Math. Soc.*, 11(4):899–965, 1998.

[31] P. Daskalopoulos, R. Hamilton, and K. Lee. All time C^∞-regularity of the interface in degenerate diffusion: a geometric approach. *Duke Math. J.*, 108(2):295–327, 2001.

[32] L. Desvillettes and K. Fellner. Entropy methods for reaction-diffusion systems. *Discrete Contin. Dyn. Syst.*, (Dynamical Systems and Differential Equations. Proceedings of the 6th AIMS International Conference, suppl.):304–312, 2007.

[33] L. Desvillettes and K. Fellner. Entropy methods for reaction-diffusion equations: slowly growing a-priori bounds. *Rev. Mat. Iberoam.*, 24(2):407–431, 2008.

[34] M. Di Francesco, K. Fellner, and P. A. Markowich. The entropy dissipation method for spatially inhomogeneous reaction—diffusion-type systems. *Proc. R. Soc. Lond. Ser. A Math. Phys. Eng. Sci.*, 464(2100):3273–3300, 2008.

[35] Marco Di Francesco and Monika Twarogowska. Asymptotic stability of constant steady states for a 22 reactiondiffusion system arising in cancer modelling. *Mathematical and Computer Modelling*, pages 1–12, 2010.

[36] Yasmin Dolak and Christian Schmeiser. The Keller-Segel model with logistic sensitivity function and small diffusivity. *SIAM J. Appl. Math.*, 66(1):286–308 (electronic), 2005.

[37] Francis Filbet, Philippe Laurençot, and Benoît Perthame. Derivation of hyperbolic models for chemosensitive movement. *J. Math. Biol.*, 50(2):189–207, 2005.

[38] Francis Filbet and Chi-Wang Shu. Approximation of hyperbolic models for chemosensitive movement. *SIAM J. Sci. Comput.*, 27(3):850–872 (electronic), 2005.

[39] W. B. Fitzgibbon, S. L. Hollis, and J. J. Morgan. Stability and Lyapunov functions for reaction-diffusion systems. *SIAM J. Math. Anal.*, 28(3):595–610, 1997.

[40] J. Folkman. Tumor angiogenesis. *Cancer Medicine, J.F.Holland, R.C.Bast, D.L.Morton, E.Frei, D.W.Kufe, R.R.Weichselbaum*, pages 181–204, 1997.

[41] M. Di Francesco and D. Donatelli. Singular convergence of nonlinear hyperbolic chemo-taxis systems to keller–segel type models. *Discrete and Continuous Dynamical Systems (B)*, 13(1):79–100, 2010.

[42] P Friedl and E B Brcker. The biology of cell locomotion within three-dimensional extracellular matrix. *Cellular and molecular life sciences CMLS*, 57(1):41–64, 2000.

[43] K. O. Friedrichs. Differential equations of symmetric type. In *Fluid Dynamics and Applied Mathematics (Proc. Sympos., Univ. of Maryland, 1961)*, pages 51–65. Gordon and Breach, New York, 1962.

[44] A. Gamba, D. Ambrosi, A. Coniglio, A. de Candia, S. Di Talia, E. Giraudo, G. Serini, L. Preziosi, and F. Bussolino. Percolation, morphogenesis, and burgers dynamics in blood vessels formation. *Phys Rev Lett*, 90(11):118101, 2003.

[45] Edwige Godlewski and Pierre-Arnaud Raviart. *Hyperbolic systems of conservation laws*, volume 3/4 of *Mathématiques & Applications (Paris) [Mathematics and Applications]*. Ellipses, Paris, 1991.

[46] S.K. Godunov. A difference scheme for numerical solution of discontinuous solution of hydrodynamic equations. *Math. Sbornik.*, 47:271–306, 1969.

[47] L. Gosse. A well-balanced flux-vector splitting scheme designed for hyperbolic systems of conservation laws with source terms. *Comput. Math. Appl.*, 39(9-10):135–159, 2000.

[48] Laurent Gosse. A well-balanced scheme using non-conservative products designed for hyperbolic systems of conservation laws with source terms. *Math. Models Methods Appl. Sci.*, 11(2):339–365, 2001.

[49] L. Graziano and L. Preziosi. Mechanics in tumor growth. In *Modeling of biological materials*, Model. Simul. Sci. Eng. Technol., pages 263–321. Birkhäuser Boston, Boston, MA, 2007.

[50] J. M. Greenberg and A. Y. Leroux. A well-balanced scheme for the numerical processing of source terms in hyperbolic equations. *SIAM J. Numer. Anal.*, 33(1):1–16, 1996.

[51] C.W. Greider and E.H. Blackburn. Telomeres, telomerase and cancer. *Scientific American*, 2:92–97, 1996.

[52] C. Gridelli. Targeted therapy developments in the treatment of non-small cell lung cancer: a promising but long and winding road. *Current Opinion in Oncology*, 20(2):145–147, 2008.

[53] Francesca Romana Guarguaglini, Corrado Mascia, Roberto Natalini, and Magali Ribot. Stability of constant states of qualitative behavior of solutions to a one dimensional hyperbolic model of chemotaxis. *Discrete Contin. Dyn. Syst. Ser. B*, 12(1):39–76, 2009.

[54] D. Hanahan and R. A. Weinberg. The hallmarks of cancer. *Cell*, 100(1):57–70, January 2000.

[55] Am Harten. High resolution schemes for hyperbolic conservation laws. *J. Comput. Phys.*, 49(3):357–393, 1983.

[56] Ami Harten and James M. Hyman. Self-adjusting grid methods for one-dimensional hyperbolic conservation laws. *J. Comput. Phys.*, 50(2):235–269, 1983.

[57] Amiram Harten, Peter D. Lax, and Bram van Leer. On upstream differencing and Godunov-type schemes for hyperbolic conservation laws. *SIAM Rev.*, 25(1):35–61, 1983.

[58] Thomas Hillen. A classification of spikes and plateaus. *SIAM Rev.*, 49(1):35–51 (electronic), 2007.

[59] Thomas Hillen and Alex Potapov. The one-dimensional chemotaxis model: global existence and asymptotic profile. *Math. Methods Appl. Sci.*, 27(15):1783–1801, 2004.

[60] K. Höllig and H.-O. Kreiss. C^∞-regularity for the porous medium equation. *Math. Z.*, 192(2):217–224, 1986.

[61] Feimin Huang, Pierangelo Marcati, and Ronghua Pan. Convergence to the Barenblatt solution for the compressible Euler equations with damping and vacuum. *Arch. Ration. Mech. Anal.*, 176(1):1–24, 2005.

[62] Feimin Huang, Ronghua Pan, and Zhen Wang. Convergence to the barenblatt solution for compressible euler equations with damping. *Archive for Rational Mechanics and Analysis*, 200:665–689, 2011. 10.1007/s00205-010-0355-1.

[63] Willem Hundsdorfer and Jan Verwer. *Numerical solution of time-dependent advection-diffusion-reaction equations*, volume 33 of *Springer Series in Computational Mathematics*. Springer-Verlag, Berlin, 2003.

[64] R. K. Jain. Normalization of tumor vasculature: An emerging concept in antiangiogenic therapy. *Science*, 307:58–62, January 2005.

[65] Juhi Jang and Nader Masmoudi. Well-posedness for compressible Euler equations with physical vacuum singularity. *Comm. Pure Appl. Math.*, 62(10):1327–1385, 2009.

[66] A. Juengel. Diffusive and nondiffusive population models. Technical report, Submitted for publication.

[67] K. Kang, T. Kolokolnikov, and M. J. Ward. The stability and dynamics of a spike in the 1D Keller-Segel model. *IMA J. Appl. Math.*, 72(2):140–162, 2007.

[68] William L. Kath and Donald S. Cohen. Waiting-time behavior in a nonlinear diffusion equation. *Stud. Appl. Math.*, 67(2):79–105, 1982.

[69] Th. Katsaounis, B. Perthame, and C. Simeoni. Upwinding sources at interfaces in conservation laws. *Appl. Math. Lett.*, 17(3):309–316, 2004.

[70] Segel L.A. Keller, E.F. Model of chemotaxis. *Jl. Theor. Biol.*, 30:225–234, 1971.

[71] S. Klainerman and A. Majda. Singular limits of quasilinear hyperbolic systems with large parameters and the incompressible limit of compressible fluids. *Comm. Pure Appl. Math.*, 34(4):481–524, 1981.

[72] Barry F. Knerr. The porous medium equation in one dimension. *Trans. Amer. Math. Soc.*, 234(2):381–415, 1977.

[73] R. Kowalczyk. Preventing blow-up in a chemotaxis model. *J. Math. Anal. Appl.*, 305(2):566–588, 2005.

[74] A. A. Lacey, J. R. Ockendon, and A. B. Tayler. "Waiting-time" solutions of a nonlinear diffusion equation. *SIAM J. Appl. Math.*, 42(6):1252–1264, 1982.

[75] Philippe G. Lefloch and Athanasios E. Tzavaras. Representation of weak limits and definition of nonconservative products. *SIAM J. Math. Anal.*, 30(6):1309–1342 (electronic), 1999.

[76] Randall J. LeVeque. *Numerical methods for conservation laws*. Lectures in Mathematics ETH Zürich. Birkhäuser Verlag, Basel, 1990.

[77] T. P. Liu and J. A. Smoller. On the vacuum state for the isentropic gas dynamics equations. *Adv. in Appl. Math.*, 1(4):345–359, 1980.

[78] Tai-Ping Liu. Compressible flow with damping and vacuum. *Japan J. Indust. Appl. Math.*, 13(1):25–32, 1996.

[79] Tai-Ping Liu and Tong Yang. Compressible Euler equations with vacuum. *J. Differential Equations*, 140(2):223–237, 1997.

[80] Tai-Ping Liu and Tong Yang. Compressible flow with vacuum and physical singularity. *Methods Appl. Anal.*, 7(3):495–509, 2000. Cathleen Morawetz: a great mathematician.

[81] Y. Lou and W.-M. Ni. Diffusion, self-diffusion and cross-diffusion. *J. Differential Equations*, 131(1):79–131, 1996.

[82] Tetu Makino and Benot Perthame. Sur les solution symtrie sphrique de lequation deulerpoisson pour levolution detoiles gazeuses. *Japan Journal of Industrial and Applied Mathematics*, 7:165–170, 1990. 10.1007/BF03167897.

[83] D. Manoussaki, S. R. Lubkin, R. B. Vernon, and J. D. Murray. A mechanical model for the formation of vascular networks *in vitro*. *Acta Biotheoretica*, 44:271–282, 1996.

[84] R. H. Martin, Jr. and M. Pierre. Nonlinear reaction-diffusion systems. In *Nonlinear equations in the applied sciences*, volume 185 of *Math. Sci. Engrg.*, pages 363–398. Academic Press, Boston, MA, 1992.

[85] H. Matano and M. Mimura. Pattern formation in competition-diffusion systems in nonconvex domains. *Publ. Res. Inst. Math. Sci.*, 19(3):1049–1079, 1983.

[86] Carlo M.Croce. Oncogenes and cancer. *The New England Journal of Medicine*, 358(5):502–511, 2008.

[87] M. Mimura. Stationary pattern of some density-dependent diffusion system with competitive dynamics. *Hiroshima Math. J.*, 11(3):621–635, 1981.

[88] M. Mimura and K. Kawasaki. Spatial segregation in competitive interaction-diffusion equations. *J. Math. Biol.*, 9(1):49–64, 1980.

[89] J. D. Murray. *Mathematical biology. I*, volume 17 of *Interdisciplinary Applied Mathematics*. Springer-Verlag, New York, third edition, 2002. An introduction.

[90] J. D. Murray. *Mathematical biology. II*, volume 18 of *Interdisciplinary Applied Mathematics*. Springer-Verlag, New York, third edition, 2003. Spatial models and biomedical applications.

[91] J. D. Murray and G. F. Oster. Cell traction models for generating pattern and form in morphogenesis. *J. Math. Biol.*, 19(3):265–279, 1984.

[92] Roberto Natalini and Magali Ribot. An asymptotic high order mass-preserving scheme for a hyperbolic model of chemotaxis. *to appear in SIAM J. Num. Anal.*

[93] W.-M. Ni. Diffusion, cross-diffusion, and their spike-layer steady states. *Notices Amer. Math. Soc.*, 45(1):9–18, 1998.

[94] O. A. Oleĭnik, A. S. Kalašinkov, and Yuĭ-Lin′ Čžou. The Cauchy problem and boundary problems for equations of the type of non-stationary filtration. *Izv. Akad. Nauk SSSR. Ser. Mat.*, 22:667–704, 1958.

[95] Kevin J. Painter and Thomas Hillen. Volume-filling and quorum-sensing in models for chemosensitive movement. *Can. Appl. Math. Quart*, 10(4):501–543, 2002.

[96] Clifford S. Patlak. Random walk with persistence and external bias. *Bull. Math. Biophys.*, 15:311–338, 1953.

[97] C. A. Perazzo and J. Gratton. Bounds of waiting-time in nonlinear diffusion. *Appl. Math. Lett.*, 17(11):1253–1259, 2004.

[98] Benoît Perthame and Chiara Simeoni. Convergence of the upwind interface source method for hyperbolic conservation laws. In *Hyperbolic problems: theory, numerics, applications*, pages 61–78. Springer, Berlin, 2003.

[99] K Post. *A system of non-linear partial differential equations modeling chemotaxis with sensitivity functions*. PhD thesis, Humboldt Univ., Berlin, 1999.

[100] A. B. Potapov and T. Hillen. Metastability in chemotaxis models. *J. Dynam. Differential Equations*, 17(2):293–330, 2005.

[101] L. Preziosi. Modelling tumour growth and progression. *Progress in industrial mathematics at ECMI 2002*, 5:53–66.

[102] L. Preziosi and A. Tosin. Multiphase modelling of tumour growth and extracellular matrix interaction: mathematical tools and applications. *J. Math. Biol.*, 58(4-5):625–656, 2009.

[103] P. L. Roe. Approximate Riemann solvers, parameter vectors, and difference schemes. *J. Comput. Phys.*, 43(2):357–372, 1981.

[104] P. L. Roe. Upwind differencing schemes for hyperbolic conservation laws with source terms. In *Nonlinear hyperbolic problems (St. Etienne, 1986)*, volume 1270 of *Lecture Notes in Math.*, pages 41–51. Springer, Berlin, 1987.

[105] P. L. Roe and J. Pike. Efficient construction and utilisation of approximate Riemann solutions. In *Computing methods in applied sciences and engineering, VI (Versailles, 1983)*, pages 499–518. North-Holland, Amsterdam, 1984.

[106] F. Rothe. *Global Solutions of Reaction-Diffusion Systems*. Lecture Notes in Mathematics. Springer-Verlag, Berlin, 1984.

[107] Guido Serini, Davide Ambrosi, Enrico Giraudo, Andrea Gamba, Luigi Preziosi, and Federico Bussolino. Modeling the early stages of vascular network assembly. *The EMBO Journal*, 22(8):1771–1779, April 2003.

[108] Y. Shizuta and S. Kawashima. Systems of equations of hyperbolic-parabolic type with applications to the discrete boltzmann equation. *Hokkaido Math. J.*, 14:249–275, 1985.

[109] B. D. Sleeman, Michael J. Ward, and J. C. Wei. The existence and stability of spike patterns in a chemotaxis model. *SIAM J. Appl. Math.*, 65(3):790–817 (electronic), 2005.

[110] J. Smoller. *Shock waves and reaction-diffusion equations*, volume 258 of *Grundlehren der Mathematischen Wissenschaften [Fundamental Principles of Mathematical Science]*. Springer-Verlag, New York, 1983.

[111] Joseph L. Steger and R. F. Warming. Flux vector splitting of the inviscid gasdynamic equations with application to finite-difference methods. *J. Comput. Phys.*, 40(2):263–293, 1981.

[112] P. K. Sweby. High resolution schemes using flux limiters for hyperbolic conservation laws. *SIAM J. Numer. Anal.*, 21(5):995–1011, 1984.

[113] E F Toro, M Spruce, and W Speares. Restoration of the contact surface in the hll-riemann solver. *Shock Waves*, 4(1):25–34, 1994.

[114] Eleuterio F. Toro. *Riemann solvers and numerical methods for fluid dynamics*. Springer-Verlag, Berlin, third edition, 2009. A practical introduction.

[115] I. Toumi. A weak formulation of Roe's approximate Riemann solver. *J. Comput. Phys.*, 102(2):360–373, 1992.

[116] A. M. Turing. The chemical basis of morphogenesis. *Philo. Trans. Roy. Soc. Lond. Ser. B*, 237:5–72, 1952.

[117] M.S. Tyler. *Developmental biology: a guide for experimental study*. Sinauer Associates, 1994.

[118] B. Vailhé, D. Vittet, and J. J. Feige. In vitro models of vasculogenesis and angiogenesis. *Laboratory investigation; a journal of technical methods and pathology*, 81(4):439–452, April 2001.

[119] B Van Leer. Flux-vector splitting for the euler equations. In E. Krause, editor, *Numerical Methods in Fluid Dynamics*, volume 170 of *Lecture Notes in Physics, Berlin Springer Verlag*, pages 507–512. Springer-Verlag, 1982.

[120] Juan L. Vázquez. The interfaces of one-dimensional flows in porous media. *Transactions of the American Mathematical Society*, 285(2):pp. 717–737, 1984.

[121] Juan Luis Vázquez. Asymptotic behaviour and propagation properties of the one-dimensional flow of gas in a porous medium. *Trans. Amer. Math. Soc.*, 277(2):507–527, 1983.

[122] Berg Linda R. Villee Claude A., Solomon Eldra Pearl. *Biologia*. Multico, 1998.

[123] L. K. Wai. Telomeres, telomerase, and tumorigenesis – a review. *MedGenMed*, 6(3):19, 2004.

[124] O. Warburg. On the Origin of Cancer Cells. *Science*, 123(3191):309–314, 1956.

[125] Chao-Jiang Xu and Tong Yang. Local existence with physical vacuum boundary condition to Euler equations with damping. *J. Differential Equations*, 210(1):217–231, 2005.